UNIVERSITAT
POLITÈCNICA
DE VALÈNCIA

DOCTORAL SCHOOL

PhD Thesis

Mound Breakwater Design in Depth-Limited Breaking Wave Conditions

AUTHOR
María Piedad HERRERA GAMBOA

SUPERVISOR
Dr. Josep Ramon MEDINA FOLGADO

VALENCIA, March 2017

NECESITO del mar porque me enseña:
no sé si aprendo música o conciencia:
no sé si es ola sola o ser profundo
o sólo ronca voz o deslumbrante
suposición de peces y navios.
El hecho es que hasta cuando estoy dormido
de algún modo magnético circulo
en la universidad del oleaje.

Pablo Neruda, “El mar”
in *Memoria de Isla Negra* 1964
(III El fuego cruel)

Agradecimientos

Esta tesis doctoral es el fruto de varios años de trabajo, pero su culminación no habría sido posible sin el apoyo y la ayuda de todas aquellas personas importantes que me rodean.

A mi padre, por su dedicación y precocupación por mí. Porque sin él, probablemente no estaría escribiendo estas líneas.

A mi madre, por su apoyo incondicional, su alegría y su capacidad de ponerse en el lugar del otro. Gracias por estar siempre a mi lado.

A mis hermanos, Patricia y Pepe, a los que quiero con locura aunque siempre estemos de 'peleillas'.

A mis amigos, porque a pesar de la distancia que nos separa, sois mi segunda familia.

A mis compañeros del LPC y departamento, Ainoha, Gloria, Quique, Vicente, Guille, Tomás, César, Pepe, Ana, Esther, Jose Alberto, Joaquín, Miguel…por la ayuda prestada.

A Jorge, por todo. Por sus ánimos, su confianza, su paciencia y su ayuda. Porque siempre has estado ahí sin esperar nada a cambio.

A mi director de tesis, Josep, quien me ha transmitido su pasión por la ingeniería marítima. Gracias por haberme ofrecido la posibilidad de trabajar contigo, por la ayuda, la confianza y la disponibilidad mostrada todos estos años.

Al Ministerio de Educación, Cultura y Deporte, por la financiación brindada a través del programa de Formación de Profesorado Universitario (FPU 13/01872) para la realización de esta tesis doctoral.

Al Ministerio de Economía y Competitividad, por la financiación del proyecto ESCOLIF (BIA2012-33967).

A Debra Westall, por revisar este documento.

Resumen

El manto principal de los diques en talud suele estar formado por escollera natural o elementos prefabricados de hormigón; su función es resistir la acción del oleaje. Una revisión del estado del arte pone de manifiesto que son numerosas las fórmulas existentes para el diseño de mantos derivadas de ensayos físicos a escala reducida con oleaje sin rotura por fondo. Sin embargo, la mayoría de diques en talud se construyen en la zona de rompientes con oleaje limitado por fondo, donde las ecuaciones de diseño habituales no son del todo válidas. En esta tesis doctoral se analiza la estabilidad hidráulica de mantos bicapa de escollera, a partir de ensayos a escala reducida con pendiente de fondo m=1/50. En base a los resultados obtenidos de los ensayos físicos, se propone una nueva relación potencial para el diseño de mantos de escollera en condiciones de oleaje limitado por fondo, válida para taludes con $\cot\alpha=1.5$, números de estabilidad $0.98\leq H_{m0}/(\Delta D_{n50})\leq 2.5$, y profundidades relativas a pie de dique de $3.75\leq h_s/(\Delta D_{n50})\leq 7.50$.

Cuando el manto principal está formado por elementos de hormigón, es habitual construir una berma de pie que proporciona apoyo a los elementos del manto y, en su caso, colabora en la protección de la zona inferior del dique contra la socavación. Dicha berma suele construirse con escollera natural y su peso está condicionado al de los elementos del manto en el caso de no haber rotura por fondo. El peso de los elementos de la berma de pie suele ser un orden de magnitud inferior al peso de las unidades del manto; sin embargo, si la pendiente de fondo es fuerte (p.e. m=1/10) y las aguas someras esta regla no se cumple ya que algunas olas rompen sobre el fondo impactando directamente sobre la berma de pie. En estos casos, el peso de la escollera de la berma puede sobrepasar el de las unidades del manto y su correcto diseño es crucial para garantizar la estabilidad del dique. Además de estudiar la estabilidad del manto principal de diques de escollera, la presente tesis doctoral analiza también la estabilidad hidráulica de bermas de pie de escollera ubicadas en fondos con pendiente m=1/10 y aguas someras ($0.5<h_s/D_{n50}<5.01$), en base a ensayos físicos a escala reducida realizados con mantos bicapa de cubos y bermas de escollera con diferentes dimensiones. En primer lugar, se propone una nueva ecuación para el

diseño de bermas escollera estándar (B_t=3D_{n50} y t_t=2 D_{n50}), tanto emergidas como sumergidas, a partir de tres parámetros: (1) altura de ola en aguas profundas, H_{s0}, (2) longitud de onda en aguas profundas, L_{0p}, (3) profundidad a pie de dique, h_s. Posteriormente, se analiza la influencia del ancho de la berma (B_t) en su estabilidad hidráulica, introduciendo dos nuevos conceptos para caracterizar bermas de pie anchas (B_t>3D_{n50}): (1) berma nominal o zona de la berma de pie sobre la que realmente apoya el manto principal, y (2) berma de sacrificio o zona de la berma de pie que protege a la berma nominal. A partir del daño de la berma de pie nominal, se propone un nuevo método para reducir el tamaño de piedra (D_{n50}) incrementando el ancho de la berma (B_t) cuando no se disponga del tamaño requerido en cantera. Finalmente, se examina el daño del manto de cubos y se analiza la influencia del método de colocación sobre el mismo, a partir de ensayos realizados con mantos bicapa de cubos con colocación aleatoria y uniforme.

Resum

El mantell principal dels dics en talús sol estar format per roca o elements prefabricats de formigó, la seva funció és resistir l'acció de l'onatge. Una revisió de l'estat de l'art manifesta que són nombroses les equacions de disseny existents per a condicions d'onatge no trencat. No obstant això, la majoria de dics en talús es construeixen a la zona de rompents amb onatge limitat per fons, on les equacions de disseny existents no són del tot vàlides. En aquesta tesi doctoral s'analitza l'estabilitat hidràulica de mantells bicapa de roca, a partir d'assajos a escala reduïda realitzats amb pendent de fons $m = 1/50$. En base als resultats obtinguts dels assajos, es proposa una relació potencial per al disseny de mantells de roca en condicions d'onatge limitat per fons vàlida per a talussos amb $\cot\alpha = 1.5$, nombres d'estabilitat $0.98 \leq H_{m0}/(\Delta D_{n50}) \leq 2.5$, i profunditats relatives a peu de dic de $3.75 \leq h_s/(\Delta D_{n50}) \leq 7.50$.

Quan mantell principal està format per elements de formigó , és habitual construir una berma de peu que proporciona suport als elements del mantell i, si escau, col·labora en la protecció de la zona inferior del dic contra la soscavació. Aquesta berma sol construir amb roca i el seu pes està condicionat al dels elements del mantell en el cas de no haver trencament per fons. El pes dels elements de la berma de peu sol ser un ordre de magnitud inferior al pes de les unitats del mantell; però, si el pendent de fons és fort (p.e. $m = 1\ /10$) i les aigües someres aquesta regla no es compleix ja que algunes onades trenquen sobre el fons impactant directament sobre la berma de peu. En aquests casos, el pes de la roca de la berma pot sobrepassar el de les unitats del mantell, i el seu correcte disseny és crucial per garantir l'estabilitat del dic. A més d'estudiar l'estabilitat del mantell principal de dics de roca, la present tesi doctoral analitza també l'estabilitat hidràulica de bermes de roca ubicades en fons amb pendents $m = 1/10$ i aigües someres ($0.5 < h_s/D_{n50} < 5.01$), utilitzant assajos a escala reduïda realitzats amb mantells de doble capa de cubs i bermes de roca amb diferents dimensions. En primer lloc, es proposa una nova equació per al disseny de bermes de roca estàndard ($B_t = 3\ D_{n50}$ i $t_t = 2\ D_{n50}$), tant emergides com submergides, a partir de tres paràmetres: (1) alçada d'ona significant

en aigües profundes, H_{s0}, (2) longitud d'ona en aigües profundes, L_{0p}, i (3) profunditat a peu de dic, h_s. Posteriorment, s'analitza la influència de l'amplada de la berma (B_t) en la seua estabilitat hidràulica, introduint dos nous conceptes per caracteritzar bermes de peu amples ($B_t > 3\ D_{n50}$): (1) berma nominal o zona de la berma de peu sobre la qual recolza el mantell principal, i (2) berma de sacrifici o zona de la berma de peu que protegeix la berma nominal. A partir del dany de la berma de peu nominal, es proposa un nou mètode per reduir el tamany de roca (D_{n50}) incrementant l'amplada de la berma (B_t) quan no es disposi de la mida requerit en pedrera. Finalment, s'examina el dany del mantell de cubs i s'analitza la influència del mètode de col·locació sobre el mateix , a partir d'assajos realitzats amb mantells bicapa de cubs amb col·locació aleatòria i uniforme.

Abstract

The design of rubble mound breakwaters usually focuses on the main armor layer. A review of the existing literature reveals that different equations are used to design rock armors in non-breaking wave conditions. However, most rubble mound breakwaters are constructed in the depth-induced breaking zone where they are attacked by waves breaking in the foreshore; in these conditions, existing design equations are not valid. Therefore, in this PhD thesis, the hydraulic stability of double-layer rock armors is analyzed through a series of small-scale tests conducted with a bottom slope m=1/50. Based on test results, a new potential relationship is given to design rock armors in depth-limited breaking wave conditions with armor slope $\cot\alpha=1.5$, stability numbers within the range $0.98 \leq H_{m0}/(\Delta D_{n50}) \leq 2.5$, and relative water depth at the toe $3.75 \leq h_s/(\Delta D_{n50}) \leq 7.50$.

When concrete units are used for the armor layer, mound breakwaters are usually protected by a toe berm. This toe berm is placed on the seafloor or underlayer, providing support for the concrete armor units which are placed later on the structure slope. Toe berm design is commonly related to the armor design; in non-breaking wave conditions, the mass of toe berm rocks is one order of magnitude lower than the units of the layer. In breaking wave conditions, however, the highest waves start breaking on the bottom and impact directly on the toe berm. This is the common case of rocky sea bottoms with m=1/10 or higher slopes and thus, a correct design of the toe berm is crucial to guarantee the armor stability. The present PhD thesis examines the hydraulic stability of rock toe berms placed on a m=1/10 bottom slope and in very shallow waters ($0.5 < h_s/D_{n50} < 5.01$). Small-scale tests were conducted with double-layer cube armored breakwaters and rock toe berms with different widths (B_t) and thicknesses (t_t). Firstly, a new equation is proposed to design emerged and submerged standard rock toe berms ($B_t=3D_{n50}$ and $t_t=2\ D_{n50}$) using three parameters: (1) deep water wave height, H_{s0}, (2) deep water wave length, L_{0p}, and (3) water depth at the toe, h_s. Secondly, the influence of toe berm width (B_t) on toe berm stability is analyzed introducing two new concepts to characterize wide toe berms ($B_t>3D_{n50}$): (1) the nominal toe berm or the most shoreward toe berm area

which effectively supports the armor layer, and (2) the sacrificial toe berm or the most seaward toe berm area which serves to protect the nominal toe berm. Considering the nominal toe berm damage, a new method is developed to reduce the rock toe berm size (D_{n50}) by increasing the toe berm width (B_t) if the required rock size is not available at the quarries. Finally, cube armor damage is examined, and the influence of the placement technique on armor stability is also characterized from physical tests conducted with cubes randomly- and uniformly- placed on the armor in two layers.

TABLE OF GENERAL CONTENTS

Agradecimientos

Resumen

Resum

Abstract

Table of general contents

Table of contents

List of figures

List of tables

Notations

Chapter

I Introduction 27

II Literature review 33

III Hydraulic stability of rock armors placed in shallow waters and on gentle sea bottoms (m=1/50) 75

IV Hydraulic stability of rock toe berms placed in very shallow waters and on steep sea bottoms (m=1/10) 125

V Conclusions and future research 183

VI References 189

VII Appendix 1 205

VIII Appendix 2 281

TABLE OF CONTENTS

I Introduction 27

I.1. Focus of the study.. 29
I.2. Background for the research.. 29
I.3. Thesis structure 30

II Literature review 33

II.1. Introduction 35
II.2. Waves in breaking conditions 35
II.2.1. Types of wave breaking... 35
II.2.2. Wave breaking criteria.. 38
II.2.2.1. Wave steepness 38
II.2.2.2. Water depth... 39
II.2.3. Distribution of shallow-water wave heights 42
II.3. Hydraulic stability of mound breakwaters 44
II.3.1. Introduction 44
II.3.2. Failure modes 45
II.3.3. Techniques to place armor units 47
II.3.4. Armor stability and damage measurements 48
II.3.4.1. Qualitative analysis.. 48
II.3.4.2. Quantitative analysis.. 51
II.3.5. Toe berm stability and damage measurements 54
II.3.5.1. Toe berm dimensions 54
II.3.5.2. Toe berm damage 57
II.4. Hydraulic stability of rock armors in depth-limited breaking wave conditions 58
II.4.1. Introduction 58
II.4.2. Hydraulic stability formulas for rock armors 59

II.5. Hydraulic stability of rock toe berms in depth-limited breaking wave conditions....64
II.5.1. Introduction....64
II.5.2. Hydraulic stability formulas for rock toe berms....65
III Hydraulic stability of rock armors placed in shallow waters and on gentle sea bottoms (m=1/50)....75
III.1. Introduction....77
III.2. Experimental design....77
III.2.1. Facilities and equipment....77
III.2.2. Physical models....79
III.2.3. Irregular tests....83
III.2.4. Measurements....85
III.2.4.1. Wave measurements....85
III.2.4.2. Wave separation. LASA-V Method....87
III.2.4.1. Damage measurements....89
III.2.5. Numerical simulations using SwanOne....90
III.3. Data analysis....91
III.3.1. Wave analysis....91
III.3.2. Damage analysis....104
III.4. New hydraulic stability formula for mound breakwaters....109
III.4.1. A new hydraulic stability formula....109
III.4.1.1. Confidence intervals....118
III.4.1.2. Comparison of measurements with existing formulas....120
IV Hydraulic stability of rock toe berms placed in very shallow waters and on steep sea bottoms (m=1/10)....125
IV.1. Introduction....127
IV.2. Experimental design....128
IV.2.1. Facilities and equipment....128
IV.2.2. Physical models....128
IV.2.3. Irregular tests....134
IV.2.4. Measurements....136
IV.2.4.1. Wave measurements....136
IV.2.4.2. Wave separation. LASA-V Method....137
IV.2.4.3. Damage measurements....138

- □ Toe berm damage 138
- □ Armor damage 138

IV.3. Data analysis 139

IV.3.1. Wave analysis 139

IV.3.2. Analysis of toe berm damage 146

IV.3.2.1. Tests conducted with standard toe berms (B_t=3D_{n50}) 146

IV.3.2.2. Additional tests conducted with three toe berm widths (B_t=3, 5 and 12 D_{n50}) 149

- □ Total toe berm damage (N_{od}) 149
- □ Nominal toe berm damage (N_{od}*) 151

IV.3.3. Analysis of armor damage 154

IV.3.3.1. Armor damage with nominal rock toe berm (B_t=3D_{n50}) 154

IV.3.3.2. Armor damage with three toe berm widths (B_t=3, 5 and 12D_{n50}) 160

IV.4. New hydraulic stability formulas for toe berms 160

IV.4.1. Standard toe berms (B_t=3D_{n50}) 161

IV.4.1.1. A new hydraulic stability formula 161

IV.4.1.2. Confidence intervals 162

IV.4.1.3. Validation with additional tests 163

IV.4.1.4. Comparison with existing formulas 164

IV.4.1.5. Example of application 166

IV.4.2. Wide toe berms (B_t>3D_{n50}) 169

IV.4.2.1. Hydraulic stability formula of wide toe berms 169

IV.4.2.2. Confidence intervals 173

IV.4.2.3. Comparison with existing formulas 174

IV.4.2.4. Example of application 176

IV.5. Influence of the placement technique on cube armor stability 177

IV.5.1. Introduction 177

IV.5.2. Artificial neural network model for armor damage 178

IV.5.3. Neural network simulations 181

V Conclusions and future research 183

V.1. Summary and Conclusions 185

V.1.1. Introduction 185

V.1.2. Hydraulic stability of rock armors placed in shallow waters and on gentle sea bottoms (m=1/50) 185

V.1.3. Hydraulic stability of rock toe berms placed in very shallow waters and on steep sea bottoms (m=1/10) 187
V.2. Future research 188
VI References 189
VII Appendix 1 205
VIII Appendix 2 281

LIST OF FIGURES

Figure II.1. Types of wave breaking. 37

Figure II.2. Breaking parameters (New et al., 1985). 38

Figure II.3. Limiting steepness in deep water (USACE, 1984). 39

Figure II.4. Example of shallow water and deep water distributions of wave heights. 42

Figure II.5. Concrete armor units for mound breakwaters (Dupray and Roberts, 2009). 45

Figure II.6. Failure modes of mound breakwaters (Bruun, 1979). 46

Figure II.7. Heterogeneous packing (HeP) failure mode (Gómez-Martín and Medina, 2014). 47

Figure II.8. View of IDa for double-layer Cubipod armor. 49

Figure II.9. View of IIDa for double-layer Cubipod armor. 49

Figure II.10. View of IDe for double-layer Cubipod armor. 49

Figure II.11. View of De for double-layer Cubipod armor. 50

Figure II.12. View of IDa for single-layer Cubipod armor. 50

Figure II.13. View of IDe for single-layer Cubipod armor. 51

Figure II.14. View of De for single-layer Cubipod armor. 51

Figure II.15. Cross section of toe berm. 55

Figure II.16. Types of toe berms (BSI, 1991). 56

Figure II.17. Toe using concrete piles (CIRIA/CUR/CETMEF, 2007). 57

Figure II.18. N_{od} classification for toe berms (Docters van Leeuwen, 1996). 58

Figure II.19. Permeability values for different structures (Van der Meer, 1988a). 61

Figure II.20. Stability number as a function of the water depth ratio (h_t/h_s) for tests conducted by Markle (1989)..66

Figure II.21. Linearized N_{od} measured in Gerding's (1993) tests and linearized N_{od} estimated with Eqs. II.27 and II.28 given by Gerding (1993) and Van der Meer (1998b). 68

Figure II.22. $N_{\%}$ measured during Ebbens' (2009) tests in the series conducted with m=1/10, D_{n50}(cm)=2.68 and h_s(cm)=7.3. 69

Figure II.23. Values of N_{od} corresponding to $N_{\%}$ measured by Ebbens (2009) as a function of the bottom slope (m), toe berm size (D_{n50}) and toe berm void porosity (n_v). 70

Figure II.24. Linearized $N_{\%}$ measured during Ebbens' (2009) tests and estimated by Eq. II.29...70

Figure II.25. Example of toe berm damage estimated by different formulas as a function of N_s. 72

Figure II.26. Example of toe berm damage estimated by different formulas as a function of h_s/D_{n50}...73

Figure III.1. Longitudinal cross section of the LPC-UPV wave flume used in the experiments with m=1/50 (dimensions in meters)......................77

Figure III.2. Piston-type wavemaker..78

Figure III.3. Piston-type wavemaker used in the experiments.......................79

Figure III.4. Passive energy absorber system used in the experiments. 79

Figure III.5. Cross section of the rock armored model (dimensions in centimeters). 80

Figure III.6. Nominal diameter for gravel G0 used in the experiments. 80

Figure III.7. Aspect ratio for gravel G0 used in the experiments. 81

Figure III.8. Blockiness for gravel G0 used in the experiments. 82

Figure III.9. Construction process of the rubble mound breakwater model: (a) drawing, (b) leveling, (c) core, (d) filter, (e) first armor layer and (f) second armor layer...83

Figure III.10. View of test conducted with breakwater model. 85

Figure III.11. View of test conducted without breakwater model. 85

Figure III.12. Capacitive wave gauges used in the experiments. 86

Figure III.13. Video and photo cameras used in the experiments. 87

Figure III.14. LASA-V software used to separate incident and reflected waves (Figueres and Medina, 2004) 87

Figure III.15. Virtual net used in the experiments to characterized armor damage. 89

Figure III.16. View of wave gauges close to the breakwater model during a test. 91

Figure III.17. Incident and reflected waves obtained at G1 when applying the LASA-V method ($0<t(s)<100$). Test conducted with structure, h_s (cm)=30, ξ_p=5.0 and H_{m0} (cm)=9. 92

Figure III.18. Reflection coefficient measured at the wave generating zone (G1 to G4) versus the dimensionless water depth. 93

Figure III.19. Comparison of experimental incident H_{m0}, $H_{1/10}$ and $H_{2\%}$ without the structure, and with the structure obtained from K_r at the wave generating zone. 94

Figure III.20. Comparison of experimental incident H_{m0}, $H_{1/10}$ and $H_{2\%}$ without the structure and estimations given by SwanOne. 96

Figure III.21. H_{m0} versus $H_{1/3}$ measured in tests without structure and estimations given by the SwanOne model combined with the CWD method. 97

Figure III.22. $H_{1/10}$ versus $H_{2\%}$ measured in tests without structure and estimations given by the SwanOne model. 97

Figure III.23. Wave heights measured at the wave generating zone in tests without structure compared to the average of G11 and G12: (a) H_{m0}, (b) $H_{1/10}$ and (c) $H_{2\%}$. 99

Figure III.24. SwanOne estimations at the G1 position compared to the average of G11 and G12: (a) H_{m0}, (b) $H_{1/10}$ and (c) $H_{2\%}$. 101

Figure III.25. Comparison of the mean values of H_{m0} and (a) $H_{1/10}$ and (b) $H_{2\%}$ measured at G11 and G12 in tests without structure. 102

Figure III.26. Comparison of the mean values of H_{m0} and (a) $H_{1/10}$ and (b) $H_{2\%}$ estimated by SwanOne at G11 and G12 positions..................... 103

Figure III.27. Stability numbers for (a) IDa and (b) IDe.............................. 105

Figure III.28. Qualitative armor damage levels for series 3.......................... 106

Figure III.29. Armor damage (S_e) as a function of the stability number (N_s=H/(ΔD_{n50})) measured in tests without structure when using (a) H=H_{m0}, (b) H=$H_{1/10}$ and (c) H=$H_{2\%}$ at G11 and G12 positions. 108

Figure III.30. Armor damage (S_e) as a function of the stability number (N_s=H/(ΔD_{n50})) estimated by SwanOne when using (a) H=H_{m0}, (b) H=$H_{1/10}$ and (c) H=$H_{2\%}$ at G11 and G12 positions.. 109

Figure III.31. Armor damage ($S_e^{1/6}$) versus the stability number N_s=H/(ΔD_{n50}) for H=H_{m0}, H=$H_{1/10}$ and H=$H_{2\%}$ obtained at G11 and G12 positions from (a) tests without structure and (b) SwanOne estimations. 112

Figure III.32. Linearized armor damage ($S_e^{1/6}$) versus the stability number N_s=H/(ΔD_{n50}) for H=H_{m0}, H=$H_{1/10}$ and H=$H_{2\%}$ obtained at G11 and G12 positions from (a) tests without structure and (b) SwanOne estimations... 113

Figure III.33. rMSE frequency histograms for measured and estimated S_e when using Eq. III.13 with H=H_{m0}, H=$H_{1/10}$ and H=$H_{2\%}$ measured in tests without structure... 114

Figure III.34. rMSE frequency histograms for measured and estimated S_e when using Eq. III.13 with H=H_{m0}, H=$H_{1/10}$ and H=$H_{2\%}$ estimated by SwanOne... 115

Figure III.35. Measured armor damage (S_e) versus S_e estimated by Eq. III.13 for H=H_{m0}, H=$H_{1/10}$ and H=$H_{2\%}$ obtained at G11 and G12 positions from (a) test measurements and (b) SwanOne estimations. 116

Figure III.36. Sketch of the distances seaward from the toe structure (d*) to determine the optimum location for wave parameter calculation in breaking wave conditions. 117

Figure III.37. Measured armor damage (S_e) as a function of the stability number (N_s=H/(ΔD_{n50})) estimated by SwanOne when using H=H_{m0} at a distance of d*=3h_s seaward from the structure toe. 118

Figure III.38. Squared armor damage errors as a function of the S_e estimated by Eq. III.13 with H=H_{m0}, K=0.066 and k_2=6.0. 119

Figure III.39. Measured S_e versus S_e estimated by Eq. III.13 with H=H_{m0} given by SwanOne at 3h_s seaward from the toe structure, K=0.066 and k_2=6.0...120

Figure III.40. Linearized measured armor damage $S^{1/6}$ versus estimations of $S^{1/6}$ given by existing formulas and 90% confidence interval of Eq. III.13 using H=H_{m0} given by SwanOne at d*=3h_s. 123

Figure IV.1. The two segments of a wide toe berm (B_t>3D_{n50}): sacrificial and nominal toe berm. 127

Figure IV.2. Longitudinal cross section of the LPC-UPV wave flume used in the experiments with m=1/10 (dimensions in meters). 128

Figure IV.3. Cross section of the cube armored model (dimensions in centimeters). 129

Figure IV.4. Configuration of toe berms: (a) B_t=3D_{n50}, (b) B_t=5D_{n50}, (c) B_t=12D_{n50}. 130

Figure IV.5. Nominal diameter for cubes and gravel G3, G4 and G5 used in the experiments..131

Figure IV.6. Resin cubes used in tests...131

Figure IV.7. Construction process of the mound breakwater model: (a) drawing, (b) cleaning material, (c) core, (d) filter, (e) toe berm and placement of cameras, and (f) armor layers...132

Figure IV.8. (a) Double-layer randomly-placed cube armor, (b) Double-layer uniformly-placed cube armor. 133

Figure IV.9. Physical model constructed with rock toe berms of D_{n50}(cm) = 3.99 (gravel G4) and (a) B_t = 3D_{n50}, (b) B_t = 5D_{n50}, and (c) B_t = 12D_{n50}.....134

Figure IV.10. Wave gauges located in the model zone...............................137

Figure IV.11. Total toe berm damage (N_{od}) and nominal toe berm damage (N_{od}*). 138

Figure IV.12. Virtual net method used in the experiments to measure cube armor damage.......... 139

Figure IV.13. Measured $H_{1/3i}$ at the wave generating zone versus deep water significant wave height, H_{s0}. 140

Figure IV.14. Comparison of H_{m0} measured at G1 and G11 for tests in the range 8≤ h_s (cm) ≤20 with standard toe berms. 141

Figure IV.15. Virtual wave flumes (dimensions in meters). 142

Figure IV.16. Comparison of H_{m0} given by SwanOne for h_s(cm)=6: (a) virtual wave flumes #1 and #2 and (b) virtual wave flumes #1 and #3. 145

Figure IV.17. Measured toe berm damage (N_{od}=N_{od}*) depending on water depth at the toe (h_s) after tests conducted with (a) H_{s0}(cm)=12 and T_p(s)=1.8, and (b) H_{s0}(cm)=16 and T_p(s)=1.8. 147

Figure IV.18. Measured toe berm damage (N_{od}=N_{od}*) depending on water depth at the toe (h_s). 147

Figure IV.19. Toe berm damage (N_{od}=N_{od}*) versus $(H_{s0}\ L_{0p})^{1/2}$ for (a) D_{n50}(cm)=3.99 and (b) D_{n50}(cm)=5.17. 149

Figure IV.20. Influence of rock size (D_{n50}) on measured total toe berm damage (N_{od}) depending on $(H_{s0}\ L_{0p})^{1/2}$. Tests with B_t=3D_{n50}. 150

Figure IV.21. Influence of toe berm width on measured toe berm damage (N_{od}). 151

Figure IV.22. Influence of toe berm width on measured nominal toe berm damage (N_{od}*). 152

Figure IV.23. Comparison of measured toe berm damage (N_{od}) and nominal toe berm damage (N_{od}*) for tests conducted with rock sizes (a) D_{n50}(cm)=3.04 and (b) D_{n50}(cm)=3.99. 153

Figure IV.24. Comparison of measured total toe berm damage (N_{od}) and measured nominal toe berm damage (N_{od}*). 154

Figure IV.25. Dimensionless armor damage S_e versus the water depth at the toe of the structure after the test conducted with H_{s0}(cm)=16 and T_p(s)=1.8 and rock toe berms with D_{n50}(cm)=3.99 and 5.17 155

Figure IV.26. Dimensionless armor damage S_e versus the water depth at the toe of the structure for all tests conducted with rock toe berms with D_{n50}(cm)=3.99 and 5.17 155

Figure IV.27. Armor damage (S_e) versus $(H_{s0}\ L_{0p})^{1/2}$ for (a) D_{n50}(cm)=3.99 and (b) D_{n50}(cm)=5.17. 156

Figure IV.28. Measured armor damage S_e versus measured armor damage N_{od}. ... 157

Figure IV.29. Armor damage N_{od} versus water depth at the toe of the structure (h_s) for all tests conducted with rock toe berms with D_{n50}(cm)=3.99 and 5.17. 158

Figure IV.30. Armor damage compared to toe berm damage measured with the parameter N_{od} for toe berm sizes (a) D_{n50}(cm)=3.99 and (b) D_{n50}(cm)=5.17. 159

Figure IV.31. Influence of toe berm width on measured armor damage, S_e. 160

Figure IV.32. Squared toe berm damage errors as a function of the N_{od} given by Eq. IV.4 162

Figure IV.33. Comparison of the N_{od}=N_{od}* measured in tests and that given by Eq. IV.4 and 90% confidence interval. 163

Figure IV.34. Comparison of the measured toe berm damage (N_{od}=N_{od}*) and the estimated toe berm damage (N_{od}=N_{od}*) using Eq. IV.4 for all tests within the range of application. 164

Figure IV.35. Measured toe berm damage (N_{od}=N_{od}*) compared to prediction formulas and 90% confidence intervals of Eq. IV.4 for tests conducted in the range $10 \leq h_s(cm) \leq 20$ (h_t>0). 165

Figure IV.36. Toe berm damage (N_{od}=N_{od}*) given by Eq. IV.4 depending on the variable $H_{s0}\ L_{0p}$, for h_s/D_{n50}=0 and h_t<0. 167

Figure IV.37. Toe berm damage (N_{od}=N_{od}*) given by Eq. IV.4 depending on the variable $H_{s0}\ L_{0p}$, for h_s/D_{n50}=2 and h_t=0. 167

Figure IV.38. Toe berm damage (N_{od}=N_{od}*) given by Eq. IV.4 depending on the variable H_{s0} L_{0p}, for h_s/D_{n50}=5 and h_t>0. 168

Figure IV.39. Toe berm damage (N_{od}=N_{od}*) given by Eq. IV.4 depending on h_s/D_{n50} for H_{s0}(m)=5 and T_p(s)=11.. 169

Figure IV.40. Measured nominal toe berm damage (N_{od}*) versus (H_{s0} L_{0p})$^{1/2}$ for tests conducted with (a) D_{n50}(cm)=3.99 with n_t=5 and D_{n50}(cm)=5.17 with n_t=3, and (b) D_{n50}(cm)=3.04 with n_t=5 and D_{n50}(cm)=3.99 with n_t=3.170

Figure IV.41. (a) Nominal toe berm (n_t=3) and (b) equivalent wider toe berm (3<n_t≤12).. 171

Figure IV.42. (a) $D_{n50,3}$ estimated with Eq. IV.4 and (b) $D_{n50,nt}$ as a function of $D_{n50,3}$ and the toe berm width (n_t). 173

Figure IV.43. Comparison of the N_{od}* measured in tests and the N_{od} given by Eq. IV.9 with μ=0.4 and 90% confidence interval................................ 174

Figure IV.44. Comparison of the N_{od}* measured in tests and that estimated by Eq. IV.9 using μ=2/17 instead of μ=0.4..................................... 175

Figure IV.45. Rock mass (M_{50}) depending on the toe berm width (B_t=n_t D_{n50}). 176

Figure IV.46. Double-layer armor with face-to-face fitting parallelepiped blocks. Mazarrón, Murcia (Spain)... 177

Figure IV.47. Uniformly-placed cube roundhead. Jávea, Alicante (Spain)......... 178

Figure IV.48. NN configuration... 179

Figure IV.49. NN performance for configurations with different numbers of neurons in the hidden layer. 180

Figure IV.50. Comparison of NN estimations and experimental observations of S_e. 180

Figure IV.51. *S_e e*stimated by NN depending on (H_{m0i} L_{0p})$^{1/2}$/ΔD_n for cubes randomly- and uniformly-placed on the armor layer. 181

Figure IV.52. S_e estimated by NN depending on h_s/ΔD_n for cubes randomly- and uniformly-placed on the armor layer. 182

Figure V.1. Final equations proposed to estimate rock armor damage. 186

Figure V.2. Final equations proposed to estimate rock toe berm damage. 188

Figure A2.1. Linear damage function obtained from the data provided by USACE (1975 and 1984). 284

LIST OF TABLES

Table II.1. Types of wave breaking as a function of Iribarren's number with the bottom slope (m) 37

Table II.2. Types of wave breaking (New et al., 1985). 38

Table II.3. Coefficients for $H_{1/3}$ and H_{max} according to Goda (2000). 44

Table II.4. Characteristic damage numbers for a range of damage levels (CIRIA/CUR/CETMEF, 2007)... 52

Table II.5. Design values of S for double-layer rock armors (Van der Meer, 1998a). 53

Table III.1. Characteristics of model materials. 82

Table III.2. Test matrix... 84

Table III.3. Wave gauge distances. 86

Table III.4. Mean values of dimensionless armor damage using visual counting and virtual net methods..106

Table III.5. t-student analysis values..110

Table III.6. Optimum values of K and k_2 in Eq. III.13 for H_{m0} estimated by SwanOne at a seaward distance d* from the toe of the structure, and rMSE and r between measured S_e and estimated S_e given by Eq. III.13. 117

Table IV.1. Characteristics of model materials. 130

Table IV.2. Irregular tests conducted with standard toe berms (B_t=3D_{n50}).......135

Table IV.3. Irregular tests conducted with h_{ss}=8cm and three toe berm widths (B_t=n_t D_{n50}, n_t=3, 5 and 12)...136

Table IV.4. Distance between wave gauges. 137

Table IV.5. Distances between points A, B, C, D, E, F, G, H and the toe of the structure (dimensions in meters). 142

Table IV.6. Spectral significant wave height at the toe, H_{m0}, provided by the SwanOne numerical model for the virtual wave flumes #1, #2 and #3. 143

Table IV.7. rMSE for H_{m0} at different points along wave flume #1 (target) when compared to values for wave flumes #2 and #3. 144

Table A2.1. Dimensionless armor damage (S) for H=Hs and H=H1/10, as a function of H/HD=0 and the damage in percent (D). 283

NOTATIONS

Symbols

a [m] or [cm] = zD_{n50}, width of the virtual net

A [m^2] or [cm^2] = area of average original profile in the cross section

A_e [m^2] or [cm^2] = eroded area in the cross section

A_{ev} [m^2] or [cm^2] = eroded area in the cross section estimated using the visual counting method

b [m] or [cm] = qD_{n50}, length of the virtual net or width of the reference area

Blc [%] = $(M_{50}/(\rho_r XYZ))100$, blockiness

B_t[cm] = $n_t D_{n50}$, toe berm width

c_{pl} [-] = plunging coefficient

c_s [-] = surging coefficient

cotα [-] = armor slope

d [cm] = minimum distance between rows through which a rock could pass

D [%] = A_e/A, percentage of original volume eroded

D_n [m] or [cm] = $(M/\rho_r)^{1/3}$, concrete armor unit nominal diameter

D_{n50} [m] or [cm] = $(M_{50}/\rho_r)^{1/3}$, rock nominal diameter

$D_{n50\text{-core}}$ [m] or [cm] = nominal diameter of the core material

$D_{n50,3}$ [m] or [cm] = nominal diameter of rocks for the nominal toe berm (n_t=3)

$D_{n50,nt}$ [m] or [cm] = nominal diameter of rocks for wider toe berms (n_t>3)

D_{50} [m] or [cm] = rock diameter that exceeds the 50% value of sieve curve

D_{15} [m] or [cm] = rock diameter that exceeds the 15% value of sieve curve

D_{85} [m] or [cm] = rock diameter that exceeds the 85% value of sieve curve

e_i = estimated values

$\bar{e}$ = average of estimated values

f [s^{-1}] = frequency

f_p [s^{-1}] = peak frequency

f_B [-] = $(B_t/3\ D_{n50})^{1/2}$, amplifier factor for wide toe berms (n_t>3)

F(H) = wave distribution function

g [m/s^2] = gravitational acceleration (=9.81)

h [m] or [cm] = water depth

h_b [m] or [cm] = breaker water depth

h_s [m] or [cm]] = water depth at the toe berm or at the toe of the structure (for rubble mound breakwaters without toe berm)

h_{ss} [m] or [cm] = water depth at the toe of the nominal toe berm

h_t [m] or [cm] = water depth above the toe berm

H [m] or [cm] = wave height

H_b [m] or [cm] = breaker wave height

$H_{D=0}$ [m] or [cm] = design wave height corresponding to D=0-5%

H_m [m] or [cm] = mean wave height

H_{max} [m] or [cm] = maximum wave height

H_{m0} [m] or [cm] = $4(m_0)^{0.5}$, spectral wave height

H_{m0i} [m] or [cm] = incident spectral wave height

H_{m0r} [m] or [cm] = reflected spectral wave height

H_{rms} [m] or [cm] = root mean square wave height

H_s [m] or [cm] = significant wave height or highest one-third wave, $H_{1/3}$

H_{s0} [m] or [cm] = deep water significant wave height

H_{tr} [m] or [cm] = transitional wave height

H_0' [m] or [cm] = equivalent deep water significant wave height

H1 [m] or [cm] = scale parameter in the composite Weibull distribution method

H2 [m] or [cm] = scale parameter in the composite Weibull distribution method

$H_{1/3i}$ [m] or [cm] = average of the highest one-third incident waves

$H_{1/10}$ [m] or [cm] = average wave height of the highest 1/10 waves

$H_{1/20}$ [m] or [cm] = average wave height of the highest 1/20 waves

$H_{1/50}$ [m] or [cm] = average wave height of the highest 1/50 waves

$H_{0.1\%}$ [m] or [cm] = wave height exceeded by 0.1% of the waves

$H_{1\%}$ [m] or [cm] = wave height exceeded by 1% of the waves

$H_{2\%}$ [m] or [cm] = wave height exceeded by 2% of the waves

H_{50} [m] or [cm] = average wave height of the 50 highest waves

I [-] = number of strips in the virtual net

Ir [-] = $\tan\alpha\,/(H/L_0)^{1/2}$, Iribarren's number

Ir* [-] = $m\,/(H/L_0)^{1/2}$, Iribarren's number with the bottom slope m

k [rad/m] = $2\pi/L_m$, wave number

$k_{m-1,0}$ [rad/m] = $2\pi/L_{m-1,0}$, number of wave based on the spectral wave length, $L_{m-1,0}$

kh_s [-] = $2\pi h_s/L_{m,toe}$, dimensionless water depth

K_D [-] = stability coefficient

K_R [-] = $H_{m0r,g}/H_{m0i,g}$=m_{0r}/m_{0i}, reflection coefficient

K_s [-] = H/H_0', shoaling coefficient

k_Δ [-] = layer coefficient

l [cm] = maximum length of a rock

L [m] or [cm] = $gT^2 \tanh(2\pi h/L)/2\pi$, wave length

$L_{m,toe}$ [m] or [cm] = $gT_m^2 \tanh(2\pi h_s/ L_{m,toe})/2\pi$, mean wave length at the toe of the structure

L_{jet} [m] or [cm] = length of the wave jet

L_{crest} [m] or [cm] = length of the wave crest

$L_{m-1,0}$ [m] or [cm] = $gT_{m-1,0}^2/2\pi$, deep water wave length based on the spectral wave period, $T_{m-1,0}$

L_0 [m] or [cm] = $gT^2/2\pi$, deep water wave length

L_{0m} [m] or [cm] = $gT^2/2\pi$, deep water wave length based on the mean period, T_m

L_{0p} [m] or [cm] = $gT_p^2/2\pi$, deep water wave length based on the peak period, T_p

LT [-] = l/d, aspect ratio

m [-] = bottom slope

m_i = i-th spectral moment

M [t] or [g] = concrete armor unit mass

M_{50} [t] or [g] = rock mass corresponding to D_{n50}

n [-] = number of armor layers

n_t [-] = number of rock rows placed on the upper layer of the toe berm

n_v [-] = void porosity

N[-] = number of displaced units

N_d [-] = N/ N_t, damage number

N_e [-] = number of extracted armor units relocated above the upper layer of the armor

N_i [-] = number of armor units whose center of gravity is within each strip in the virtual net method

N_{od} [-] = $N/(b/D_{n50})$, damage parameter

N_{od}*[-] = $N/(b/D_{n50})$, damage parameter of the nominal toe berm

N_p [-] = number of free parameters in the neural network

N_s [-] = $H/(\Delta D_n)$, stability number

N_s*[-] = $H_m /(\Delta D_{n50})$, stability number for regular waves

N_t [-] = total number of units within the reference area

N_z [-] = number of waves

N_Δ[-] = $A_e \rho_b 9D_{50}/(\rho_r D_{50}^3 \pi/6)$, damage parameter

$N_\%$[-] = $N D_{n50}^3/((1- n_v)V_{total})$, damage parameter

P [-] = armor permeability

p [-] or [%] = $(1- \Phi/n)$, armor porosity

p_i[-] or [%] = armor porosity in each strip of the virtual net after wave action

p_{0i} [-] or [%] = initial armor porosity in each strip of the virtual net

q [-] = number of rows in each strip of the virtual net

$R_{d1\%}$ [m] or [cm] = maximum run-down level

R_{up} [m] or [cm] = run-up

s[-] = H/L, wave steepness for regular waves

s_0 [-] = H_0/L_0, deep water wave steepness

s_p [-] = H_s/L_{0p} or H_{m0}/L_{0p}, wave steepness based on the peak period, T_p

s_{0p} [-] = H_{s0}/L_{0p}, wave steepness based on the peak period, T_p

s_m [-] = H_s/L_{0m}, wave steepness based on the mean period, T_m

$s_{m,toe}$ [-] = $H_{m0}/L_{m,toe}$, local wave steepness based on the mean period, T_m

S [-] = A_e/D_n^2, dimensionless armor damage measured with a profiler

S(f) = wave spectra

S(t) [-] = mean dimensionless armor damage at time, t

S_e [-] = equivalent dimensionless armor damage

S_i [-] = dimensionless armor damage in each strip of the virtual net

S_v [-] = visual dimensionless armor damage

S_0 [m^{-1}] =1.521 m/H_0, breaking parameter for solitary waves

t [s] = time

t_i = target values

$\bar{t}$ = average of target values

t_t [cm] = toe berm thickness

T [s] = wave period

T_m [s] = mean wave period

$T_{m-1,0}$ [s] = m_{-1}/m_0, spectral wave period based on the spectral moment, m_{-1}

T_p [s] = peak wave period

T_s [s] = $T_{1/3}$, significant wave period

VAR [-] = variance

V_{total} [cm^3] or [m^3] = apparent volume of the toe berm

W [N] = unit weight

X [cm] = maximum rectangular dimension of the smallest hypothetical box that would enclose a rock

Y [cm] = intermediate rectangular dimension of the smallest hypothetical box that would enclose a rock

Z [cm]	= minimum rectangular dimension of the smallest hypothetical box that would enclose a rock
z [-]	= number of units per row in a reference area
ε [-]	= error, difference between estimated and measured values
ξ [-]	= $\tan\alpha\ /(H/L_0)^{1/2}$, surf similarity parameter
ξ_m [-]	= $\tan\alpha/(H_s/\ L_m)^{1/2}$, surf similarity parameter based on the mean period, T_m
ξ_{mc}[-]	= $((c_{pl}/c_s)P^{0.31}(\tan\alpha)^{0.5})^{1/(P+0.5)}$, critical breaker parameter
ξ_{s-1} [-]	= $\tan\alpha/(H_s/\ L_{m-1,0})^{1/2}$, surf similarity parameter based on the spectral period, $T_{m-1,0}$
ξ_p [-]	= $\tan\alpha/(H_{m0}/\ L_{0p})^{1/2}$, surf similarity parameter based on the peak period, T_p and spectral wave height, H_{m0}
ξ^* [-]	= $m/(H/L_0)^{1/2}$ or surf similarity parameter with the bottom slope, m
$\xi_0{}^*$[-]	= $m/(H_0/L_0)^{1/2}$, surf similarity parameter in deep water
$\xi_p{}^*$ [-]	= $m/(H_s/L_{0p})^{1/2}$, surf similarity parameter with the bottom slope m based on the peak period, T_p
α [rad or °]	= angle of the armor slope
γ [-]	= JONSWAP spectra parameter
γ_b[-]	= H_b/h_b, breaker index
Ω_b[-]	= H_b/H_0, breaker height index
Δ [-]	= (ρ_r/ρ_w)-1, relative submerged mass density
ω [s^{-1}]	= wave impulse
ρ_b [t/m^3] or [g/cm^3]	= bulk density of the material
ρ_r [t/m^3] or [g/cm^3]	= armor unit density
ρ_c [t/m^3] or [g/cm^3]	= concrete density
ρ_w[t/m^3] or [g/cm^3]	= water density
φ [units/m^2]	= placing density
Φ [-]	= n(1-p), packing density
Φ_i [-]	= $n(1-p_i)$, packing density of each strip in the virtual net after wave action
Φ_{i0} [-]	= $n(1-p_{i0})$, initial packing density of each strip in the virtual net

η [cm] = water surface elevation

$\hat{u}_{\delta}$ [m/s] = $\pi H_s / (T_{m-1,0} \sinh(k_{m-1,0} h_t))$, characteristic wave velocity

Acronyms

CAU = Concrete armor unit

CWD = Composite Weibull distribution

De = Destruction

G0 = Gravel used in the armor in physical models

G1 = Gravel used in the filter in physical models

G2 = Gravel used in the core in physical models

HeP = Heterogeneous Packing

IDa = Initiation of Damage

IDe = Initiation of Destruction

IIDa = Initiation of Iribarren's Damage

LPC-UPV = Laboratory of Ports and Coasts (UPV)

MSE = Mean squared error

NN = Neural Network

PSE = Predicted squared error

r = Correlation coefficient

rMSE = Relative mean squared error

SWL = Still water level

UPV = Universitat Politècnica de València (ES)

Chapter I

Introduction

Roses, Cataluña (Spain). August, 2016.

I.1. Focus of the study

Most coastal structures around the world are constructed close to the shoreline in the depth-induced wave breaking zone; however, guidance is currently needed to design mound breakwaters in depth-limited breaking wave conditions. There are numerous variables affecting the hydraulic stability of mound breakwaters in breaking wave conditions; the sea bottom slope and the water depth at the construction site are the two determining parameters in the mound breakwater design in these conditions. Gentle sea bottoms and shallow waters are typical of sandy coasts; in these situations, the breakwater design usually focuses on the main armor. In contrast, steep sea bottoms and very shallow waters are typical of rocky coasts, where waves induce very high loads; in these situations, the toe berm stability is critical to ensure the overall armor stability and thus the stone size required for the toe berm may significantly exceed the armor unit size.

The main objective of this PhD thesis is to analyze the hydraulic stability of rock armors placed on gentle sea bottoms (m=1/50) and to develop new equations for toe berm design in very shallow waters with steep sea bottoms (m=1/10). To this end, small-scale laboratory tests were conducted in the Laboratory of Ports and Coasts at the *Universitat Politècnica de València* (LPC-UPV).

Six specific objectives were established for this PhD thesis:

- To review the literature regarding wave breaking phenomena and the existing methods to determine wave height distributions in the depth-induced wave breaking zone.
- To examine the literature regarding formulas used to design rock armors in breaking wave conditions.
- To assess the literature regarding formulas used to design rock toe berms for mound breakwaters in breaking wave conditions.
- To develop new equations to design double-layer rock armors in breaking wave conditions with a bottom slope m=1/50.
- To establish a new method to design rock toe berms in breaking wave conditions with a bottom slope m=1/10.
- To evaluate the stability of cube-armored breakwaters with random and uniform placement in breaking wave conditions with a bottom slope m=1/10.

I.2. Background for the research

The present PhD thesis is the result of research conducted by the author and funded by the Spanish Ministry of Education (*Ministerio de Educación, Cultura y Deporte*) through the FPU program (*Formación del profesorado Universitario,* grant FPU13/01872). Most of the thesis results are based on the research Project **ESCOLIF**

(***ES**tabilidad hidráulica de los mantos de escollera, cubos y **C**ubípodos frente a **O**leaje **LI**mitado por el **F**ondo*, grant BIA2012-33967), awarded by the Spanish Ministry of Economy and Competitiveness (*Ministerio de Economía y Competitividad*). The goal of ESCOLIF was to enhance our knowledge regarding the hydraulic stability of mound breakwaters in depth-limited breaking wave conditions.

Results of this PhD research have been published in the following papers:

- Herrera, M.P., Hoyos, A., Medina, J.R., 2017. Toe stability in very shallow water combined with steep sea bottom. Proc. 35th International Conference on Coastal Engineering (ICCE 2016), in press.
- Herrera, M.P., Molines, J., Medina, J.R., 2016. Hydraulic stability of nominal and sacrificial toe berms for mound breakwaters on steep sea bottoms. Coastal Engineering 114, 361-368 (D1).
- Herrera, M.P., Medina, J.R., 2015. Toe berm design for very shallow waters on steep sea bottoms. Coastal Engineering 103, 67-77 (D1).
- Herrera, M.P., Hoyos, A., Molines, J., Medina, J.R., 2015. Influence of placement technique on double-layer cube armor stability of breakwaters constructed on steep foreshores. Proc. 36th IAHR World Congress, 28 June-3 July, 2015 (The Hague, the Netherlands), in press.
- Herrera, M.P., Molines, J., Medina, J.R., 2015. Colocación de bloques cúbicos y estabilidad hidráulica del manto principal. Libro XIII Jornadas Españolas de Costas y Puertos, 24-25 June, 2015 (Avilés, Asturias), in press.
- Hoyos, A., Herrera, M.P., Medina, J.R., 2015. Diseño de la berma de pie en diques rompeolas. Libro XIII Jornadas Españolas de Costas y Puertos, 24-25 June, 2015 (Avilés, Asturias), in press.
- Herrera, M.P., Molines, J., Medina, J.R., 2014. Toe protection stability for rubble mound breakwaters in very shallow waters. Proc. 5th International Conference on the Application of Physical Modelling to Port and Coastal Protection, 231-239.
- Herrera, M.P., Molines, J., Pardo, V., Gómez-Martín, M.E., González-Escrivá, J.A., Medina, J.R., 2014. Characterizing wave breaking on rubble mound breakwaters on steep bottom slopes. Proc. 3rd IAHR Europe Congress. ISBN 978-989-96479-2-3.

Appendix 1 provides a selection of the above cited papers.

I.3. Thesis structure

The PhD thesis has been structured in five chapters and two appendixes.

- Chapter I explains the motivation, focus and background of the present PhD thesis.
- Chapter II provides a review of the literature related to the design of coastal structures when attacked by breaking waves. Firstly, wave transformation

in the breaking zone is described and the main methods developed to estimate waves in breaking conditions are mentioned. Secondly, a general description of hydraulic stability of mound breakwaters is provided. Thirdly, hydraulic stability formulas for the design of rock armors in breaking wave conditions are examined. Finally, the most relevant hydraulic stability formulas to design rock toe berms are listed.

- Chapter III centers on the hydraulic stability of rock armors placed in shallow waters and on gentle sea bottoms (m=1/50). First, the physical model tests conducted with double-layer rock armors in the LPC-UPV are described. Second, the main results of the experimental data are shown and wave measurements are compared with numerical simulations given by the SwanOne model. Finally, a new hydraulic stability formula is developed for rock armors, and a simple method is provided to determine the characteristic wave height in the depth-induced breaking zone.
- Chapter IV focuses on the hydraulic stability of rock toe berms placed in very shallow waters and on steep sea bottoms (m=1/10). The physical model tests conducted in the LPC-UPV with double-layer cube armors and rocks on the toe berm are first described. Secondly, experimental results are presented. Thirdly, a new hydraulic stability formula is given for emerged and submerged rock toe berms, and the influence of toe berm width is analyzed introducing the concepts of nominal and sacrificial toe berms. Finally, the hydraulic stability of randomly- and uniformly-placed double-layer cube armors is studied, using artificial neural networks (NN).
- Chapter V provides the main conclusions of the study and future research.
- Appendix 1 contains a selection of the published papers related to the present PhD thesis.
- Appendix 2 summarizes the methodology used by Medina et al. (1994) to re-write the armor design equation proposed by Hudson (1959) in terms of armor damage, adapted to this study.

The references cited herein are listed at the end of the document.

Chapter II

Literature review

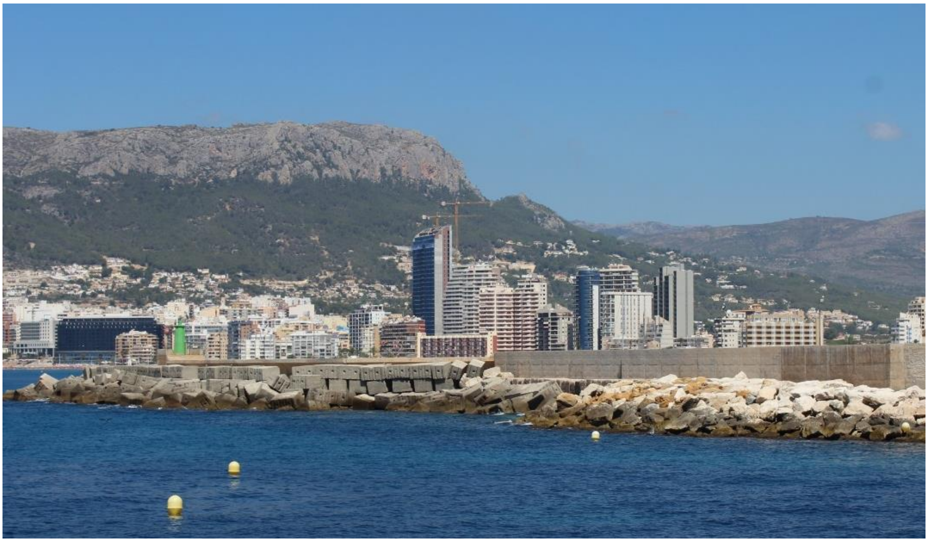

Calpe, Alicante (Spain). July, 2016.

II.1. Introduction

The design of mound breakwaters usually focuses on the main armor layer, and most armor hydraulic stability formulas are based on small-scale tests in non-breaking wave conditions. Formulas for armors have been provided by USACE (1984) and USACE (2006) for different Concrete Armor Units (CAUs), Van der Meer (1988a) for rocks, Van der Meer (1988c) for cubes, Tetrapods and Accropodes, and Burcharth and Liu (1992) for Dolosses. However, in breaking wave conditions, these equations are not fully valid. The depth-limiting breaking conditions cause larger waves to break in advance, which significantly changes the wave forces and currents affecting the breakwater. As a result, empirical modifications and specific small-scale models are frequently needed to validate existing formulas for breaking wave conditions.

To design coastal structures in depth-limited breaking wave conditions, it is necessary to estimate the incident wave height in the depth-induced breaking zone. This wave height is commonly considered the significant wave height $H_s= H_{1/3}$ (highest one-third wave) or a wave height with a prescribed low exceedance probability ($H_{1\%}$, $H_{2\%}$, etc.). When wave heights follow a Rayleigh distribution (non-breaking wave conditions), $H_{1\%}$ and $H_{2\%}$ are strongly correlated to H_s; however, this does not occur when the wave height distribution is influenced by depth-induced wave breaking and other non-linear effects. Different models exist to obtain wave height distributions in the breaking zone. Most methods are based on the use of a Weibull distribution (see Glukhovsky, 1966), a Beta-Rayleigh distribution (see Hughes and Borgman, 1987), a composite Weibull distribution (CWD) (see Battjes and Groenendijk, 2000) or a modified distribution (see Mendez et al., 2004). Nevertheless, it is not usual for the hydraulic stability formulas to consider the wave height distribution changes that take place in the surf zone.

In this chapter, the primary methods to estimate wave height distributions in the breaking zone are first described. Secondly, the hydraulic stability of mound breakwaters is analyzed as well as the main failure modes; existing parameters to quantify armor and toe berm damage are also given. Thirdly, equations for designing rock armors in breaking wave conditions are mentioned. Finally, existing formulas for rock toe berm design are examined.

II.2. Waves in breaking conditions

II.2.1. Types of wave breaking

Waves affect coastal structures. To obtain a reliable estimation of waves, it is necessary to understand their transformation during their propagation towards the shore. Incoming waves can be changed by refraction, shoaling, diffraction and coastal breaking. Wave breaking results in a significant dissipation of energy, and it is usually the major limiting factor for the wave height and loads on the structures.

Two types of wave breaking can be found in the literature: (1) wave breaking caused by exceeding maximum wave steepness (s=H/L too large) or (2) wave breaking caused by water depth (H/h too large), where H is the wave height, L is the wave length and h is the water depth. Wave breaking caused by water depth is typical of shallow water areas where most mound breakwaters are built.

In shallow waters, wave breaking may be classified depending on the value of the bottom slope and wave characteristics (see Iribarren and Nogales, 1950; Galvin, 1968; Weggel, 1972; Svendsen et al., 1978; Dean and Dalrymple, 1991; or Gourlay, 1992). Wave breaking can be grouped in four categories (see Fig. II.1): *Spilling, plunging, collapsing* and *surging*, as a function of the Iribarren number, Ir* (see Iribarren and Nogales, 1950), also called the surf similarity parameter, ξ* (Battjes, 1974) with the bottom slope m (Eq. II.1).

$$I_r{}^* = \xi^* = \frac{m}{\sqrt{\dfrac{H}{L_0}}} \qquad [II.1]$$

where $L_0 = gT^2/2\pi$ is the deep water wave length, g is the gravitational acceleration, and T is the wave period.

In *spilling* breakers, the wave produces a foamy water surface given the unstable wave crest. Spilling breakers are also characterized by their symmetrical wave contours. This type of breaker is typical of very gentle beach slopes.

Plunging waves produce a high splash, coming from the crest that curls over the shoreward face of the wave. The wave front is initially very vertical, then starts to curl and finally falls. Wave energy is dissipated during this process. This kind of breaking is observed on gentle to intermediate beach slopes.

Collapsing waves are classified between surging and plunging waves. The crest is not breaking, but the lower part of the shoreward face rises up and falls. An irregular turbulent water face is created.

On very steep beaches, *surging* waves occur; the wave does not break. The front of the wave reaches the beach with minor breaking. The wave goes up and down on the slope and only forms a small amount of foamy water.

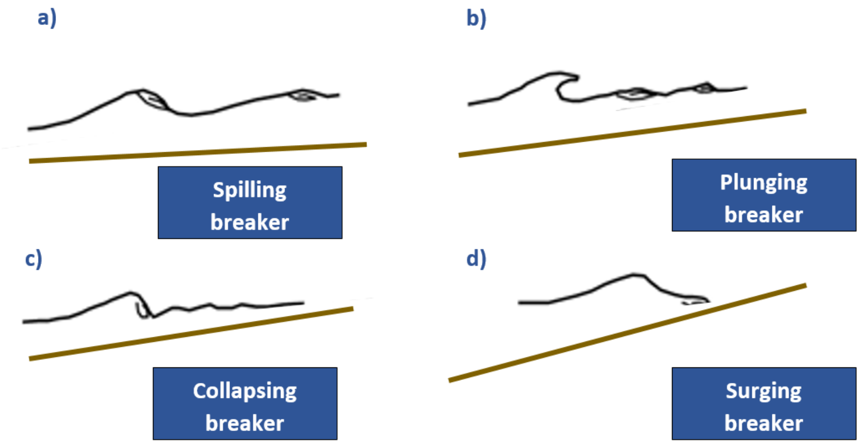

Figure II.1. Types of wave breaking.

Table II. 1 summarizes the types of wave breaking according to Iribarren and Nogales (1950).

Breaker Types	Ir*
Spilling	Ir*<0.5
Plunging	0.5<Ir*<2.5
Collapsing	2.5<Ir*<3.0
Surging	Ir*>3.0

Table II.1. Types of wave breaking as a function of Iribarren's number with the bottom slope (m).

In situations with complex bathymetry featuring bars, platforms and steps, Iribarren's number or the surf similarity parameter is not considered a good estimator of the breaker type (Smith and Kraus, 1991; Mead and Black, 2001; Scarfe et al., 2003; Blenkinsopp and Chaplin, 2008).

Other classifications have been proposed as a function of wave geometry at the breaking point (e.g. Peregrine, 1983; New et al., 1985; Bonmarin, 1989 or Qiao and Duncan, 2001). Among these, New et al. (1985) established another criterion as a function of the crest length (L_{crest}) above the still water level (SWL) and the length of the jet (L_{jet}), using the parameter S_{jet} given by Eq. II.2 (see Fig. II.2). These authors only distinguished between spilling and plunging breakers (see Table II.2).

$$S_{jet} = \frac{L_{jet}}{L_{crest}} \qquad [II.2]$$

Breaker Types	S_{jet}
Spilling	$S_{jet}<3/100$
Plunging	$S_{jet}>1/10$

Table II.2. Types of wave breaking (New et al., 1985).

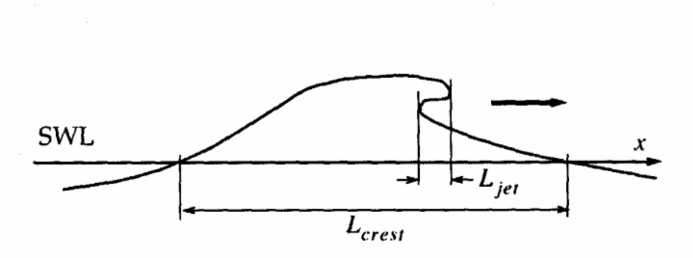

Figure II.2. Breaking parameters (New et al., 1985).

Wave breaking has also been characterized by analyzing wave vortex parameters (Longuet-Higgins, 1982) and wave plunge distances (Smith and Kraus, 1991), with empirical and numerical methods (Vinje and Brevig, 1980; Cooker et al., 1990; Li, 2000; Khayyer et al., 2008).

II.2.2. Wave breaking criteria

II.2.2.1. Wave steepness

Breaking caused by excessive wave steepness is the primary limiting factor in deep and medium water depths. The most well-known criterion was provided by Michell (1893), who established the limiting wave steepness, s=H/L, as 0.142 in deep water for a crest angle equal to 120° (see Fig. II.3).

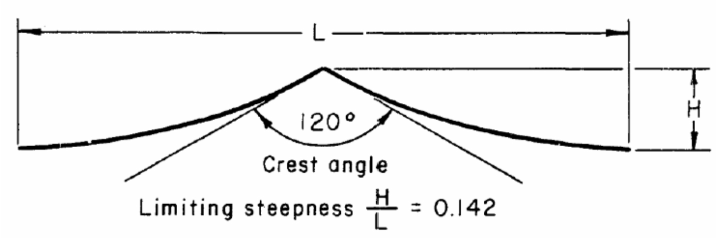

Figure II.3. Limiting steepness in deep water (USACE, 1984).

Miche (1944) found that the limiting wave steepness for waves in depths less than $L_0/2$ was $(H/L)_{max}=0.142\ \tanh(2\pi H/L)$. Danel (1952) proposed re-adapting the constant value of 0.142 to 0.12 when applying Miche's (1944) formula to horizontal seafloors. Ostendorf and Madsen (1979) revisited Miche's formula to consider the beach slope on the wave breaking height. Other studies based on laboratory tests established the limit of $H/gT^2=0.021$ and results obtained from measurements in the North Sea indicated a limit of $H/gT^2=0.0067$ for wave breaking. Longuet-Higgins (1983) concluded that the acceleration of the wave at the breaking point is -0.388g. In this thesis, only waves broken by depth limitation have been considered for further analysis.

II.2.2.2. Water depth

The breaking criterion due to water depth is commonly given by a non-dimensional parameter called the breaker index, defined as the maximum wave height to depth ratio H/h, at the breaking point.

$$\frac{H}{L} \leq \gamma_b = \left(\frac{H}{h}\right)_{\max} = \frac{H_b}{h_b} \qquad [II.3]$$

where H_b is the breaker wave height at the water depth h_b.

The definition of the breaking point still varies from author to author. Fenton (1972), Kamphuis (1991) and Rattanapitikon et al. (2003) defined breaking as occurring when the wave reaches its maximum height while Iverson (1952), Seyama and Kimura (1988), Smith and Kraus (1991), Grilli et al. (1997) and Blenkinsopp and Chaplin (2008) defined breaking as being when the front wave profile becomes vertical. Johnson (2009) referred to the instant that the crest particle velocity is equal to the wave celerity. Kraus and Larson (1988) and Haller and Catalan (2005) proposed waiting until white water appears to indicate the wave has begun to break.

Apart from γ_b, another commonly-used parameter is the breaker height index, Ω_b, defined as the ratio between the breaker wave height, H_b, and the deep water wave height, H_0.

$$\Omega_b = \frac{H_b}{H_0} \qquad [II.4]$$

Numerous criteria exist to predict the value of these indexes (Eqs. II.3 and II.4). A review of these can be found in Rattanapitikon and Shibayama (2000) or Robertson et al. (2013). According to Robertson et al. (2013), breaker index formulas can be divided into six types depending on the parameters included: (1) constant breaker index, (2) breaker index as a function of the bottom slope, (3) breaker index as a function of the surf similarity parameter, (4) breaker index as a function of the hyperbolic tangency of breaking wavelength and height, (5) breaker index as a function of the offshore wavelength and height and the bottom slope, and (6) breaker index as a function of the offshore wavelength and height and the exponential of the bottom slope.

The first constant value of the breaker depth index for regular waves was given by McCowan (1894) for a solitary wave traveling over a horizontal bottom. This author introduced $\gamma_b = 0.78$ as the breaking criteria. Munk (1949) maintained the value of 0.78 for γ_b, and defined the breaker height index for a solitary wave as $\Omega_b = 1/(3.3s_0)^{1/3}$. Yamanda et al. (1968) updated the breaking depth index to $\gamma_b = 0.8261$.

Based on laboratory tests, Camfield and Street (1968), Galvin (1968), Collins and Weir (1969) and Madsen (1976) developed different equations to estimate γ_b as a function of the bottom slope. USACE (1984) published experimental data which were re-analyzed by Le Roux (2007), proposing another equation using the sea bottom angle measured in degrees instead of the sea bottom slope, m.

Battjes (1974) proposed the first equation to estimate the breaker index as a function of the surf similarity parameter. To extend its range of application, Sunamura (1980) updated Battjes' (1974) equation for a range of bottom slopes $0.02<m<0.3$. Larson and Kraus (1989) and Kaminsky and Kraus (1993) published new equations with better correlations.

Le Mehaute and Koh (1967) were the first to include both the bottom slope and the offshore wave steepness to predict the wave breaking height. Sunamura and Horikawa (1974) recalibrated this equation, armed with Godas' (1970) laboratory data. Singamsetti and Wind (1980) and Ogawa and Shuto (1984) proposed similar equations to estimate the breaker index, γ_b. However, Gourlay (1992) noted that the breaker height was not sensitive to the beach slope, although some years later, Rattanapitikon and Shibayama (2000) found Gourlay's equation to have poor performance. Rattanapitikon et al. (2003) reported the correlation between H_0/L_0 and H_b/L_b, proposing a new breaker height formula to estimate H_b, this being updated later in Rattanapitikon and Shibayama (2006). Tsai et al. (2005) investigated breaking conditions on steep bottom slopes because most existing equations were based on gentle bottom slopes. Camenen and Larson (2007) compared some of the aforementioned equations and concluded that none achieved more than 50% accuracy, so they proposed a new one which combined trigonometric and offshore steepness relationships. Based on new experiments with a non-emergent beach slope, Yao et al. (2012) estimated γ_b, distinguishing between the breaker index on the fore-reef slope and on the post-reef platform.

Several exponential relationships have been developed to estimate the breaker index or the breaking height. Goda (1970) proposed an exponential dependence of the breaking wave height on the breaking depth based on regular laboratory tests with bottom slopes in the range $0.05<m<0.2$. Goda (1975) presented a random wave breaking model, re-adapting the proposed equation for regular waves to irregular waves. Muttray and Oumeraci (2000) proposed a new coefficient for Goda's formula which resulted in a better agreement for bottom slopes over 1/30, and Tsai et al. (2005) concluded that Goda's equation overestimated the wave height on steep slopes.

Weggel (1972) proposed a high estimation of the breaker height to be used for coastal design; this overestimation was confirmed by Camenen and Larson (2007). Dally et al. (1985) included the effects of oblique wave incidence and Smith and Kraus (1991) recalibrated the coefficients used in Weggel's (1972) equation. Rattanapitikon and Shibayama (2000) modified the equation given by Goda (1975), which was again recalibrated by Goda (2010) for a better fit to the laboratory data on steep slopes.

CIRIA/CUR/CETMEF (2007) recommended the formulas given by Goda (1970) and Weggel (1972) to estimate the breaker index for regular waves, normally incident, on a uniform slope (Eqs. II.5 and II.6, respectively).

$$\gamma_b = \frac{H_b}{h_b} = 0.17 \ \frac{L_0}{h_b} \left\{ 1 - \exp\left[-1.5\pi \frac{h_b}{L_0} \left(1 + 15 \ m^{4/3} \right) \right] \right\} \qquad [II.5]$$

Goda (1975) suggested modifing the value of 0.17 (valid for regular waves) to values between 0.18 and 0.12 when applied to irregular waves. Goda (2010) reduced the constant value of 15 to 11, for a better fit to the laboratory data on steep slopes.

$$\gamma_b = \frac{H_b}{h_b} = \frac{b(m)}{1 + a(m)\dfrac{h_b}{L_0}} = b(m) - a(m)\frac{H_b}{L_0} \qquad [II.6]$$

where $a(m) = 6.96\,[1-\exp(-19m)]$ and $b(m) = 1.56\,[1+\exp(-19.5m)]^{-1}$.

Additionally, the criterion given by Rattanapitikon and Shibayama (2000) and Rattanapitikon et al. (2003) was recommended by CIRIA/CUR/CETMEF (2007) for practical use (Eq. II.7). This criterion is a function of the wavelength calculated at the depth h_b using the linear wave theory, L_b.

$$\frac{H_b}{L_b} = \left[-1.40\,m^2 + 0.57\,m + 0.23 \right] \left(\frac{H_0}{L_0} \right)^{0.35} \qquad [II.7]$$

II.2.3. Distribution of shallow-water wave heights

In deep water, the water surface elevation usually follows a Gaussian process and the distribution can be approximated as being Rayleighan (Longuet-Higgins, 1952). When assuming a Rayleigh distribution, all characteristics wave heights are theoretically correlated.

In shallow water, the situation is completely different. Wave transformation distorts the wave profile and the surface elevation no longer follows a Gaussian process. In the breaking zone, those waves that exceed the breaking limit will break (see Goda, 2000).

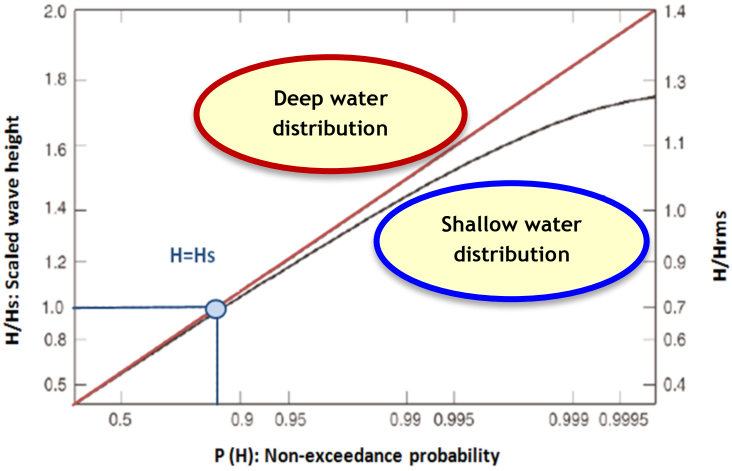

Figure II.4. Example of shallow water and deep water distributions of wave heights.

Since Collins (1970), several random wave breaking models have been developed. Battjes and Janssen (1978) presented a frequently applied model to estimate the transformation of random breaking waves in shallow waters and based on the wave energy dissipation (bore-type dissipation model) due to the breaking phenomena in the depth-induced breaking zone. Mase and Iwagaki (1982), Dally and Dean (1986), Dally (1990, 1992) and Kuriyama (1996) also described different methods to calculate the distribution of wave height in shallow waters. Baldock et al. (1998) modified the model proposed by Battjes and Janssen (1978), providing explicit expressions for the fraction of broken waves and the energy dissipation rate within the surf zone. Massel and Sobey (2000) published a revision of the existing literature about statistical models for the distribution of the highest wave in a given sea state.

The most common approach to deal with distributions of depth-limited breaking wave heights consists of empirical or semi-empirical adaptations to the Rayleigh distribution considering the effects of breaking, as described in Glukhovsky (1966), Tayfun (1981), Hughes and Borgman (1987), Klopman (1996), or Tayfun (1999). Batjjes and Groenendijk (2000) proposed the Composite Weibull Distribution (CWD) valid for the modeling of depth-limited waves. The CWD method uses the cumulative distribution function given by Eq. II.8 to describe the distribution of individual waves.

$$F(H)=\begin{cases}1-\exp\left[-\left(H/_{H1}\right)^{k1}\right] & ifH\le H_{tr}\\ 1-\exp\left[-\left(H/_{H2}\right)^{k2}\right] & ifH\ge H_{tr}\end{cases} \qquad [II.8]$$

where H_{tr}= (0.35+5.8m)h is a transitional wave height which depends on the bed slope and the local water depth, H1 and H2 are the scale parameters and the exponents k1 and k2 have been given the values of k1=2.0 and k2=3.6 as the best fit to laboratory test data with five bottom slopes. The CWD method requires knowing the variance of the surface elevation, m_0, or the significant spectral wave height, H_{m0}, to estimate the root mean square wave height as H_{rms}=[0.6725+0.2025(H_{m0}/h)]. Battjes and Groenendijk (2000) provided a table with the non-dimensional characteristic values of $H_{1/3}$/ H_{rms}, $H_{1/10}$/H_{rms}, $H_{2\%}$/H_{rms}, $H_{1\%}$/H_{rms}, and $H_{0.1\%}$/H_{rms}.

The CWD method has been cited in different engineering manuals (e.g. CIRIA/CUR/CETMEF (2007), Pullen et al. (2007) or IEC (2009), among others). Mai et al. (2010) reported the distributions of wave heights measured at three stations in the North Sea and compared these with the CWD method proposed by Battjes and Groenendijk (2000).

Goda (2000) used Eqs. II.9 and II.10 to estimate the significant wave height, H_s=$H_{1/3}$, and the maximum wave height, H_{max}, in the surf zone, as a function of the equivalent deep water significant wave height, H_0', the shoaling coefficient, K_s=H/H_0', the ratio h/L_0 based on the significant wave period, $T_{1/3}$, and the bottom slope, m. Diagrams were also provided to directly obtain $H_{1/3}$ and H_{max} for m=1/10. 1/20, 1/30 and 1/100.

$$H_{1/3}=\begin{cases}\left(K_S H_0'\right) & for \quad h/L_0\ge 0.2\\ \min\ \left[\left(\beta_0\,H_0'+\beta_1\,h\right),\ \left(\beta_{\max}\,H_0'\right),\ \left(K_S\,H_0'\right)\right] & for \quad h/L_0<0.2\end{cases} \qquad [II.9]$$

$$H_{\max}=H_{1/250}=\begin{cases}\left(1.8\,K_S\,H_0'\right) & for \quad h/L_0\ge 0.2\\ \min\ \left[\left(\beta_0*H_0'+\beta_1*h\right),\left(\beta_{\max}*H_0'\right),\left(1.8K_S\,H_0'\right)\right] & for \quad h/L_0<0.2\end{cases} \qquad [II.10]$$

The coefficients β_0, β_1, β_{max}, β_0*, β_1* and β_{max}* were formulated as listed in Table II.3.

Coefficients for $H_{1/3}$	Coefficients for H_{max}
$\beta_0 = 0.028\,(H_0'/L_0)^{-0.38} \exp\,(20\, m^{1.5})$	$\beta_0{*} = 0.052\,(H_0'/L_0)^{-0.38} \exp\,(20\, m^{1.5})$
$\beta_1 = 0.52\ \exp\,(4.2\, m)$	$\beta_1{*} = 0.63\ \exp\,(3.8\, m)$
$\beta_{max} = \max\left\{0.92,\ 0.32\,(H_0'/L_0)^{-0.29} \exp\,(2.4\, m)\right\}$	$\beta_{max}{*} = \max\left\{1.65,\ 0.53(H_0'/L_0)^{-0.29} \exp\,(2.4\, m)\right\}$

Table II.3. Coefficients for $H_{1/3}$ and H_{max} according to Goda (2000).

CIRIA/CUR/CETMEF (2007) described a method to determine the significant spectral wave height, H_{m0}, in shallow water based on Van der Meer (1990). Five graphs were provided for different wave steepnesses in deep water, s_{0p}, which gave the ratio H_{m0}/h as a function of h/L_{0p} for bottom slopes gentler than m=1/50, where $L_{0p}=gT_p^2/2\pi$ is the deep water wave length based on the peak period, T_p.

Assuming the model of energy dissipation given by Battjes and Janssen (1978), Méndez et al. (2004) proposed an analytical expression of the wave height probability density function on planar beaches. Méndez and Castanedo (2007) presented a probability density function for depth-limited maximum wave height distribution based on the modeling of the physical process and combining the probability density function provided by Méndez et al. (2004) with the correlation between consecutive waves given by Kimura (1980). Caires and Van Gent (2012) suggested calibrating the CWD method to obtain a better fit with the Rayleigh distribution when dealing with deep water conditions.

II.3. Hydraulic stability of mound breakwaters

II.3.1. Introduction

Mound breakwaters are the most commonly used typology for coastal structures to protect harbor areas from wave action. They consist of many layers of rock material protected by large rocks or concrete armor units (CAUs) which force waves to break on the slope. Structural strength (massive, bulky and slender), placement technique (uniform, patterned, oriented and random) and number of layers (single or double layer) are the armor characteristics which will determine the type of unit to be used in the armor layer. Fig. II.5 shows ten types of CAUs used to construct mound breakwaters according to Dupray and Roberts (2009). Developed in 2005 at the

Universitat Politècnica de València, the Cubipod is the latest armor unit, which can be placed in one or two layers.

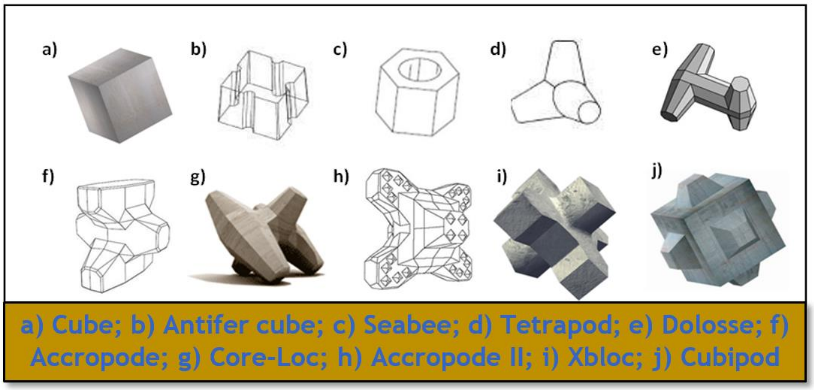
a)
b)
c)
d)
e)
f)
g)
h)
i)
j)
a) Cube; b) Antifer cube; c) Seabee; d) Tetrapod; e) Dolosse; f) Accropode; g) Core-Loc; h) Accropode II; i) Xbloc; j) Cubipod

Figure II.5. Concrete armor units for mound breakwaters (Dupray and Roberts, 2009).

Mound breakwaters are usually protected by a toe berm when CAUs are used for the armor layer. This toe berm is placed on the sea bottom or a bed layer, providing support for the units which are placed later on the structure slope (USACE, 2006).

It is also common practice to construct a superstructure or crown wall on the top of the mound breakwater to reduce overtopping rates.

II.3.2. Failure modes

When analyzing the stability of a mound breakwater, it is first necessary to know the main failure modes. According to Bruun (1979), eleven failure modes can be identified in conventional mound breakwaters (see Fig. II.6).

1. Loss of armor units from the armor layer during run-up events.
2. Loss of armor units from the armor layer during run-down events.
3. Sliding of the armor layer due to a lack of friction with the layer below.
4. Rocking of the armor units; breaking is due to fatigue.
5. Undermining of the crown wall.
6. Damage to inner slope by wave overtopping.
7. Lack of compactness in the underlying layers, causing transmission of energy to the core of the breakwater; this might lift the breakwater cap and the interior layers.
8. Erosion of the breakwater toe or the breakwater interior.

9. Settlement or collapsing of the subsoil.
10. Loss of the mechanical characteristics of the materials.
11. Construction errors.

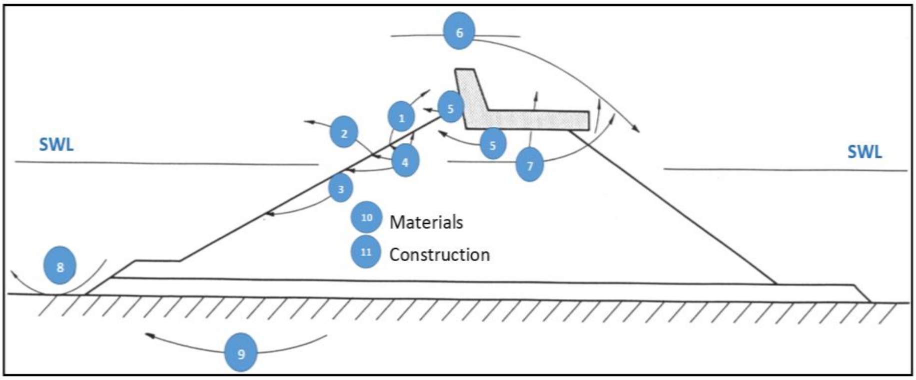

Figure II.6. Failure modes of mound breakwaters (Bruun, 1979).

In this thesis, only the hydraulic stability of the armor layer and the erosion of the toe caused by wave action on the structure are analyzed. Regarding the hydrodynamic stability of the armor layer, three causes of armor erosion are considered: (1) armor unit extractions, (2) armor layer sliding as a whole, and (3) slight armor settlements parallel to the slope which is known as Heterogeneous Packing (HeP). The HeP failure mechanism reduces the packing density of the armor layer near the still water level (SWL) without extracting elements, generating segments with low porosity and others with high porosity (see Gómez-Martín and Medina, 2014). The impact of the HeP failure mode mainly depends on four parameters:

1. Type of armor unit
2. Difference between the initial porosity and the minimum porosity
3. Slope of the armor layer
4. Friction coefficient between the armor layer and the secondary layer

When cubes or parallelepiped blocks are placed on the main armor, the HeP failure mode should be taken into account because these units tend to change positions favoring face-to-face fitting, even though no block is extracted from the armor during wave attack (see Fig. II.7). The Cubipod CAU was invented to prevent HeP observed on conventional double-layer randomly-placed cube armors.

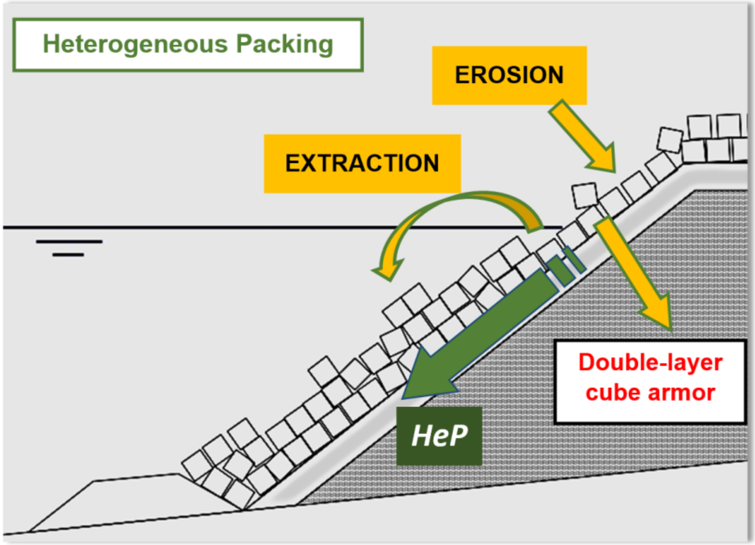

Figure II.7. Heterogeneous packing (HeP) failure mode (Gómez-Martín and Medina, 2014).

II.3.3. Techniques to place armor units

Armor units can be placed uniformly, patterned, oriented or randomly. The specific placement technique is directly related to armor porosity (p%) and interlocking, which significantly affects armor stability. Van der Meer (1999), Yagci and Kapdasli (2003), Bakker et al. (2005), and Medina et al. (2014) among others, analyzed a variety of CAUs and reported a significant influence of armor porosity on hydraulic stability. Porosity is also directly related to the number of units in the armor, material consumption and hence the construction cost. Thus, significant differences between design and prototype porosities can affect material provisions, construction costs and also the probability of failure.

According to Medina et al. (2010), porosity is a general concept referring to the percentage of voids in a granular system. To calculate armor porosity, first armor thickness should be defined, and this can be fixed for CAUs placed uniformly or in patterns, but it is difficult to determine porosity for randomly-placed units. For single- and double-layer armors, the armor thickness usually refers to one or two times the equivalent cube size or nominal diameter, $D_n=(M/\rho_r)^{1/3}$ where M and ρ_r are mass and density of the units, respectively. However, most engineering manuals recommend fixed nominal armor porosities (p%) for different armor units associated to a layer coefficient or layer thickness factor (k_Δ), which is arbitrarily fixed. Only the placing density (φ[units/m^2]) can be controlled by the placement grid, and this is related to both nominal armor porosity (p%) and layer coefficient (k_Δ). According to the formula given by USACE (1984), the placing density is given by Eq. II.11.

$$\varphi = \frac{N_t}{A} = \frac{n(k_\Delta)(1-p\%)}{D_n^2} \qquad [II.11]$$

where N_t is the number of armor units placed on a surface A, n is the number of armor layers, k_Δ is the layer coefficient and p% is the nominal armor porosity, while W/γ_r= volume of CAU, where W is the weight of the unit and γ_r the specific weight. It is clear that different pairs of layer coefficients, k_Δ, and nominal porosities, p%, lead to the same placing density, φ. Frens (2007) summarized problems caused by different researchers using different criteria regarding the layer coefficient and the porosity concept. To prevent misunderstandings, Medina et al. (2014) suggested referring armor porosity $p(\%)=(1-\Phi/n)$ to a layer coefficient of $k_\Delta=1.00$ using the dimensionless placing density $\Phi=\varphi D_n^2$.

Different criteria can be used to classify armor units depending on the placement technique. Bakker et al. (2003) distinguished six groups of CAUs which consider the placement technique, the number of layers and the geometry of the unit. Gómez-Martín (2015) distinguished eighteen groups of CAUs (seven groups for double-layer armors and eleven groups for single-layer armors). Whatever the armor unit orientation required, some units are placed using a specific placement grid whose characteristics depend on the type of armor unit and design considerations. The placement grid provides the exact planar X-Y coordinates, indicating how each unit must be placed by the crawler crane, which is often equipped with precise GPS positioning (see Pardo et al., 2012, 2014).

Conventional cube and Cubipod armors are commonly constructed with random placement; however, cube armors can be also placed with a uniform pattern like the cube revetment of the Maasvlakte 2, recently built in Rotterdam (see Loman et al., 2012), or the Boa Vista breakwater (Cape Verde) built with a single layer of uniformly-placed cubes (see Van Gent and Luis, 2013).

II.3.4. Armor stability and damage measurements

Armor damage can be analyzed from both qualitative and quantitative points of view.

II.3.4.1. Qualitative analysis

Two qualitative armor damage levels are frequently considered: Initiation of Damage (IDa) and Initiation of Destruction (IDe). “Initiation of Damage”, “No Damage” or “Start of Damage” have been used for decades to refer to the limit below which armor units do not move significantly. IDe, or Failure, has been used to refer to the limit above which progressive failure can occur.

Losada et al. (1986) and Vidal et al. (1991) described four damage levels for double-layer armors of mound breakwaters:

1. Initiation of Damage (IDa), when the upper armor layer has lost several units.

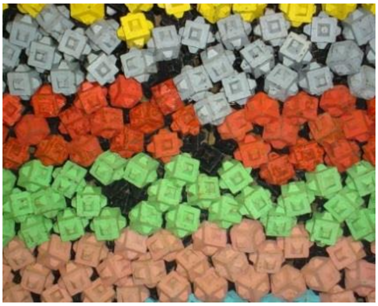

Figure II.8. View of IDa for double-layer Cubipod armor.

2. Initiation of Iribarren's Damage (IIDa), when damage in the upper area has spread over an area large enough to allow units to be extracted from the filter armor layer.

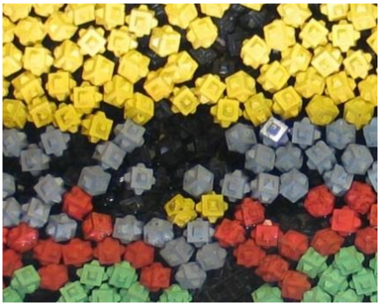

Figure II.9. View of IIDa for double-layer Cubipod armor.

3. Initiation of Destruction (IDe), when at least one unit has been lost from the bottom armor layer and the filter is clearly visible.

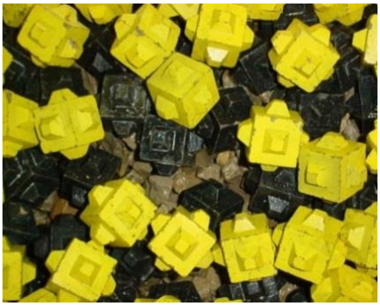

Figure II.10. View of IDe for double-layer Cubipod armor.

4. Destruction (De), when several units have been removed from the filter layer.

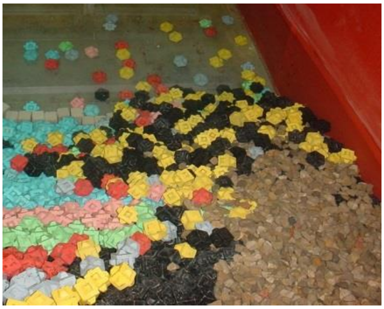

Figure II.11. View of De for double-layer Cubipod armor.

These damage levels are based on the visual analysis conducted after tests.

Gomez-Martín (2015) described three levels of damage to single-layer Cubipod armors because IIDa is not possible. Due to the capacity of realignment of Cubipod units, the definitions of the other damage levels were modified.

1. Initiation of Damage (IDa), when the armor layer has lost some units.

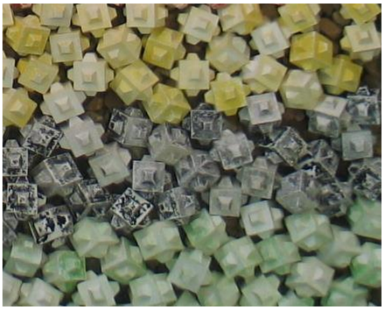

Figure II.12. View of IDa for single-layer Cubipod armor.

2. Initiation of Destruction (IDe), when several contiguous armor units have been removed or there is a fissure in the armor and the filter is clearly visible.

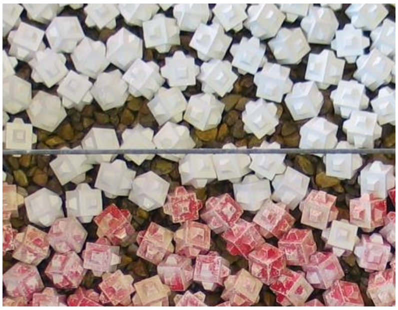

Figure II.13. View of IDe for single-layer Cubipod armor.

3. Destruction (De), when several filter units have been extracted and several armor units have moved from their original positions, so that the collapse of the structure is only a matter of time.

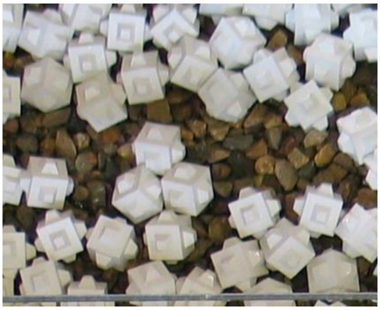

Figure II.14. View of De for single-layer Cubipod armor.

II.3.4.2. Quantitative analysis

Although it is easy to describe armor damage, it is not so simple to formulate quantitative armor damage definitions valid for all kinds of armor units, slopes, sizes and armor layers. Quantitative measurements of armor damage are usually given in terms of unit loss from the armor layer; therefore, most methods consider armor unit extraction as the main failure mode to describe armor erosion.

In the quantitative analysis, the damage is measured by counting the number of displaced units or by measuring the eroded surface profile of the armor slope (USACE, 2002). If the damage is measured by counting the displaced units, which is mostly done in the case of CAUs, CIRIA/CUR/CETMEF (2007) proposed the damage numbers N_d (Eq. II.12) and N_{od} (Eq. II.13).

$$N_d = \frac{N}{N_t} \qquad [II.12]$$

$$N_{od} = \frac{N}{b/D_n} \qquad [II.13]$$

where N is the number of displaced units, N_t is the total number of units within the reference area, and b is the width of the reference area.

CIRIA/CUR/CETMEF (2007) provided typical values of N_d and N_{od} for three damage levels: (1) start of damage, (2) intermediate damage and (3) failure (Table II.4).

Armor type	Damage number	Damage level		
		Start of Damage	Intermediate damage	Failure
Cube	N_{od}	0.2-0.5	1	2
Tetrapod		0.2-0.5	1	1-5
Accropode		0	-	>0.5
Cube	N_d	-	4%	-
Dolos		0-2%	-	≥15%
Accropode		0%	1-5%	≥10%

Table II.4. Characteristic damage numbers for a range of damage levels (CIRIA/CUR/CETMEF, 2007).

For rock armors, it is common practice to characterize armor damage as a function of the eroded area. The first authors to calculate armor damage in this way were Iribarren (1938) and Hudson (1959). Hudson (1959) defined the damage as the percentage of original volume eroded:

$$D = \frac{A_e}{A} \qquad [II.14]$$

where A_e is the eroded area in the cross section, and A is the area of average original profile.

Thompson and Shuttler (1975) defined another damage parameter, N_Δ:

$$N_\Delta = \frac{A_e \rho_b 9 D_{50}}{\rho_r D_{50}^3 \frac{\pi}{6}} \qquad [II.15]$$

where ρ_b is the bulk density of the material as placed on the slope, and D_{50} is the rock diameter that exceeds 50% value of the sieve curve value.

The advantage of this formula is that the damage is independent of initial number of units placed on the armor, compared to formulas that use a percentage of damage. The disadvantages are the measurement of the bulk density and the use of the sieve diameter instead of the actual mass of the stone. The most common damage parameter based on the eroded area was proposed by Broderick (1983) and popularized later by Van der Meer (1988b):

$$S = \frac{A_e}{D_{n50}^2} \qquad [II.16]$$

where $D_{n50}=(M_{50}/\rho_r)^{1/3}$ is the nominal diameter of armor unit, defined as the equivalent cube size of the unit with a mass, M_{50}, and a density, ρ_r.

According to Van der Meer (1998a), the slope angle of the structure significantly influences the limits of damage, S. Table II.5 provides the limits of S for double-layer rock armors as a function of armor slopes for initial damage, intermediate damage and failure.

Slope	Initial damage	Intermediate damage	Failure (under layer visible)
1:1.5	2	3-5	8
1:2	2	4-6	8
1:3	2	6-9	12
1:4	3	8-12	17
1:6	3	8-12	17

Table II.5. Design values of S for double-layer rock armors (Van der Meer, 1998a).

The eroded area (A_e) in Eqs. II.14 to II.16 is usually estimated with a mechanical or laser profiler. However, it can also be measured by computing the planar eroded area on the outer layer of the armor, using a digital image processing technique, or by counting the armor units removed from the armor layers (Vidal et al., 2006). If the eroded area is estimated with the visual counting method (A_{ev}), the dimensionless damage parameter, S_v, , according to Vidal et al. (2006), can be obtained as follows:

$$S_v = \frac{A_{ev}}{D_{n50}^2} = \frac{N_e D_{n50}}{(1-p)b} \qquad [II.17]$$

where N_e is the number of extracted units relocated above the upper layer, p is the armor porosity and b is the width of the eroded area.

Vidal et al. (2003 and 2006), Gómez-Martín and Medina (2006) and Lomónaco et al. (2009) characterized the armor damage to trunks and roundheads using the visual counting method together with laser or mechanical profilers. They concluded that if only a few units are displaced, S_v is more accurate than S measured with a profiler. However, as armor damage levels increase, profile-based armor damage estimations are more reliable.

The main disadvantages of the aforementioned damage numbers are that they do not consider the HeP failure mode. When HeP is significant, the porosity of the armor layer changes in time and space, and Eqs. II.14 to II.17 are no longer valid. To consider armor unit extraction, armor layer sliding as a whole and HeP failure modes, Gómez-Martín and Medina (2006) developed the virtual net method. This method divides the armor into individual strips of a constant width ($a=q\ D_{n50}$) and length ($b=z\ D_{n50}$); it allows the dimensionless damage in each strip (S_i) to be measured considering porosity evolution in time and space. Integrating this dimensionless armor damage over the slope, the equivalent dimensionless armor damage parameter (S_e) can be obtained using Eq. II.18.

$$S_e = \sum_{i=1}^{I} S_i = \sum_{i=1}^{I} q\left(1 - \frac{1-p_i}{1-p_{i0}}\right) = \sum_{i=1}^{I} q\left(1 - \frac{\phi_i}{\phi_{i0}}\right) \quad \forall S_i \geq 0 \qquad [II.18]$$

in which q is the number of rows in each strip, $p_i=1-(N_i D_n^2/a\,b)$ and $\phi_i=n(1-p_i)$ are the armor porosity and packing density of the strip i respectively, N_i is the number of armor units whose center of gravity is within each strip, p_{0i} and ϕ_{i0} are the initial armor porosity and packing density of the strip i, and I is the number of strips.

For the present research, both the visual counting and the virtual net methods were used to measure damage to rock armors. For cube armors, only the virtual net method was used. The damage was also characterized using the qualitative approach described by Losada et al. (1986) and Vidal et al. (1991).

II.3.5. Toe berm stability and damage measurements

II.3.5.1. Toe berm dimensions

When mound breakwaters are constructed with CAUs, a toe berm is usually placed on the sea bottom or bed layer to provide support for the armor. Fig. II.15 shows a typical cross section for a conventional mound breakwater with a toe berm placed on a bed layer, where h_s is the sea bottom water depth at the toe, h_t is the water depth above the toe berm, B_t is the toe berm width, and t_t is the toe berm thickness.

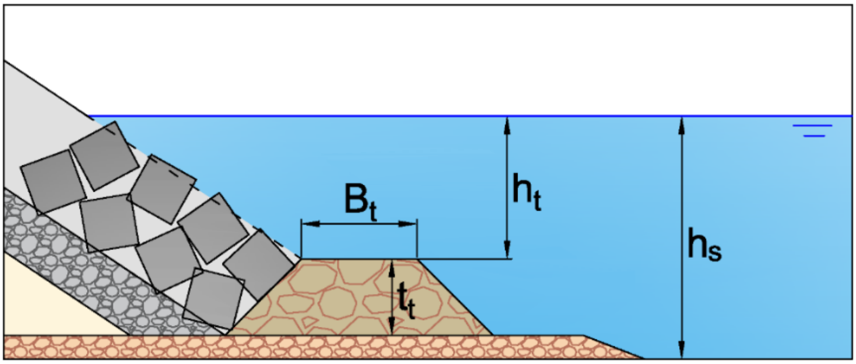

Figure II.15. Cross section of toe berm.

Toe berms are usually constructed with rocks, although CAUs can also be used for the toes of mound breakwaters (see Burchart and Liu, 1995, or Van Gent and Van der Werf, 2014). BSI (1991) specified five structure types for toes, including the circumstances in which they should be applied:

1. A toe berm of underlayer material (for $h_t>2H_s$)
2. A toe berm of armor material (for $h_s<2H_s$)
3. Lower armor units resting in a trench (for $h_s <1.5H_s$ and rock bottom)
4. A toe berm on top of bed protection and replacement material (for an original bed of soft material)
5. A toe berm on an extended anti-scour apron.

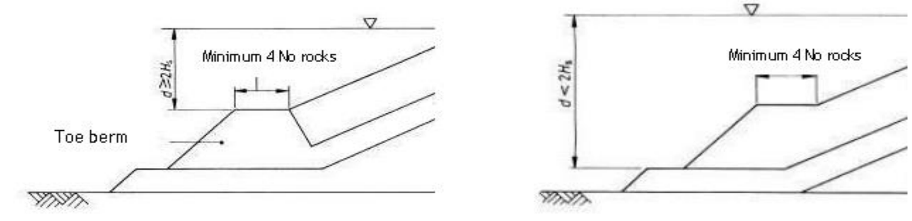
Minimum 4 No rocks
d≥2Hs
Toe berm
Minimum 4 No rocks
d<2Hs

(a) Deep water case

(b) Shallow water case

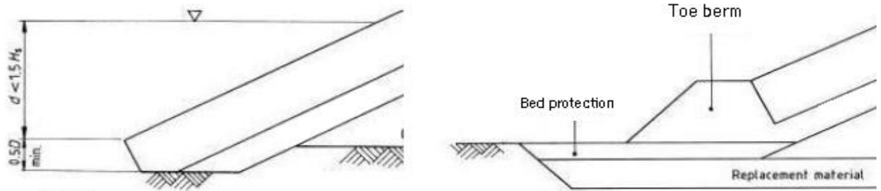
d<1.5Hs
0.5D min.
Trench
Toe berm
Bed protection
Replacement material

(c) Rock at bed level

(d) Soft material at bed level

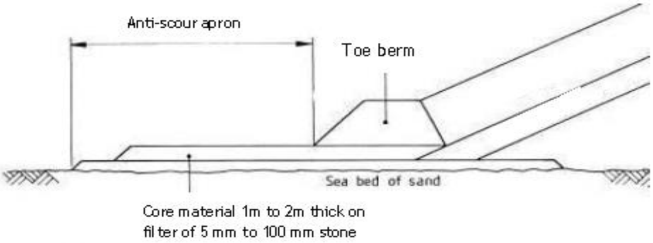
Anti-scour apron
Toe berm
Sea bed of sand
Core material 1m to 2m thick on
filter of 5 mm to 100 mm stone

(e) Protective toe apron

Figure II.16. Types of toe berms (BSI, 1991).

CIRIA/CUR/CETMEF (2007) also mentioned different types of toe berms depending on the sea bottom (sandy or rocky) and the water depth (deep or shallow). For relatively deep water conditions and sandy sea bottoms, it is common for units in the toe berm to be smaller than in the main armor layer. However, in shallow water conditions, units may be larger in the toe berm than in the armor itself. For shallow waters in combination with steep foreshores (m≈1/10 bottom slope), CIRIA/CUR/CETMEF (2007) recommended constructing the toe in a dredged trench or moving the breakwater to a shallower or deeper water location where there is no breaking.

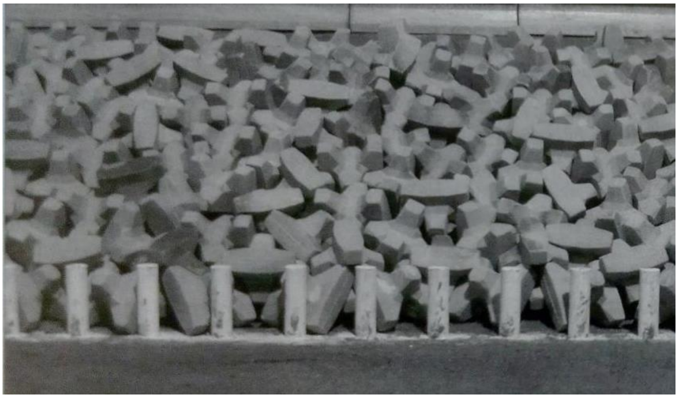

Figure II.17. Toe using concrete piles (CIRIA/CUR/CETMEF, 2007).

According to USACE (1984), the toe berm width, B_t, should in general allow at least two stones to be placed. BSI (1991) recommended at least four stones and according to CIRIA/CUR/CETMEF (2007), B_t should, in general, allow at least three stones to be placed; while the thickness, t_t, should, in general, allow at least two stones to be placed. However, a wider toe berm can be designed for breakwaters in zones at risk of severe scour.

II.3.5.2. Toe berm damage

Toe berm damage is usually characterized with the damage numbers N_d and N_{od} (Eqs. II.12 and II.13) but considering D_{n50} instead of D_n when rocks are used for the toe berm. Ebbens (2009) introduced a new damage parameter to characterize toe berm damage:

$$N_{\%} = N \cdot \frac{{D_{n50}}^3}{(1-n_v)\cdot V_{total}} \tag{II.19}$$

where n_v is the void porosity, and V_{total} is the apparent volume of the toe berm.

From a qualitative point of view, CIRIA/CUR/CETMEF (1991) established the following criteria for the damage levels and the damage measured in percentage:

1. 0-3 %: no movement of stones (or only a few) in the toe.
2. 3-10 %: the toe flattens out but still functions with the damage being acceptable.
3. >20 %: failure.

Van der Meer et al. (1995) defined three damage levels as a function of the damage number, N_{od}. The CIRIA/ CUR/ CETMEF (2007) criteria for a standard toe berm size of 3-5 rocks wide and 2-3 rocks thick was represented as follows:

1. N_{od}=0.5: start of damage.
2. N_{od}=2: some flattening out occurs.
3. N_{od}=4: toe berm failure.

For N_{od} classification, Docters van Leeuwen (1996) offered Fig. II.18 with the following values:

1. N_{od}=0.5: start of damage.
2. N_{od}=1: acceptable damage.
3. N_{od}=4: unacceptable damage.

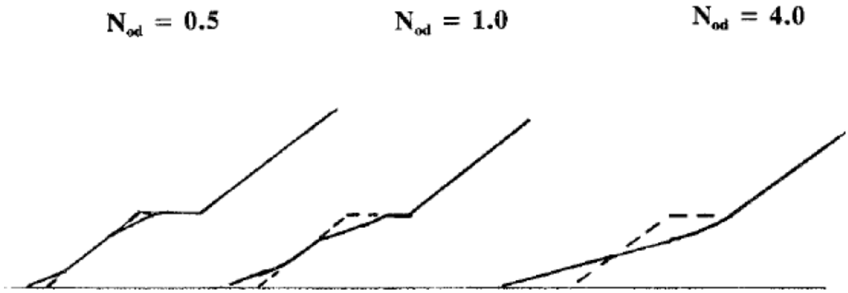

Figure II.18. N_{od} classification for toe berms (Docters van Leeuwen, 1996).

II.4. Hydraulic stability of rock armors in depth-limited breaking wave conditions

II.4.1. Introduction

Until 1933 no methods were availabe to design mound breakwater armors. Breakwaters were built using the experience obtained from previously constructed ones. However, this qualitative knowledge was not sufficient to construct breakwaters given the complexity of the phenomena involved (wave characteristics, wave behavior, etc). As a result, different hydraulic stability formulas have been developed since then to design armor layers.

The most popular hydraulic stability formulas for rock armors were devised by Iribarren (1938, 1965), Hudson (1959), USACE (1975, 1984), Losada and Gimenez-Curto (1979), Van der Meer (1988a), Melby and Kobayashi (1998), Van Gent et al. (2003), Vidal et al. (2006) and others. Most were developed for relatively deep water wave conditions at the toe of the structure with no wave breaking on the foreshore. However, certain modifications were introduced later to be applied in depth-limited wave conditions (varying coefficients or the wave height used), but in most cases without providing contrasting experimental data.

II.4.2. Hydraulic stability formulas for rock armors

The most commonly-used formulas to design non-overtopped rock armors of mound breakwaters in breaking wave conditions are examined in this section. The stability number, $N_s=H/(\Delta D_{n50})$, is used to characterize hydraulic stability, where D_{n50} is the nominal diameter of the rocks in the armor, $\Delta = (\rho_r-\rho_w)/\rho_w$ is the relative submerged mass density, ρ_r is the mass density of the rocks, ρ_w is the mass density of the sea water, and H is the design wave height.

Eq. II.20 was introduced by Hudson (1959), based on the work of Iribarren (1938) and popularized by USACE (1975, 1984); Eq. II.20 was obtained from regular tests in non-breaking wave conditions. This was modified later for breaking wave conditions through the stability coefficient (K_D) which also considers the geometry of the armor unit, the number of layers, and the breakwater segment (trunk or head).

$$\frac{H}{\Delta D_{n50}} = \left(K_D \cot\alpha\right)^{1/3} \qquad [II.20]$$

where cotα is the armor slope. USACE (1975) and USACE (1984) recommended using $H=H_s$ and $H_{1/10}=1.27H_s$ respectively. When using $H=H_s$, the stability coefficient for rough angular randomly-placed rocks is $K_D=3.5$ for breaking waves and $K_D=4.0$ for non-breaking waves. When using $H=H_{1/10}$, the stability coefficient for rough angular randomly-placed rocks is $K_D=2.0$ for breaking waves and $K_D=4.0$ for non-breaking waves. USACE (1984) introduced a considerable safety factor compared to the practice based on USACE (1975) (see USACE, 2006). USACE (1975,1984) provided a method to estimate a breaker wave height, H_b, as a function of the deep-water wave height, the wave period and the bottom slope; nevertheless, no clear specifications were given about which H should be used in Eq. II.20 when dealing with depth-limited waves.

Feuillet et al. (1987) conceived a method to use Eq. II.20 for shallow water conditions taking into account the influence of shoaling and wave capping. The method provided the design wave height (H) to be used in Eq. II.20 for m=1/100, 1/20 and 1/10 bottom slopes, as a function of the wave steepness, the water depth at the toe, and the offshore highest tenth wave, $H_{1/10\ \mathrm{offshore}}$. Vidal et al. (1995) and Jensen et al. (1996) introduced a representative height larger than $H=H_s$ or $H=H_{1/10}$, on the basis of the statistics of large waves in incident wave trains; Jensen et al. (1996) recommended $H_{1/20}$ to characterize irregular waves. Kobayashi et al. (1990a, 1990b) examined the critical incident wave profile for the initiation of armor movement, considering that one wave height alone may not represent irregular waves.

Eq. II.20 refers to moderate damage (0-5% of the volume of armor units displaced from the breakwater active zone given a specific H). In order to determine the damage levels, Van der Meer (1988a) and Medina et al. (1994) proposed two equations based on the dimensionless armor damage parameter $S=A_e/D_{n50}^2$ for double-layer armors of rough rocks in deep water conditions. To this end, they used the damage values recommended by USACE (1975) as a function of the relative wave height $H/H_{D=0}$, where $H_{D=0}$ is the wave height that causes zero armor damage obtained from Hudson's formula. Following the methodology given by Medina et al. (1994), Eq. II.20 was related in this study to higher damage levels, using the data provided by USACE (1975, 1984) for rough rocks, as described in Appendix 2.

To consider the storm duration in armor damage, Medina (1996) developed an exponential model applicable to individual waves attacking the breakwater, and compared the results with the models of Teisson (1990), Smith et al. (1992), and Vidal et al. (1995). However, no experimental contrast was provided.

Van der Meer (1988a) proposed Eqs. II.21a and II.21b to predict rock stability under wave attack, using data from irregular laboratory tests performed at Delft Hydraulics and the work conducted earlier by Thompson and Shuttler (1975). Most of the tests were carried out in non-breaking wave conditions covering a wide range of armor slopes ($\cot\alpha=1.5$, 2, 3, 4 and 6), stability numbers ($1\leq H_s/\Delta D_{n50}\leq 4$), a grading armor material of $D_{n85}/D_{n15}<2.5$ and different structure geometries (i.e. structures with an impermeable core, structures with a permeable core, and homogeneous structures). The wave steepness was varied in the range of $0.01<s_m=H_s/L_{0m}<0.06$, where $L_{0m}=gT_m^2/2\pi$ is the deep water wavelength corresponding to the mean period, T_m. Armor damage was measured with a surface profiler after every 1000 waves up to 5000 waves. Eqs. II.21a and II.21b distinguish between "plunging" and "surging" conditions, but refer only to the type of wave breaking on the armor slope (not on the foreshore).

$$\frac{H_s}{\Delta D_{n50}}=c_{pl}S^{0.2}P^{0.18}N_z^{-0.1}\xi_m^{-0.5} \quad \text{for } \xi_m<\xi_{mc} \text{ (Plunging waves)} \qquad \text{[II.21a]}$$

$$\frac{H_s}{\Delta D_{n50}}=c_sS^{0.2}P^{-0.13}N_z^{-0.1}(\cot\alpha)^{0.5}\xi_m^{P} \quad \text{for } \xi_m>\xi_{mc} \text{ (Surging waves)} \qquad \text{[II.21b]}$$

in which $\xi_{mc}=((c_{pl}/c_s)P^{0.31}(\tan\alpha)^{0.5})^{1/(P+0.5)}$ is the critical breaker parameter, $c_{pl}=6.2$ and $c_s=1.0$ are two coefficients, $0.1\leq P\leq 0.6$ is a parameter which considers the permeability of the structure, N_z is the number of waves, and $\xi_m=\tan\alpha/(2\pi H_s/(gT_m^2)^{0.5})$ is the surf similarity parameter based on T_m. Fig. II.19 illustrates the values of P given by Van der Meer (1988a) for different structures.

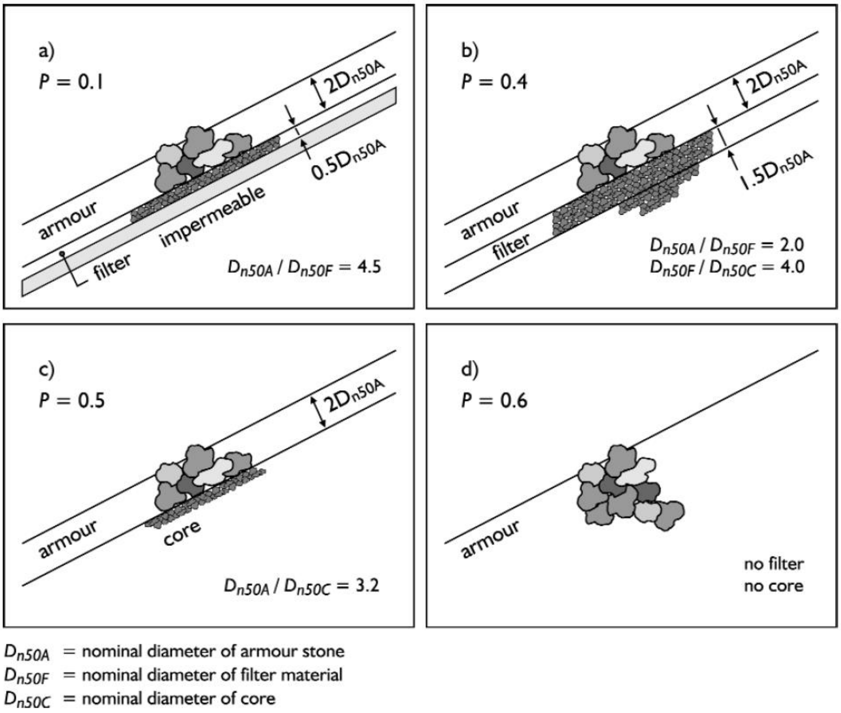
a)
P = 0.1
2Dn50A
0.5Dn50A
armour
impermeable
filter
Dn50A / Dn50F = 4.5
b)
P = 0.4
2Dn50A
1.5Dn50A
armour
filter
Dn50A / Dn50F = 2.0
Dn50F / Dn50C = 4.0
c)
P = 0.5
2Dn50A
armour
core
Dn50A / Dn50C = 3.2
d)
P = 0.6
armour
no filter
no core
Dn50A = nominal diameter of armour stone
Dn50F = nominal diameter of filter material
Dn50C = nominal diameter of core

Figure II.19. Permeability values for different structures (Van der Meer, 1988a).

Eqs. II.21a and II.21b are valid for non-depth-limited wave conditions. Additionally, Van der Meer (1988a) conducted 16 physical tests in depth-limited breaking wave conditions with a m=1/30 bottom slope and a permeable structure with rock nominal diameter D_{n50} (cm)=3.6, armor slope cotα=2, $1.6 \leq H_s/\Delta D_{n50} \leq 2.5$ and $3.3 \leq h_s/\Delta D_{n50} \leq 6.5$. For breaking wave conditions, Van der Meer (1988a) replaced H_s in Eqs. II.21a and II.21b by $H_{2\%}/1.4$; however, the factor 1.4 corresponds to the ratio $H_{2\%}/H_s$ in the Rayleigh distribution.

Van der Meer (1998c) also introduced an equation for two-layer non-overtopped armored slopes with concrete cubes, but this equation was only valid for non-depth limited wave conditions. For depth-limited conditions, no equation or modification was provided.

Lamberti et al. (1994) analyzed the influence of the water depth on ‘reshaping’ rubble mound breakwaters in deep and shallow water conditions. They conducted physical model tests with a horizontal bottom slope to represent deep water conditions, and with bottom slope, m=1/20, followed by a gentler bottom slope, m=1/100, to represent shallow water conditions. They concluded that to describe the stability of the rock armor of a berm breakwater, $H_{1/50}$ is a good representative wave height for any water conditions.

Melby and Kobayashi (1998) studied the progression and variability of armor damage on rubble mound breakwaters through physical tests conducted in breaking wave conditions with a bottom slope m=1/20 and water depth at the toe h_s(m)=11.9 and 15.8. Damage to a double-layer rock armor with cotα=2 and D_{n50}(cm)=3.64 was measured using a profiler after three test series of long duration. Eq. II.22 was proposed to estimate the temporal progression of the mean armor damage (S) for the wave parameters varying in steps in the ranges $1.6 \le H_s/\Delta D_{n50} \le 2.5$ and $2.0 \le h_s/\Delta D_{n50} \le 2.6$.

$$S(t) = S(t_n) + 0.025 \left(\frac{H_s}{\Delta D_{n50}} \right)_n^5 \frac{\left(t^{0.25} - t_n^{0.25} \right)}{\left(T_m \right)_n^{0.25}} \quad \text{for } t_n \le t \le t_{n+1} \qquad [II.22]$$

where S(t) and S(t_n) are the mean dimensionless armor damage at times t and t_n, respectively, with $t > t_n$. Incident wave parameters were estimated in the breaker zone using the methodology described by Kobayashi et al. (1990a, b) based on linear wave theory. Eq. II.22 was calibrated with H_s measured at a distance of 0.91m from the model. According to Melby (1999), this distance was roughly $5H_s$ for the largest measured waves, following the recommendation given by Goda (1985) for vertical breakwaters.

Eqs. II.21a and II.21b were modified by Van Gent et al. (2003) based on tests by Smith et al. (2002) and new physical model tests with deep and shallow water conditions. Tests were conducted with two bottom slopes (m=1/30 and 1/100), two armor slopes (cotα =2 and 4), three rock nominal diameters (D_{n50}(cm)=2.2, 2.6 and 3.5) with an aspect ratio of 2.1, a grading armor material of $1.4 < D_{n85}/D_{n15} < 2.0$, and different structure geometries (i.e. structures with permeable and impermeable cores). The wave steepness based on the mean period was varied in the range of $0.01 < s_m = H_s/L_{0m} < 0.06$. Armor damage was measured after 1000 or 3000 waves using a surface profiler. Eqs. II.23a and II.23b are the modified formulas reported by Van Gent et al. (2003) to be valid for both deep and shallow water conditions in the ranges $0.5 \le H_s/\Delta D_{n50} \le 4.5$ and $1.5 < h_s/\Delta D_{n50} < 11$. These equations consider the real wave height exceeded by 2% of the waves, $H_{2\%}$, with the coefficients re-calibrated to $c_{pl}=8.4$ and $c_s=1.3$.

$$\frac{H_{2\%}}{\Delta D_{n50}} = c_{pl} S^{0.2} P^{0.18} N_z^{-0.1} \xi_{s-1}^{-0.5} \quad \text{for } \xi_{s-1} < \xi_{mc} \text{ (Plunging waves)} \qquad [II.23a]$$

$$\frac{H_{2\%}}{\Delta D_{n50}} = c_s S^{0.2} P^{-0.13} N_z^{-0.1} (\cot\alpha)^{0.5} \xi_{s-1}^{P} \quad \text{for } \xi_{s-1} > \xi_{mc} \text{ (Surging waves)}$$

[II.23b]

in which $\xi_{S-1}=tan\alpha/(2\pi H_s/(g\ T_{m-1,0}{}^2)^{0.5})$ is the surf similarity parameter based on the spectral period $T_{m-1,0}=\frac{m_{-1}}{m_0}$, where m_i is the *i-th* spectral moment, $m_i=\int_0^\infty S(f)\cdot f^i\cdot df$, being *S(f)* the wave spectra.

Based on the aforementioned tests, Van Gent et al. (2003) provided a new stability formula (Eq. II.24) to introduce the nominal diameter of the core material ($D_{n50\text{-}core}$).

$$\frac{H_s}{\Delta D_{n50}}=1.75\cot\alpha^{0.5}(1+D_{n50-core}/D_{n50})\left(\frac{S}{N_z}\right)^{0.2} \qquad [II.24]$$

H_s at the toe of the structure was selected as the characteristic wave height.

Hovestad (2005) conducted specific physical tests in breaking wave conditions to determine the effect of the bottom slope on armor stability. A conventional rubble mound breakwater with cotα=2 and D_{n50}(cm)=1.57 was tested, with two different bottom slopes, a gentle slope m=1/30 and a steep slope m=1/8. After re-analysing Hovestad's data, Muttray and Reedijk (2008) concluded that with identical wave conditions at the wavemaker, the most significant increase in damage occurred in tests with plunging breakers in the steep sea bottom. Verhagen et al. (2006) also pointed out that with steep sea bottoms, non-linear effects and wave loads on mound breakwaters significantly increase. CIRIA/CUR/CETMEF (2007) recommended reducing the stability number of single-layer armors by 10% when dealing with depth-limited wave heights and steep sea bottoms.

Using data from Thompson and Shuttler (1975), Vidal et al. (2006) demonstrated that the average wave height of the 50 highest waves attacking the breakwater, H_{50}, is the wave parameter that best represents the damage evolution with the number of waves in a sea state (note that for N_z=1000 waves, H_{50} is very similar to $H_{2\%}$). Using H_{50}, Eqs. II.21a and II.21b were transformed into a sea-state damage evolution formula, assuming a Rayleigh distribution:

$$\frac{H_{50}}{\Delta D_{n50}}=c_{pl}S^{0.2}P^{0.18}\xi_m{}^{-0.5} \qquad \text{for } \xi_m<\xi_{mc} \text{ (Plunging waves)} \qquad [II.25a]$$

$$\frac{H_{50}}{\Delta D_{n50}}=c_sS^{0.2}P^{-0.13}(\cot\alpha)^{0.5}\xi_m{}^P \qquad \text{for } \xi_m\geq\xi_{mc} \text{ (Surging waves)} \qquad [II.25b]$$

in which c_{pl}=4.44 and c_s=0.716.

In order to demonstrate that H_{50} is representative of rock armor damage for Rayleigh and regular sea states, Vidal et al. (2006) conducted additional physical model tests.

Experiments were designed with a flat bottom and non-breaking wave conditions, one armor slope (cotα =1.5) and one rock nominal diameter (D_{n50}(cm)=2.95). Twelve regular tests of 500 waves, twelve irregular tests of 1000 waves, and two long irregular tests of 1000 waves were carried out with two surf similarity parameters ($\xi=\tan\alpha/(2\pi H/(gT^2))^{0.5}=2.5$ and 3.5 for regular tests and $\xi_p=\tan\alpha/(2\pi H_{m0}/(gT_p^2))^{0.5}=2.5$ and 3.5 for irregular tests). Armor damage was measured after each test with a surface profiler, a digital image processing technique, and counting the removed rocks settled over the original armor layer. The dimensionless armor damage parameter was estimated using the visual counting method following Eq. II.17.

Prevot et al. (2012) conducted specific physical model tests in breaking wave conditions with a bottom slope m=1/30 to compare the damage measured in a double-layer rock armor and the estimations given by Eqs. II.23a, II.23b and II.24, and Eq. II.20 when using the method given by Feuillet et al. (1987). According to these authors, the best fit was found with Eqs. II.23a and II.23b.

The literature reviewed for rubble mound breakwater design suggests that most design equations were developed for deep water conditions (non-depth-limited waves), although they are also commonly used in depth-limited wave conditions. Only Melby and Kobayashi (1998) and Van Gent et al. (2003) obtained rock armor hydraulic stability formulas based on specific laboratory tests in breaking wave conditions for a bottom slope m=1/20 with armor slope cotα=2, and bottom slopes m=1/30 and 1/100 with cotα=2 and 4. Nevertheless, no equations are available to design rubble mound breakwaters built with steeper armor slopes (cotα<2) and placed in shallow waters. In addition, most equations require knowing H_s or $H_{2\%}$ at the toe of the structure, but they do not specify a standard procedure to estimate them, nor the exact point at which they should be determined in breaking conditions, which may lead to relevant errors (note that these equations were validated with waves measured by gauges located at a certain distance from the structure toe). Thus, in this study (Section III), a new hydraulic stability formula is presented for rock armors with cotα=1.5, after conducting an analysis to identify which characteristic wave height and distance from the toe structure best determine armor damage evolution in depth-limited breaking wave conditions.

II.5. Hydraulic stability of rock toe berms in depth-limited breaking wave conditions

II.5.1. Introduction

Several empirical formulas have been used to predict the damage to rock toe berms. Markle (1989) carried out physical tests with regular waves on a bottom slope m=1/10; the water depth ratio (h_t/h_s) was identified as the governing parameter for toe berm stability. Gerding (1993) performed tests with random waves on a bottom slope m=1/20; the toe berm damage was characterized using the damage number N_{od} and h_t/D_{n50} was selected as the explanatory variable. Docters Van Leeuwen (1996) performed tests on a bottom slope m=1/50 to analyze the influence of the relative submerged mass density ($\Delta = (\rho_r - \rho_w)/\rho_w$) on Gerding's formula; this author concluded that Δ was well reproduced as different stone mass densities gave similar results for $H_s/(\Delta D_{n50})$ as a function of h_t/D_{n50}. Gerding's tests were later re-analyzed by Van der Meer (1998b) using the water depth ratio (h_t/h_s) as the explanatory variable. Ebbens (2009) performed tests with random waves considering three bottom slopes (m=1/50, 1/20 and 1/10) and studied the influence of the slope on the toe berm stability. Test results published by Markle (1989), Gerding (1993) and Ebbens (2009) were re-examined by Muttray (2013) who included the ratio between the water depth above toe berm and the significant wave height (h_t/H_s) as the explanatory. Finally, Van Gent and Van der Werf (2014) analyzed the influence of different toe berm widths conducting specific tests with random waves with a bottom slope m=1/30.

The design toe berm formulas found in the literature are only valid for submerged toe berms ($h_t>0$); however, breakwaters and seawalls constructed in very shallow water along rocky coasts with steep seafloors may require emerged toe berms ($h_t<0$) built with large rocks.

II.5.2. Hydraulic stability formulas for rock toe berms

The most relevant formulas to design rock toe berms, as described in this section, use the stability number, $N_s=H_s/(\Delta D_{n50})$, with the significant wave height H_s measured at the toe of the structure.

Markle (1989) conducted physical tests in breaking wave conditions, with a foreshore slope m=1/10 and proposed Eq. II.26 to design rock toe berms. Tests were carried out with regular waves generated with increasing mean wave heights ($9.1<H_m(cm)<22.9$) and mean wave periods ($1.32<T_m(s)<2.82$) for a fixed water depth at the toe berm (h_s(cm)=12.2, 15.2, 18.3, 21.3, 24.4, 27.4), where H_m is the average wave height at the toe of the structure. Four rock sizes were used (D_{n50}(cm)=2.58, 2.95, 3.30, 4.06) for toe berms with fixed $t_t=2D_{n50}$ and $B_t=3D_{n50}$. Eq. II.26 is the lower bound formula obtained from Markle's data (see Muttray, 2013), in which the water depth ratio (h_t/h_s) was identified as the determining parameter for toe berm stability. Damage levels were not taken into account in the formula. The results refer only to moderate damage.

$$N_s{*} = \frac{H_m}{\Delta D_{n50}} = 1.6 + 5.5\left(\frac{h_t}{h_s}\right)^3 \qquad [II.26]$$

where $N_s^* = H_m/(\Delta D_{n50})$ is the stability number for regular waves. For the central bound of Eq. II.26, the coefficient 1.6 is replaced by 2.0.

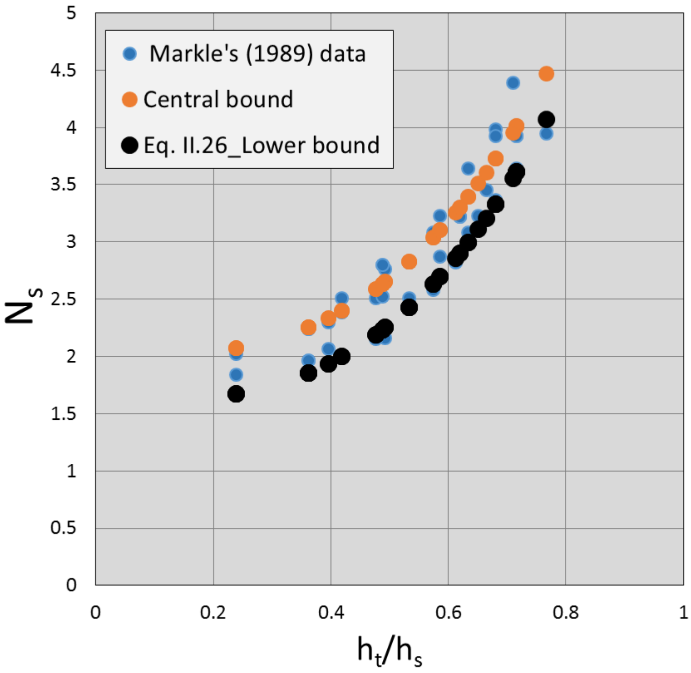

Figure II.20. Stability number as a function of the water depth ratio (h_t/h_s) for tests conducted by Markle (1989).

Gerding (1993) measured the toe berm damage in physical tests with wave runs of 1000 random waves and a bottom slope m=1/20. Tests were conducted with a constant wave steepness at the wave generating zone ($s_p=H_s/L_{0p}$=0.02 and 0.04), an increasing significant wave height at the wave generator (H_s(cm)=15, 20, 25) and a fixed water depth at the toe (h_s(cm)=30, 40 and 50). Four rock nominal diameters were studied (D_{n50}(cm)=1.7, 2.5, 3.5 or 4.0), with three toe berm heights (t_t(cm)=8, 15 and 22), and three toe berm widths (B_t(cm)=12, 20 and 30). Gerding (1993) was the first author to introduce the damage number N_{od} (Eq. II.13) to quantify the damage observed on the toe berm.

$$N_{od}=\frac{1}{\left(0.24\left(\frac{h_t}{D_{n50}}\right)+1.6\right)^{1/0.15}}\left(N_s\right)^{1/0.15} \qquad [II.27]$$

After each test, N_{od} was calculated and the model was rebuilt, so no cumulative damage was measured.

Continuing the work done by Lamberti and Aminti (1994), Donnars and Benoit (1996) analyzed the influence of rock toe berms on armor stability, conducting small-scale tests with four rock toe berm sizes and rock armors with two slopes (cotα=1.5 and

1.25) in the wave flume at the University of Bologna. They concluded that the stability of the toe berm significantly affected the armor stability, but only minor effects of main armor on toe berm stability were observed.

Aminti and Lamberti (1996) conducted tests with a bottom slope m = 1/100 to analyze the interaction between the main armor and the toe berm damage. To this end, a rubble mound breakwater with rock armor size D_{n50} (cm)=2.3 and slope cotα=1.5 and 2.5 was tested with no toe berm, a narrow rock toe berm ($B_t=3D_{n50}$) and a wide toe berm ($B_t=10D_{n50}$) for two rock toe berm sizes D_{n50} (cm)=2.04 and 2.30. Based on test results, Aminti and Lamberti (1996) modified Eq. II.27, introducing the effect of wave steepness.

Docters van Leeuwen (1996) conducted tests on a bottom slope m=1/50 to analyze the influence of the relative submerged mass density ($\Delta=(\rho_r-\rho_w)/\rho_w$) on Gerding's formula, concluding that Δ was well reproduced since different stone mass densities gave similar results for N_s as a function of h_t/D_{n50}.

Van der Meer (1998b) re-analyzed the data given by Gerding (1993) for rock toe berms, using the water depth ratio (h_t/h_s) as the explanatory variable; this formula can be re-written as follows:

$$N_{od} = \frac{1}{\left(6.2\left(\frac{h_t}{h_s}\right)^{2.7}+2.0\right)^{1/0.15}}\left(N_s\right)^{1/0.15} \qquad [II.28]$$

Fig. II.21 shows the measured values of N_{od} during Gerding's (1993) tests and the estimated N_{od} using Eqs. II.27 and II.28. Only $N_{od}\leq 20$ was represented in Fig. II.21.

CIRIA/ CUR/ CETMEF (2007) makes reference to the formulas given by Gerding (1993) and Van der Meer (1998b) to calculate the rock size for mound breakwaters. Gerding (1993) recommended using $N_{od}=2$ for a safe design, while Van der Meer (1998b) recommended $N_{od}=0.5$ for a conservative design.

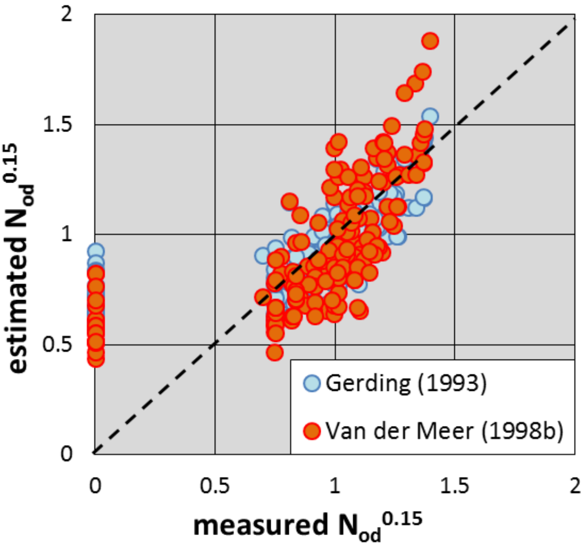

Figure II.21. Linearized N_{od} measured in Gerding's (1993) tests and linearized N_{od} estimated with Eqs. II.27 and II.28 given by Gerding (1993) and Van der Meer (1998b).

Sayao (2007) examined the influence of the surf similarity parameter and the bottom slope on the stability number of rock toe berms.

Ebbens (2009) performed laboratory tests to analyze the influence of different bottom slopes (m=1/50, 1/20 and 1/10). Random wave runs were generated with seven water depths at the toe ($7.3 \leq h_s(cm) \leq 25.3$). The four lowest water levels ($h_s(cm)$=7.3, 9.3, 11.3 and 13.3) were tested with two values for wave steepness at the wave generating zone ($s_p=H_s/L_{0p}$=0.04 and 0.02). Tests with the three highest water levels ($h_s(cm)$=15.3, 20.3, or 25.3) were only performed with s_p=0.03 for calibration. For each water level, wave runs were generated with four significant wave heights at the wave generator ($H_{s,g}(cm)$=6, 8, 10 or 12). Three rock sizes were tested ($D_{n50}(cm)$=1.88, 2.15 and 2.68) with toe berm thickness $t_t(cm)$=6 and toe berm width $B_t(cm)$=10 (above a 2cm-thick bed layer). Three rock void porosities were used for each D_{n50} (n_v=0.36, 0.33, 0.32). For m=1/50, only $D_{n50}(cm)$=1.88 and 2.15 were tested; for m=1/10, only $D_{n50}(cm)$=2.15 and 2.68 were tested. The damage parameter $N_{\%}$ given by Eq. II.19 was used to quantify toe berm damage.

During Ebbens' tests, damage levels fluctuated when varying the wave steepness from s_p=0.04 to s_p=0.02. Steeper waves (s_p=0.04) led mainly to a downward movement of rocks, while longer waves (s_p=0.02) pushed rocks in an upward direction. Therefore, for tests with s_p=0.04, only downward rock movements were considered. For tests with s_p=0.02, the number of displaced rocks was counted considering the number of stones moving downwards (away from the toe berm) and upwards.

Using $N_{\%}$, Ebbens (2009) and Baart et al. (2010) proposed the following design equation for toe berm stability:

$$N_{\%} = 0.038 \left(\xi_p *\right)^{3/2} \left(N_s\right)^3 \qquad [II.29]$$

where $\xi_p^*=m/(H_s/L_{0p})^{1/2}$ is the surf similarity parameter in which 1/m is the bottom slope, and $L_{0p}=gT_p^2/2\pi$ is the deep water wave length. $N_{\%}$=0% if no toe rock is moved and $N_{\%}$=100% if all toe rocks are removed from the toe berm. Although higher toe berm damage was measured during the tests, Eq. II.29 only provides reliable values if $N_{\%}<0.3$.

The toe berm was not rebuilt after each test but rather before each change in the water level. The cumulative toe berm damage did not always increase for a certain water depth, but it sometimes decreased when wave steepness increased (s_p=0.04 after s_p=0.02). Fig. II.22 shows the fluctuation in damage levels during a test series conducted with m=1/10, D_{n50}(cm)=2.68 and h_s(cm)=7.3.

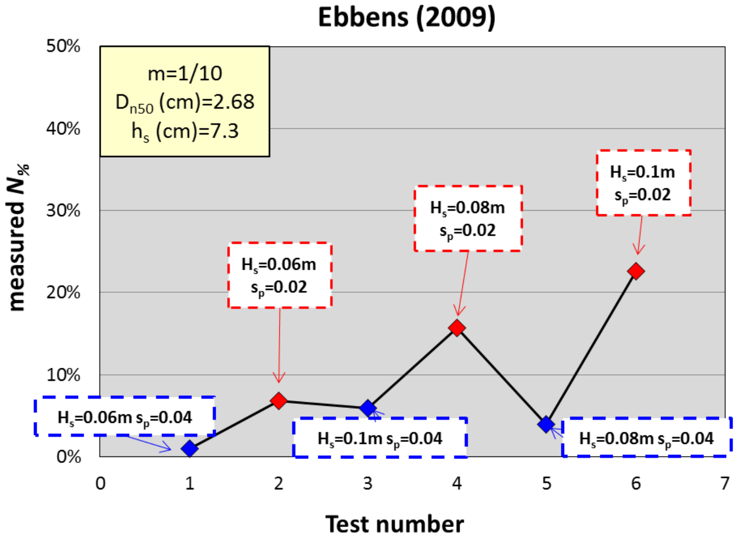

Figure II.22. $N_{\%}$ measured during Ebbens' (2009) tests in the series conducted with m=1/10, D_{n50}(cm)=2.68 and h_s(cm)=7.3.

Fig. II.23 represents the experimental results given by Ebbens (2009), who recommended using $N_{\%}$ = 5% (N_{od}≈0.5) as a safe toe berm design level for swell waves and $N_{\%}$=10% (N_{od}≈1.0) for wind waves. Fig. II.23 indicates that N_{od} is approximately one order of magnitude higher than the damage number $N_{\%}$. Fig. II.24 shows the $N_{\%}$ measured during Ebbens' (2009) tests and the $N_{\%}$ estimated by Eq. II.29.

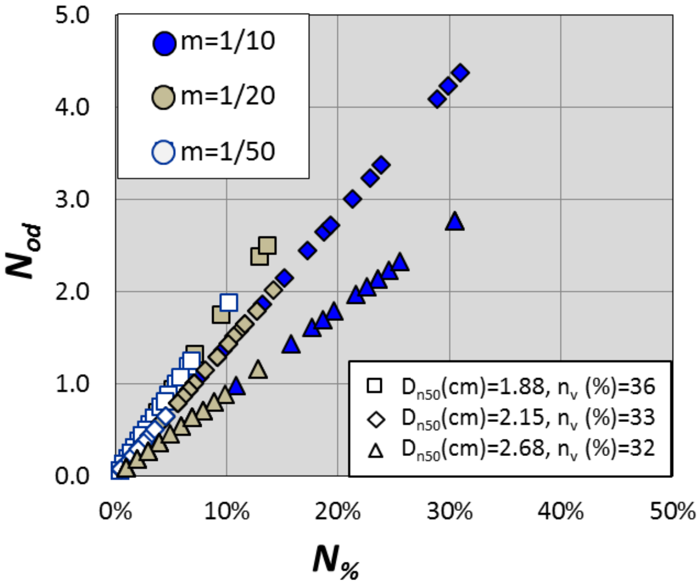

Figure II.23. Values of N_{od} corresponding to $N_{\%}$ measured by Ebbens (2009) as a function of the bottom slope (m), toe berm size (D_{n50}) and toe berm void porosity (n_v).

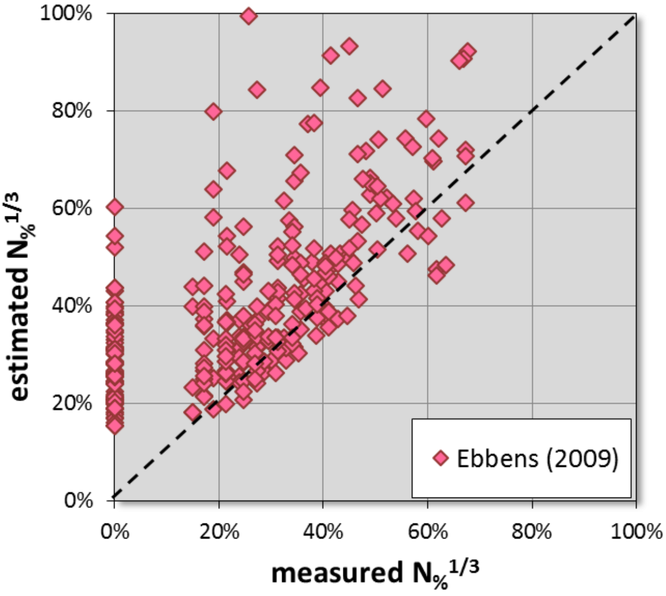

Figure II.24. Linearized $N_{\%}$ measured during Ebbens' (2009) tests and estimated by Eq. II.29.

Muttray (2013) re-analyzed the experimental results obtained by Markle (1989), Gerding (1993) and Ebbens (2009) and proposed Eq. II.30 to estimate N_{od}.

$$N_{od} = \left(0.58 - 0.17 \cdot \frac{h_t}{H_s}\right)^3 (N_s)^3 \qquad [II.30]$$

where H_s is the significant wave height measured at the toe of the structure.

Van Gent and Van der Werf (2014) carried out irregular tests with a m=1/30 bottom slope. Three water levels in front of the toe (h_s(cm)=20, 30, and 40) were considered, and most tests were done without severe wave breaking on the foreshore. Two wave steepness values were considered at the wave generating zone ($s_p=H_s/L_{0p}=0.015$ and 0.04) increasing the significant wave height until reaching a high damage level or H_s(cm)=28. Two rock sizes were used (D_{n50}(cm)=1.46 and 2.33) for a thickness $t_t=2D_{n50}$ and $4D_{n50}$, and a width $B_t=3D_{n50}$ and $9D_{n50}$. Cumulative damage was considered as the model was rebuilt after each test series of four or seven wave runs of increasing H_s. Eq. II.31 was proposed to estimate damage to the toe berm.

$$N_{od} = 0.032\left(\frac{t_t}{H_s}\right)\left(\frac{B_t}{H_s}\right)^{0.3}\left(\frac{\hat{u}_\delta}{\sqrt{g \cdot H_s}}\right)(N_s)^3 \qquad [II.31]$$

where $\hat{u}_\delta = \frac{\pi \cdot H_s}{T_{m-1,0}} \frac{1}{\sinh(k_{m-1,0} h_t)}$ and $k_{m-1,0} = \frac{2\pi}{L_{m-1,0}} = \frac{2\pi}{\frac{g}{2\pi} \cdot T_{m-1,0}{}^2}$.

Given a design wave storm (H_s, $T_{m-1,0}$), the larger the toe berm (B_t or t_t), the larger the N_{od}. For $3D_{n50}<B_t \leq 9D_{n50}$, Van Gent and Van der Werf (2014) multiplied the design N_{od} value by a factor f_B:

$$f_B = \left(\frac{B_t}{3D_{n50}}\right)^{1/2} = \left(\frac{n_t}{3}\right)^{1/2} \qquad [II.32]$$

where n_t is the number of rock rows placed on the upper layer of the toe berm.

Eqs. II.27 and II.28 can be used to estimate the damage caused by a wave storm characterized by a wave height measured at the toe of the structure and a mean or peak period. Eqs. II.29, II.30 and II.31 consider cumulative damage caused by some specific wave climates as the model was not rebuilt after each test.

Fig. II.25 shows the toe berm damage estimated by Eqs. II.27 to II.31 as a function of the stability number, N_s, for a toe berm with a width $B_t=3D_{n50}$ and thickness $t_t=2D_{n50}$. The wave steepness at the toe was established as $s_p=H_s/L_{0p}=0.02$, the relative berm height was $h_t/h_s=0.78$, and the relative water depth at the toe,

h_s/D_{n50}=9.4. The damage parameter obtained from Eq. II.29, $N_{\%}$, was considered one order of magnitude lower than the damage number, N_{od} (N_{od}=10 $N_{\%}$).

Fig. II.26 shows the toe berm damage estimated by Eqs. II.27 to II.31 for the relative water depth, h_s/D_{n50}, for a toe berm with a width $B_t=3D_{n50}$ and a thickness $t_t=2D_{n50}$. The wave steepness at the toe was established as $s_p=H_s/L_{0p}=0.026$ and the stability number N_s=2.8.

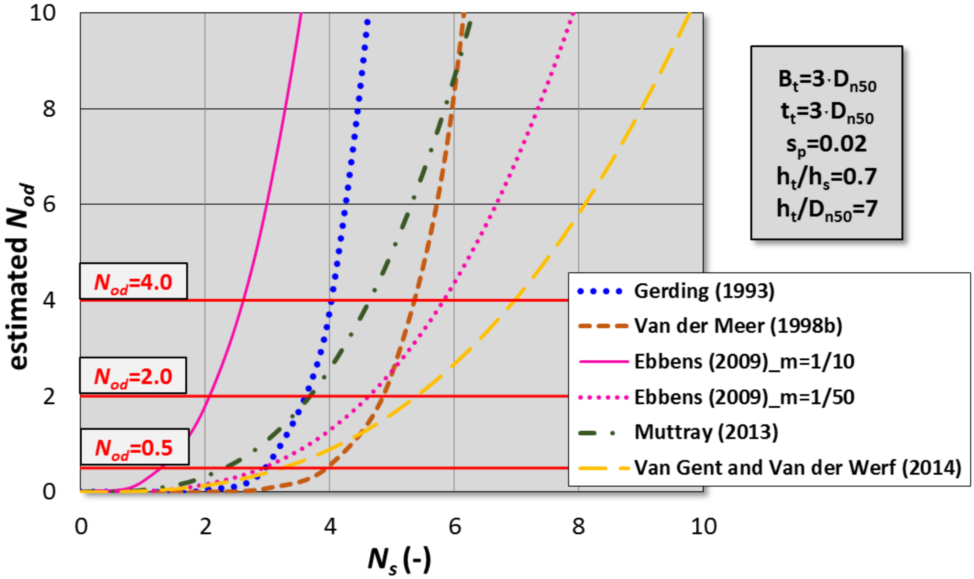

Figure II.25. Example of toe berm damage estimated by different formulas as a function of N_s.

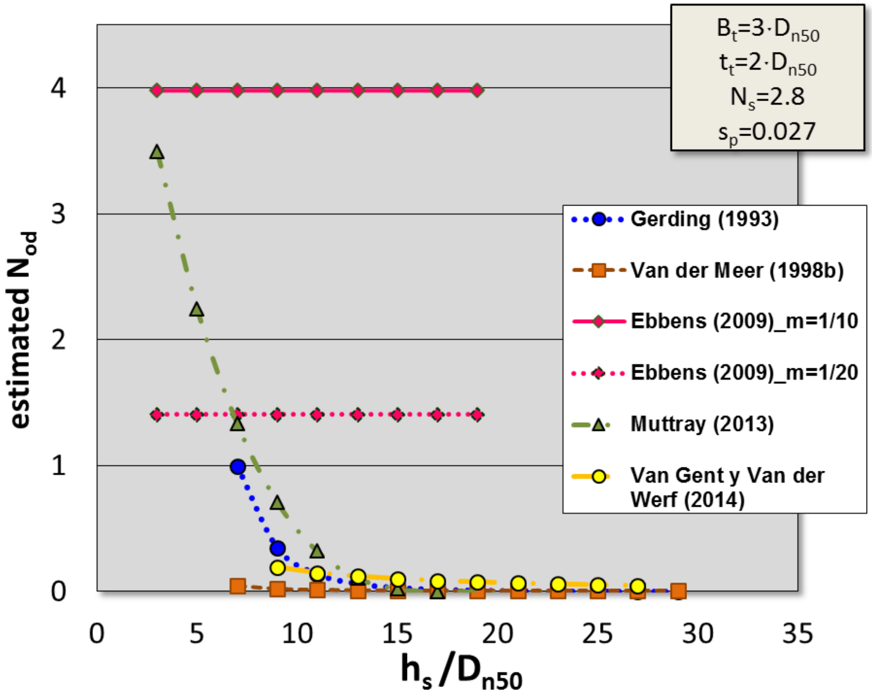

Figure II.26. Example of toe berm damage estimated by different formulas as a function of h_s/D_{n50}.

Figs. II.25 and II.26 illustrate a relevant scatter of toe berm damage estimations obtained with Eqs. II.27 to II.31.

The existing literature for submerged toe structures in depth-limited conditions and gentle seafloors suggests that the primary parameters for toe stability are the relative water depth at the toe and the stability number. However, the influence of the water depth on toe berm damage seems to be quite variable when existing equations are used. For emergent toe structures and steeper seafloors no information is available. Only Ebbens (2009) performed physical tests with random waves and a steep bottom (m=1/10). Nevertheless, the effect of water depth on toe berm stability was not considered (see Fig. II.26) nor was the stability of emerged toe berms. Thus, in this study (Section IV), a new equation is proposed to characterize the damage of emerged and submerged toe berms placed on a m=1/10 bottom slope considering the influence of the water depth at the toe, deep water wave parameters and rock size.

On the other hand, although the aforementioned equations were obtained from small-scale tests with different toe berm geometries, the toe berm width (B_t) and thickness (t_t) were not usually introduced as explanatory parameters of the observed toe berm damage; only Van Gent and Van der Werf (2014) included B_t and t_t as explanatory parameters of toe berm damage. When considering wider and/or higher toe berms, common damage numbers (N_{od} or $N_{\%}$) are not suitable to characterize toe berm stability since a larger number of rocks must be displaced from the toe (N) to significantly damage larger toe berms. Thus, in this study (Section IV), two new concepts are introduced to better characterize the damage to wide toe berms.

Chapter III

Hydraulic stability of rock armors placed in shallow waters and on gentle sea bottoms (m=1/50)

Port Saplaya, Valencia (Spain). October, 2015.

III.1. Introduction

Within the framework of the ESCOLIF project, hydraulic stability of double-layer rock armors was characterized in depth-limited breaking wave conditions. 2D physical model tests were carried out with a bottom slope m=1/50 in the wind and wave test facility of the LPC-UPV.

In order to establish a rational procedure to determine the wave characteristics in the depth-induced breaking zone, experimental wave measurements were compared to the estimations provided by the SwanOne numerical model (see Verhagen et al., 2008). SwanOne is a wave transformation numerical model which considers the depth-induced breaking phenomena. Using both experimental results and SwanOne estimations, an analysis was conducted to identify the characteristic wave height that best determines armor damage evolution, and the exact location at which it should be obtained when dealing with depth-limited waves.

In this chapter, the experimental design and SwanOne simulations are first described. Secondly, the results are analyzed. Thirdly, a new hydraulic stability formula for rock armors in depth-limited breaking wave conditions is given and compared to existing formulas. Finally, conclusions are drawn.

III.2. Experimental design

III.2.1. Facilities and equipment

2D physical model tests were conducted with a bottom slope m=1/50 in the wave flume (30 x 1.2 x1.2 m) of the Laboratory of Ports and Coasts at the *Universitat Politècnica de València* (LPC-UPV).

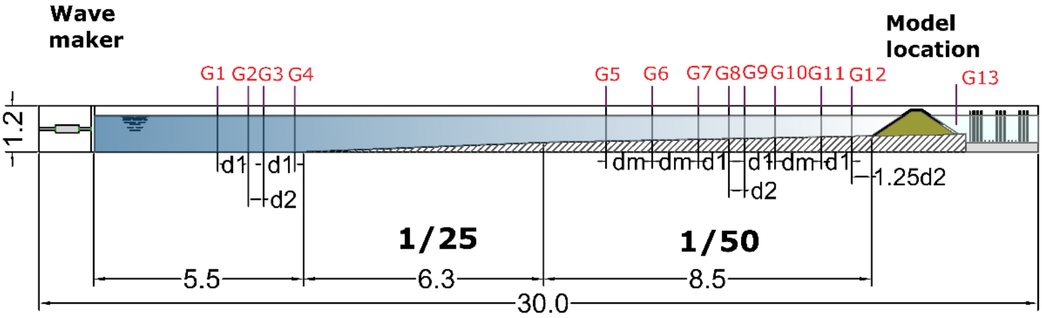

Figure III.1. Longitudinal cross section of the LPC-UPV wave flume used in the experiments with m=1/50 (dimensions in meters).

Two bottom slopes were placed in the flume to study wave propagation from deep or relatively deep water to shallow water where the physical model was placed. At the wave generating zone, there was a 5.5m-long horizontal bottom. The first ramp corresponded to a 6.3m-long and m=1/25 bottom slope; and the second one, corresponded to a 8.5m-long and m=1/50 bottom slope. Above this, the breakwater model was placed. The wave flume allowed the water to be recirculated through a false bottom of 25cm in height. The walls were transparent to observe what happened inside.

At one end of the wave flume, the wave generator system was located and at the opposite end, there was a passive system to dissipate the energy (see Fig. III.4). The physical model was located right in front of the absorber energy system.

The wave generator was a piston-type wavemaker with a maximum stroke of S_0(cm)=90 (see Fig. III.2); the AWACS Active Wave Absorption System was implemented to avoid multi-reflections in the wave flume.

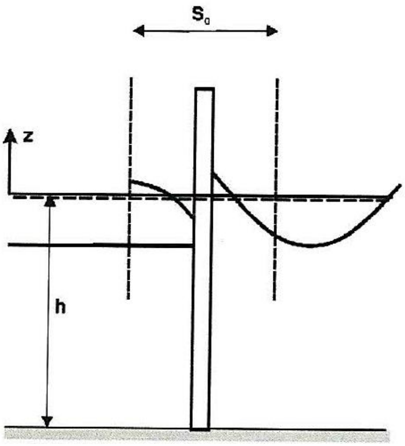

Figure III.2. Piston-type wavemaker.

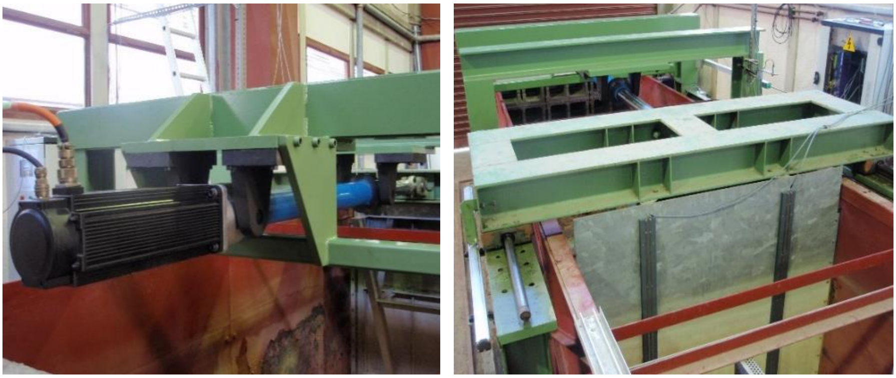

Figure III.3. Piston-type wavemaker used in the experiments.

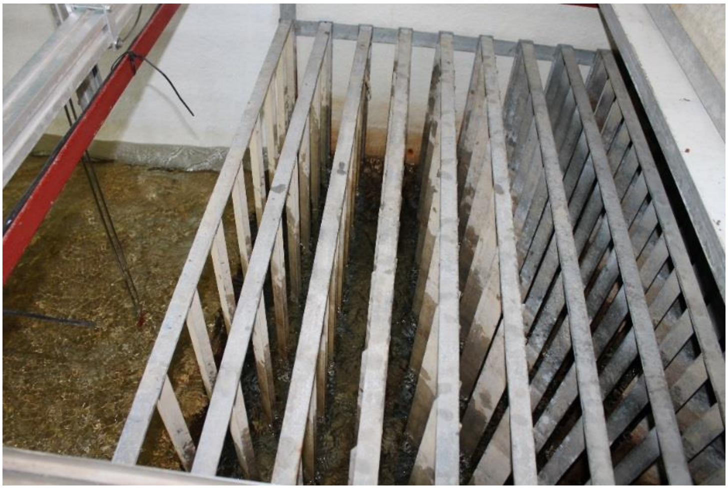

Figure III.4. Passive energy absorber system used in the experiments.

III.2.2. Physical models

The model tested corresponded to a conventional $\cot\alpha=1.5$ non-overtopped mound breakwater without a toe berm, protected with a double-layer, randomly-placed rock armor with nominal diameter $D_{n50}(cm)=3.18$ and mass density $\rho_r(g/cm^3)=2.677$ (Fig. III.5). Considering a reference scale 1/40, this structure corresponds to a double-layer 5.5-tonne rock armor.

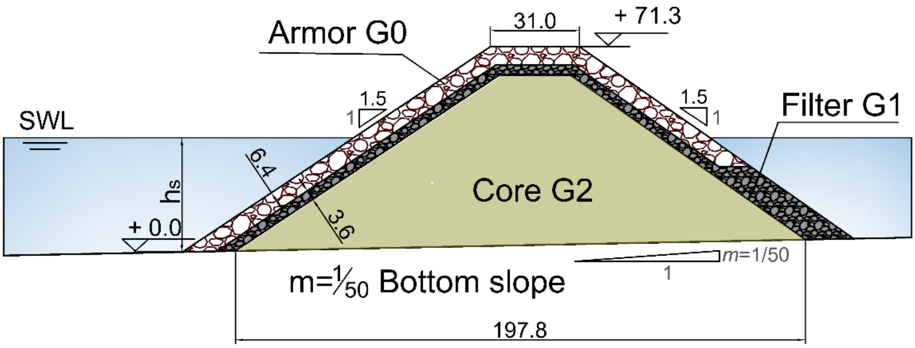
Armor G0
31.0
+ 71.3
1.5
1
1.5
1
Filter G1
SWL
6.4
hs
Core G2
+ 0.0
3.6
m=1/50
m=$\frac{1}{50}$ Bottom slope
1
197.8

Figure III.5. Cross section of the rock armored model (dimensions in centimeters).

Fig. III.6 shows the nominal diameter of the rough angular gravel (G0) used in the armor for twenty-five randomly selected resamples.

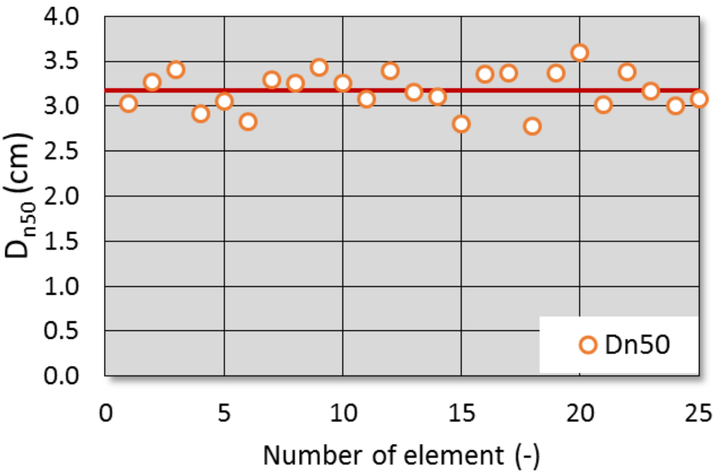

Figure III.6. Nominal diameter for gravel G0 used in the experiments.

The mean value of the measured packing density of the tested armor layer was ϕ=1.26 value, recommended by USACE (1984). The shape of rough angular rocks in the armor was characterized using the length-to-thickness ratio (Eq. III.1), also called aspect ratio (LT), and the Blockiness (BLc) (Eq. III.2) described by CIRIA/ CUR/ CETMEF (2007). The mean values of the two parameters were LT=1.8 and BLc=42%.

$$LT = \frac{l}{d} \qquad [III.1]$$

$$Blc = \left(\frac{M_{50}}{\rho_r}\frac{1}{XYZ}\right) 100 \qquad [III.2]$$

where l is the maximum length of the unit, d is the minimum distance between rows through which the unit could pass, and X, Y and Z are the maximum, intermediate and minimum rectangular dimensions of the smallest hypothetical box that would enclose the unit.

Figs. III.7 and 8 show the aspect ratio and blockiness of the rocks used in the armor layer. In this case, twenty resamples were randomly selected.

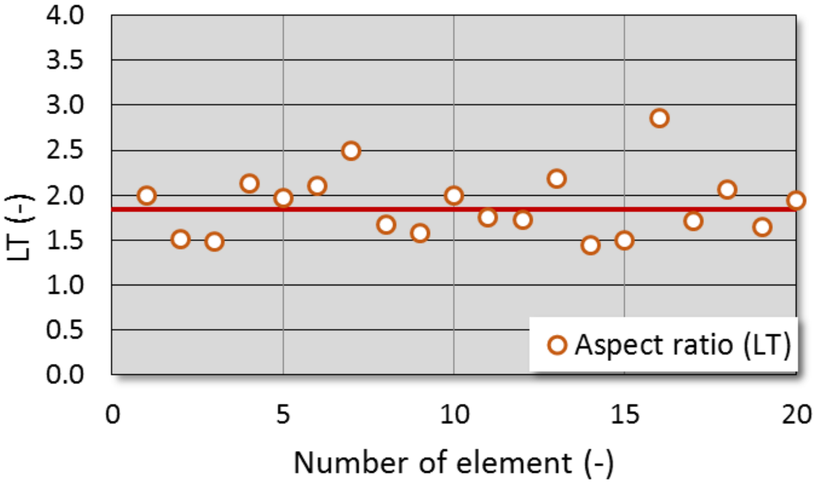

Figure III.7. Aspect ratio for gravel G0 used in the experiments.

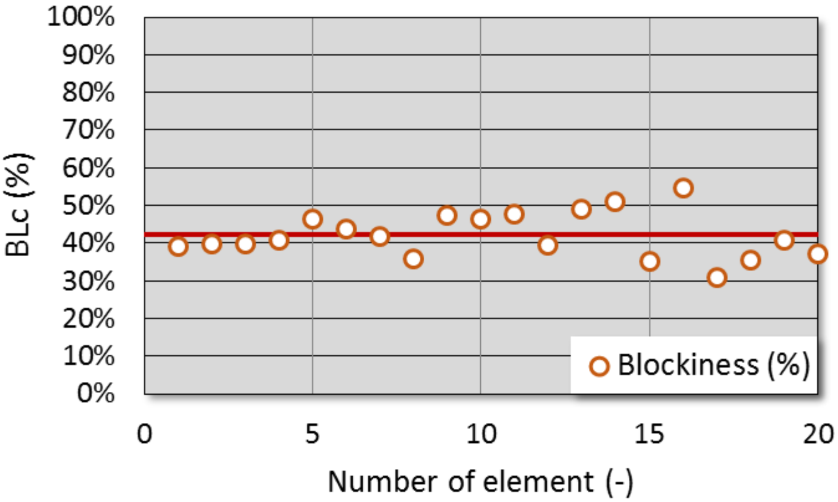

Figure III.8. Blockiness for gravel G0 used in the experiments.

The rock armor was placed on a filter layer with D_{n50}(cm)=1.78 and D_{n85}/D_{n15}=1.35. The characteristics of the core material were D_{n50}(cm)=0.68 and D_{n85}/D_{n15}=1.64. Table III.1 summarizes the characteristics of the materials used in the physical tests.

Gravel	M_{50}[g]	D_{n50}[cm]	ρ_r[g/cm^3]
G0	86.18	3.18	2.677
G1	15.40	1.78	2.729
G2	0.86	0.68	2.722

Table III.1. Characteristics of model materials.

Fig. III.9 shows the construction process of the rubble mound breakwater used in the wave flume. First, the cross section was drawn on the walls of the flume at the proper scale. Second, the core was constructed with gravel G2. Third, the filter layer (gravel G1) was built on top of the core layer. Finally, the first (yellow rocks) and second (black, red, grey and blue rocks) layers of the armor were placed on the filter layer.

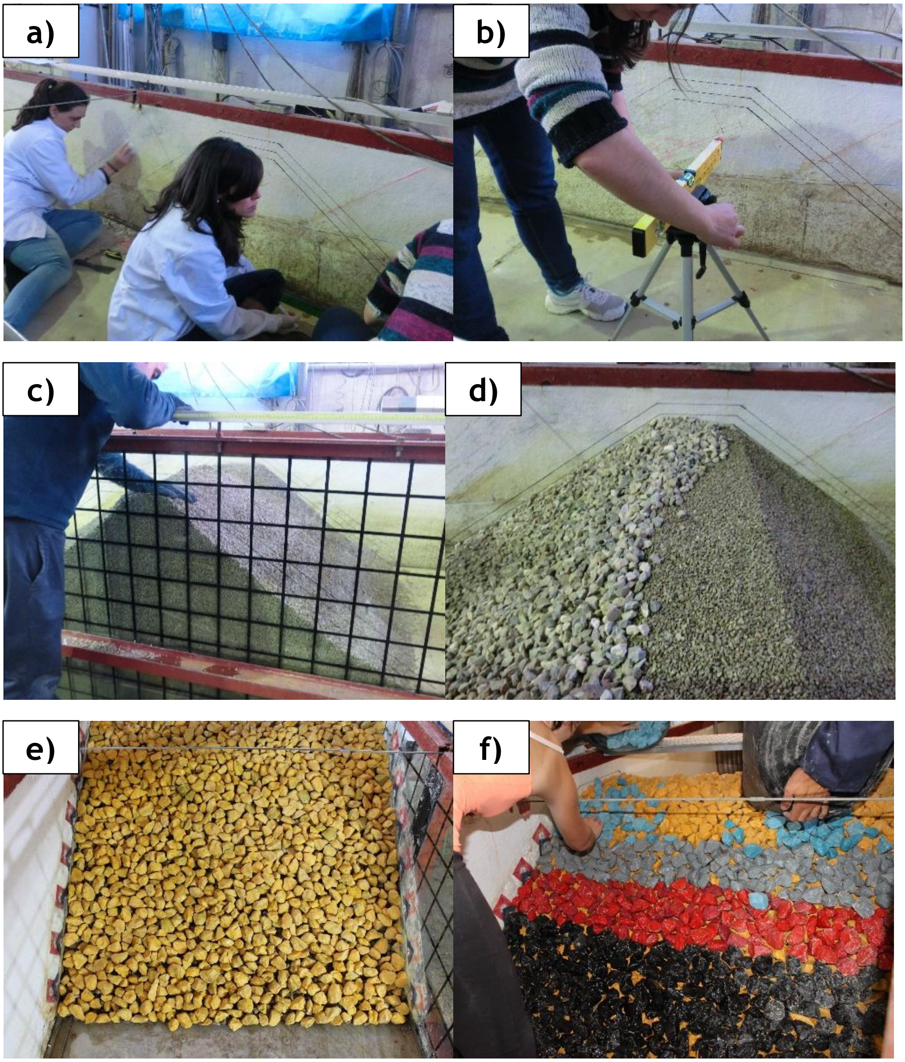

Figure III.9. Construction process of the rubble mound breakwater model: (a) drawing, (b) leveling, (c) core, (d) filter, (e) first armor layer and (f) second armor layer.

III.2.3. Irregular tests

Irregular wave trains of 1000 waves were generated with JONSWAP (γ=3.3) spectra (Eq. III.3). Reflected waves were absorbed using the AWACS Active Wave Absorption System.

$$S(f)=\alpha g^2 f^{-5}\exp\left[-\frac{5}{4}\left(\frac{f}{f_p}\right)^{-4}\right]\gamma\exp\left[\frac{-\left(\frac{f}{f_p}-1\right)^2}{2\sigma^2}\right]$$

[III.3]

where α=0.0081; γ=1 a 10; $\sigma=\begin{cases}0.07 sif \prec f_p \\ 0.09 sif \succ f_p\end{cases}$; $f_p=\frac{1}{T_p}$

The minimum and maximum frequencies were fixed at $f_{mín}=0.7f_p$ y $f_{máx}=2.5f_p$.

Three water depths at the toe of the structure were tested (h_s(cm)=20, 30 and 40). For each water depth, tests were grouped in two series of a constant surf similarity parameter with the target values of $\xi_p=\tan\alpha/(2\pi H_{m0}/(gT_p^2))=3.0$ and 5.0, corresponding to a target wave steepness of $s_p=2\pi H_{m0}/(gT_p^2)=0.049$ and 0.018. For h_s(cm)=40, tests conducted with ξ_p =5.0 were eliminated because some overtopping was observed during the experiments. Spectral significant wave height at the wave generating zone, $H_{m0}=4(m_0)^{1/2}$, was increased progressively in steps of 1 cm from zero-damage to initiation of destruction or wave breaking at the wave generating zone. Table III.2 summarizes the test characteristics.

Irregular tests							
Series	h_s(cm)	ξ_p	s_p	H_{m0}(cm)	T_p(s)	#Tests	#Waves, N_z
1	20	3.0	0.049	8.0-18.0	1.02-1.53	11	1000
2	20	5.0	0.018	8.0-15.0	1.70-2.32	8	1000
3	30	3.0	0.049	8.0-17.0	1.02-1.48	10	1000
4	30	5.0	0.018	8.0-14.0	1.70-2.25	7	1000
5	40	3.0	0.049	8.0-16.0	1.02-1.44	9	1000

Table III.2. Test matrix.

When all tests were completed, tests were repeated without the structure to more accurately measure the incident wave heights close to the model. To reduce undesired reflection, an energy absorber was placed at the end of the wave flume.

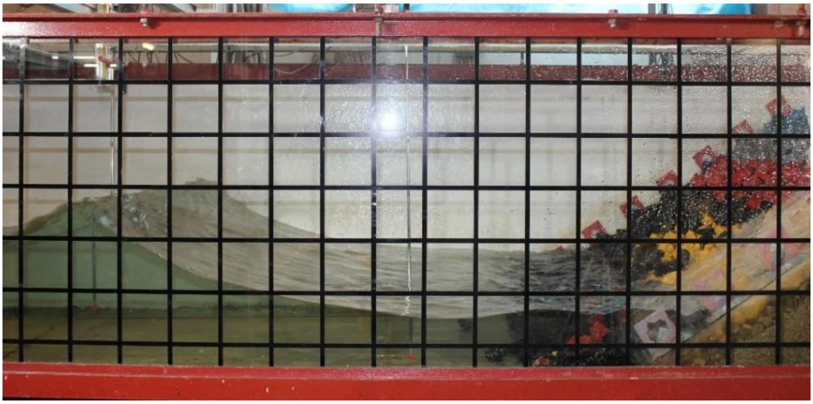

Figure III.10. View of test conducted with breakwater model.

Figure III.11. View of test conducted without breakwater model.

III.2.4. Measurements

III.2.4.1. Wave measurements

Surface elevation was measured using thirteen capacitive wave gauges. One group of wave gauges (G1, G2, G3 and G4) was placed near the wavemaker, the other group was placed along the wave flume and near the model (G5, G6, G7, G8, G9, G10, G11 and G12), and one wave gauge (G13) was placed behind the model to control the sea level at the rear of the structure (see Fig. III.1).

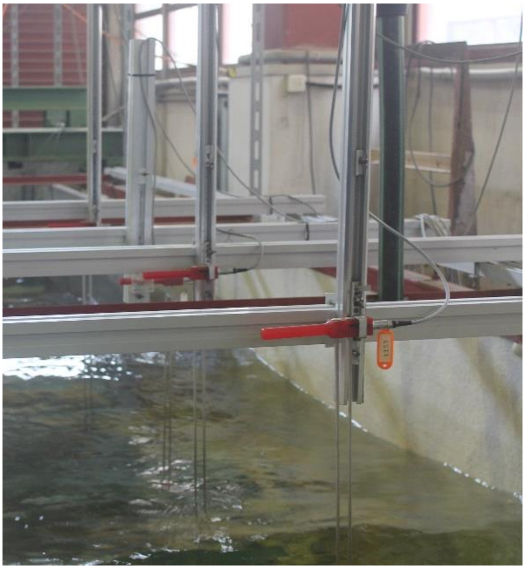

Figure III.12. Capacitive wave gauges used in the experiments.

Incident and reflected waves were separated at the wave generating zone. To this end, wave gauges were distanced according to the criterion given by Mansard and Funke (1980), depending on the wave length (Eq. III.4).

$$\left.\begin{array}{c} d_1 \approx \frac{L}{10} \\ \frac{L}{6} < d_1 + d_2 < \frac{L}{3} \\ d_1 + d_2 \neq \frac{L}{5} \\ d_1 + d_2 \neq \frac{3L}{10} \end{array}\right\} \qquad [III.4]$$

Table III.3 shows the distances between wave gauges (see also Fig. III.1).

Zone	Wave gauges	d_1[cm]	d_2[cm]	d_m[cm]
Wave generator	G1, G2, G3 and G4	80	40	120
Model	G4, G5, G6, G7, G8, G9, G10, G11	80	40	120

Table III.3. Wave gauge distances.

Additionally, all tests were recorded using video and photo cameras from two perspectives: one profile and another perpendicular to the slope. Thus, both wave breaking on the slope and armor damage evolution could be observed during the experiments.

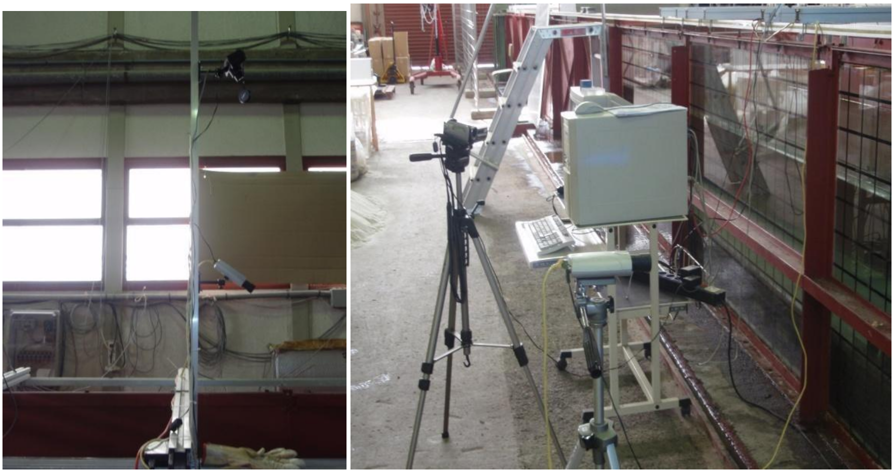

Figure III.13. Video and photo cameras used in the experiments.

III.2.4.2. Wave separation. LASA-V Method

Incident and reflected waves were estimated at the wave generating zone (wave gauges G1, G2, G3 and G4), using the LASA-V method developed by Figueres and Medina (2004). The LASA-V method allows wave separation into non-linear and non-stationary waves.

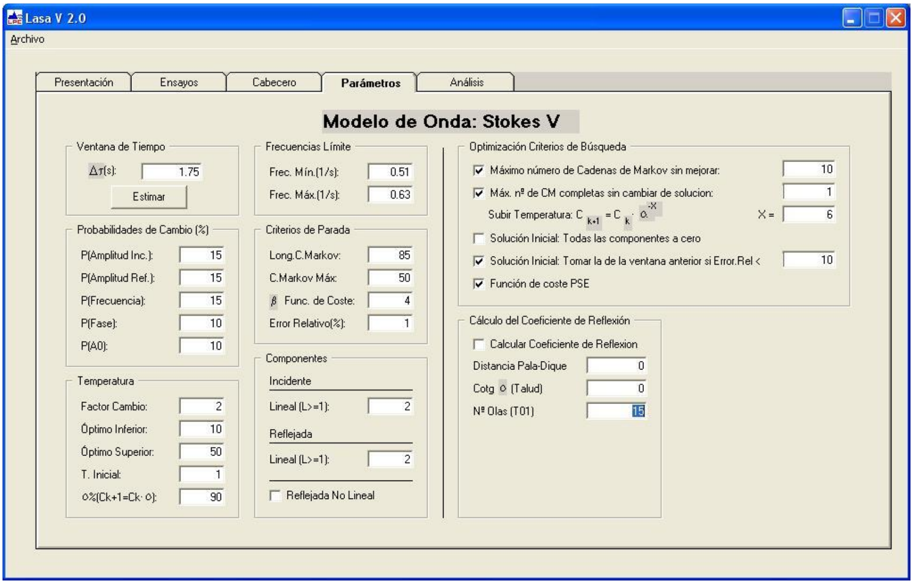

Modelo de Onda: Stokes V

Ventana de Tiempo
Δτ(s): 1.75

Probabilidades de Cambio (%)
P(Amplitud Inc.): 15
P(Amplitud Ref.): 15
P(Frecuencia): 15
P(Fase): 10
P(A0): 10

Temperatura
Factor Cambio: 2
Óptimo Inferior: 10
Óptimo Superior: 50
T. Inicial: 1
α%(Ck+1=Ck·α): 90

Frecuencias Límite
Frec. Mín.(1/s): 0.51
Frec. Máx.(1/s): 0.63

Criterios de Parada
Long.C.Markov: 85
C.Markov Máx: 50
β Func. de Coste: 4
Error Relativo(%): 1

Componentes
Incidente
Lineal (L>=1): 2
Reflejada
Lineal (L>=1): 2
☐ Reflejada No Lineal

Optimización Criterios de Búsqueda
☑ Máximo número de Cadenas de Markov sin mejorar: 10
☑ Máx. nº de CM completas sin cambiar de solucion: 1
Subir Temperatura: $C_{k+1} = C_k \cdot \alpha^{-X}$ X = 6
☐ Solución Inicial: Todas las componentes a cero
☑ Solución Inicial: Tomar la de la ventana anterior si Error.Rel < 10
☑ Función de coste PSE

Cálculo del Coeficiente de Reflexión
☐ Calcular Coeficiente de Reflexion
Distancia Pala-Dique 0
Cotg α (Talud) 0
Nº Olas (T01) 15

Figure III.14. LASA-V software used to separate incident and reflected waves (Figueres and Medina, 2004).

The LASA (Local Aproximation using Simulated Annealing) method allows for the analysis of the incident and reflected waves in the time domain, unlike other methods such as the 2-point model by Goda and Suzuki (1976), which performs the analysis in the frequency domain without respecting the principle of causality. The general procedure for local approximation separation of incident and reflected waves can be described in three stages:

- Eliminate noise.
- Set windows for estimating central points.
- Define a local approach model.

LASA is based on the use of triangular windows with linear superposition. The wave model initially proposed by Medina (2001) used linear and Stokes II for trains incident and reflected wave components. Four equations govern the model of local wave 2 + 2:

$$z_{Ie}(x,t,m\Delta\tau) = A_0+A1_{1m}\cos(k_{1m}x-\omega_{1m}t+\varepsilon_{1m})+A1_{2m}\cos(k_{2m}x-\omega_{2m}t+\varepsilon_{2m})+CNI \qquad [III.5]$$

$$CNI = A2_{1m}\cos[2(k_{1m}x-\omega_{1m}t+\varepsilon_{1m})]+A2_{2m}\cos[2(k_{2m}x-\omega_{2m}t+\varepsilon_{2m})] \qquad [III.6]$$

$$z_{Re}(x,t,m\Delta\tau) = A1_{3m}\cos(k_{3m}x+\omega_{3m}t+\varepsilon_{3m})+A1_{4m}\cos(k_{4m}x+\omega_{4m}t+\varepsilon_{4m})+CNR \qquad [III.7]$$

$$CNR = A2_{3m}\cos[2(k_{3m}x+\omega_{3m}t+\varepsilon_{3m})]+A2_{4m}\cos[2(k_{4m}x-\omega_{4m}t+\varepsilon_{4m})] \qquad [III.8]$$

The impulses (w) and wave numbers (k) are related by the linear dispersion, $w^2=g\,k\,\tanh(kh)$.

The local approximation model described by Eqs. III.5 to III.8 has 17 parameters to be estimated in each time window. These 17 parameters are optimized in each window, minimizing the error detected in the sensors. The criterion used for optimization is to minimize the mean squared error.

The LASA - V method (Figueres and Medina, 2004) is applied in the same conditions as the original LASA, but it is also valid for highly non-linear waves. Very asymmetric waves occur both in physical scale models and reality, limiting the effectiveness of many wave separation methods. For the analysis of these non-linear waves, it is necessary then to set a wave pattern of a higher order than Stokes – II, used by LASA. In this case, LASA-V uses an empirical model Stokes - V type, which allows for a better adjustment with highly asymmetric waves.

The LASA method uses simulated annealing as optimization technique, which is necessary to reach the optimum efficiently without stagnating in a local minimum. The method therefore requires the definition of a cost function and a mechanism of generation. The cost function evaluates the validity (by the mean squared error) of each possible solution, while the generation mechanism finds a new solution in the vicinity of any other known solution. The algorithm is developed in series, keeping the solution found or jumping to another until the "crystallized" process converges to the global optimum.

III.2.4.1. Damage measurements

Armor damage was measured after each test run considering the cumulative number of rocks displaced during the test series of h_s and ξ_p constant. Comparing the photographs taken perpendicularly to the armor slope before and after each test, the damage was characterized with the virtual net method described by Gómez-Martín and Medina (2006).

A virtual net was projected over each photograph, dividing the armor into six strips (five 16cm-wide strips and one 28cm-wide strip). Dimensionless armor damage was calculated for each strip (S_i); integrating this dimensionless armor damage over the slope, the equivalent dimensionless armor damage parameter was obtained (S_e), according to Eq. II.18.

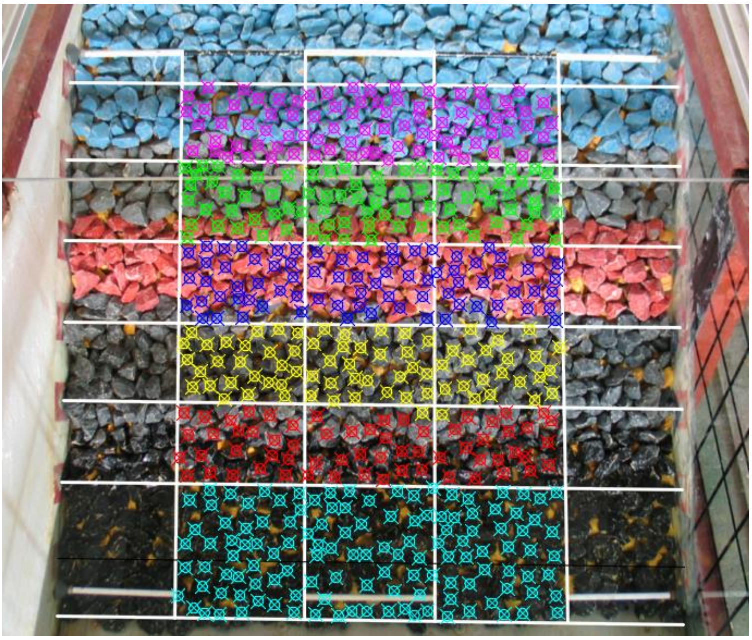

Figure III.15. Virtual net used in the experiments to characterized armor damage.

Armor damage was also characterized using the visual counting method described by Vidal et al. (2006). Eq. II.17 was used to estimate the visual dimensionless armor damage, S_v.

Note that the visual counting method assumes a constant armor porosity, so changes in the porosity from Heterogeneous Packing (HeP) are not considered with this method. In contrast, the virtual net method takes into account armor-unit extractions, sliding of the armor layer as a whole and HeP simultaneously (see Gómez-Martín and Medina, 2014).

III.2.5. Numerical simulations using SwanOne

After conducting the physical tests, numerical simulations were carried out using SwanOne software (TUDelft, 2016). SwanOne, a popular, free wave propagation model developed by Delft University of Technology, is appropriate to estimate wave propagation in 1D bathymetry (wave flume). The SwanOne model simulates the following physical phenomena:

- Wave propagation in time and space, shoaling, refraction due to currents and depth, frequency shifting due to currents and non-stationary depth.
- Wave generation by wind.
- Non-linear wave-wave interactions (both quadruplets and triads).
- Depth-induced breaking.
- Blocking of waves by currents.

In this study, SwanOne was used to estimate incident wave parameters close to the breakwater model because wave gauges can give inaccurate wave measurements due to air entrapment (see Fig. III.16), and methods to separate incident and reflected waves are not reliable in the breaking zone.

SwanOne estimated only wave propagation, simulating the depth-induced breaking phenomena. The test program (see Table III.2) was repeated with the same bottom profile and wave characteristics as in the physical experiments. To analyze wave parameters, virtual data were taken at the positions of the thirteen wave gauges used in the physical tests. SwanOne provided the values of H_{m0}, T_p, T_m and $T_{m-1,0}$ at these positions. The Composite Weibull Distribution (CWD) method, proposed by Battjes and Groenendijk (2000), was then implemented to estimate $H_{1/3}$, $H_{1/10}$ and $H_{2\%}$ in the depth-induced breaking zone from the H_{m0} values.

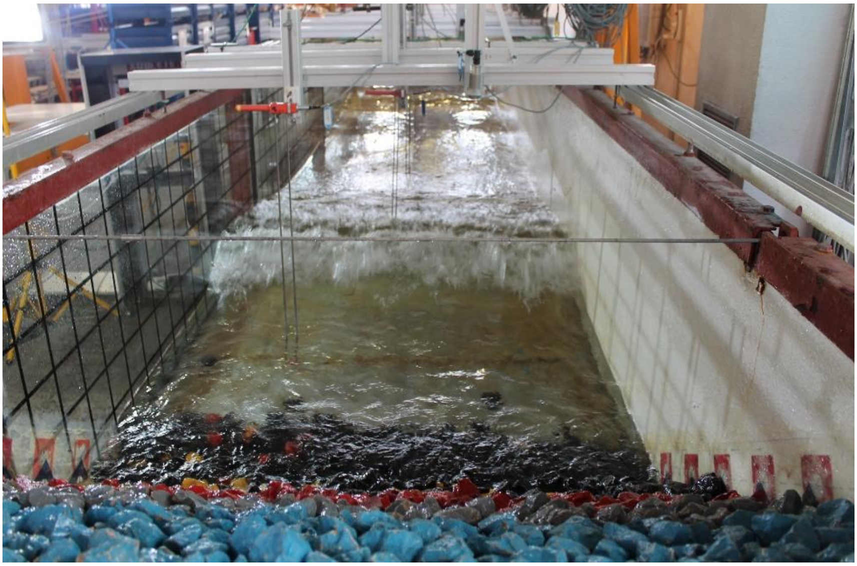

Figure III.16. View of wave gauges close to the breakwater model during a test.

III.3. Data analysis

III.3.1. Wave analysis

Wave characteristics obtained from the physical tests and SwanOne numerical simulations were analyzed. H_{m0}, $H_{2\%}$ and $H_{1/10}$ were used for the analysis because they can be obtained directly from SwanOne, and they are the most common characteristic wave heights used in the armor hydraulic stability formulas (see Section II.4).

Firstly, using the measured surface elevations, wave height distributions and spectral moments were estimated from the laboratory tests with and without the structure.

In the tests conducted without the structure, the measured waves directly corresponded to the incident waves since an effective absorber system was placed at the end of the flume.

In those tests conducted with the structure, incident and reflected waves were separated in the wave generating zone (G1 to G4) using the LASA-V method developed by Figueres and Medina (2004) because available methods to separate incident and reflected waves are not reliable when applied near the structure in breaking wave conditions. Fig. III.17 shows an example of separating incident and reflected surface elevation (η) when applying the LASA-V method from a recording of wave gauge G1.

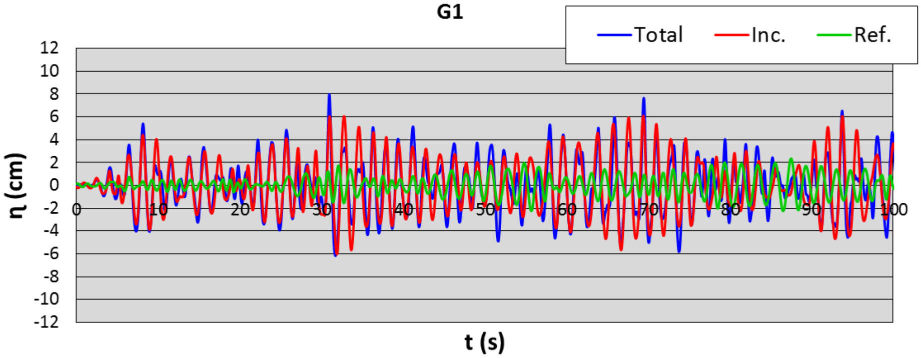

Figure III.17. Incident and reflected waves obtained at G1 when applying the LASA-V method (0<t(s)<100). Test conducted with structure, h_s (cm)=30, ξ_p=5.0 and H_{m0} (cm)=9.

From incident and reflected waves obtained at the wave generating zone (G1 to G4) in tests with the structure, the reflection coefficient was obtained using Eq. III.9.

$$K_r = \frac{H_{m0r}}{H_{m0i}} \tag{III.9}$$

where H_{m0r} and H_{m0i} are the reflected and incident wave height at the wave generating zone, respectively.

Fig. III.18 plots the K_r obtained at the wave generating zone (G1 to G4) compared to the dimensionless water depth $kh_s=2\pi h_s/L_{m,toe}$ where $L_{m,toe}$ is the mean wave length at the toe of the structure.

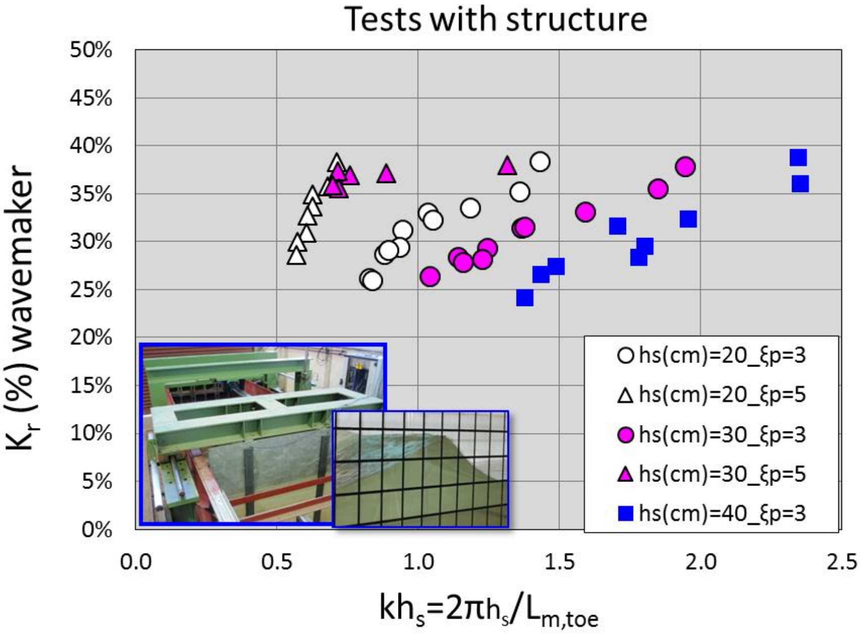

Figure III.18. Reflection coefficient measured at the wave generating zone (G1 to G4) versus the dimensionless water depth.

Considering the reflection coefficient measured at the wave generating zone (G1 to G4) constant along the flume, incident waves were estimated close to the model (average between G11 and G12) from the total register. Fig. III.19 compares incident H_{m0}, $H_{1/10}$ and $H_{2\%}$ estimated in the physical tests conducted with the structure, with those measured in the physical tests without the structure at G11 and G12 (average value).

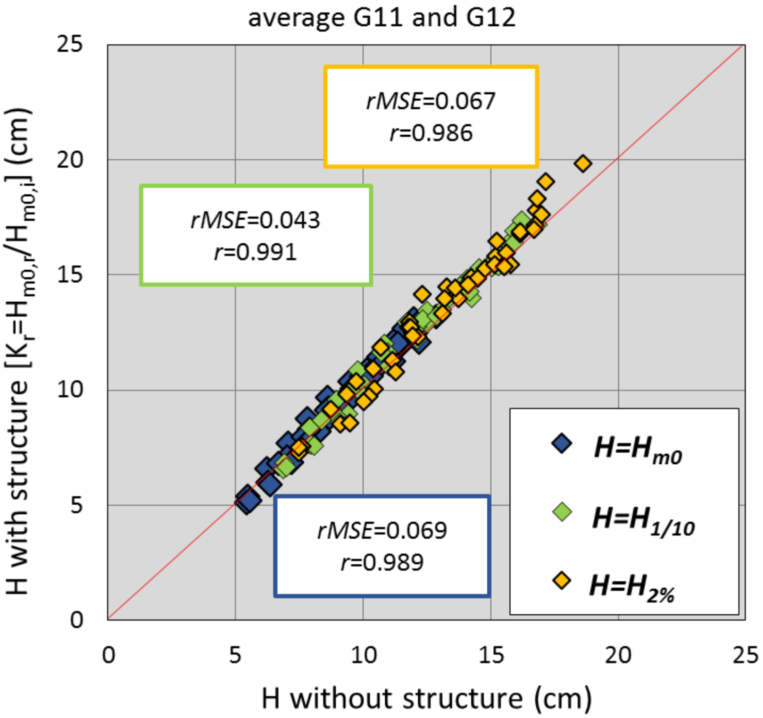

Figure III.19. Comparison of experimental incident H_{m0}, $H_{1/10}$ and $H_{2\%}$ without the structure, and with the structure obtained from K_r at the wave generating zone.

The relative mean squared error (rMSE) and the correlation coefficient (r) were used to measure the goodness of fit in the comparison (Eqs. III.10 and III.11).

$$rMSE = \frac{MSE}{VAR} = \frac{\frac{1}{N_o}\sum_{i=1}^{N_o}(t_i - e_i)^2}{\frac{1}{N_o}\sum_{i=1}^{N_o}(t_i - \bar{t})^2} \qquad [III.10]$$

$$r = \frac{\sum_{i=1}^{N_o}(t_i - \bar{t})(e_i - \bar{e})}{\sqrt{\sum_{i=1}^{N_o}(t_i - \bar{t})^2 \sum_{i=1}^{N_o}(e_i - \bar{e})^2}} \qquad [III.11]$$

where MSE is the mean squared error, N_o is the number of observations, t_i is the target value, e_i is the estimated value, VAR is the variance of target values, and $\bar{t}$

and $\bar{e}$ are the average of target and estimated values, respectively. $0 \leq rMSE \leq 1$ estimates the proportion of variance not explained by the model, and $0 \leq r \leq 1$ measures the degree of correlation; the lower the rMSE and the higher the r, the better the predictions.

For H_{m0}, the rMSE was 0.069 and the r was 0.989; for $H_{1/10}$, the rMSE was 0.043 and the r was 0.991, and for $H_{2\%}$, the rMSE was 0.067 and the r was 0.986. For the three considered wave heights, the errors between the mean values of the incident wave heights obtained with and without the structure in the gauges G11 and G12 were lower than 7%. Therefore, the wave height values, obtained from the K_r measured in the wave generating zone, are good estimators of the real incident wave heights that reach the breakwater when $K_r \leq 40\%$. Since measurements without the structure are more accurate to estimate incident wave parameters, only the values obtained in tests without the breakwater model are considered for further analysis when referring to wave measurements.

Secondly, numerical simulations were analyzed and compared to experimental results. Fig. III.20 shows the mean value of $H_{m0,}$ $H_{1/10}$ and $H_{2\%}$ provided by SwanOne at the position of the wave gauges G11 and G12, compared to the mean value measured in the laboratory tests without the structure. For H_{m0}, the rMSE was 0.058 and the r was 0.995; for $H_{1/10}$, the rMSE was 0.059 and the r was 0.964, and for $H_{2\%}$, the rMSE was 0.105 and the r was 0.952. For the three considered wave heights, there was also a high correlation between the laboratory measurements and the SwanOne predictions.

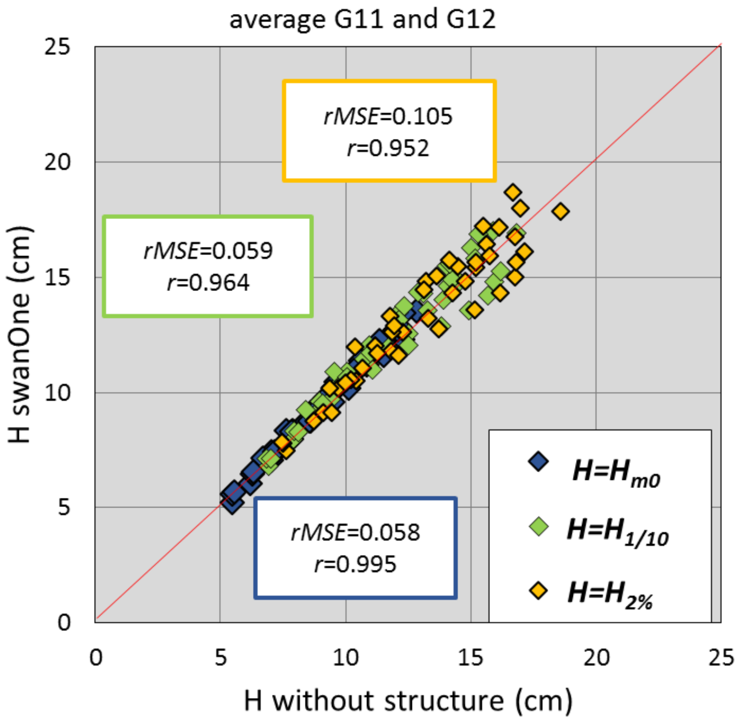

Figure III.20. Comparison of experimental incident H_{m0}, $H_{1/10}$ and $H_{2\%}$ without the structure and estimations given by SwanOne.

$H_{1/3}$ was not used in the analysis because the SwanOne model does not directly provide this characteristic wave height and it is very similar to H_{m0}, which can be directly obtained from SwanOne. In order to analyze the differences between H_{m0} and $H_{1/3}$, $H_{1/3}$ was estimated, from the H_{m0} values given by SwanOne, using the CWD method proposed by Batjjes and Groenendijk (2000). H_{m0} and $H_{1/3}$ were also compared using the test measurements without the structure (see Fig. III.21). In both cases the relationship was approximately $H_{1/3}=1.05H_{m0}$. $H_{2\%}$ was also compared with $H_{1/10}$ for both test measuments without structure and SwanOne estimations (see Fig. III.22); the relationship was approximately $H_{2\%}=1.07H_{1/10}$.

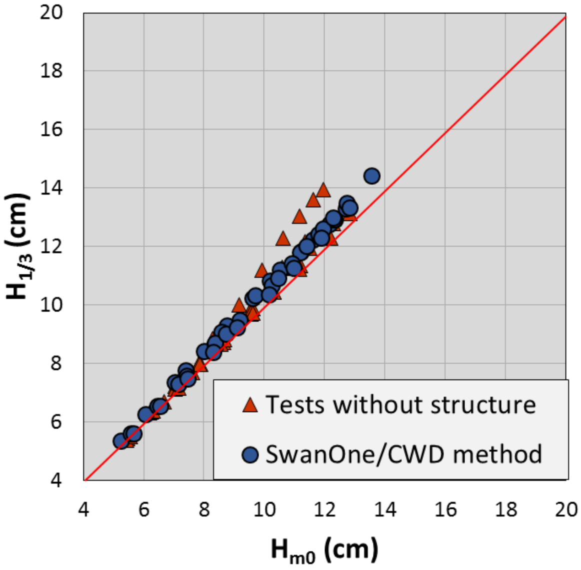

Figure III.21. H_{m0} versus $H_{1/3}$ measured in tests without structure and estimations given by the SwanOne model combined with the CWD method.

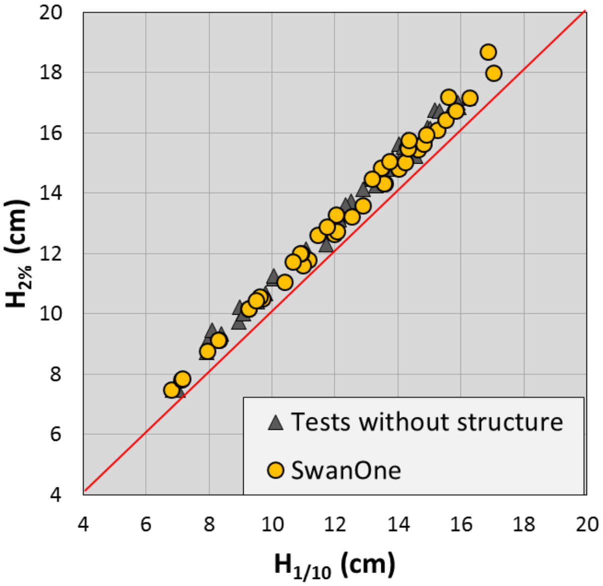

Figure III.22. $H_{1/10}$ versus $H_{2\%}$ measured in tests without structure and estimations given by the SwanOne model.

The influence of the water depth on wave height distribution variations was also analyzed for both experimental results and numerical simulations. Depending on test characteristics, H_{m0}, $H_{1/10}$ and $H_{2\%}$ increased or decreased along the flume due to shoaling or breaking processes. Close to the wavemaker, waves were Rayleigh-distributed ($H_{1/10}/H_{m0}≈1.27$ and $H_{2\%}/H_{m0}≈1.4$). In contrast, the ratio of $H_{1/10}/H_{m0}$ close to the breakwater model (G11 and G12) varied from 1.19 to 1.40 (physical tests) and from 1.20 to 1.32 (numerical simulations); the ratio of $H_{2\%}/H_{m0}$ close to the breakwater model (G11 and G12) varied from 1.24 to 1.51 (physical tests) and from 1.26 to 1.46 (numerical simulations).

Figs. III.23 and III.24 show the values of H_{m0}, $H_{1/10}$ and $H_{2\%}$, obtained in tests (Fig. III.23) and provided by the SwanOne numerical model (Fig. III.24) at G1 (wave generating zone) and at G11 and G12 (model zone), as a function of the water depth at the toe (h_s) and the surf similarity parameter (ξ_p). Lower h_s and ξ_p led to lower values of H_{m0} and $H_{2\%}$ at the toe of the structure.

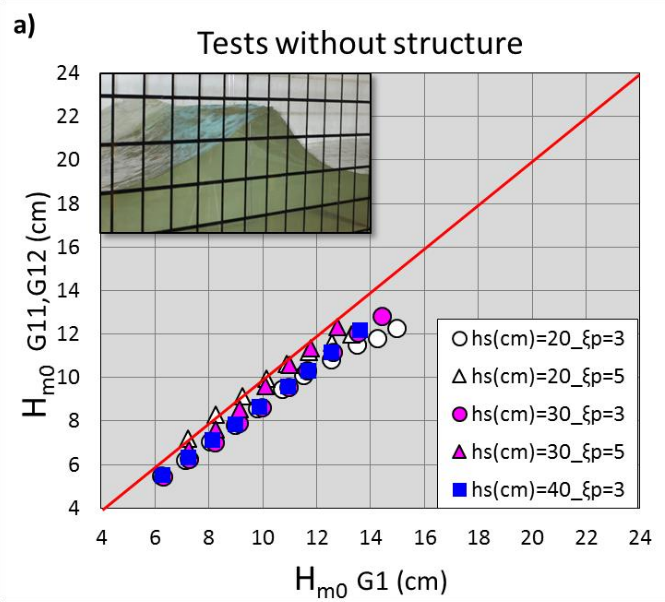

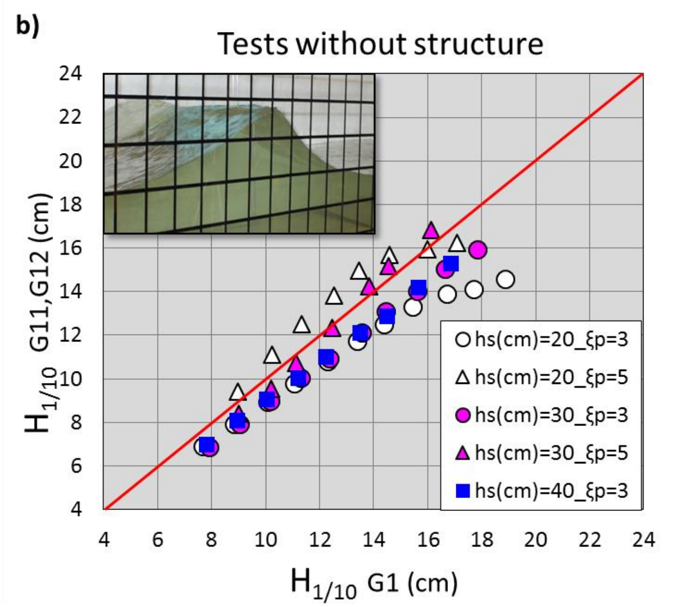

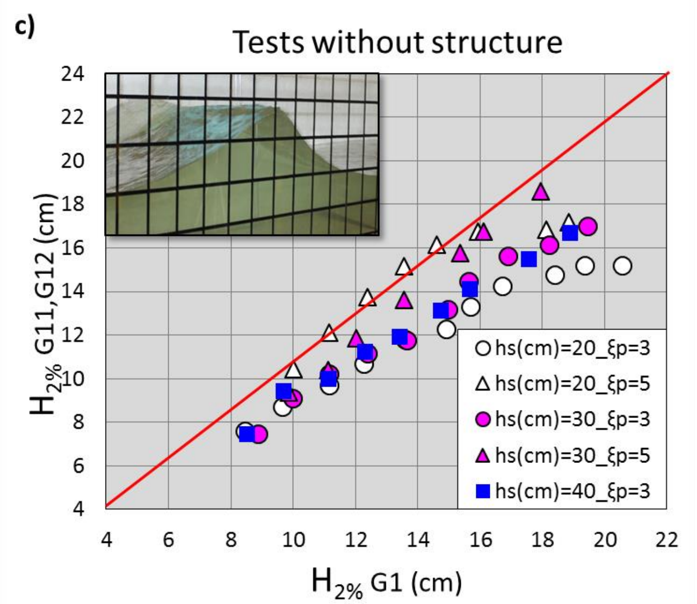

Figure III.23. Wave heights measured at the wave generating zone in tests without structure compared to the average of G11 and G12: (a) H_{m0}, (b) $H_{1/10}$ and (c) $H_{2\%}$.

a)

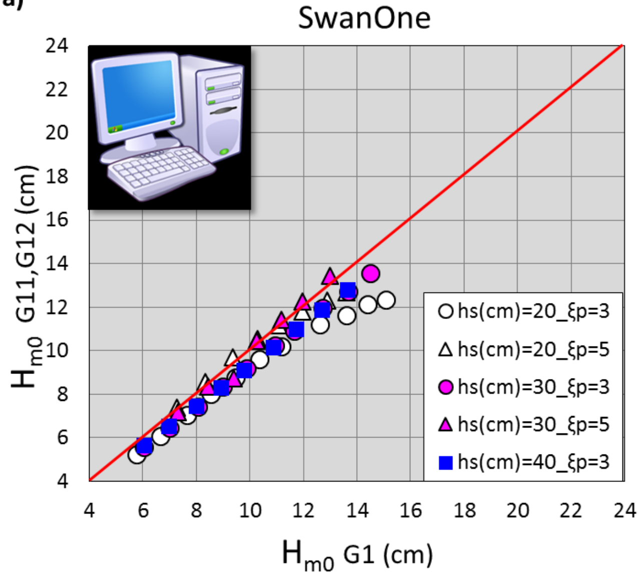
SwanOne
24
22
20
18
16
14
12
10
8
6
4
H_{m0} G11,G12 (cm)
4
6
8
10
12
14
16
18
20
22
24
H_{m0} G1 (cm)
○ hs(cm)=20_ξp=3
△ hs(cm)=20_ξp=5
● hs(cm)=30_ξp=3
▲ hs(cm)=30_ξp=5
■ hs(cm)=40_ξp=3

b)

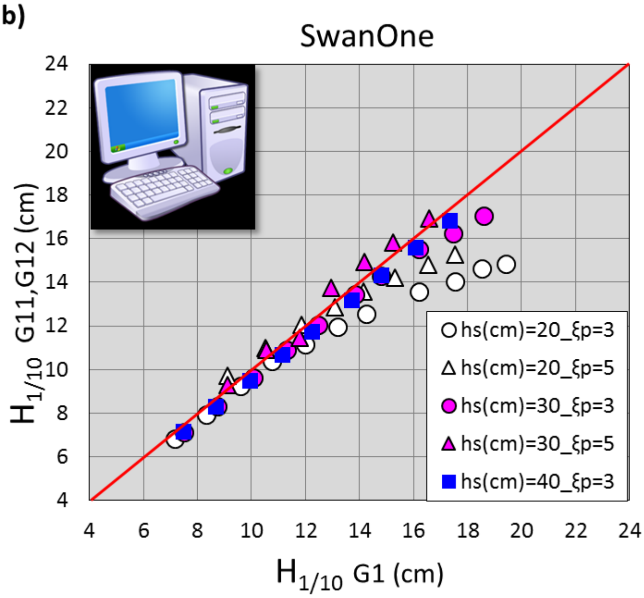
SwanOne
24
22
20
18
16
14
12
10
8
6
4
$H_{1/10}$ G11,G12 (cm)
4
6
8
10
12
14
16
18
20
22
24
$H_{1/10}$ G1 (cm)
○ hs(cm)=20_ξp=3
△ hs(cm)=20_ξp=5
● hs(cm)=30_ξp=3
▲ hs(cm)=30_ξp=5
■ hs(cm)=40_ξp=3

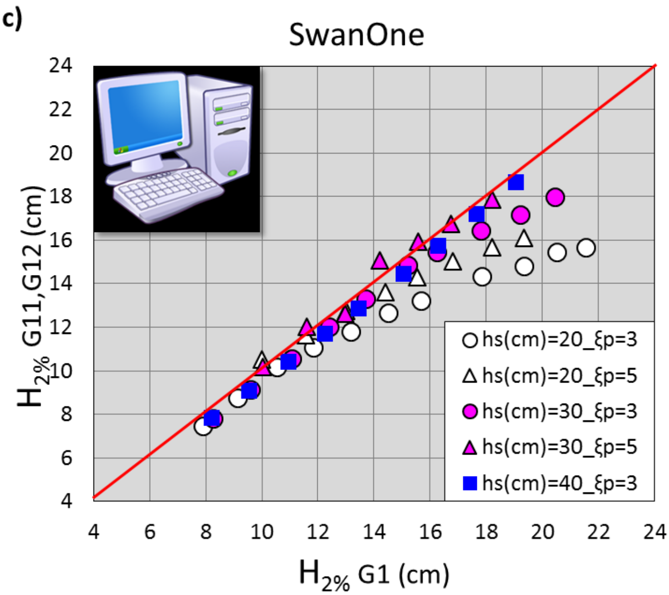

Figure III.24. SwanOne estimations at the G1 position compared to the average of G11 and G12: (a) H_{m0}, (b) $H_{1/10}$ and (c) $H_{2\%}$.

Figs. III.25 and III.26 show the average estimations of H_{m0} compared to the average estimations of $H_{1/10}$ and $H_{2\%}$, obtained in tests without the structure (Fig. III.25) and given by SwanOne (Fig. III.26) at the G11 and G12 positions. In general, lower h_s led to lower values of $H_{1/10}/H_{m0}$ and $H_{2\%}/H_{m0}$ at the toe of the structure (in numerical simulations this tendency is clearer due to the lower dispersion of results).

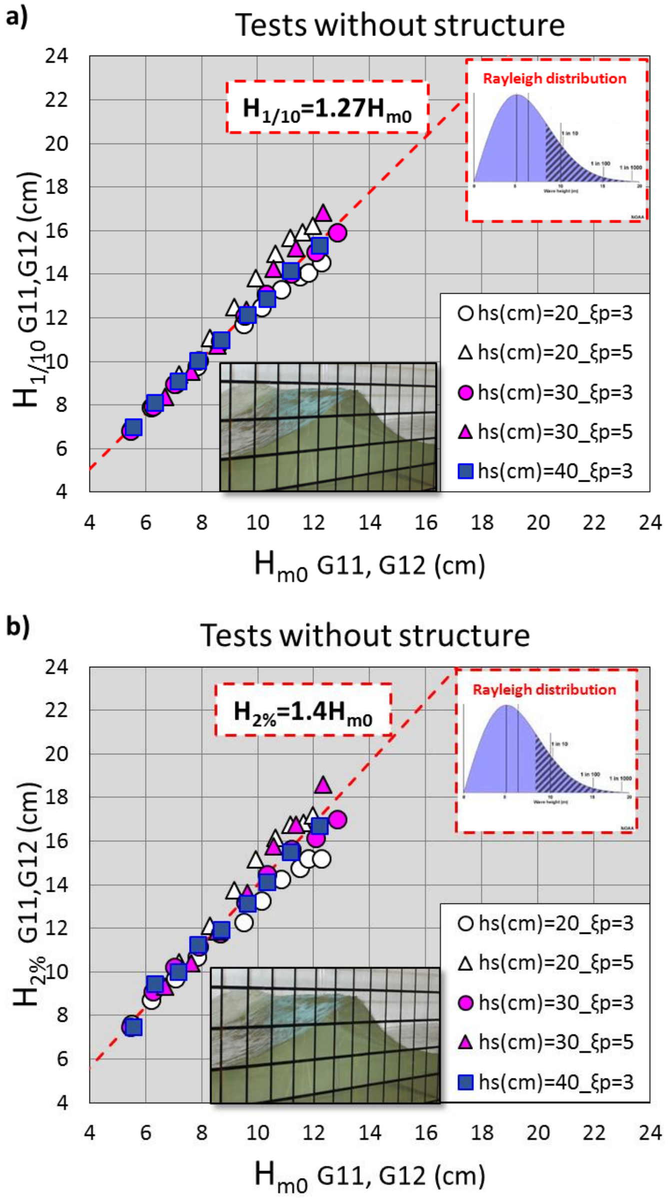

Figure III.25. Comparison of the mean values of H_{m0} and (a) $H_{1/10}$ and (b) $H_{2\%}$ measured at G11 and G12 in tests without structure.

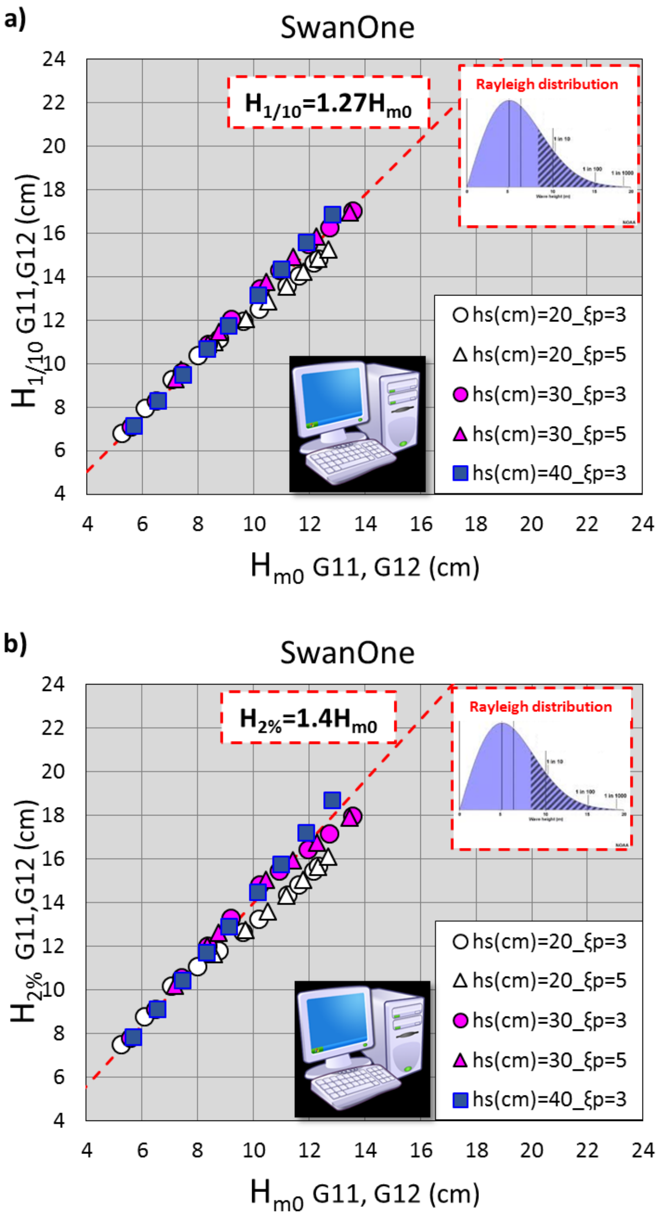

Figure III.26. Comparison of the mean values of H_{m0} and (a) $H_{1/10}$ and (b) $H_{2\%}$ estimated by SwanOne at G11 and G12 positions.

III.3.2. Damage analysis

After each test, cumulative armor damage was measured using the visual counting and virtual net methods (see Section III.2.4). The visual dimensionless damage parameter (S_v) and the equivalent dimensionless damage parameter (S_e) were obtained. Additionally, four qualitative armor-damage levels, described in Section II.3.4, were identified: Initiation of Damage (IDa), Initiation of Iribarren's Damage (IIDa), Initiation of Destruction (IDe), and Destruction (De).

Figs. III.27a and III.27b provide the stability numbers, $N_s=H/(\Delta D_{n50})$, obtained in test measurements and SwanOne estimations for Initiation of Damage (IDa) and Initiation of Destruction (IDe), when using $H=H_{m0}$ or $H=H_{2\%}$. The damage seems to be independent of wave steepness $s_p=2\pi H_{m0}/gT_p^2$. For $H=H_{m0}$, N_s (IDa)≈1.38 and N_s(IDe)≈2.09; for $H=H_{2\%}$, N_s(IDa)≈1.95 and N_s(IDe)≈2.89.

a)

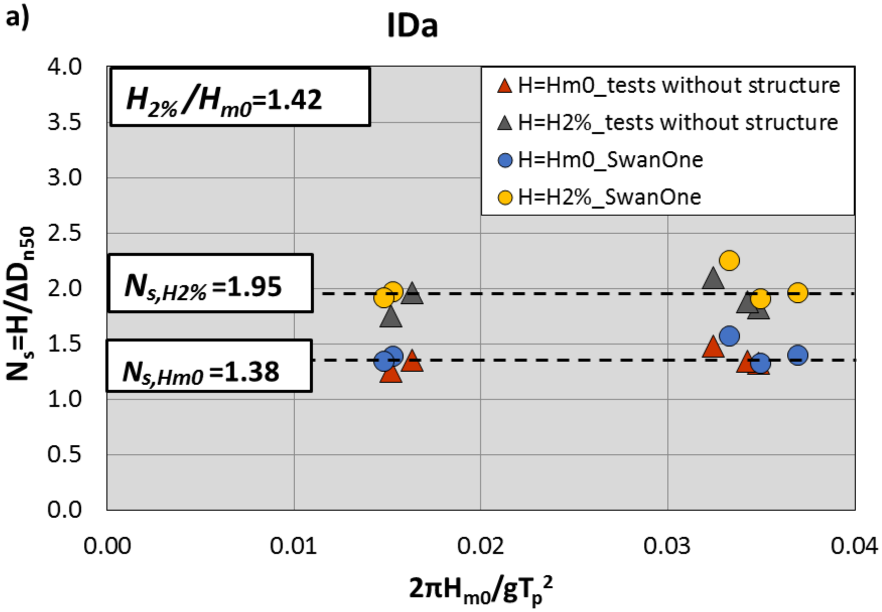

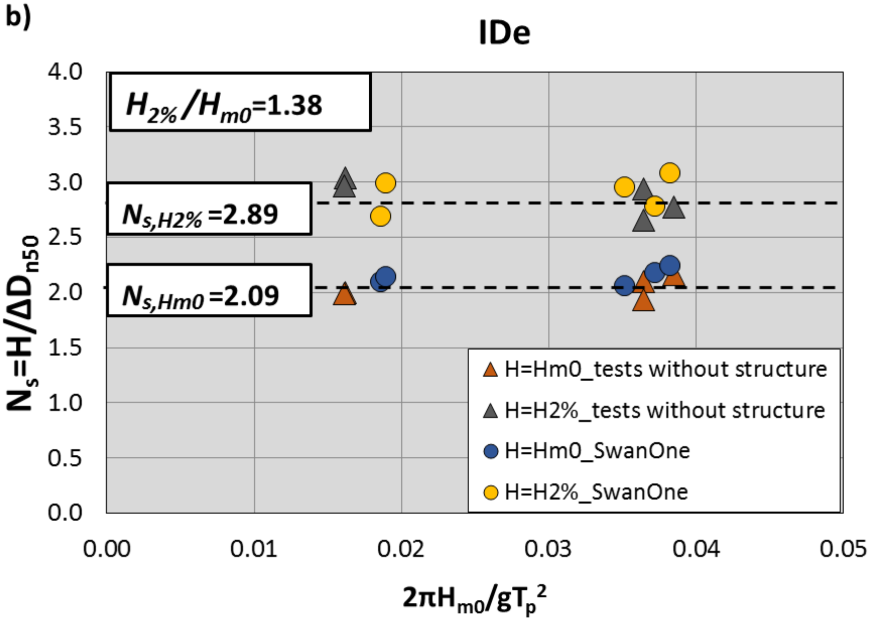

Figure III.27. Stability numbers for (a) IDa and (b) IDe.

Fig. III.28 shows photos taken perpendicularly to the armor slope with h_s(cm)=30 and ξ_p=3.0. Table III.4 provides the mean values for S_v and S_e obtained using the visual counting and virtual net methods for the IDa, IIDa and IDe identified after each test series.

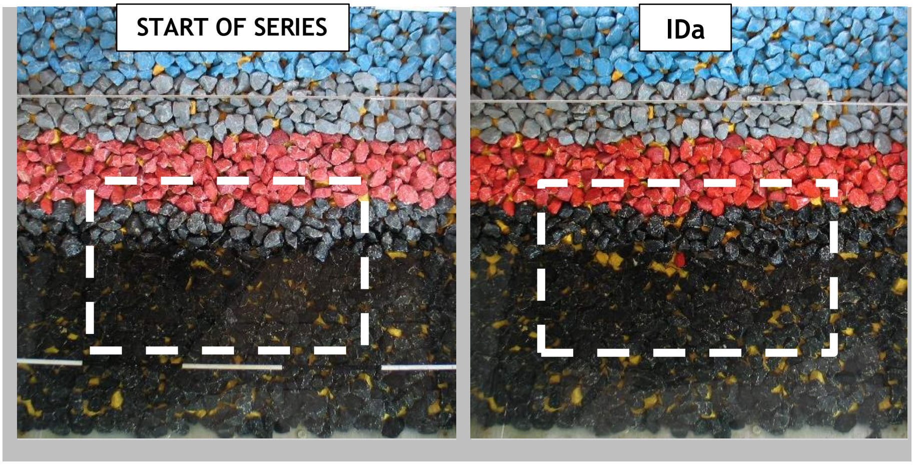

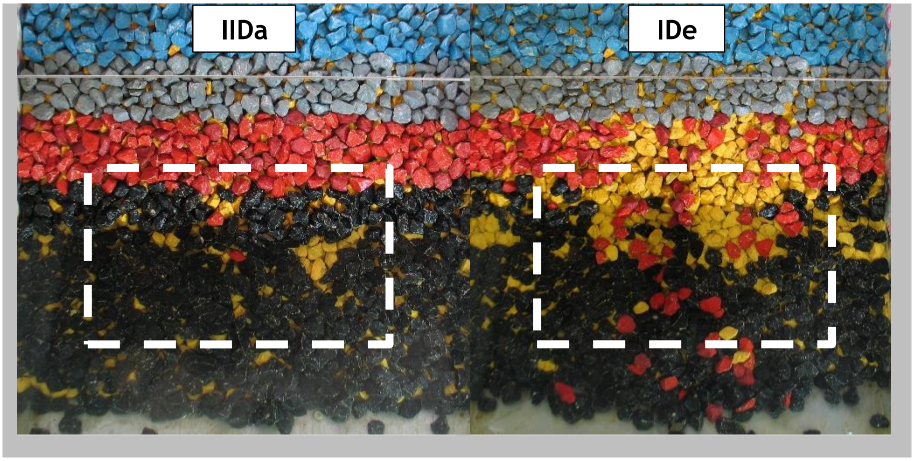

Figure III.28. Qualitative armor damage levels for series 3.

Series	Damage level	Armor damage measurements	
		Visual counting (S_v)	Virtual net (S_e)
1	IDa	0.3	0.3
	IIDa	2.7	2.7
	IDe	6.5	6.4
2	IDa	0.6	0.6
	IIDa	1.8	1.9
	IDe	3.8	4.4
3	IDa	0.5	0.7
	IIDa	1.3	1.3
	IDe	7.1	7.0
4	IDa	0.5	0.5
	IIDa	1.7	1.7
	IDe	7.5	7.4
5	IDa	0.2	0.3
	IIDa	1.5	1.5
	IDe	6.0	6.0

Table III.4. Mean values of dimensionless armor damage using visual counting and virtual net methods.

Table III.4 indicates that S_v and S_e were very similar; heterogeneous packing was not relevant, as armor damage was caused by rock extraction.

Figs. III.29 and III.30 show the S_e after each test as a function of the stability number, $N_s=H/(\Delta D_{n50})$, for $H=H_{m0}$, $H=H_{1/10}$ and $H=H_{2\%}$ obtained from test measurements (Fig. III.29) and SwanOne estimations (Fig. III.30) at G11 and G12 positions. S_e and N_s showed a potential relationship; the lower the dispersion, the better the estimation $S_e(N_s)$. Figs. III.29 and III.30 show that H_{m0} seems to be a better wave height estimator than $H_{1/10}$ and $H_{2\%}$ for the armor damage. A larger dispersion was observed for the experimental wave measurements compared to the numerical simulations. Results with $H_{1/10}$ were very similar to $H_{2\%}$.

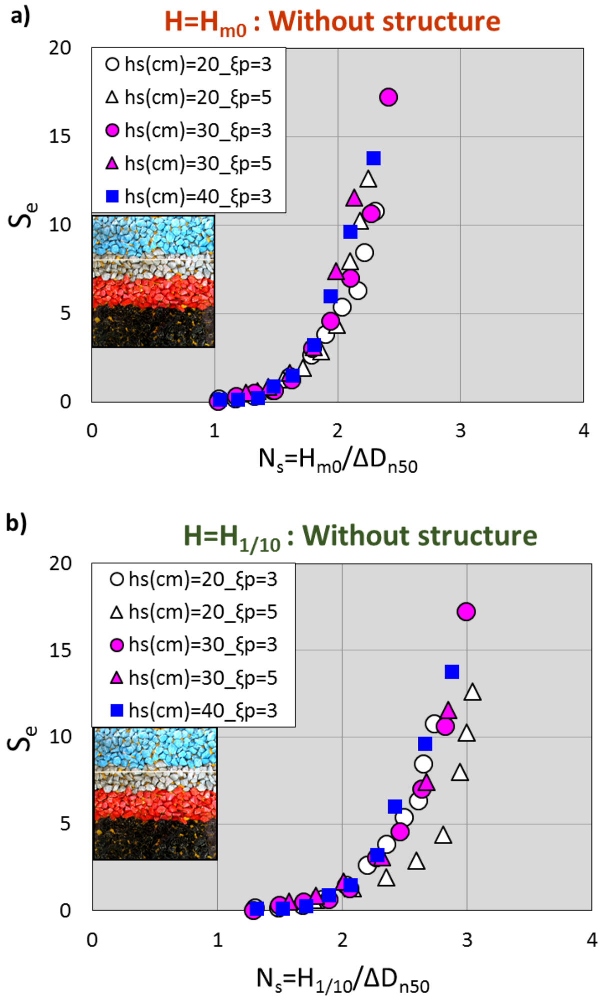

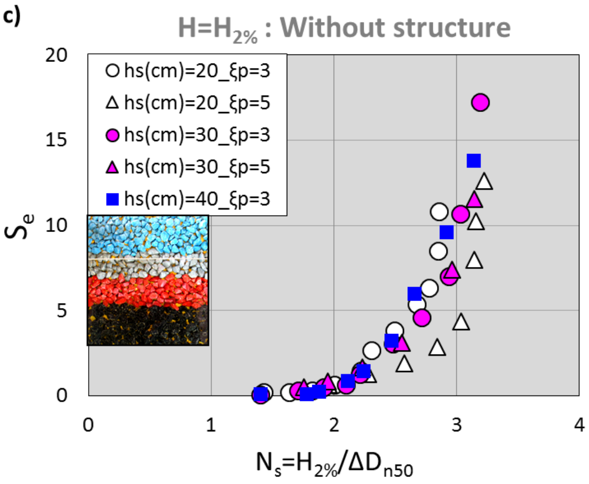

Figure III.29. Armor damage (S_e) as a function of the stability number ($N_s=H/(\Delta D_{n50})$) measured in tests without structure when using (a) $H=H_{m0}$, (b) $H=H_{1/10}$ and (c) $H=H_{2\%}$ at G11 and G12 positions.

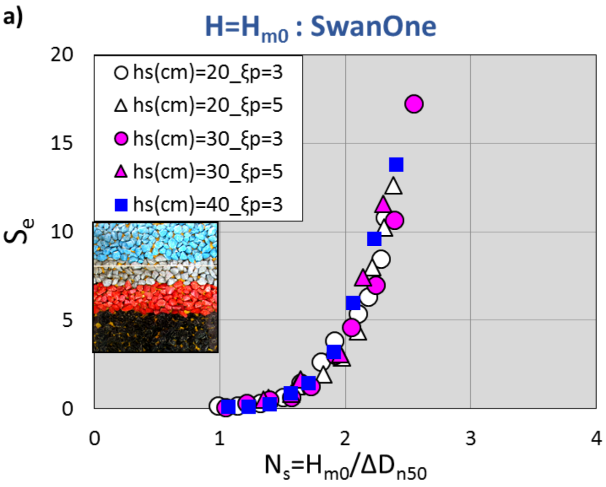

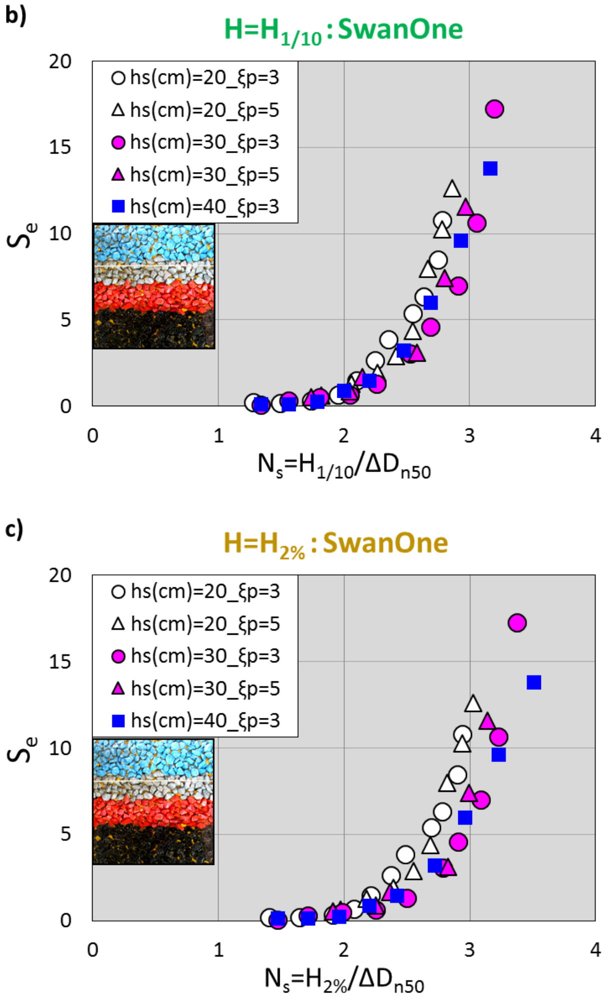

Figure III.30. Armor damage (S_e) as a function of the stability number ($N_s=H/(\Delta D_{n50})$) estimated by SwanOne when using (a) $H=H_{m0}$, (b) $H=H_{1/10}$ and (c) $H=H_{2\%}$ at G11 and G12 positions.

III.4. New hydraulic stability formula for mound breakwaters

III.4.1. A new hydraulic stability formula

A new hydraulic stability formula was developed to include the most relevant parameters affecting the stability of rock armors attacked by breaking waves (m=1/50 bottom slope). The stability number, $N_s=H/(\Delta D_{n50})$, the local wave steepness based on the mean wave length at the toe of the structure, $s_{m,toe}=H_{m0}/L_{m,toe}$, and the water depth at the toe of the structure, h_s, were initially considered as potential explanatory parameters of armor damage, S_e. The initial model used to characterize armor damage was based on the linear model given by Eq. III.12:

$$\log(S_e)=k_1+k_2\log\left(\frac{H}{\Delta D_{n50}}\right)+k_3\log\left(s_{m,toe}\right)+k_4\log\left(h_s\right) \qquad [III.12]$$

in which k_1, k_2, k_3 and k_4 are four fitting parameters.

A t-student test (5% significance error) was used later to select significant variables. Table III.5 and Figs. III.31 and III.32 show the t-values and probability values for the analysis conducted with $H=H_{m0}$, $H=H_{1/10}$ and $H=H_{2\%}$ measured in tests without the structure and estimated by SwanOne at the positions of G11 and G12. For $H=H_{m0}$, $H=H_{1/10}$ and $H=H_{2\%}$, the wave steepness and the water depth at the toe were eliminated in the statistical analysis.

Tests without structure						
Variables	H_{m0}		$H_{1/10}$		$H_{2\%}$	
	t-value	Pr > |t|	t-value	Pr > |t|	t-value	Pr > |t|
log ($H/(\Delta D_{n50})$)	35.015	<0.0001	27.236	<0.0001	24.099	<0.0001
log($s_{m,toe}$)	-0.440	0.6622	-0.275	0.7845	-0.745	0.4609
log(h_s)	2.349	0.0238	2.300	0.0267	1.696	0.0977
SwanOne						
Variables	H_{m0}		$H_{1/10}$		$H_{2\%}$	
	t-value	Pr > |t|	t-value	Pr > |t|	t-value	Pr > |t|
log ($H/(\Delta Dn50)$)	32.088	<0.0001	26.306	<0.0001	22.337	<0.0001
log($s_{m,toe}$)	-1.409	0.1664	-1.623	0.1124	-1.986	0.0539
log(h_s)	1.376	0.1764	-0.193	0.8482	-0.699	0.4888

Table III.5. t-student analysis values.

The P-values were lower than 5% only for the variable log $(H/(\Delta D_{n50}))$ when using $H=H_{m0}$, $H=H_{1/10}$ and $H=H_{2\%}$ measured in tests and estimated with SwanOne. Thus, the wave steepness and water depth at the toe were eliminated in the statistical analysis, and Eq. III.12 was re-written as follows, depending only on the stability number:

$$S_e = 10^{k_1}\left(\frac{H}{\Delta D_{n50}}\right)^{k_2} = K\left(\frac{H}{\Delta D_{n50}}\right)^{k_2} \qquad [III.13]$$

Eq. III.13 was calibrated using $H=H_{m0}$, $H=H_{1/10}$ and $H=H_{2\%}$, obtained with both laboratory measurements and SwanOne estimations at G11 and G12 positions (average value). When using $H=H_{m0}$ measured in tests without the structure, the calibration led to K =0.083 and $k_2=6$; when using $H=H_{1/10}$, the calibration led to K =0.012 and $k_2=6$; when using $H=H_{2\%}$, the calibration led to K =0.019 and $k_2=6$. For SwanOne estimations, when using $H=H_{m0}$, the calibration led to K =0.066 and $k_2=6$; when using $H=H_{1/10}$, the calibration led to K =0.016 and $k_2=6$; when using $H=H_{2\%}$, the calibration led to K =0.01 and $k_2=6$. Fig. III.31 compares the measured armor damage (S_e) and the stability number $N_s=H/(\Delta D_{n50})$ for $H=H_{m0}$, $H=H_{1/10}$ and $H=H_{2\%}$ obtained from test measurements and SwanOne estimations. The calibrated equations are also depicted in Fig. III.31.

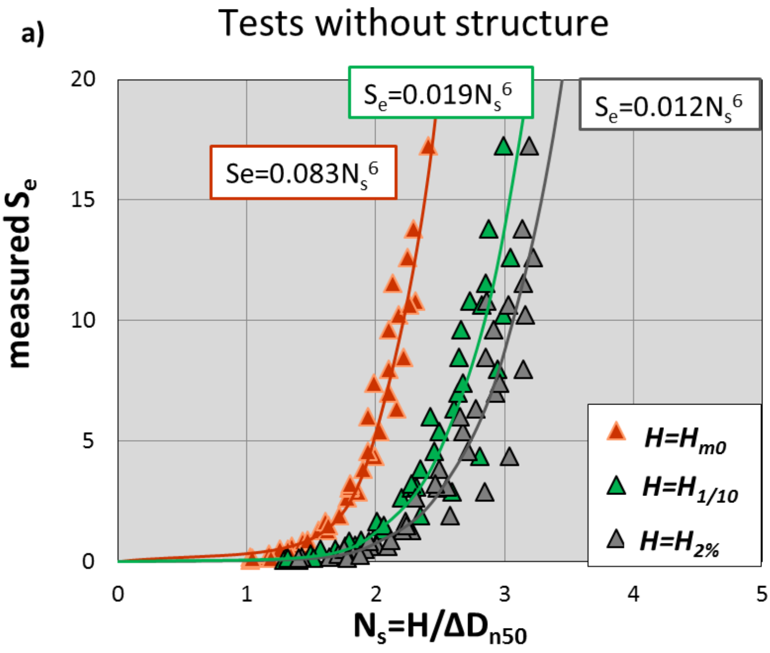

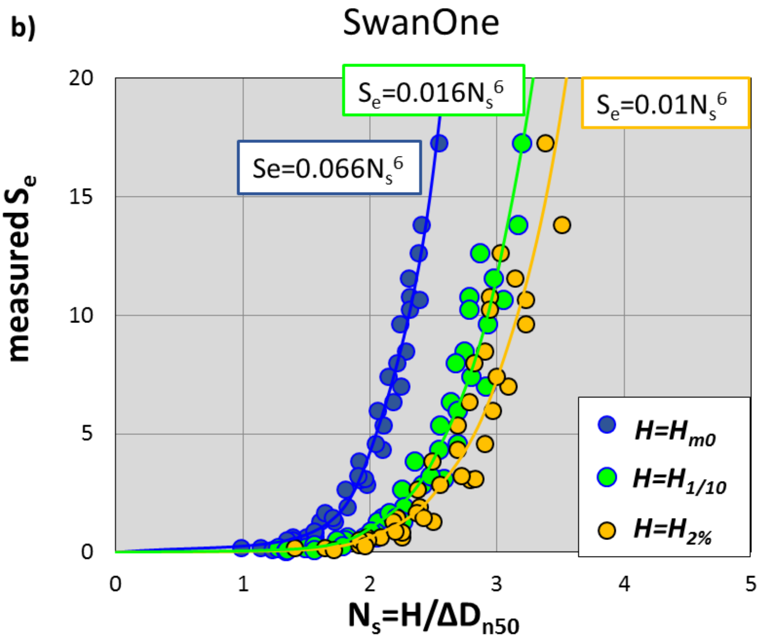

Figure III.31. Armor damage ($S_e^{1/6}$) versus the stability number N_s=H/(ΔD$_{n50}$) for H=H$_{m0}$, H=H$_{1/10}$ and H=H$_{2\%}$ obtained at G11 and G12 positions from (a) tests without structure and (b) SwanOne estimations.

Fig. III.32 compares the linearized armor damage ($S_e^{1/6}$) and the stability number N_s=H/(ΔD$_{n50}$) for H=H$_{m0}$, H=H$_{1/10}$ and H=H$_{2\%}$ obtained from test measurements and SwanOne estimations at the positions of G11 and G12, with the mean values of S_e measured during tests for IDa, IIDa and IDe: S_e(IDa)=0.5, S_e(IIDa)=1.8 and S_e(IDe)=6.2.

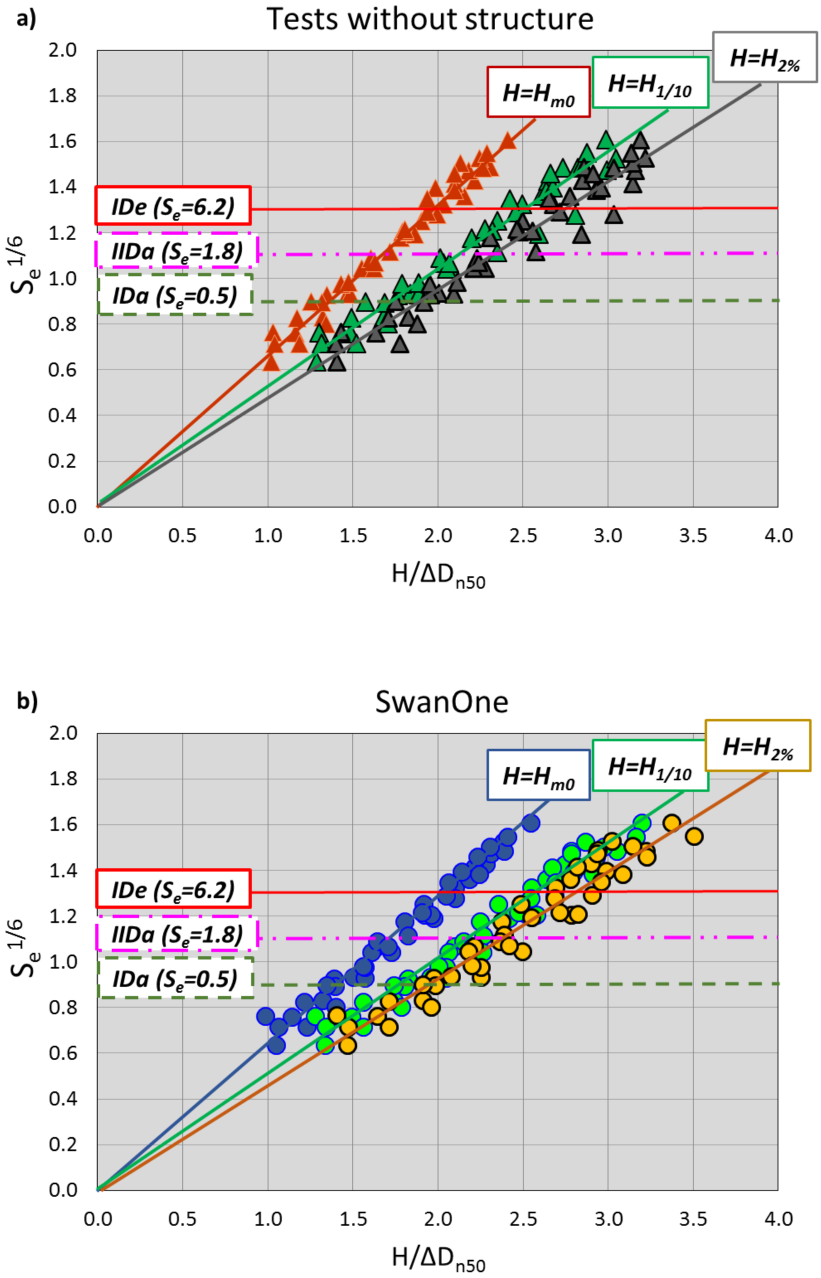

Figure III.32. Linearized armor damage ($S_e^{1/6}$) versus the stability number $N_s=H/(\Delta D_{n50})$ for $H=H_{m0}$, $H=H_{1/10}$ and $H=H_{2\%}$ obtained at G11 and G12 positions from (a) tests without structure and (b) SwanOne estimations.

To analyze the variability in the errors when considering H_{m0}, $H_{1/10}$ or $H_{2\%}$, a bootstrap resample technique was used following Van Gent et al. (2007). A bootstrapping resample is a random selection of N data taken from the original N dataset, with the probability 1/N that a particular datum is selected each time. In the case of this study, 1000 resamples were considered with S_e estimated by Eq. III.13 with $H=H_{m0}$, 1000 resamples for S_e estimated by Eq. III.13 with $H= H_{1/10}$ and 1000 resamples for S_e estimated by Eq. III.13 with $H=H_{2\%}$. The rMSE between measured and estimated S_e of each resample was used to define the discrete frequency histograms (see Figs. III.33 and III.34). The rMSE distributions followed a normal distribution when using $H=H_{m0}$, $H=H_{1/10}$ and $H=H_{2\%}$ (measurement and numerical simulations at wave gauges G11 and G12) to estimate armor damage (S_e). The errors were much lower with $H=H_{m0}$ for both test measurements and SwanOne estimations.

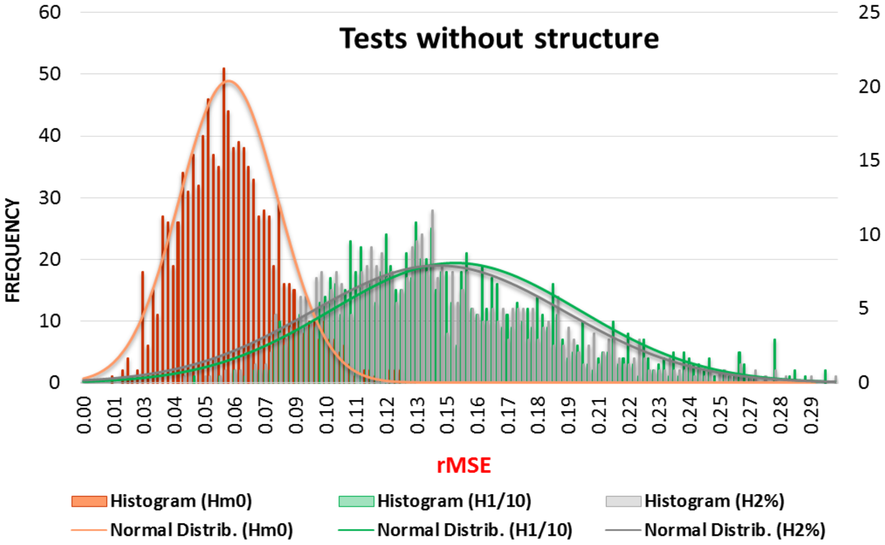

Figure III.33. rMSE frequency histograms for measured and estimated S_e when using Eq. III.13 with $H=H_{m0}$, $H=H_{1/10}$ and $H=H_{2\%}$ measured in tests without structure.

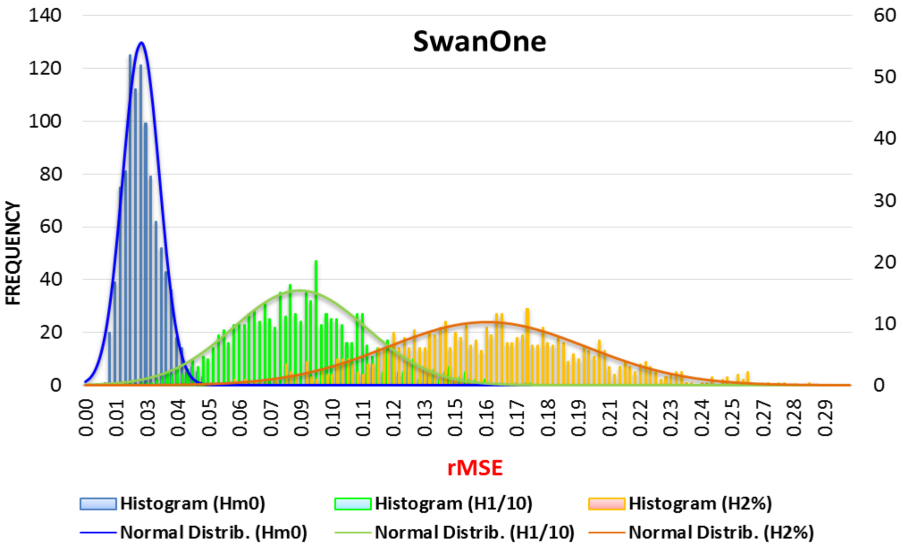

Figure III.34. rMSE frequency histograms for measured and estimated S_e when using Eq. III.13 with $H=H_{m0}$, $H=H_{1/10}$ and $H=H_{2\%}$ estimated by SwanOne.

Fig. III.35 shows the cross validation for measured S_e and S_e estimated by Eq. III.13 when using $H=H_{m0}$, $H=H_{1/10}$ and $H=H_{2\%}$ measured in tests (Fig. III.35a) and estimated by SwanOne (Fig. III.35b) at G11 and G12 positions. The agreement between measured and estimated S_e was reasonable in all cases (rMSE lower than 15%). However, S_e errors were lower when using $H=H_{m0}$ (rMSE=0.057 and r=0.973 with test measurements; rMSE=0.022 and r=0.989 with SwanOne estimations) than when using $H=H_{1/10}$ (rMSE =0.142 and r=0.926 with test measurements; rMSE=0.080 and r=0.959 with SwanOne estimations) and $H=H_{2\%}$ (rMSE=0.137 and r=0.927 with test measurements; rMSE=0.151 and r=0.922 with SwanOne estimations). Thus, H_{m0} was selected to describe armor damage. Due to the similarity between the wave heights measured in laboratory tests and those obtained in the numerical simulations, H_{m0} given by SwanOne was finally chosen in this study to describe S_e in Eq. III.13.

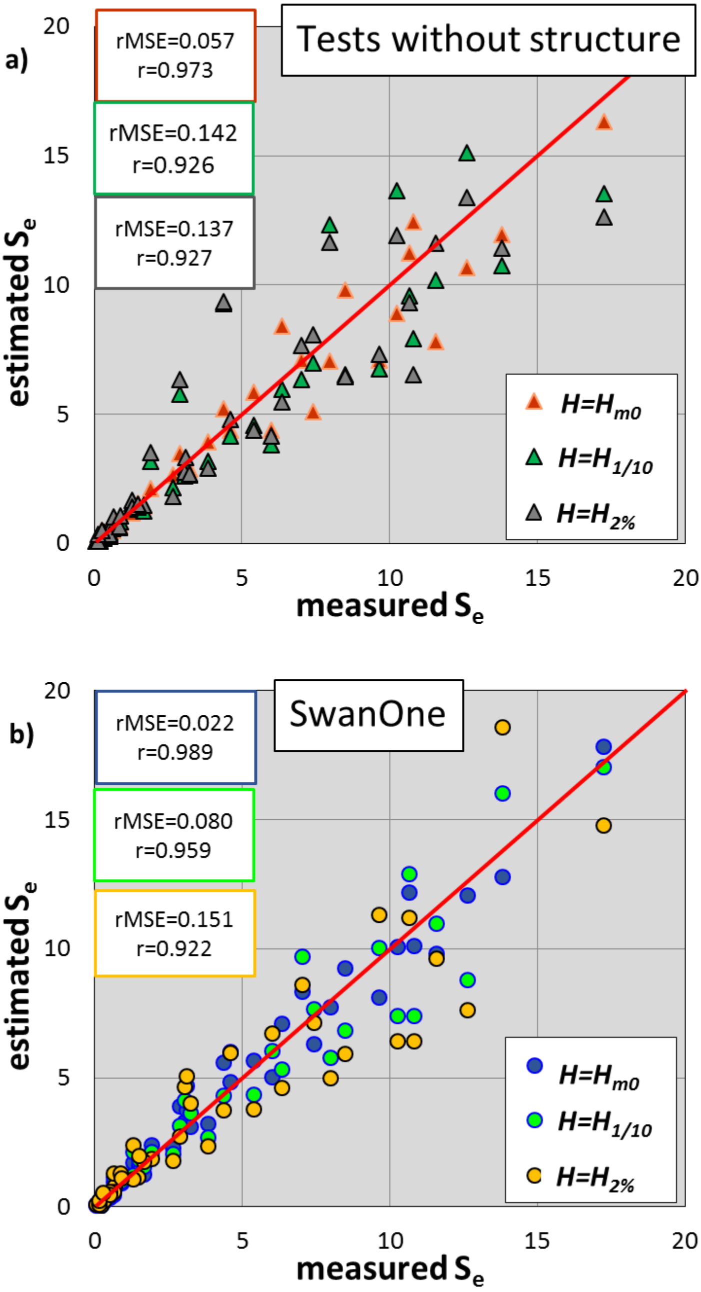

Figure III.35. Measured armor damage (S_e) versus S_e estimated by Eq. III.13 for $H=H_{m0}$, $H=H_{1/10}$ and $H=H_{2\%}$ obtained at G11 and G12 positions from (a) test measurements and (b) SwanOne estimations.

The aforementioned analysis was conducted with wave measurements and estimations at wave gauges G11 and G12, situated at a distance of 0.8m and 0.5m seaward from the structure toe, respectively. However, for design purposes it is necessary to specify the exact point at which the wave parameters are determined when dealing with breaking waves. In order to identify the optimum location to determine H_{m0} to calculate armor damage, this characteristic wave height was also estimated by SwanOne model at five points: just at the toe of the structure, and at a distance of h_s, 2 h_s, 3 h_s and 4 h_s seaward from the structure toe ($d^*=0$, h_s, 2 h_s, 3 h_s and 4 h_s).

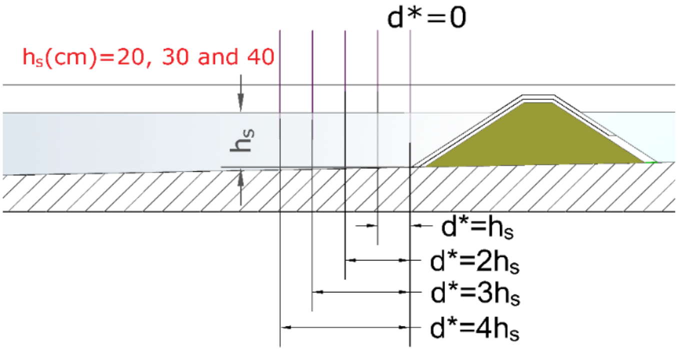

Figure III.36. Sketch of the distances seaward from the toe structure (d^*) to determine the optimum location for wave parameter calculation in breaking wave conditions.

Table III.6 shows the optimum values of K and k_2 in Eq. III.13 when using H_{m0} estimated by SwanOne at the specified locations ($d^*=0$, h_s, 2 h_s, 3 h_s and 4 h_s). The rMSE and the r between the values of S_e measured in tests and the S_e estimated by Eq. III.13 for each case are also listed in Table III.6.

Seaward distance from the toe, d*	K	k_2	rMSE	r
0 (TOE)	0.071	6.0	0.031	0.984
hs	0.069	6.0	0.026	0.987
2hs	0.068	6.0	0.024	0.987
3hs	0.066	6.0	0.023	0.988
4hs	0.065	6.0	0.024	0.987

Table III.6. Optimum values of K and k_2 in Eq. III.13 for H_{m0} estimated by SwanOne at a seaward distance d* from the toe of the structure, and rMSE and r between measured S_e and estimated S_e given by Eq. III.13.

The best agreement was found for H_{m0} estimated at a distance of three times the water depth at the toe ($d^*=3h_s$) seaward from the structure (rMSE=0.023 and r=0.988). This distance corresponds approximately to the distance of $5H_s$ proposed by Goda (1985) for vertical breakwaters, when considering H_s in breaking wave conditions. Thus, H_{m0} estimated at a distance of $d^*=3h_s$ seaward from the structure toe was finally selected in this study to describe the armor damage, S_e, given by Eq. III.13 with K =0.066 and $k_2=6.0$. Note that for m=1/50, the errors were low and very similar for all cases ($0.023 \leq rMSE \leq 0.031$ and $0.984 \leq r \leq 0.988$). However, with steeper bottom slopes, significant differences may be observed when considering different points to estimate the design wave parameters.

Fig. III.37 shows the S_e measured after each test as a function of the stability number, $N_s=H_{m0}/(\Delta D_{n50})$, for H_{m0} estimated by SwanOne at the distance of $3h_s$ seaward from the structure toe.

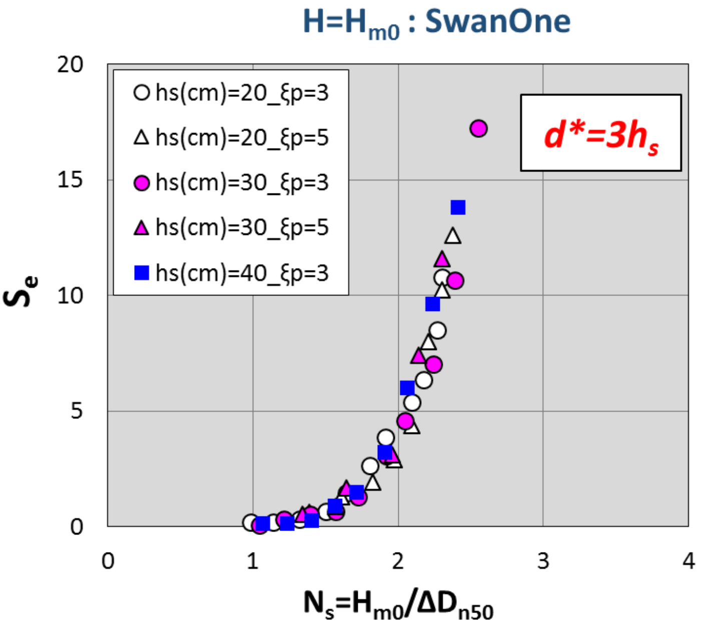

Figure III.37. Measured armor damage (S_e) as a function of the stability number ($N_s=H/(\Delta D_{n50})$) estimated by SwanOne when using $H=H_{m0}$ at a distance of $d^*=3h_s$ seaward from the structure toe.

III.4.1.1. Confidence intervals

The 90% confidence interval for the armor damage estimation given by Eq. III.13, with $H=H_{m0}$ estimated by SwanOne at $3h_s$ seaward from the structure toe, K=0.066, and $k_2=6.0$, is given by Eq. III.14, assuming a Gaussian error distribution.

$$S_e\Big|_{5\%}^{95\%} = S_e \pm 1.64 \cdot \sqrt{VAR(\varepsilon)} \qquad \text{[III.14]}$$

where VAR(ε) is the variance in the estimation errors, considered as a linear function of S_e. S_e data were ordered and grouped to nine data sets, and the MSE was calculated for each data set (see Fig. III.38). As the MSE increases with increasing S_e, the variance in the errors can be estimated by:

$$VAR(\varepsilon) = 0.1 \cdot S_e \qquad \text{[III.15]}$$

where S_e is given by Eq. III.13 with $H=H_{m0}$, $K=0.066$ and $k_2=6.0$. The 90% confidence interval is given by:

$$S_e\Big|_{5\%}^{95\%} = S_e \pm 1.64 \cdot \sqrt{(0.1 \cdot S_e)} = S_e \pm 0.52 \cdot \sqrt{S_e} \qquad \text{[III.16]}$$

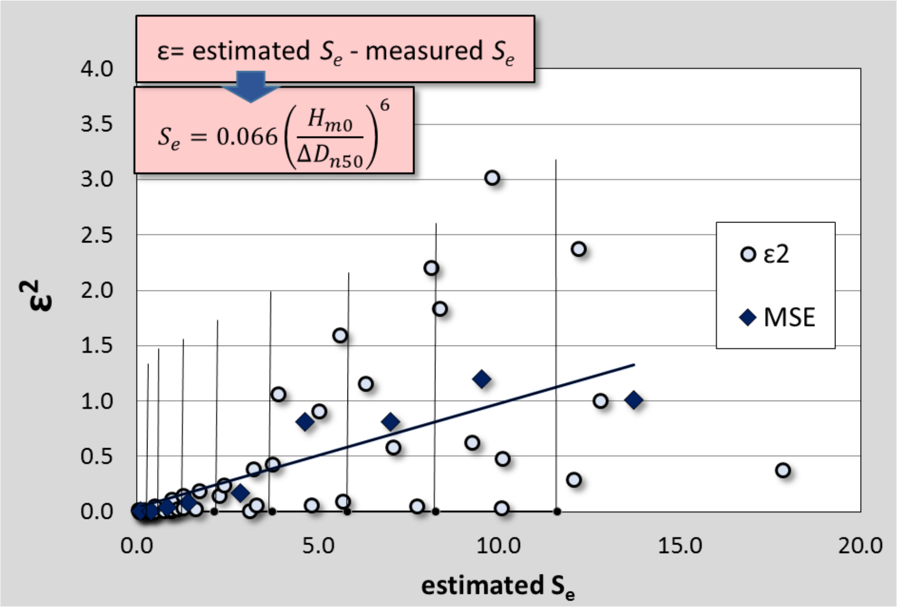

Figure III.38. Squared armor damage errors as a function of the S_e estimated by Eq. III.13 with $H=H_{m0}$, $K=0.066$ and $k_2=6.0$.

Fig. III.39 compares the measured S_e and that estimated by Eq. III.13 with $H=H_{m0}$ given by SwanOne at $d^*=3h_s$. Additionally, the 90% confidence interval given by Eq. III.16 is depicted in Fig. III.39. The rMSE=0.023 and the r=0.988 were used to determine the goodness of fit between the values of S_e measured in tests and the S_e given by Eq. III.13.

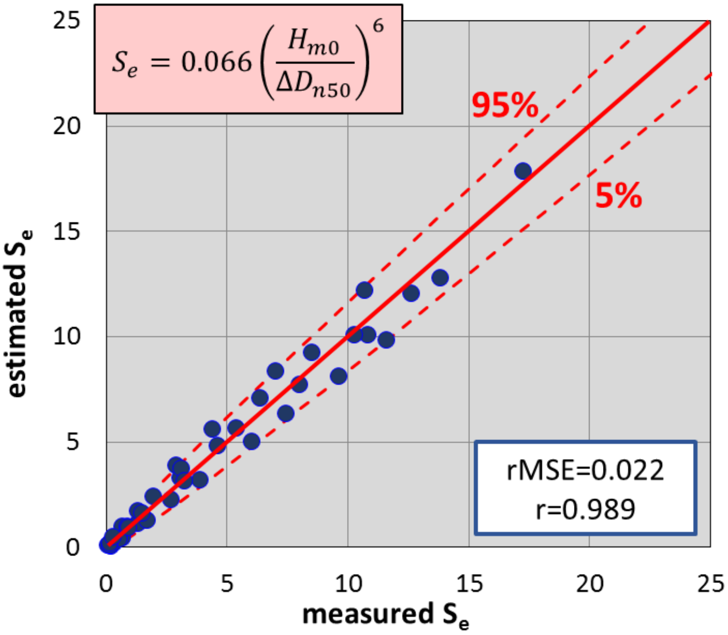

Figure III.39. Measured S_e versus S_e estimated by Eq. III.13 with $H=H_{m0}$ given by SwanOne at $3h_s$ seaward from the toe structure, K=0.066 and k_2=6.0.

III.4.1.2. Comparison of measurements with existing formulas

Different formulas are commonly used to estimate rock armor damage although not all of them should be used for breaking wave conditions, as described in Section II.4 (Eqs. II.20 to II.25). Eqs. II.20 and II.25 were developed for non-breaking wave conditions; Eqs. II.21a and II.21b given by Van der Meer (1988a) were developed from irregular tests, mostly in non-breaking wave conditions, and adapted to breaking wave conditions replacing H_s by $H_{2\%}/1.4$ (note that $H_{2\%}/\ H_s$ =1.4 is only valid for Rayleigh distribution); Eqs. II.23a and II.23b given by Van Gent et al. (2003) were obtained by modifying Eqs. II.21a and II.21b to consider the spectral wave period $T_{m-1,0}$; Eq. II.22 given by Melby and Kobayashi (1998), and Eq. II.24, given by Van Gent et al. (2003), were specifically obtained from tests developed in breaking and non-breaking wave conditions.

In this section, a comparison is made between the armor damage measured in the present study and the predictions given by Eqs. II.20 to II.25 which can be re-written in terms of armor damage, S. To this end, the dimensionless armor damage S_v, similar to S_e measured in the laboratory tests, was related to the dimensionless armor damage $S=S_e$ used in Eqs. II.20 to II.25.

To estimate the evolution of armor damage in a succession of sea states using Eqs. II.21a, II.21b, II.23a, II.23b and II.24, the methodology proposed by Van der Meer (1985) was followed, with a permeability value of P=0.4 (permeable filter and core):

Step 1. For the first sea state composed of N_z waves, Eqs. II.21a, II.21b, II.23a, II.23b and II.24 were directly used to estimate armor damage, S, with the wave parameters estimated by the SwanOne model.

Step 2. For the next sea state, an equivalent number of waves, N_{zi}, which produce the damage estimated in the previous sea state was computed using Eqs. II.21a, II.21b, II.23a, II.23b and II.24 with the new sea state parameters. The aforementioned waves were added to the number of waves in the present sea state, N_{z2}, to calculate the final damage using Eqs. II.21a, II.21b, II.23a, II.23b and II.24.

Step 3. Step 2 was repeated until the final sea state.

Eq. II.29 was used as in Appendix 2, but with the K_D value proposed by USACE (1975) for breaking waves and rough angular randomly-placed rocks with $H=H_s$ (K_D=3.5), and the K_D value proposed by USACE (1984) for breaking waves and rough angular randomly-placed rocks with $H=H_{1/10}$ (K_D=2.0).

Figs. III.40a and III.40b show the linearized armor damage, $S^{1/6}$, measured in laboratory tests and the predictions given by Eqs. II.20 to II.25. The 90% confidence intervals of the proposed equation (Eq. III.13) given by Eq. III.16 are also depicted in Fig. III.40. The significant wave height $H_s=H_{1/3}$ used in Eq. II.20 (USACE 1975) and Eq. II.24 was obtained from the average spectral wave height (H_{m0}) estimated by SwanOne at the structure toe, using the CWD method proposed by Battjes and Groenendijk (2000). For Eq. II.22, $H_s=H_{1/3}$ was estimated at a distance of 5.7hs seaward from the toe, following the methodology for the tests conducted by Melby and Kobayashi (1998). H_s was replaced by $H_{2\%}/1.4$ in Eqs. II.21a and II.21b, recommended value for depth-limited waves, with $H_{2\%}$ estimated by SwanOne at the toe. H_{50} was considered equal to $H_{2\%}$ in Eq. II.25, as in Vidal et al. (2006), when N_z=1000. $H_{1/10}$ used in Eq. II.20 by USACE (1984) was obtained from SwanOne at the toe (note that $H_{1/10}\approx1.27H_s$ is only valid for a Rayleigh distribution).

A clear difference in predictions given by Eq. II.20 can be observed in Fig. III.40a when using USACE (1975) and USACE (1984). Eq. II.20 (USACE, 1975) gave fair predictions for low levels of armor damage but underestimated high levels of armor damage (implicit safety factor lower than 1.0). Eq. II.20 (USACE, 1984) significantly overestimated armor damage for all damage levels (implicit safety factor much higher than 1.0). Eq. II.20 was based on regular tests in non-breaking wave conditions. USACE (1984) imposed much higher safety factors than USACE (1975).

Eq. II.24 given by Van Gent et al. (2003) overestimated armor damage. Eq. II.24 was developed from irregular tests in breaking and non-breaking wave conditions. Eq. II.24 is valid for bottom slopes m=1/30 and 1/100, armor slopes cotα=2 and 4, stability number in the range of $0.5\leq H_s/\Delta D_{n50}\leq4.5$ and $1.5<h_s/\Delta D_{n50}<11$. Gómez-

Martín (2005) pointed out that armor damage measured with profiles and visual counting method may differ up to 20%.

The estimations given by Eqs. II.21 to II.23 and II.25 showed two tendencies depending on the surf similarity parameter used in tests. For tests conducted with ξ_p=5.0, Eqs. II.21a, II.21b, II.22, II.23a, II.23b and II.25 gave higher values of damage than for tests conducted with ξ_p=3.0. For ξ_p=5.0, Eqs. II.21a, II.21b, II.23a and II.23b overestimated armor damage; however, for tests conducted with ξ_p=3.0, Eqs. II.23a and II.23b also overestimated armor damage, but Eqs. II.21a and II.21b gave good predictions (most values fall within the 90% confidence interval of Eq. III.13). Eq. II.22 underpredicted armor damage for high damage levels, and Eqs. II.25a and II.25b overpredicted armor damage for low damage values, but underpredicted armor damage for high damage values, as in Vidal et al. (2006) (note that Eqs. II.25a and II.25b are only valid for non-breaking conditions).

Fig. III.40 shows that the estimations given by Eqs. II.20 to II.25 led to a significant scatter for most of the test results used in this study. Note that Eqs. II.21a, II.21b, II.23a, II.23b and II.24 were used applying a method to estimate the equivalent numbers of waves required to consider the cumulative damage caused by a succession of sea states. Eq. II.22 was also based on a method proposed by Melby (2001) to consider cumulative damage; CIRIA/CUR/CETMEF (2007) pointed out that this method gives lower damage values than Van der Meer's (1985) approach. Eq. III.13 proposed in this study implicitly considers the cumulative damage of minor storms attacking the breakwater in breaking wave conditions for a given wave steepness and water depth.

Additionally, it is not clear at which distance the wave parameters should be calculated when using Eqs. II.20 to II.25. Most of equations propose obtaining H_s or $H_{2\%}$ at the toe of the structure. However, these equations were validated with incident waves measured with gauges located at a certain distance from the breakwater, which may lead to errors, especially with the steeper bottom slopes. Eq. III.13 proposed in this study was validated with waves estimated at a distance of 3hs seaward from the structure toe, given that this distance was found to be the optimum location to determine wave parameters for a bottom slope m=1/50.

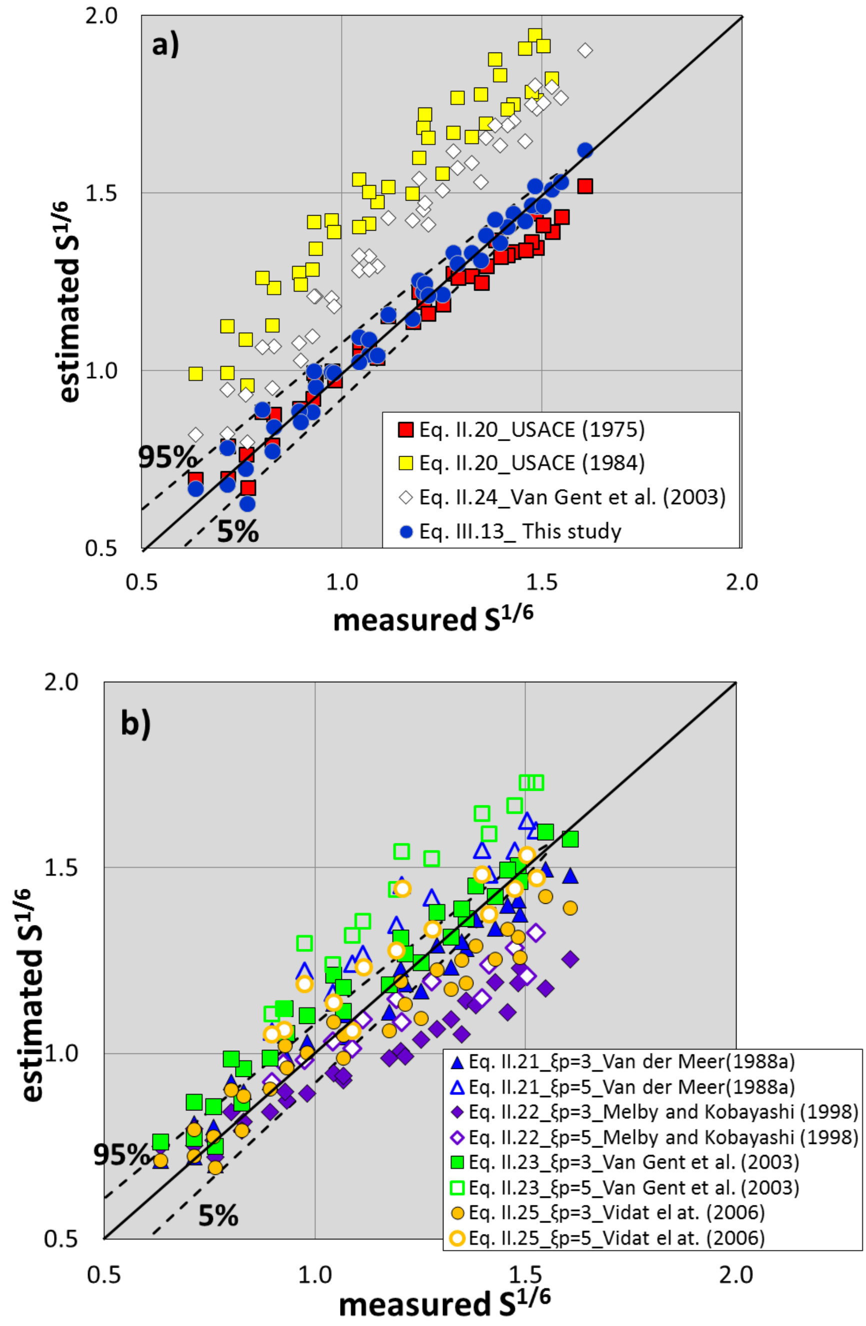

Figure III.40. Linearized measured armor damage $S^{1/6}$ versus estimations of $S^{1/6}$ given by existing formulas and 90% confidence interval of Eq. III.13 using $H=H_{m0}$ given by SwanOne at $d^*=3h_s$.

Chapter IV

Hydraulic stability of rock toe berms placed in very shallow waters and on steep sea bottoms (m=1/10)

Mazarrón, Murcia (Spain). August, 2013.

IV.1. Introduction

Within the framework of ESCOLIF project, additional physical model tests were carried out in the wave flume at the LPC-UPV to analyze the hydraulic stability of rock toe berms in very shallow waters and a m=1/10 steep sea bottom. Tests were conducted with a conventional non-overtopped mound breakwater with a double-layer randomly- and uniformly-placed cube armor, and submerged and emerged rock toe berms.

Since toe berm stability is even more critical than armor stability with very shallow waters and steep sea bottoms, the hydraulic stability of emerged and submerged rock toe berms was first characterized. To this end, standard rock toe berms with $B_t=3D_{n50}$ and $t_t=2D_{n50}$ were analyzed with a wide range of water depths ($-2 \leq h_s(cm) \leq 20$), and a new design equation was provided. The damage to the major part of the toe berm occurred when the still water level (SWL) was close to the crest of the toe berm ($h_t \approx 0$). Thus, in these conditions ($h_t \approx 0$), additional tests were later conducted with wider toe berms ($3D_{n50}<B_t \leq 12D_{n50}$). As mentioned in Section II.5, common toe berm damage parameters (N_{od} or $N_{\%}$) are not suitable to measure the damage to wide toe berms ($B_t>3D_{n50}$) as wider toe berms tend to have higher damage levels. Thus, two new concepts were introduced to better characterize damage to wide toe berms: (1) the most shoreward toe berm area which effectively supports the armor layer, in this study referred to as the “nominal” toe berm and (2) the most seaward toe berm area which serves to protect the nominal toe berm, in this study called the “sacrificial” toe berm (see Fig. IV.1). Damage to the nominal toe berm was used to describe hydraulic stability of wider toe berms ($B_t>3D_{n50}$).

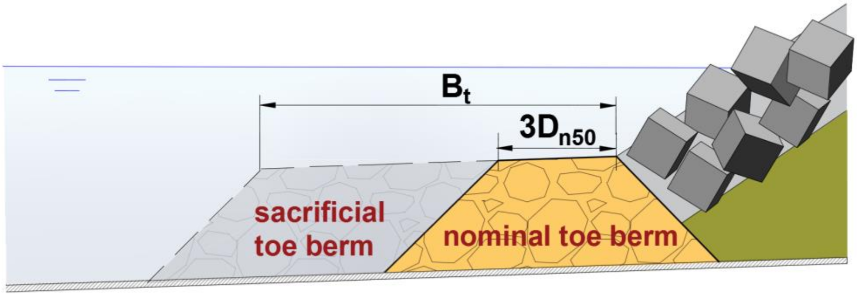

Figure IV.1. The two segments of a wide toe berm ($B_t>3D_{n50}$): sacrificial and nominal toe berm.

Secondly, the hydraulic stability of the double-layer cube armor was characterized. Using the virtual net method, armor damage was measured after each test conducted with cubes randomly- and uniformly-placed. Since the armor unit placement technique is a critical consideration in the design phase (see Medina et al., 2014), the influence of the placement technique on armor stability was analyzed using artificial neural networks.

In this chapter the experimental design is first described. Secondly, wave data and toe berm and armor damage measurements are analyzed. Thirdly, a new design method for nominal and wider rock toe berms is provided. Finally, the influence of the placement technique on double-layer cube armor is examined.

IV.2. Experimental design

IV.2.1. Facilities and equipment

2D physical model tests were conducted with a bottom slope m=1/10 in the wind and wave flume (30 x 1.2 x1.2 m) at the LPC-UPV.

At one end of the wave flume, the wavemaker system was located and at the opposite end, there was a system to dissipate the energy. The physical model was located in front of the absorber energy system. The wavemaker and absorber energy system are described in Section III.2.1.

Three bottom slopes were placed along the wave flume to simulate wave propagation from deep or relatively deep water to shallow water where the physical model was placed. The first ramp corresponded to a 6.3m-long and m=1/25 bottom slope, the second corresponded to a 5.7m-long and m=1/50 bottom slope, and the third was 2.6m-long with a m=1/10 bottom slope (see Fig. IV.2).

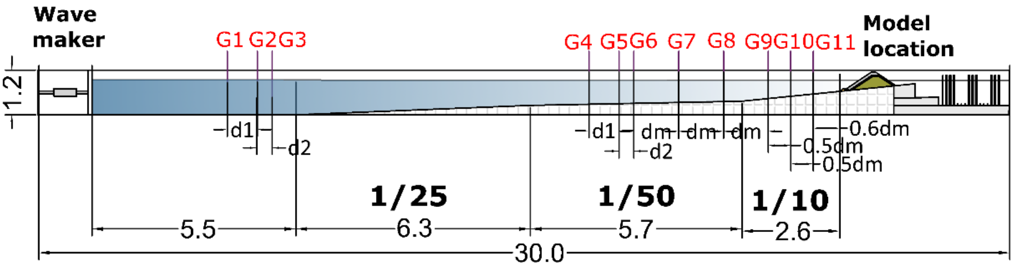

Figure IV.2. Longitudinal cross section of the LPC-UPV wave flume used in the experiments with m=1/10 (dimensions in meters).

IV.2.2. Physical models

The test model corresponded to a conventional cotα=1.5 non-overtopped mound breakwater, protected with a double-layer cube armor (Fig. IV.3). Resin cubes, with nominal diameter D_n(cm)=3.97 and mass M(g)=141.5, were randomly- and uniformly-placed on the armor; cube faces were parallel to the slope in uniform placement.

The mean value of the measured packing density of the tested armor layers was ϕ=1.16 in both cases, very close to the recommended value ϕ=1.17 given by CIRIA/ CUR/ CETMEF (2007).

The cube armor was built on a filter layer with D_{n50}(cm)=1.78 and D_{n85}/D_{n15}=1.35. The granulometric characteristics of the core material were D_{n50}(cm)=0.68 and D_{n85}/D_{n15}=1.64. Considering a reference scale 1/50, this structure corresponds to a double-layer 17.8-tonne cube armor.

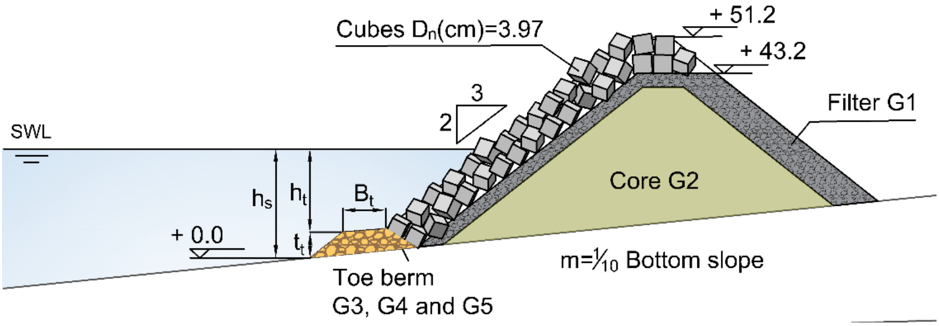

Figure IV.3. Cross section of the cube armored model (dimensions in centimeters).

Rocks with D_{n50}(cm)=3.99 and 5.17 and mass density ρ_r(g/cm^3)=2.70 (gravel G4 and G5 in Table IV.1) were used to construct a standard toe berm configuration (CIRIA/ CUR/ CETMEF (2007) with $B_t=3D_{n50}$, $t_t=2D_{n50}$, and in this study this was the “nominal toe berm”.

Additional tests were conducted later to characterize the stability of wider toe berms ($B_t \geq 3D_{n50}$). An extra rock toe berm size was tested, D_{n50}(cm)=3.04 (gravel G3 in Table IV.1). For D_{n50}(cm)=3.04 and 3.99, three toe berm widths were applied ($B_t=n_t D_{n50}$ with n_t=3, 5 and 12) maintaining the thickness at $t_t=2D_{n50}$, where n_t is the number of rock rows placed on the upper layer of the toe berm (see Fig. IV.4). The nominal toe berm was considered as the most shoreward area of the berm with a width of three times the rock nominal diameter ($B_t=3D_{n50}$) necessary to support the armor, and the sacrificial toe berm as the most seaward area of the berm. The nominal toe berm was placed first; later, the sacrificial toe berm was built with rocks painted in different colors (see Fig. IV.9). These tests were conducted with a fixed water depth measured at the toe of the nominal toe berm, h_{ss}, for all configurations (see Table IV.3). Note that $h_s=h_{ss}$ only when $B_t=3D_{n50}$.

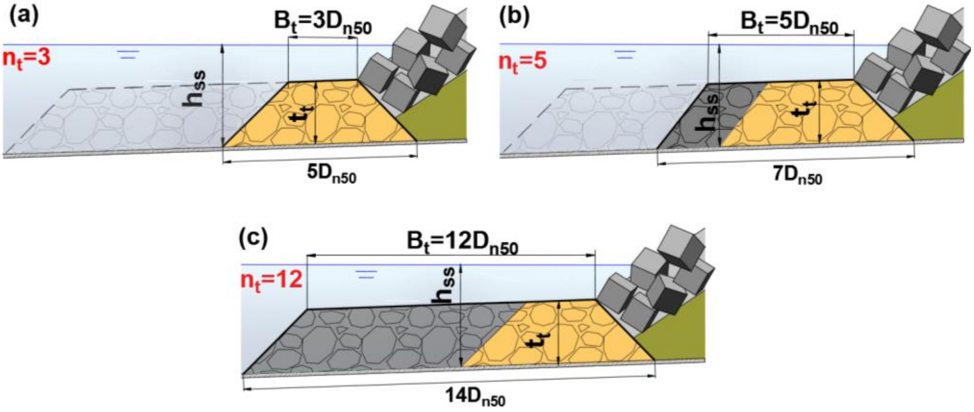
(a)
B_t=3D_{n50}
n_t=3
h_{ss}
t_t
5D_{n50}
(b)
B_t=5D_{n50}
n_t=5
h_{ss}
t_t
7D_{n50}
(c)
B_t=12D_{n50}
n_t=12
h_{ss}
t_t
14D_{n50}

Figure IV.4. Configuration of toe berms: (a) B_t=3D_{n50}, (b) B_t=5D_{n50}, (c) B_t=12D_{n50}.

Gravel	M_{50}[g]	D_{n50}[cm]	ρr[g/cm³]
G1	15.40	1.78	2.729
G2	0.86	0.68	2.722
G3	73.0	3.04	2.589
G4	168.0	3.99	2.630
G5	359.2	5.17	2.589
CAUs	**M [g]**	**D_n [cm]**	**ρr[g/cm³]**
Cubes	141.5	3.97	2.270

Table IV.1. Characteristics of model materials.

Fig. IV.5 shows the nominal diameter of armor cubes and toe berm rocks for twenty randomly-selected resamples. Fig. IV.6 shows the resin cubes used in the model.

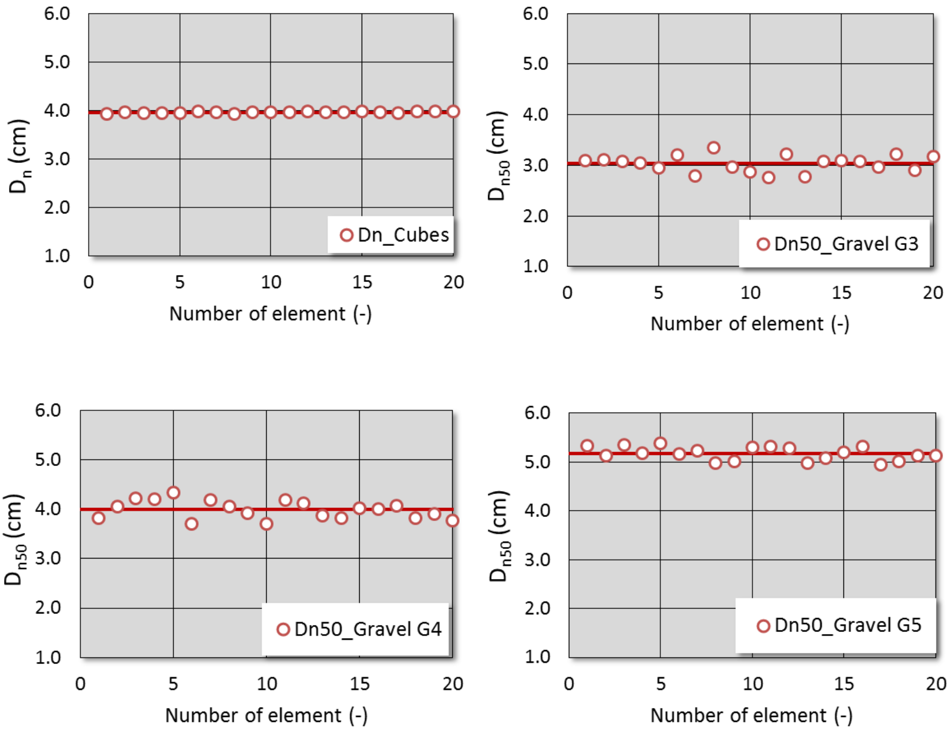

Figure IV.5. Nominal diameter for cubes and gravel G3, G4 and G5 used in the experiments.

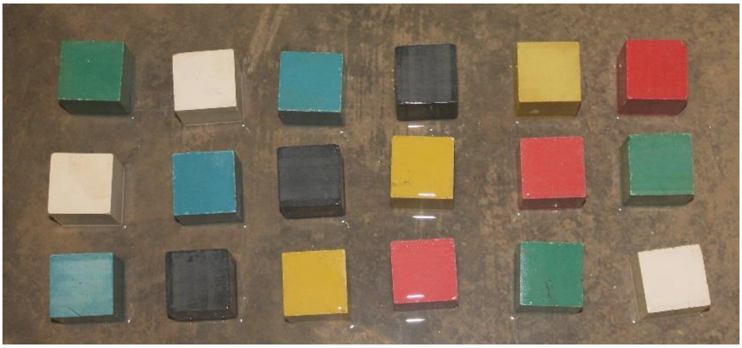

Figure IV.6. Resin cubes used in tests.

Fig. IV.7 shows the process to construct the breakwater model tested in the experiments. Firstly, the cross section was drawn on the walls of the flume and the materials were washed and properly characterized. Secondly, the core was constructed with gravel G2. Thirdly, the filter layer (gravel G1) was placed above the core layer. Fourthly, the toe berm was constructed using gravel G3, G4 or G5. Finally, cubes were placed on the main armor.

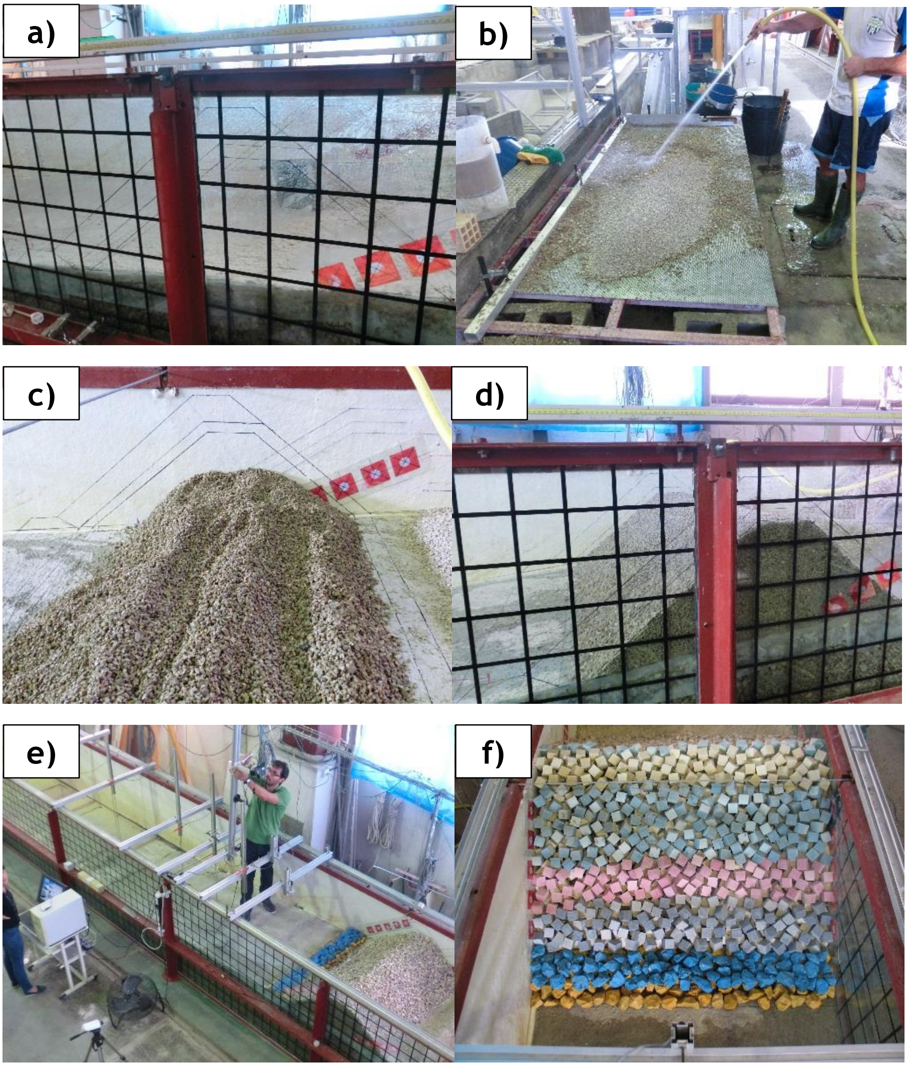

Figure IV.7. Construction process of the mound breakwater model: (a) drawing, (b) cleaning material, (c) core, (d) filter, (e) toe berm and placement of cameras, and (f) armor layers.

Fig. IV.8 shows the photos taken perpendicular to the armor with randomly- and uniformly-placed cubes. The uniformly-placed cube armor was only tested with standard toe berm configurations ($B_t=3D_{n50}$).

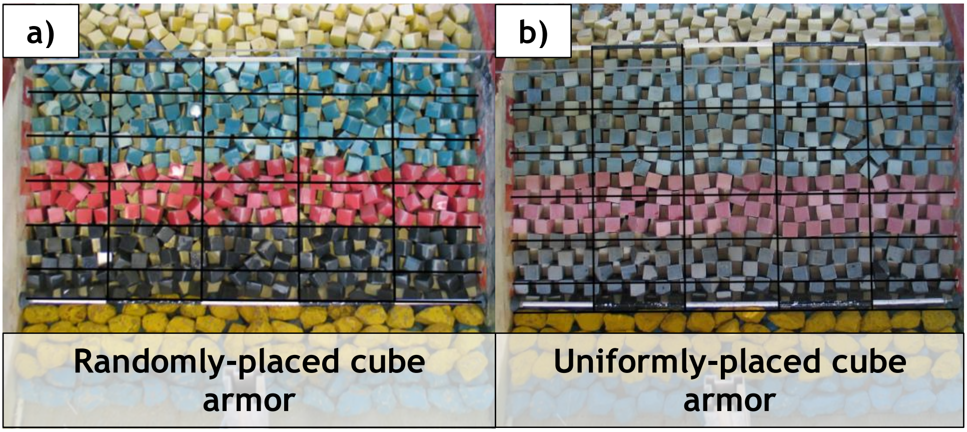
a)
b)
Randomly-placed cube armor
Uniformly-placed cube armor

Figure IV.8. (a) Double-layer randomly-placed cube armor, (b) Double-layer uniformly-placed cube armor.

Fig. IV.9 shows the breakwater model constructed with toe berms using rocks of D_{n50}(cm)=3.99 (gravel G4) and (a) $B_t=3D_{n50}$, (b) $B_t=5D_{n50}$ and (c) $B_t=12D_{n50}$. Yellow and blue rocks correspond to the first and second layer of the nominal toe berm.

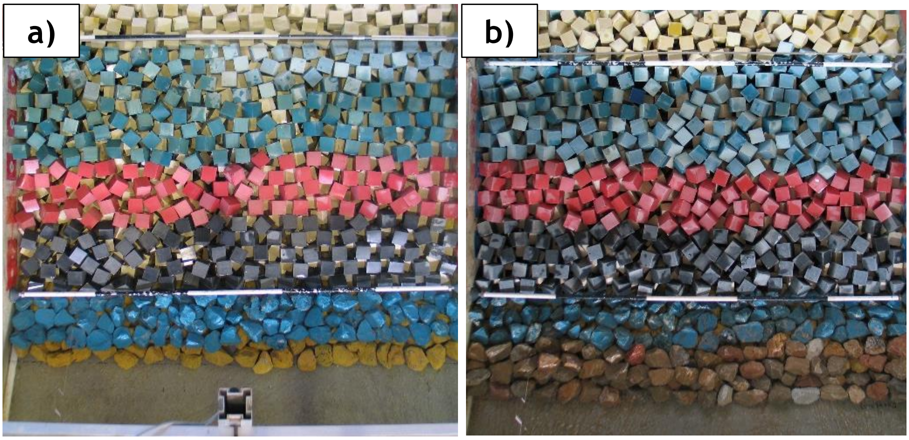

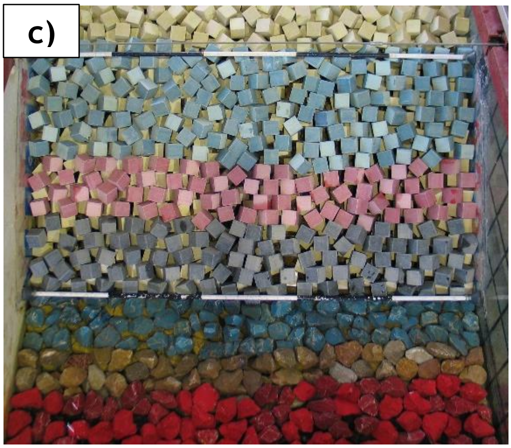

Figure IV.9. Physical model constructed with rock toe berms of D_{n50}(cm) = 3.99 (gravel G4) and (a) $B_t = 3D_{n50}$, (b) $B_t = 5D_{n50}$, and (c) $B_t = 12D_{n50}$.

IV.2.3. Irregular tests

Irregular wave trains of 500 waves were generated following JONSWAP (γ=3.3) spectra (Eq. III.3), and reflected waves were absorbed using the AWACS Active Wave Absorption System.

Twelve test series were carried out considering different water depths at the toe, h_s. For a given water depth, five wave periods were tested (T_p(s)=1.20, 1.50, 1.80, 2.20 and 2.40); for each peak period, wave heights were generated from values which caused no damage to those which caused wave breaking in the wave generating zone due to steepness (s=H/L). With these conditions, wave heights were varied in the range of $8 \leq H_{m0}(cm) \leq 20$, having characterized all values of wave height in which waves break due to depth limitation for a specific period.

The tested water depths at the toe of the structure were h_s(cm)=-2, 0, 2, 4, 6, 8, 10, 12, 14, 16, 18 and 20 with the toe berm configuration of $B_t=3D_{n50}$, $t_t=2D_{n50}$, and D_{n50}(cm)=3.99 and 5.17. The methodology used in these experiments took into account that seawalls in very shallow water and on steep seafloors must withstand not only a design storm, but also numerous wave storms slightly less intense than the design storm. In all, 1150 tests were performed, half of these (775) with cubes randomly-placed on the armor layer, and the other half (775) with cubes uniformly-placed on the armor layer.

Irregular tests with standard toe berms B_t = $3D_{n50}$		
Parameter	*Symbol*	*Value*
Waves	-	Random
Bottom slope (-)	m	1/10
Armor unit	-	Cube
Armor placement	-	Random and Uniform
Cube armor size (cm)	D_{n50}	3.97
Rock toe berm size (cm)	D_{n50}	3.99 and 5.17
Relative toe width (-)	$n_t=B_t/D_{n50}$	3
Relative toe thickness (-)	t_t/D_{n50}	2
Water depth at toe (cm)	h_s	-2, 0, 2, 4, 6, 8, 10, 12, 14, 16, 18, 20
Peak wave period (s)	T_p	1.2, 1.5, 1.8, 2.2, 2.4
Spectral significant wave height at wave generating zone (cm)	H_{m0}	8, 10, 12, 14, 16, 18, 20
Wave steepness at wave generating zone (-)	$s_p=H_{m0}/L_{0p}$	0.008-0.08
Number of waves per run	N_z	500

Table IV.2. Irregular tests conducted with standard toe berms ($B_t=3D_{n50}$).

After these tests series, it was observed that water depths close to the crest of the toe berms (h_s(cm)≈8) led to extremely high values of toe berm damage. Thus, new tests were conducted with the fixed water depth measured at the toe of the nominal toe berm of h_{ss}(cm)=8, and three toe berm widths ($B_t=n_t\ D_{n50}$, for n_t=3, 5 and 12) with D_{n50}(cm)=3.04 and 3.99. As mentioned earlier, the toe berm thickness was fixed at $t_t=2D_{n50}$ and only armors with randomly-placed cubes were considered.

Additional irregular tests with three toe berm widths		
Parameter	*Symbol*	*Value*
Waves	-	Random
Bottom slope (-)	m	1/10
Armor unit	-	Cube
Armor placement	-	Random
Cube armor size (cm)	D_{n50}	3.97
Rock toe berm size (cm)	D_{n50}	3.04 and 3.99
Relative toe width (-)	$n_t=B_t/D_{n50}$	3, 5 and 12
Relative toe thickness (-)	t_t/D_{n50}	2
Water depth at toe of the nominal toe berm (cm)	h_{ss}	8
Peak wave period (s)	T_p	1.2, 1.5, 1.8, 2.2, 2.4
Spectral significant wave height at wave generating zone (cm)	H_{m0}	8, 10, 12, 14, 16, 18, 20
Wave steepness at wave generating zone (-)	$s_p=H_{m0}/L_{0p}$	0.008-0.08
Number of waves per run	N_z	500

Table IV.3. Irregular tests conducted with h_{ss}=8cm and three toe berm widths ($B_t=n_t D_{n50}$, n_t=3, 5 and 12).

IV.2.4. Measurements

IV.2.4.1. Wave measurements

Surface elevation was measured using eleven capacitive wave gauges. One group of wave gauges (G1, G2 and G3) was placed near the wavemaker (see Fig. IV.2), and other group was placed along the wave flume and near the model (G4, G5, G6, G7, G8, G9, G10 and G11).

Incident and reflected waves were separated at the wave generating zone. To this end, wave gauges were separated according to the criterion given by Mansard and Funke (1980), depending on the wave length (see Eq. III.4).

Table IV.4 shows the distances between wave gauges shown in Fig. IV.2.

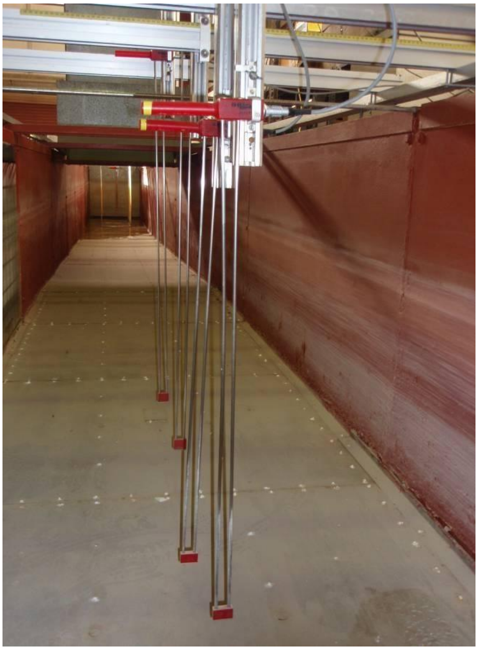

Figure IV.10. Wave gauges located in the model zone.

Zone	Wave gauges	d_1[cm]	d_2[cm]	d_m[cm]
Wave generator	G1, G2, G3	80	40	120
Model	G4, G5, G6, G7, G8, G9, G10, G11	80	40	120

Table IV.4. Distance between wave gauges.

Additionally, all tests were recorded using video and photo cameras as described in Section III.2.4.

IV.2.4.2. Wave separation. LASA-V Method

Incident and reflected waves were estimated at the wave generating zone (waves gauges G1, G2 and G3), using the LASA-V method developed by Figueres and Medina (2004), described in Section III.2.4.1.

IV.2.4.3. Damage measurements

- **Toe berm damage**

Most tests were conducted with a toe berm configuration of $B_t=3D_{n50}$ and $t_t=2D_{n50}$. In these tests, the common damage parameter N_{od} was used (Eq. II.13) to characterize toe berm damage.

N_{od} takes into account the total number of rocks displaced from the toe (N). Thus, for wide toe berms N is not suitable to characterize toe berm damage because the wider toe berm, the larger N_{od}, even though the toe berm is more resistant. Therefore, for tests conducted on toe berms with $B_t=5$ and 12 D_{n50}, two damage parameters were measured after each test: (1) N_{od}, corresponding to the total damage to the toe berm of width $B_t=n_t D_{n50}$ ($n_t\geq3$), and (2) N_{od}^* corresponding only to the damage to the nominal toe berm of $n_t=3$; N_{od}^* was determined using also Eq. II.13 but considering only the number of rocks displaced from the inner part of the toe berm with a width of three times the nominal diameter (see Fig. IV.11).

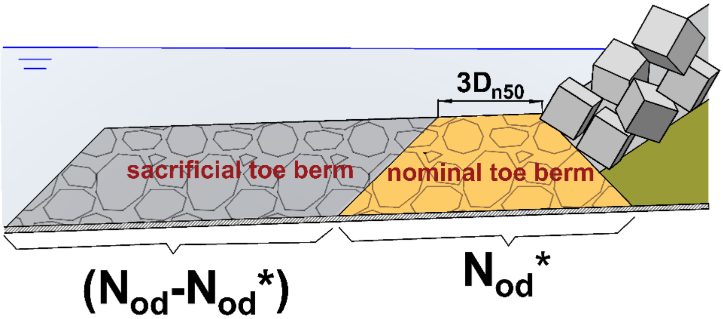

Figure IV.11. Total toe berm damage (N_{od}) and nominal toe berm damage (N_{od}^*).

Both damage parameters considered the cumulative damage from each test series. In contrast to the methodologies applied by the authors mentioned in Section II.5, this study considered significant cumulative damage since the model was not rebuilt for a given water depth. The method used in this study took into account that wave storms do not usually occur in isolation, but less intense storms also occur before the design waves attack the structure.

- **Armor damage**

Armor damage was measured after each test run for both double-layer randomly-placed and double-layer uniformly-placed cube armors. Comparing the photographs taken perpendicularly to the slope after each test, armor damage was quantified using the virtual net method described by Gómez-Martín and Medina (2014). A virtual net was projected over each photograph, dividing the armor into four $3D_n$-wide strips (strips A, B, C and D) and another $2D_n$-wide strip (strip E). Dimensionless armor damage was calculated for each strip (S_i); integrating this dimensionless armor damage over the slope, the equivalent dimensionless armor damage parameter was obtained (S_e), following Eq. II.18.

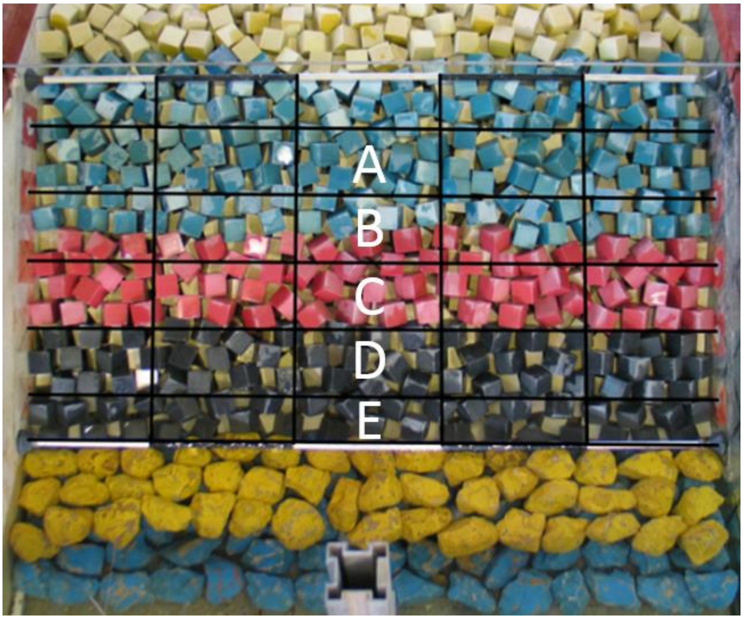

Figure IV.12. Virtual net method used in the experiments to measure cube armor damage.

Armor damage was also measured using the definition of the damage parameter N_{od}. With this definition, heterogeneous packing was not taken into account; only the armor unit extractions were considered.

IV.3. Data analysis

IV.3.1. Wave analysis

Using the calculated surface elevations, wave height distributions and spectral moments were obtained. The incident significant wave heights measured at the wavemaker were propagated to deep water using the coefficients proposed by Goda (2000). The average of the highest one-third incident waves ($H_{1/3,i}$) measured at G1, G2 and G3 was used to estimate the deep water significant wave height (H_{s0}) using the shoaling coefficients given by Goda (2000). Fig. IV.13 shows the measured $H_{1/3,i}$ compared to the deep water significant wave height (H_{s0}) estimated using the methodology described in Goda (2000).

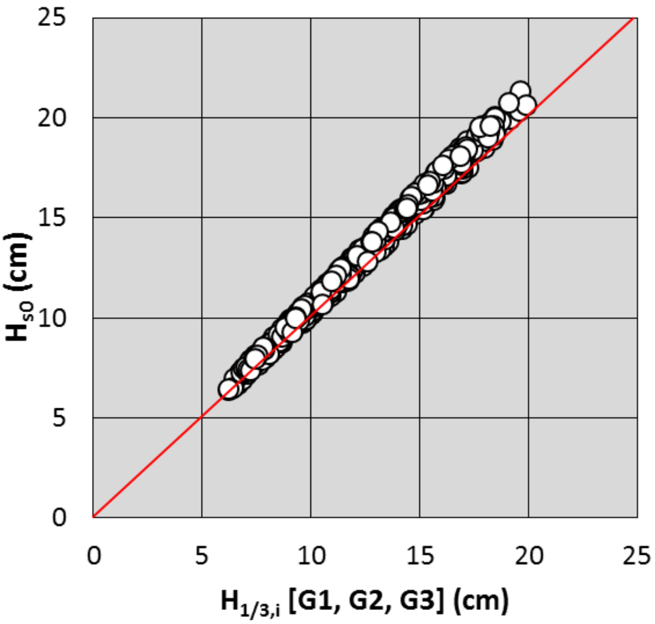

Figure IV.13. Measured $H_{1/3i}$ at the wave generating zone versus deep water significant wave height, H_{s0}.

Deep water wave condition is a clear reference when dealing with incident and reflected waves in the breaking zone. Wave gauges and available softwares to separate incident and reflected waves are not reliable in the surf zone, near the structure (Baldock and Simmonds, 1999; Battjes et al., 2004). In some of the tests in this study, the water depth was null or even negative ($h_s<h_t<0$). Only in tests conducted with h_s(cm)≥8 was it possible to obtain reliable wave measurements near the structure. Thus, it was necessary to refer all measurements to a location independent from the toe berm. Fig IV.14 shows the estimated H_{m0} compared to the incident H_{m0} estimated at G11, assuming constant along the flume the reflection coefficient ($K_r=H_{m0r}/H_{m0i}$) obtained at the wave generating zone, for tests in the range $8\leq h_s(cm)\leq 20$ with standard toe berms ($h_s=h_{ss}$). Note that for each h_s, five T_p were considered with increasing values of H_{m0}.

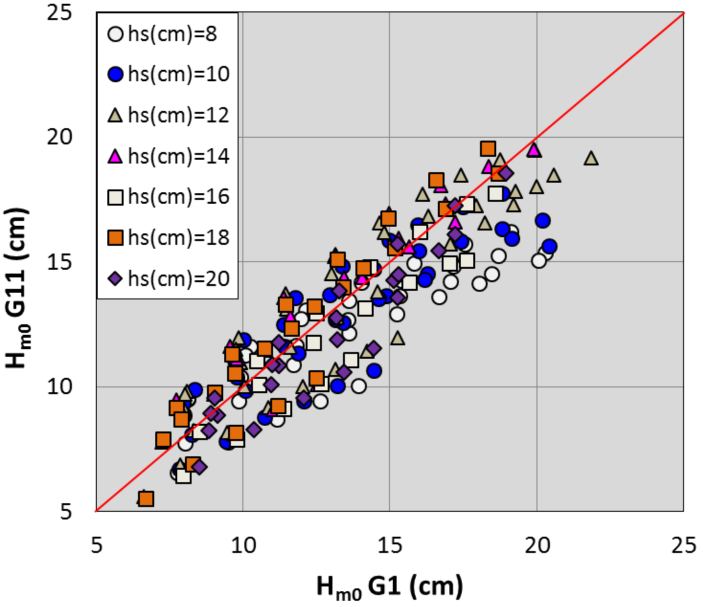

Figure IV.14. Comparison of H_{m0} measured at G1 and G11 for tests in the range $8 \leq h_s$ (cm) ≤ 20 with standard toe berms.

Wave transformation corresponding to the steep sea bottom m=1/10 in the breaking zone may be different depending on the foreshore. Thus, the numerical model SwanOne was used to compare the values of significant wave height estimated at several points near the structure (A, B, C, D, E, F, G, H and Toe) in three virtual wave flumes with different bottom configurations (see Fig. IV.15). Virtual wave flume #1 (Fig. IV.15a) corresponded to the real configuration used in the experiments; virtual wave flume #2 (Fig. IV.15b) and virtual wave flume #3 (Fig. IV.15c) considered different lengths of the bottom slope m=1/10 and different water depths at the wave paddle. The distances from the points A, B, C, D, E, F, G, H to the toe of the structure are listed in Table IV.5.

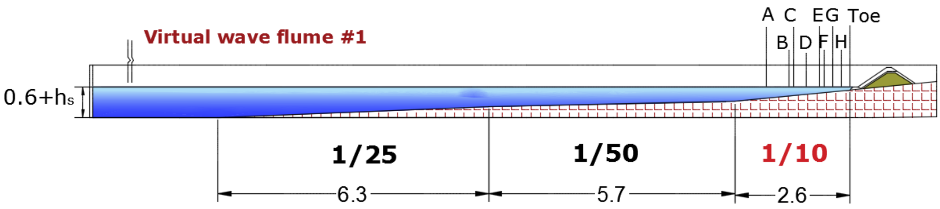

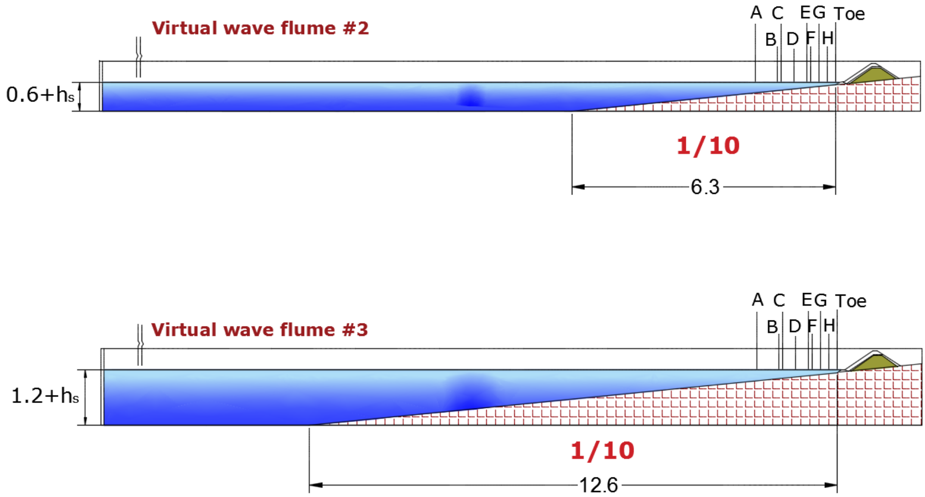
Virtual wave flume #2
A C EG Toe
B D F H
0.6+hs
1/10
6.3
Virtual wave flume #3
A C EG Toe
B D F H
1.2+hs
1/10
12.6

Figure IV.15. Virtual wave flumes (dimensions in meters).

Point	A (G9)	B	C (G10)	D	E (G11)	F	G	H
Toe distance (m)	1.9	1.4	1.3	1.0	0.7	0.6	0.4	0.2

Table IV.5. Distances between points A, B, C, D, E, F, G, H and the toe of the structure (dimensions in meters).

The analysis was done for different water depths at the toe, h_s, peak periods, T_p, and deep water significant wave heights, H_{s0}. Table IV.6 shows the input data for the SwanOne model. The values of T_p and H_{s0} used in the simulations were values obtained in the real tests. In the three virtual wave flumes (#1, #2 and #3), the input energy to the model was exactly the same since the target values of H_{s0} and T_p were not varied. H_{m0} values given by SwanOne at the toe of the structure were taken to characterize the influence of the bottom profile on waves attacking the structure.

Deep water			Toe				Toe	
Input data			Depth	H_{m0}			Relative H_{m0}	
Case	T_p (s)	H_{s0} (cm)	h_s (cm)	H_{m0}#1 (cm)	H_{m0}#2 (cm)	H_{m0}#3 (cm)	H_{m0}#2/ H_{m0}#1 (-)	H_{m0}#3/ H_{m0}#1 (-)
1	1.2	11.4	4	4.78	4.69	4.77	0.981	0.998
2	1.5	15.8	4	5.85	5.84	5.85	0.999	0.999
3	2.2	16.8	4	5.92	5.92	5.91	1.000	0.999
4	1.2	11.4	6	6.27	6.25	6.25	0.997	0.997
5	1.5	15.6	6	7.43	7.43	7.46	0.999	1.004
6	2.2	17.2	6	8.82	8.82	8.82	1.000	1.000
7	1.2	10.9	14	9.68	9.68	9.44	1.000	0.975
8	1.5	14.6	14	11.91	11.98	11.76	1.005	0.987
9	1.8	15.3	14	12.67	13.01	12.90	1.027	1.019
10	1.2	11.4	18	10.33	10.41	10.12	1.008	0.980
11	1.5	15.8	18	13.46	13.53	13.21	1.006	0.982
12	2.2	17.7	18	16.27	16.37	16.51	1.006	1.015

Table IV.6. Spectral significant wave height at the toe, H_{m0}, provided by the SwanOne numerical model for the virtual wave flumes #1, #2 and #3.

The rMSE (Eq. III.10) was used to measure the error between two spectral wave heights estimated by the SwanOne numerical model for two different virtual flumes (Table IV.7). Virtual wave flume #1 was taken as reference (target) because it corresponded to the wave flume actually used in the physical experiments of this study.

rMSE		
Point	H_{m0}#2	H_{m0}#3
A	0.040	0.036
B	0.028	0.027
C	0.023	0.025
D	0.016	0.019
E	0.009	0.014
F	0.007	0.014
G	0.002	0.010
H	0.003	0.005
TOE	0.001	0.002

Table IV.7. rMSE for H_{m0} at different points along wave flume #1 (target) when compared to values for wave flumes #2 and #3.

At the toe of the structure, the rMSE of virtual wave flumes #2 and #3 were 0.1% and 0.2%, respectively. These errors are very low, especially at the points near the tested structure.

Fig. IV.16 shows the H_{m0} values given by the SwanOne model for wave flume #1, compared to the H_{m0} values given for wave flumes #2 and #3 (water depth at the toe h_s(cm)=6). The parameter h is the existing water depth at each measuring point (A, B, C, D, E, F, G, H and Toe) for this case.

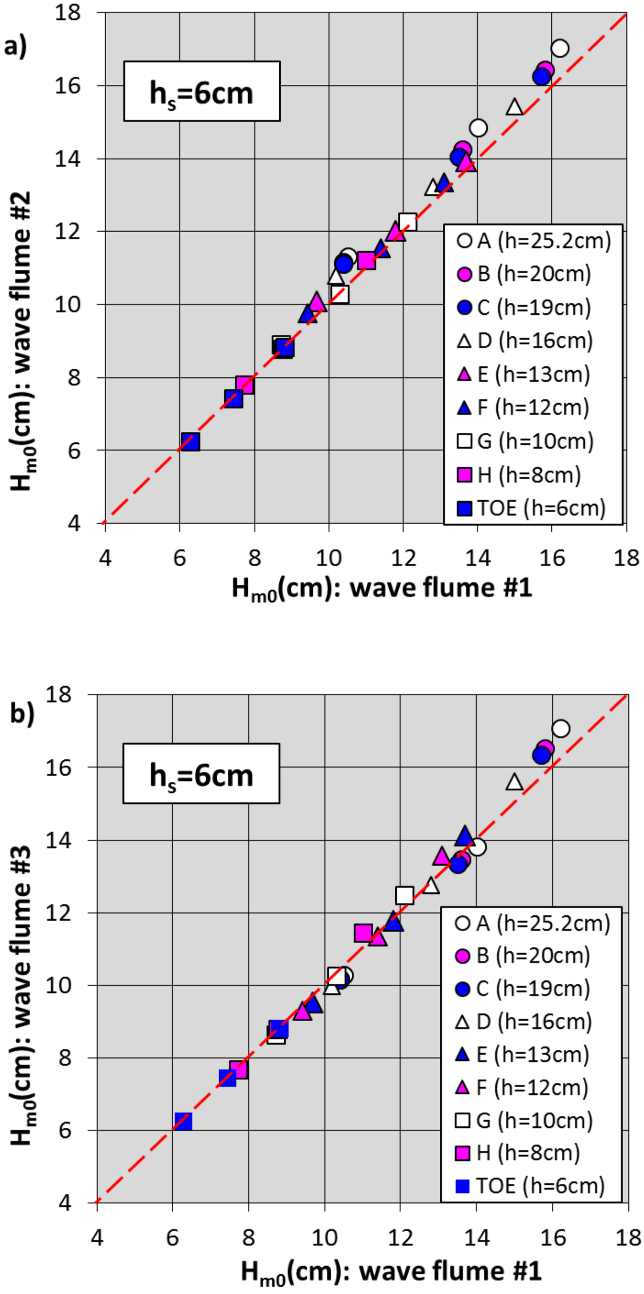

Figure IV.16. Comparison of H_{m0} given by SwanOne for h_s(cm)=6: (a) virtual wave flumes #1 and #2 and (b) virtual wave flumes #1 and #3.

Changes in the bottom profile did not significantly affect the H_{m0} near the model, regardless of bottom configurations far from the structure. Thus, if the breakwater is placed in very shallow water and on a bottom slope m=1/10, this bottom slope determines the waves that can reach the toe berm. In this study, the wave storm attacking the structure was well characterized by its parameters in deep water conditions. Deep water wave storm characteristics and the m=1/10 bottom slope near the structure determined the waves attacking the structure.

IV.3.2. Analysis of toe berm damage

IV.3.2.1. Tests conducted with standard toe berms ($B_t=3D_{n50}$)

The number of rocks displaced from the toe berm was recorded after each test to measure the damage to the standard toe berms ($B_t=3D_{n50}$, $t_t=2D_{n50}$) and rock sizes D_{n50}(cm)=3.99 and 5.17. Note that for standard toe berms $N_{od}=N_{od}$ * and $h_s=h_{ss}$ (see Figs. IV.4 and IV.11).

Because this study dealt with structures in shallow water breaking wave conditions, the influence of the water depth at the toe on toe berm stability was studied first. Fig. IV.17 shows the evolution of the observed toe berm damage depending on the water depth at the toe (h_s) after the tests conducted with H_{s0}(cm)=12 and T_p(s)=1.8 (Fig. IV.17a) and H_{s0}(cm)=16 and T_p(s)=1.8 (Fig. IV.17b). For a given T_p(s)=1.8, toe berm damage ($N_{od}=N_{od}$*) was greater with increasing H_{s0}.

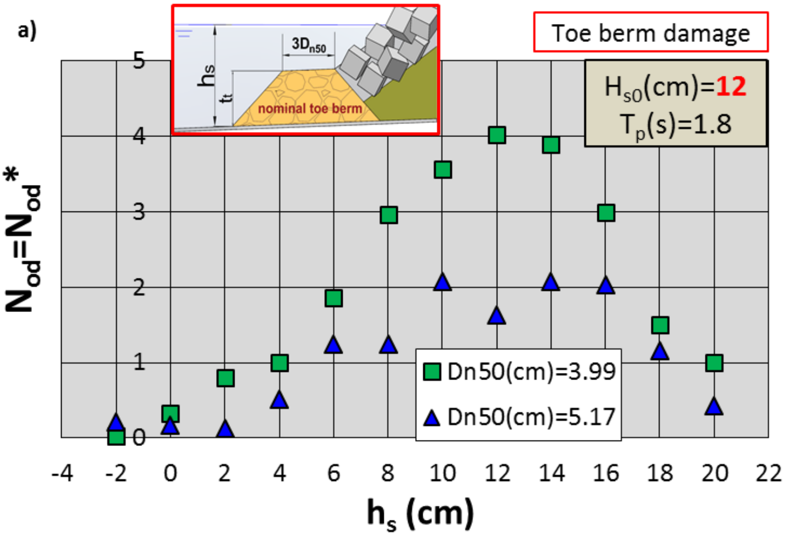

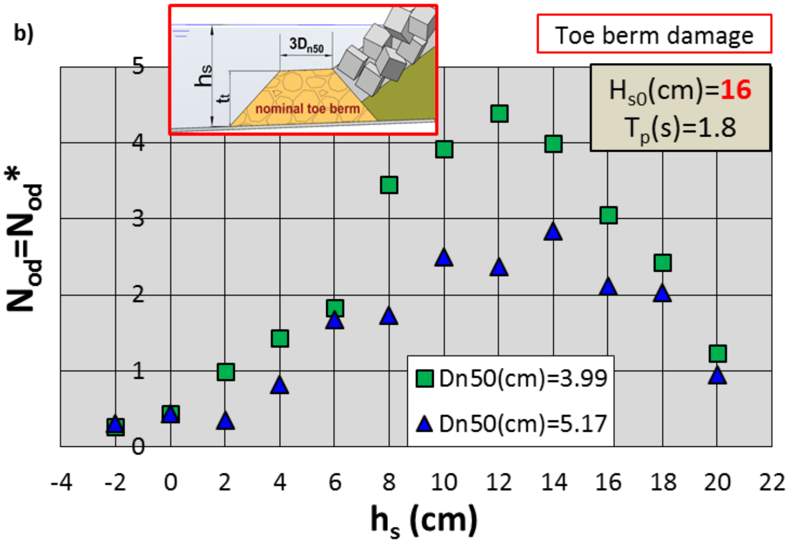

Figure IV.17. Measured toe berm damage ($N_{od}=N_{od}$*) depending on water depth at the toe (h_s) after tests conducted with (a) H_{s0}(cm)=12 and T_p(s)=1.8, and (b) H_{s0}(cm)=16 and T_p(s)=1.8.

Fig. IV.18 illustrates the evolution of the observed toe berm damage to standard toe berms (B_t=3D_{n50} and t_t=2D_{n50}), depending on the water depth at the toe (h_s) for all tests conducted with D_{n50}(cm)=3.99 and 5.17. Figs. IV.17 and IV.18 show that toe berm damage ($N_{od}=N_{od}$*) generally increased with the water depth up to h_s(cm)=12 and decreased from there up to h_s(cm)=20.

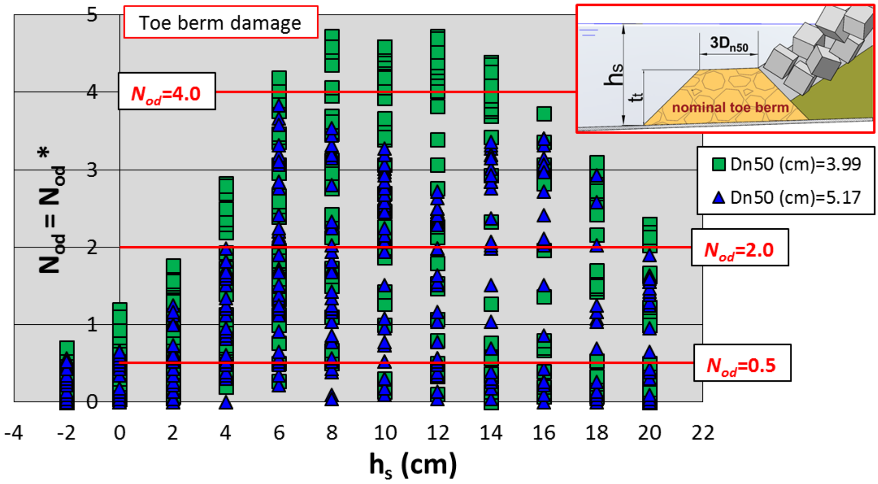

Figure IV.18. Measured toe berm damage ($N_{od}=N_{od}$*) depending on water depth at the toe (h_s).

Toe berm damage mainly occurred during the run-down events. Run-up and run-down levels chiefly depend on the wave height and the period of incident waves. According to Hunt (1959), the run-up, R_{up}, on a structure can be estimated by Eq. IV.1.

$$R_{up} = (H\,L_0)^{1/2}\ \tan\alpha \qquad \text{[IV.1]}$$

where H is the wave height, L_0 is the deep water wave length and tanα is the slope of the breakwater.

Different formulas were obtained later to characterize wave run-up and run-down based on Eq. IV.1. The variable $(H\,L_0)^{1/2}$ has been widely used to estimate run-up and run-down levels. Eq. IV.2 was obtained re-writing the formula given by CIRIA/ CUR/ CETMEF (2007) to estimate the maximum run-down level on porous slopes, $R_{d1\%}$, derived from test results by Thompson and Shuttler (1975):

$$\frac{R_{d1\%}}{H_s} = 0.34\,\xi_p - 0.17$$

$$R_{d1\%} = 0.34\,\left(H_s\ L_{0p}\right)^{1/2}\ \tan\alpha\ -\ 0.17\ H_s; \qquad \text{[IV.2]}$$

Fig.IV.19 shows the toe berm damage (N_{od}=N_{od}*) as a function of $(H_{s0}\,L_{0p})^{1/2}$ and the water depth at the toe (h_s) for tests carried out with D_{n50}(cm)=3.99 and 5.17. For a given water depth, the toe berm damage increased almost linearly with $(H_{s0}\,L_{0p})^{1/2}$. Straight lines correspond to h_s(cm)=-2, 0, 2, 4 and 6.

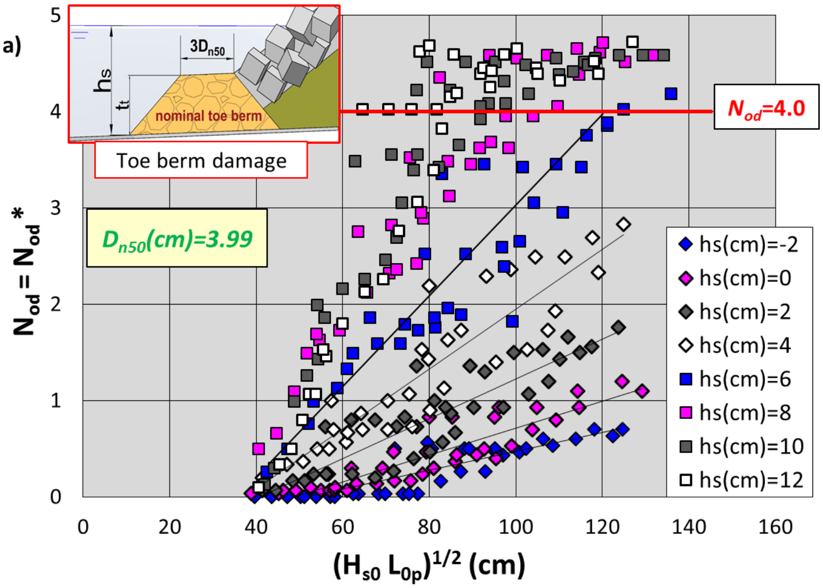

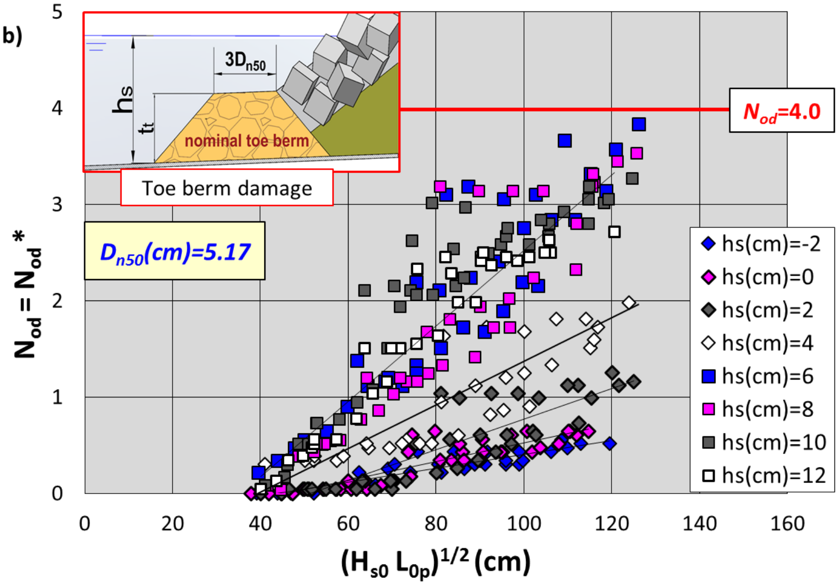

Figure IV.19. Toe berm damage ($N_{od}=N_{od}^*$) versus $(H_{s0}\ L_{0p})^{1/2}$ for (a) D_{n50}(cm)=3.99 and (b) D_{n50}(cm)=5.17.

For high levels of damage ($N_{od}=N_{od}^*>4$), an increase in $(H_{s0}\ L_{0p})^{1/2}$ did not significantly increase the toe berm damage because the toe berm was already severely damaged (failure according to CIRIA/ CUR/ CETMEF, 2007). Only tests with $N_{od}\leq 4$ were selected for the following analysis.

IV.3.2.2. Additional tests conducted with three toe berm widths (B_t=3, 5 and 12 D_{n50})

The total toe berm damage (N_{od}) and the nominal toe berm damage (N_{od}^*) were used to characterize the damage to wide toe berms in this section. Only the values obtained at the highest H_{s0} of each T_p are represented in the following figures to facilitate understanding.

- **Total toe berm damage (N_{od})**

The influence of the rock size on the total N_{od} was first studied. Fig.IV.20 shows the measured N_{od} depending on the variable $(H_{s0}\ L_{0p})^{1/2}$ and the rock size (D_{n50}(cm)=3.04, 3.99 and 5.17) for tests conducted with $B_t=3D_{n50}$. N_{od} increased almost linearly with the variable $(H_{s0}\ L_{0p})^{1/2}$ for all tested toe berm sizes. N_{od} was larger when reducing the rock nominal diameter. (N_{od} (D_{n50}(cm)=3.04) > N_{od} (D_{n50}(cm)=3.99) > N_{od} (D_{n50}(cm)=5.17).

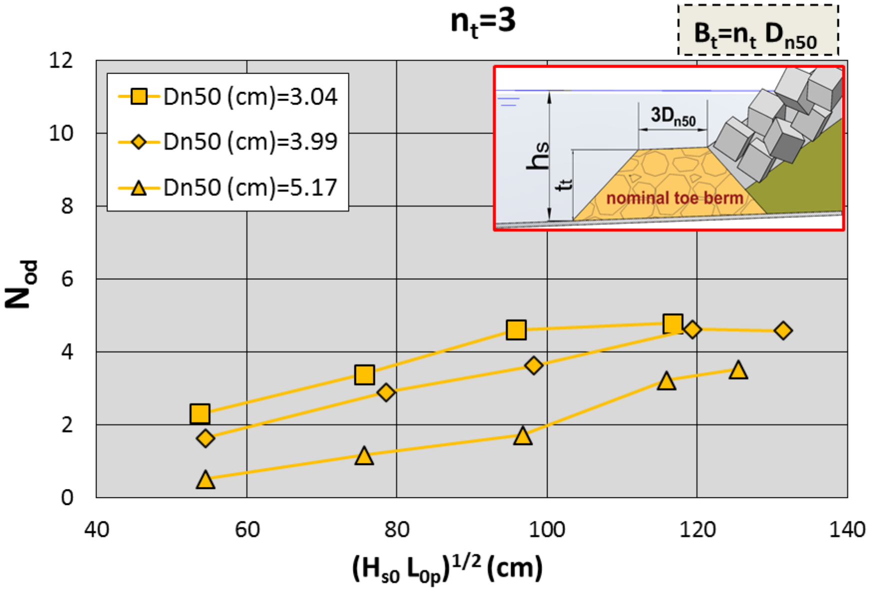

Figure IV.20. Influence of rock size (D_{n50}) on measured total toe berm damage (N_{od}) depending on $(H_{s0} L_{0p})^{1/2}$. Tests with B_t=3D_{n50}.

Secondly, the influence of the toe berm width (B_t=n_t D_{n50}) on N_{od} was analyzed for the three tested configurations (n_t=3, 5 and 12). Fig. IV.21 shows the measured N_{od} depending on the variable $(H_{s0} L_{0p})^{1/2}$ and the toe berm width for tests conducted with D_{n50}(cm)=3.04, D_{n50}(cm)=3.99 and D_{n50}(cm)=5.17. There is a clear influence of the toe berm width on the damage. For each D_{n50}, N_{od} increased with the number of rocks placed on the second layer of the toe berm (n_t). Thus, larger toe berms had larger values of N_{od}.

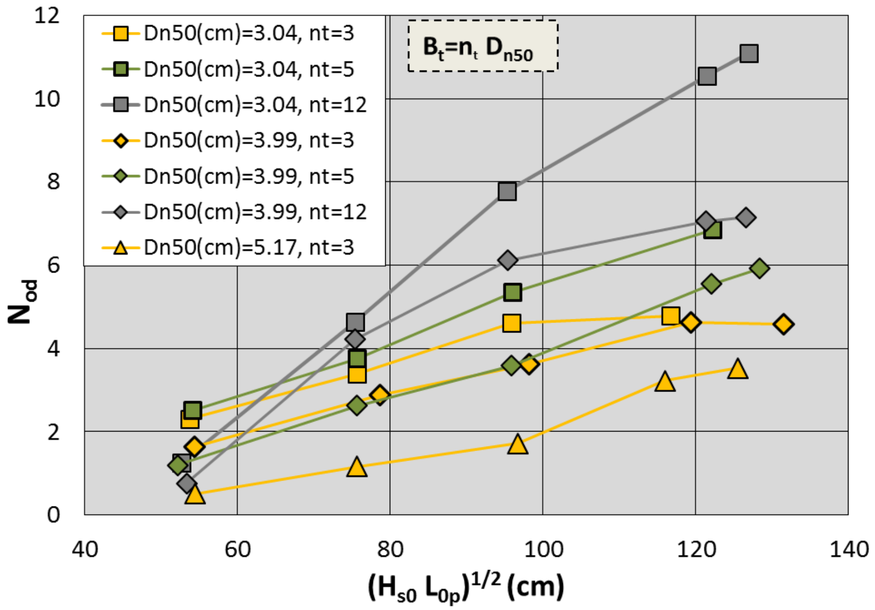

Figure IV.21. Influence of toe berm width on measured toe berm damage (N_{od}).

- **Nominal toe berm damage (N_{od}*)**

Fig. IV.22 illustrates the measured N_{od}* depending on the variable $(H_{s0}\ L_{0p})^{1/2}$ for the toe berms tested. Given a rock size (D_{n50}), N_{od}* increased when reducing the number of rocks placed on the second layer of the toe berm (n_t). Larger toe berms had lower values of N_{od}*.

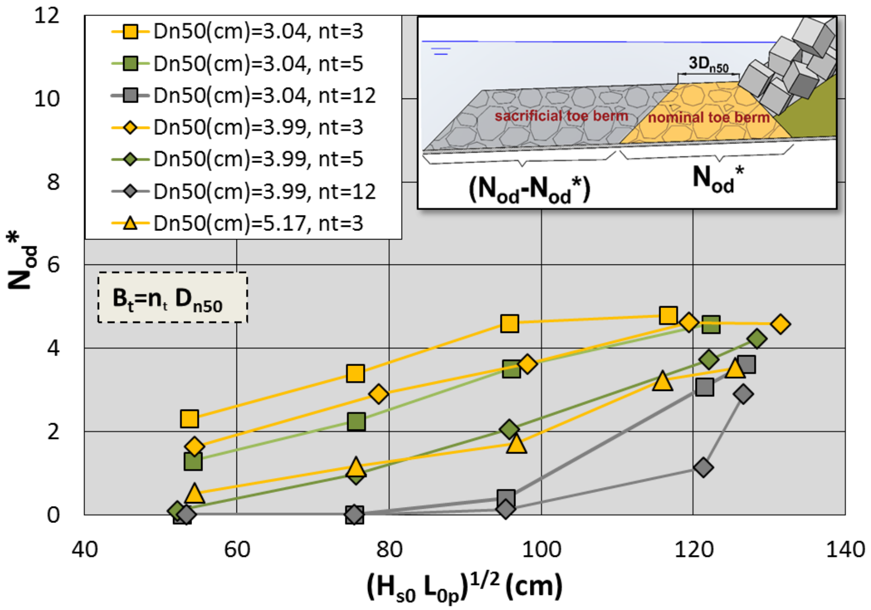

Figure IV.22. Influence of toe berm width on measured nominal toe berm damage (N_{od}*).

When comparing the toe berm width with N_{od}*, the behavior is opposite to that observed when using N_{od} (see Fig. IV.23). If N_{od} is considered, the wider the toe berm, the larger the N_{od}. However, for a specific D_{n50}, a wider toe berm is more resistant than a narrower one instead of having more displacements. Thus, the total N_{od} is not a good estimator of toe berm stability when dealing with wide toe berms (B_t>$3D_{n50}$); the N_{od}* corresponding to the damage to the nominal toe berm, which really supports the armor layer, should be taken into account. Damage observed on the sacrificial toe berm is not relevant when analyzing the hydraulic performance of mound breakwaters.

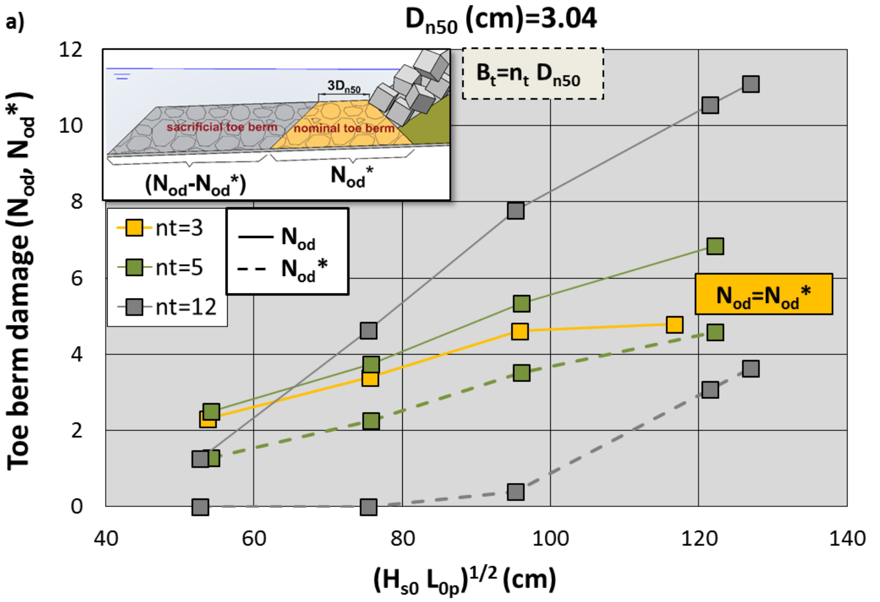

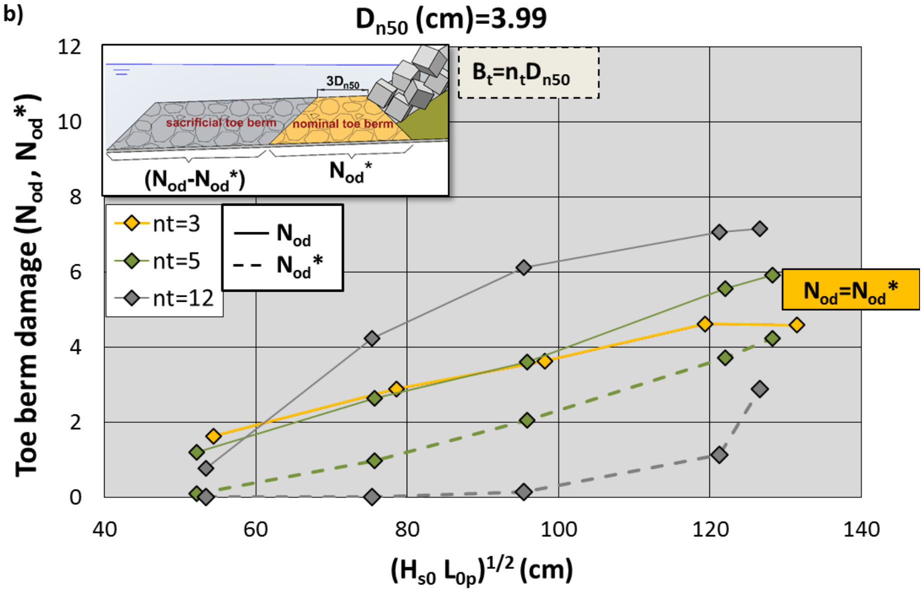

Figure IV.23. Comparison of measured toe berm damage (N_{od}) and nominal toe berm damage (N_{od}*) for tests conducted with rock sizes (a) D_{n50}(cm)=3.04 and (b) D_{n50}(cm)=3.99.

Fig. IV.24 compares measured total toe berm damage (N_{od}) and nominal toe berm damage (N_{od}*) for all tests conducted.

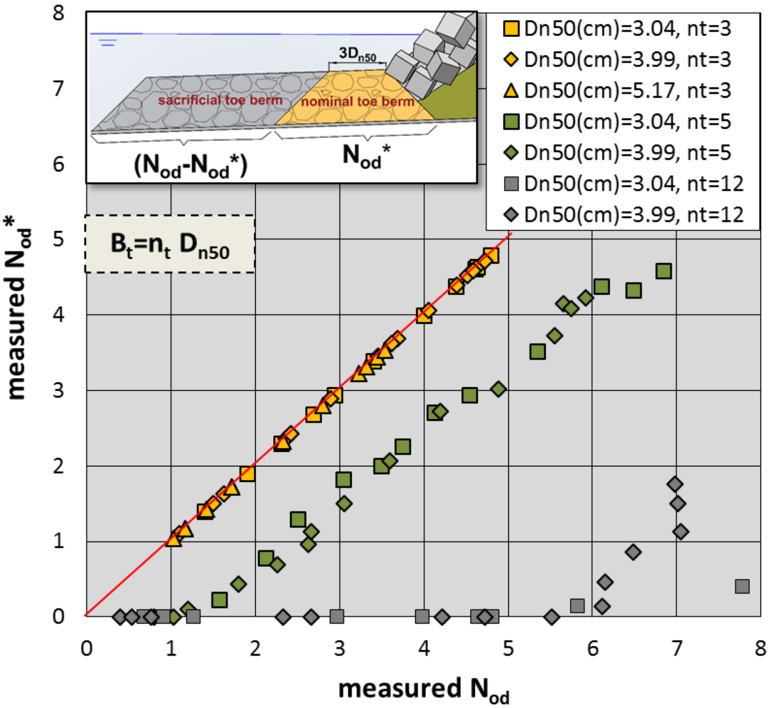

Figure IV.24. Comparison of measured total toe berm damage (N_{od}) and measured nominal toe berm damage (N_{od}*).

IV.3.3. Analysis of armor damage

The damage to double-layer cube armors is examined in this section, when standard (B_t=3D_{n50}) and wide (B_t>3D_{n50}) rock berms are used in the toe of the structure. Only tests conducted with randomly-placed cubes are considered here. Only data obtained from tests with cubes placed uniformly on the armor were used in Section IV.5 to analyze the influence of placement technique on armor stability.

IV.3.3.1. Armor damage with nominal rock toe berm (B_t=3D_{n50})

Fig. IV.25 shows the relation between the armor damage obtained with the virtual net method proposed by Gómez-Martín and Medina (2006), and the water depth (h_s=h_{ss}) for H_{s0}(cm)=16 and T_p(s)=1.8. Armor damage increased up to the water depth of h_s(cm)=16. From approximately h_s(cm)=16, armor damage decreased because the role of the toe protection became less relevant. Armor damage in tests conducted with a toe berm of D_{n50}(cm)=5.17 was less than for D_{n50}(cm)=3.99. Fig. IV.26

illustrates the evolution of the observed armor damage depending on the water depth at the toe (h_s) for all tests conducted with D_{n50}(cm)=3.99 and 5.17, B_t=3D_{n50} and t_t=2D_{n50}.

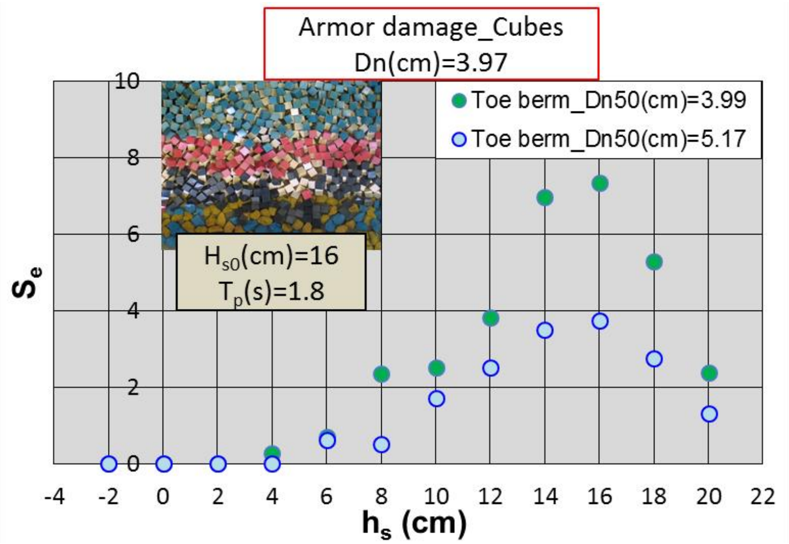

Figure IV.25. Dimensionless armor damage S_e versus the water depth at the toe of the structure after the test conducted with H_{s0}(cm)=16 and T_p(s)=1.8 and rock toe berms with D_{n50}(cm)=3.99 and 5.17.

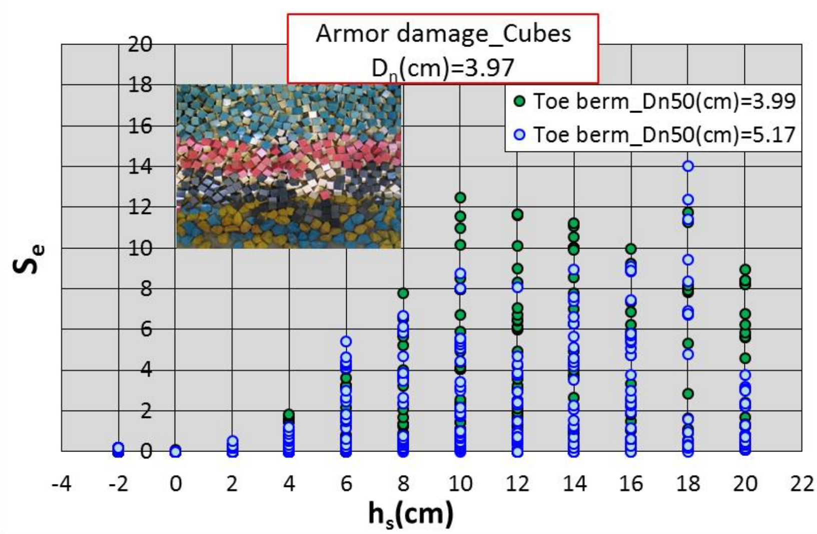

Figure IV.26. Dimensionless armor damage S_e versus the water depth at the toe of the structure for all tests conducted with rock toe berms with D_{n50}(cm)=3.99 and 5.17.

Armor damage was also influenced by the wave variable $(H_{s0}\ L_{0p})^{1/2}$. Fig. IV.27 shows the armor damage (S_e) as a function of $(H_{s0}\ L_{0p})^{1/2}$ and the water depth at the toe (h_s) for tests carried out with D_{n50}(cm)=3.99 and 5.17. For a given water depth, the armor damage increased almost linearly with $(H_{s0}\ L_{0p})^{1/2}$. Straight lines correspond to h_s(cm)=-2, 4, 6, 8 and 14.

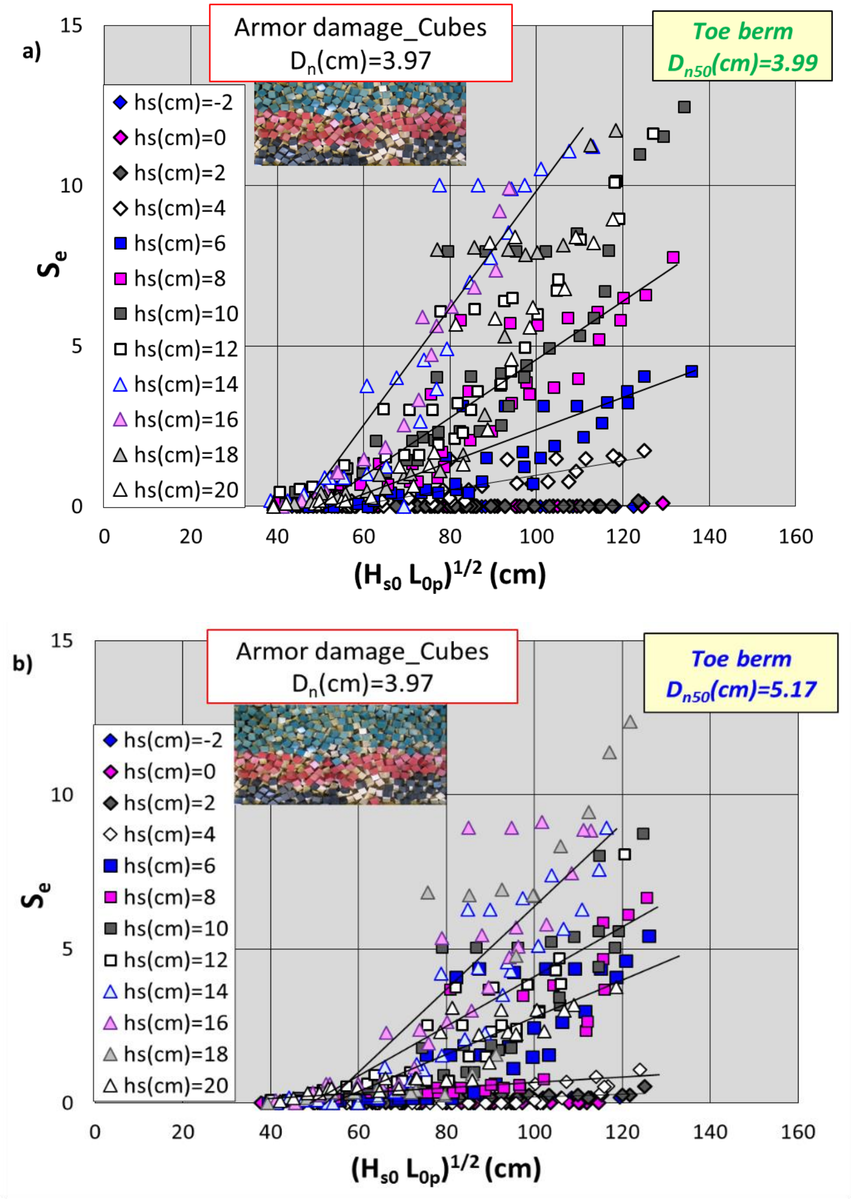

Figure IV.27. Armor damage (S_e) versus $(H_{s0}\ L_{0p})^{1/2}$ for (a) D_{n50}(cm)=3.99 and (b) D_{n50}(cm)=5.17.

The damage parameter N_{od} was also used to characterize armor damage. Fig. IV.28 shows the measured armor damage when using S_e and the measured armor damage with the damage parameter N_{od}. When using N_{od}, heterogeneous packing was not taken into account; only the armor unit extractions were considered. S_e was approximately 1.7 times N_{od}.

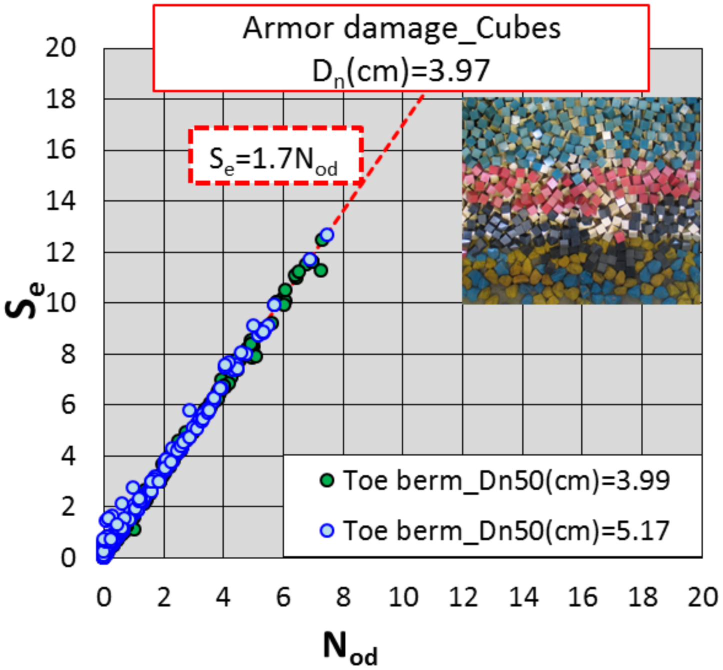

Figure IV.28. Measured armor damage S_e versus measured armor damage N_{od}.

Fig. IV.29 shows the measured N_{od} depending on the water depth at the toe (h_s) for all tests conducted with D_{n50}(cm)=3.99 and 5.17, $B_t=3D_{n50}$ and $t_t=2D_{n50}$.

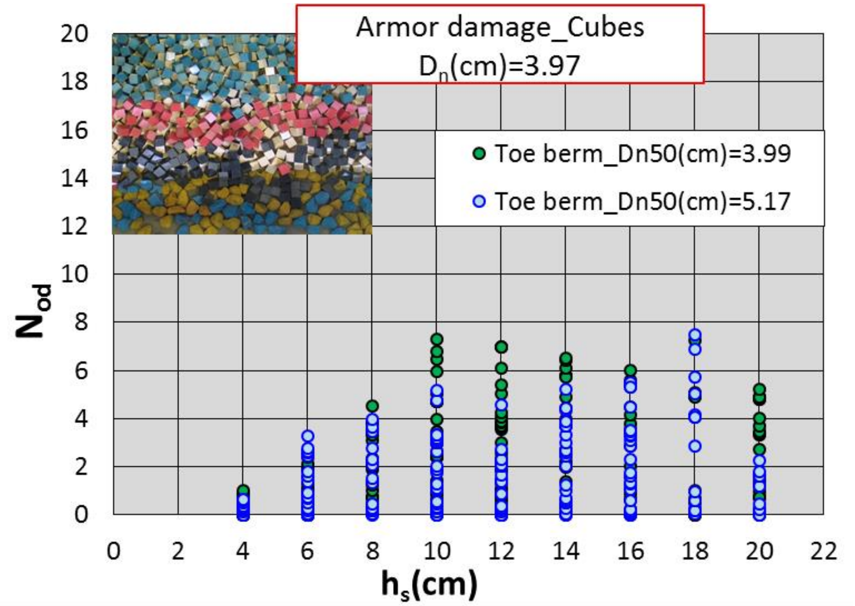

Figure IV.29. Armor damage N_{od} versus water depth at the toe of the structure (h_s) for all tests conducted with rock toe berms with D_{n50}(cm)=3.99 and 5.17.

Additionally, measured toe berm damage N_{od} was compared to measured armor damage N_{od}. Fig. IV.30 shows the relation between the armor and toe damage for each test as a function of the water depth h_s. With low water depths, toe stability was essential for the whole armor stability, and most of the damage was absorbed by the toe protection. However, greater water depths led to more armor damage than toe berm damage. For the toe berm size D_{n50}(cm)=3.99 and low water depths, armor damage was greater than for the toe berm size D_{n50}(cm)=5.17.

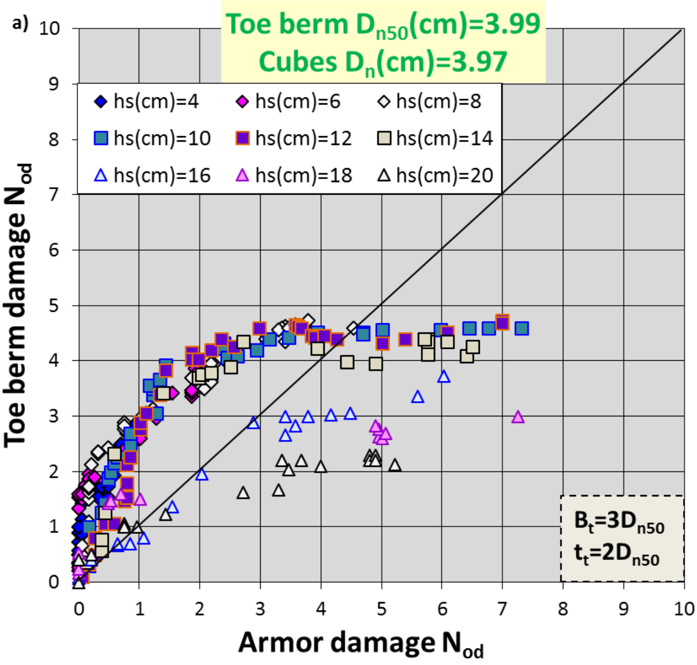

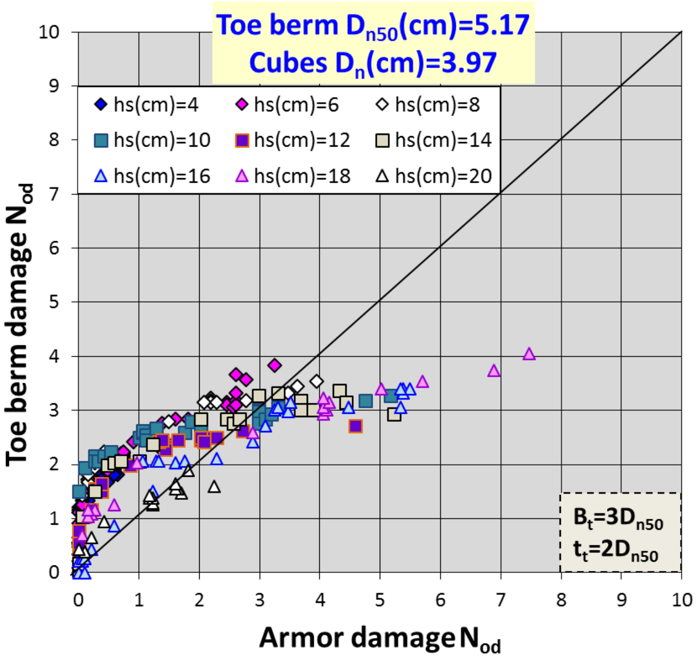

Figure IV.30. Armor damage compared to toe berm damage measured with the parameter N_{od} for toe berm sizes (a) D_{n50}(cm)=3.99 and (b) D_{n50}(cm)=5.17.

IV.3.3.2. Armor damage with three toe berm widths (B_t=3, 5 and 12D_{n50})

The influence of toe berm width and size on cube armor damage was examined. Fig. IV.31 shows the measured equivalent armor damage S_e compared to the wave variable $(H_{s0} L_{0p})^{1/2}$ for tests conducted with wide toe berms (B_t=3, 5 and 12D_{n50}) and a water depth at the toe of the nominal toe berm h_{ss}(cm)=8. Given a rock toe berm size (D_{n50}), S_e increased when reducing the toe berm width (n_t). Given a toe berm width (n_t), S_e increased when reducing the toe berm size (D_{n50}). Therefore, larger rock toe berm sizes as well as wider toe berms had less cube armor damage S_e. A proper design of the toe berm is therefore crucial for the armor stability.

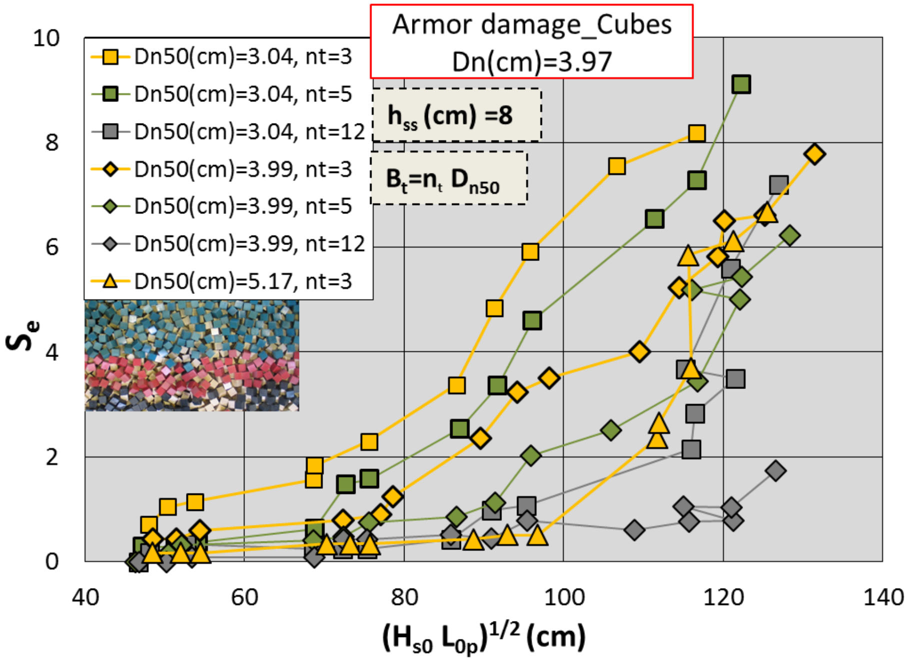

Figure IV.31. Influence of toe berm width on measured armor damage, S_e.

IV.4. New hydraulic stability formulas for toe berms

Based on the data analysis, a new hydraulic stability formula was developed to design submerged (h_t>0) and emerged (h_t<0) standard toe berms (B_t=3D_{n50} and t_t=2D_{n50}) placed on a m=1/10 bottom slope (Section IV.4.1). The required rock size given by the proposed equation for a nominal toe berm (B_t=3D_{n50}) was modified to account for wider toe berms (n_t>3) based on damage measurements of the nominal toe berm (Section IV.4.2).

IV.4.1. Standard toe berms ($B_t=3D_{n50}$)

IV.4.1.1. A new hydraulic stability formula

A formula was developed here to include the most relevant parameters, previously discussed, affecting the hydraulic stability of standard toe berms ($B_t=3D_{n50}$ and $t_t=2D_{n50}$). The relative water depth, h_s/D_{n50}, and the ratio $(H_{s0}\,L_{0p})^{1/2}/\Delta D_{n50}$, were the explanatory dimensionless variables used in the formula. Note that for standard toe berms, $N_{od}=N_{od}$ * and $h_s=h_{ss}$.

Because N_{od} increased almost linearly with the variable $(H_{s0}\,L_{0p})^{1/2}/\Delta D_{n50}$, for a given relative water depth h_s/D_{n50}, up to $N_{od}=4$, the corresponding general formula is

$$N_{od}=N_{od}{*}=\left(\frac{(H_{s0}\;L_{0p})^{1/2}}{\Delta D_{n50}}-c\right)f\left(\frac{h_s}{D_{n50}}\right) \qquad [IV.3]$$

where c is a constant, and f (h_s/D_{n50}) is a function of the relative water depth h_s/D_{n50}.

To calibrate the design formula, only tests corresponding to the maximum significant wave height generated for each peak period and water depth were taken into account. In each test series defined by a water depth at the toe (h_s), toe berm damage generally increased with increasing deep water significant wave heights (H_{s0}) and peak periods (T_p). However, for a specific T_p, the lowest H_{s0} did not significantly increase the toe berm damage N_{od}. Therefore, only the cumulative damage obtained at the highest H_{s0} of each T_p series was considered for the calibration.

One should take into consideration that toe berm damage is associated to a specific wave condition (H_{s0}, T_p), which includes as well the cumulative damage from the previous tests with lower H_{s0} and T_p for a given h_s.

The calibration of Eq. IV.3 with test results led to the following formula for toe berm design (see Herrera and Medina, 2015).

$$N_{od}=N_{od}{*}=\left(\frac{(H_{s0}\;L_{0p})^{1/2}}{\Delta D_{n50}}-5.5\right)\left[\left(-0.2\frac{h_s}{D_{n50}}+1.4\right)\exp\left(0.25\frac{h_s}{D_{n50}}-0.65\right)\right]^{1/0.15}$$

[IV.4]

Eq. IV.4 is valid for standard toe berms ($B_t=3D_{n50}$ and $t_t=2D_{n50}$) placed on steep seafloors (m=1/10) in the range $N_{od}\leq 4.0$, $0.02<s_{0p}=2\pi H_{s0}/gT_p^2<0.07$, $-0.15<h_s/H_{s0}<1.5$ and $-0.5\leq h_s/D_{n50}\leq 5.01$. Eq. IV.4 considers that given a wave storm (H_{s0}, T_p), N_{od} is highest for $h_s/D_{n50}=3.0$ ($h_t/D_{n50}=1.0$). From $h_s/D_{n50}=3.0$, N_{od} decreases when increasing h_s/D_{n50}.

IV.4.1.2. Confidence intervals

Assuming a Gaussian error distribution, the 90% confidence interval for the toe damage estimation given by Eq. IV.4 is

$$N_{od}\Big|_{5\,\%}^{95\,\%} = N_{od} \pm 1.64\ \sqrt{Var(\varepsilon)} \qquad [IV.5]$$

where N_{od} is given by Eq. IV.4 and Var(ε) is the variance in the estimation errors. Var(ε) was considered as a linear function of N_{od} given by Eq. IV.5. N_{od} data were ordered and grouped in ten data sets as shown in Fig. IV.32. The MSE was calculated for each data set (black rhombus in Fig. IV.32). As the MSE increases with increasing N_{od}, the variance in the errors can be estimated by:

$$Var(\varepsilon) = 0.14\ N_{od} + 0.05 \qquad [IV.6]$$

where N_{od} is given by Eq. IV.4. The 90% confidence interval is given by:

$$N_{od}\Big|_{5\%}^{95\%} = N_{od} \pm 1.64\ \sqrt{(0.14\ \ N_{od} + 0.05)} \qquad [IV.7]$$

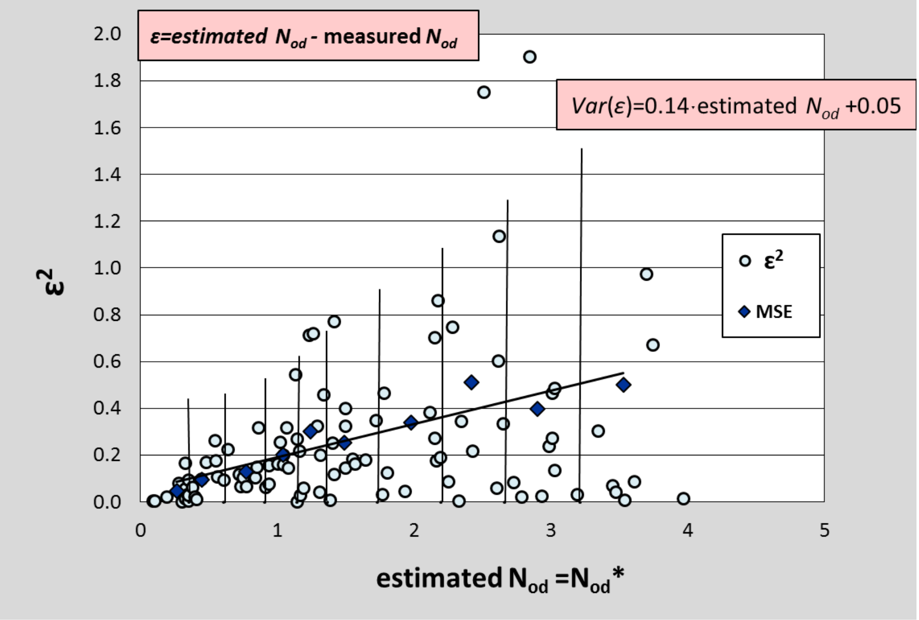

Figure IV.32. Squared toe berm damage errors as a function of the N_{od} given by Eq. IV.4.

Fig. IV.33 compares measured N_{od} and N_{od} estimated by Eq. IV.4 as well as the 90% confidence interval given by Eq. IV.7. The rMSE and the correlation coefficient (r) were used to determine the goodness of fit between the values of N_{od} measured in tests and that given by Eq. IV.4.

The rMSE=0.208 indicates the proportion of variance for N_{od} not explained by Eq. IV.4, and r=0.89 indicates the correlation between measured and estimated values of N_{od}.

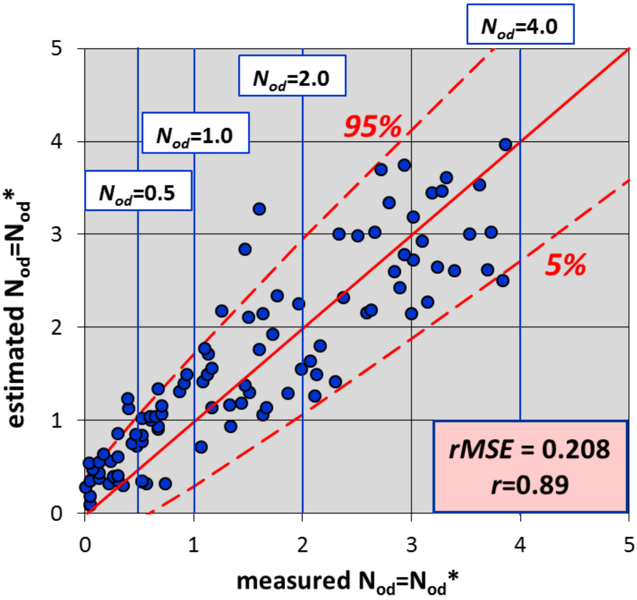

Figure IV.33. Comparison of the $N_{od}=N_{od}^*$ measured in tests and that given by Eq. IV.4 and 90% confidence interval.

IV.4.1.3. Validation with additional tests

Those tests carried out with lower wave heights and not used to calibrate Eq. IV.4, were used later for validation purposes. Only tests with parameters defined within the range of application of the proposed equation were considered in this analysis.

Fig. IV.34 compares the measured toe berm damage N_{od} and the estimated N_{od} using Eq. IV.4. Most tests results fall within the 90% confidence interval with a rMSE=12.4%. Thus, Eq. IV.4 is valid for all data within its range of application ($0.02<s_{0p}<0.07$, $-0.15<h_s/H_{s0}<1.5$ and $-0.5<h_s/D_{n50}<5.01$).

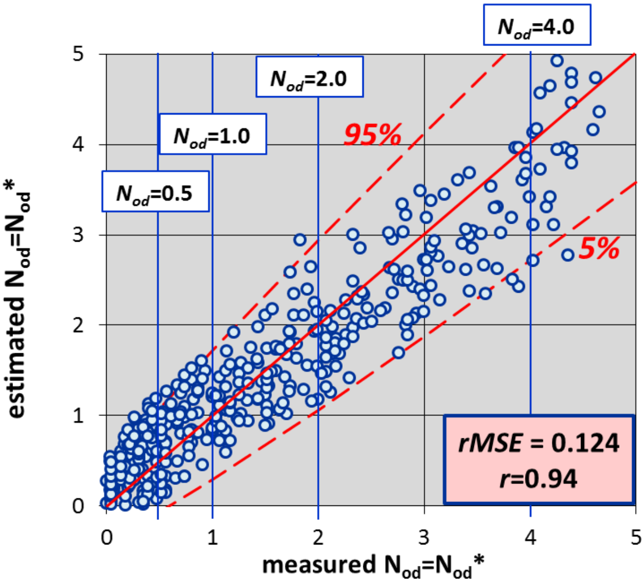

Figure IV.34. Comparison of the measured toe berm damage ($N_{od}=N_{od}^*$) and the estimated toe berm damage ($N_{od}=N_{od}^*$) using Eq. IV.4 for all tests within the range of application.

Four levels of toe berm damage were identified in this study:

(1) no significant movement of toe berm rocks ($N_{od}=N_{od}^*<0.5$)

(2) significant rock movements ($N_{od}=N_{od}^*=1$)

(3) moderate damage but toe berm still provides support to the armor layer ($N_{od}=N_{od}^*=2$)

(4) toe berm failure ($N_{od}=N_{od}^*=4$)

With this classification, a value of $N_{od}=N_{od}^*=1$ was considered a reasonable design criteria when using Eq. IV.4.

IV.4.1.4. Comparison with existing formulas

Different formulas can be used to predict toe berm damage (see Section II.5.2,). Most of them were obtained from laboratory tests with different conditions and foreshore slopes; however, they have been used in this section to compare their damage estimations with the measured toe berm damage. Only tests conducted with submerged toe berms ($h_t>0$) were used in this comparison. The significant wave height measured at G11 was used to estimate the wave height at the toe in the prediction formulas.

Fig. IV.35 shows the N_{od}=N_{od}* measured for those tests conducted in the range 10≤h_s(cm)≤20 (h_t>0) and the toe berm damage prediction given by the existing equations to predict rock toe berm damage. The 90% confidence intervals of the proposed equation (Eq. IV.4) are also depicted in this figure.

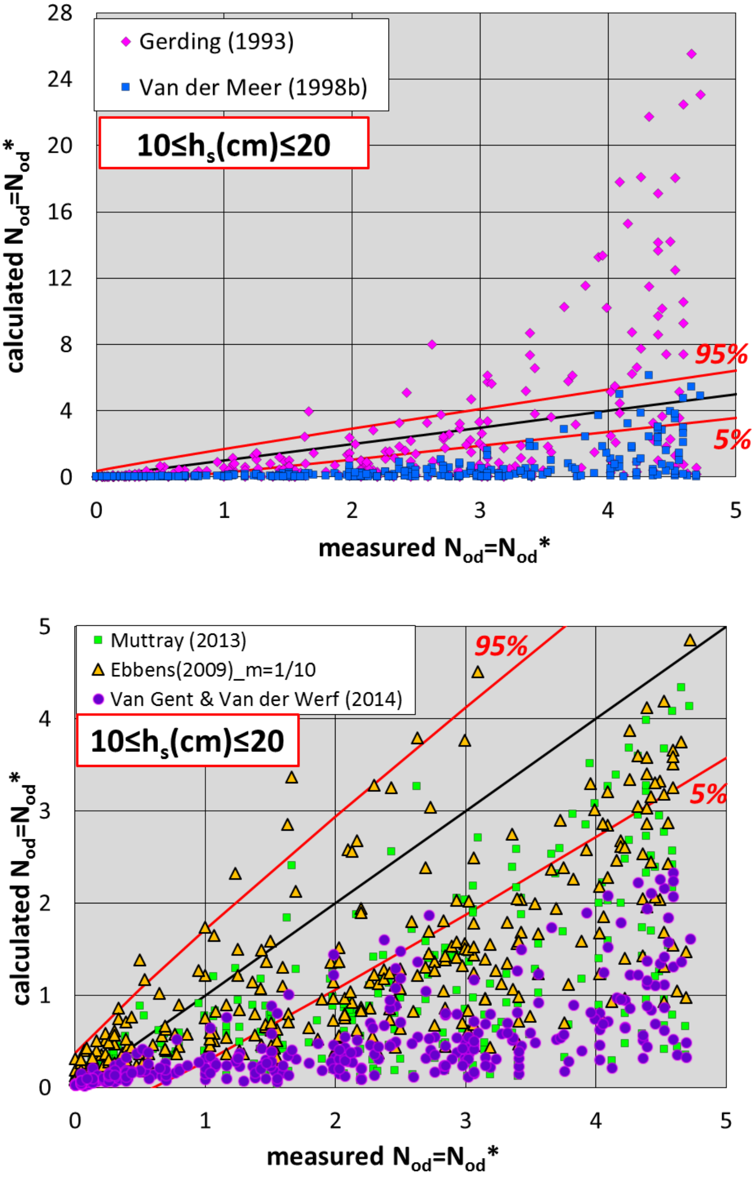

Figure IV.35. Measured toe berm damage (N_{od}=N_{od}*) compared to prediction formulas and 90% confidence intervals of Eq. IV.4 for tests conducted in the range 10≤h_s(cm)≤20 (h_t>0).

Although only tests performed with high water depths were compared, most of equations were based on tests with deeper waters, milder bottom slopes and distinct definitions of damage. Compared to existing equations, Eq. IV.4 provides conservative predictions for cumulative toe berm damage.

IV.4.1.5. Example of application

In this section, examples of application of Eq. IV.4 are given for a standard rock toe berm ($B_t=3D_{n50}$ and $t_t=2D_{n50}$) within its validity ranges.

Three different situations were compared depending on h_s/D_{n50}: (1) $h_s/D_{n50}=0$ and $h_t<0$, (2) $h_s/D_{n50}=2$ and $h_t=0$, and (3) $h_s/D_{n50}=5$ and $h_t>0$. For each case, three stone sizes were considered ($M_{50}(t)=3$, 6 and 12) with a mass density of $\rho_r(t/m^3)=2.70$. A wave climate typical of the Alboran Sea ($H_{s0}(m)=5$, $T_p(s)=11$) was considered.

Figs. IV.36, 37 and 38 show the toe berm damage ($N_{od}=N_{od}^*$) given by Eq. IV.4 depending on the design wave climate for $h_t<0$, $h_t=0$ and $h_t>0$, respectively. For the cases $h_s/D_{n50}=0$ and $h_t<0$ (Fig. IV.36) and $h_s/D_{n50}=5$ and $h_t>0$ (Fig. IV.38), Eq. IV.4 provides reasonable values of N_{od} for the three rock sizes when considering $H_{s0}(m)=5$ and $T_p(s)=11$ ($N_{od}\approx1$ with the medium rock size M_{50} $(t)=6$). If waves are stronger, for instance $H_{s0}(m)=8$ and $T_p(s)=14$, moderate damage ($N_{od}\approx2$) is estimated for this rock size ($M_{50}(t)=6$, $D_{n50}=1.30$).

For the case $h_s/D_{n50}=2$ and $h_t=0$ (Fig. IV.37), the values of N_{od} given by Eq. IV.4 with $H_{s0}(m)=5$ and $T_p(s)=11$ are significantly higher ($N_{od}\approx3$ with the medium rock size M_{50} $(t)=6$); only less intense wave storms can be resisted when $h_s/D_{n50}=2$ and $h_t=0$. One should take into consideration that Eq. IV.4 does not provide reliable values for $N_{od}=N_{od}^*$ above $N_{od}=N_{od}^*=4.0$.

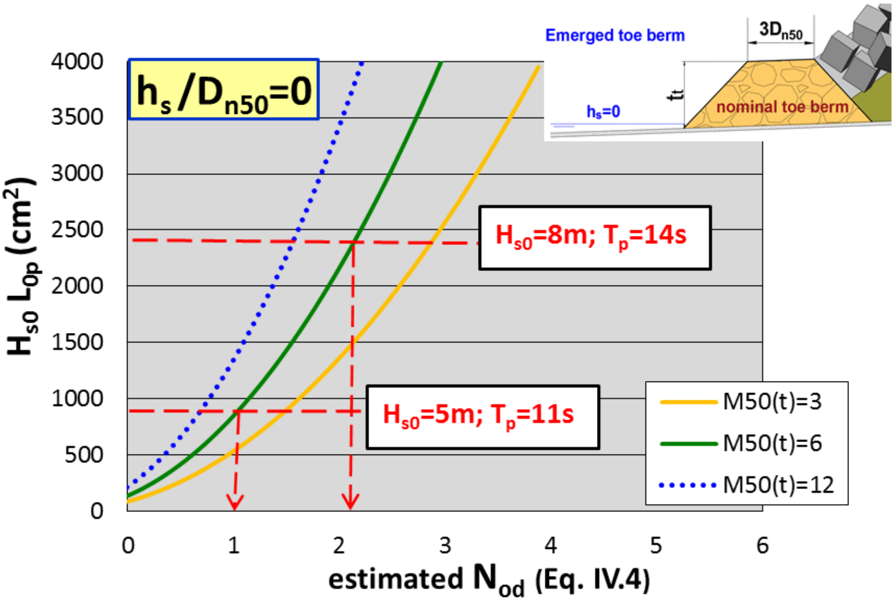

Figure IV.36. Toe berm damage ($N_{od}=N_{od}^*$) given by Eq. IV.4 depending on the variable $H_{s0}\,L_{0p}$, for $h_s/D_{n50}=0$ and $h_t<0$.

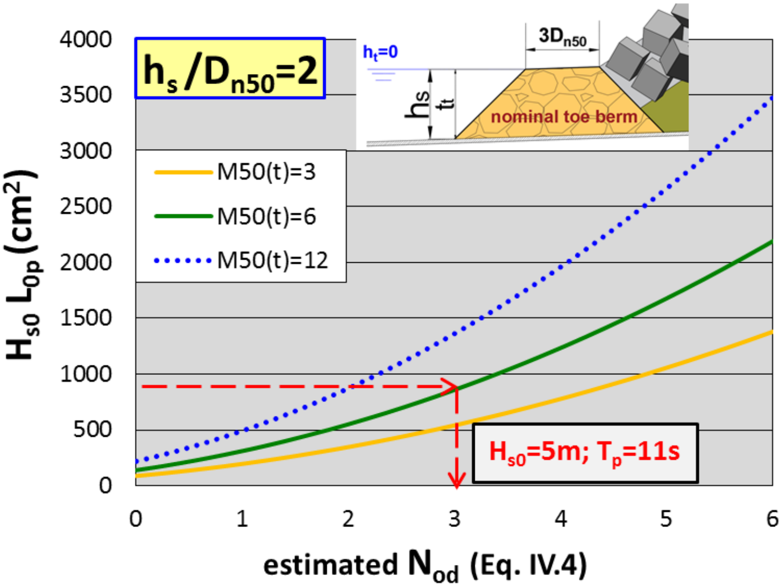

Figure IV.37. Toe berm damage ($N_{od}=N_{od}^*$) given by Eq. IV.4 depending on the variable $H_{s0}\,L_{0p}$, for $h_s/D_{n50}=2$ and $h_t=0$.

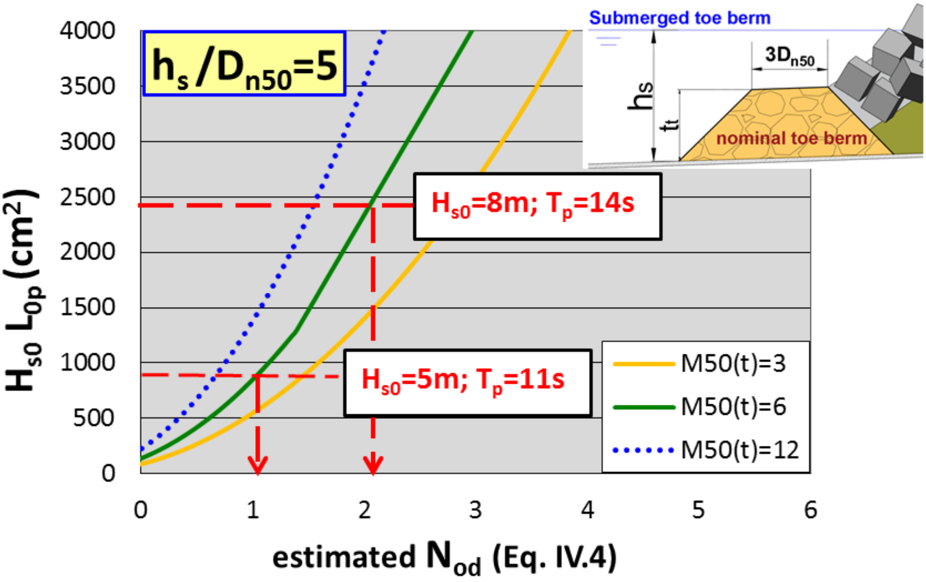

Figure IV.38. Toe berm damage (N_{od}=N_{od}*) given by Eq. IV.4 depending on the variable H_{s0} L_{0p}, for h_s/D_{n50}=5 and h_t>0.

Fig. IV.39 illustrates the toe berm damage (N_{od}=N_{od}*) given by Eq. IV.4 depending on h_s/D_{n50} when H_{s0}(m)=5 and T_p(s)=11 is the design wave storm. Toe berm damage is greatest when h_s/D_{n50}=3 (h_t=D_{n50}); toe berm damage is reduced by removing from the worst situation (h_t=D_{n50}), either h_t>D_{n50} or h_t<D_{n50}. Eq. IV.4 can be used to determine a more stable toe berm position, converting the nominally submerged toe berm into an emergent or completely submerged toe berm within the range $-0.5 \le h_s/D_{n50} \le 5.01$.

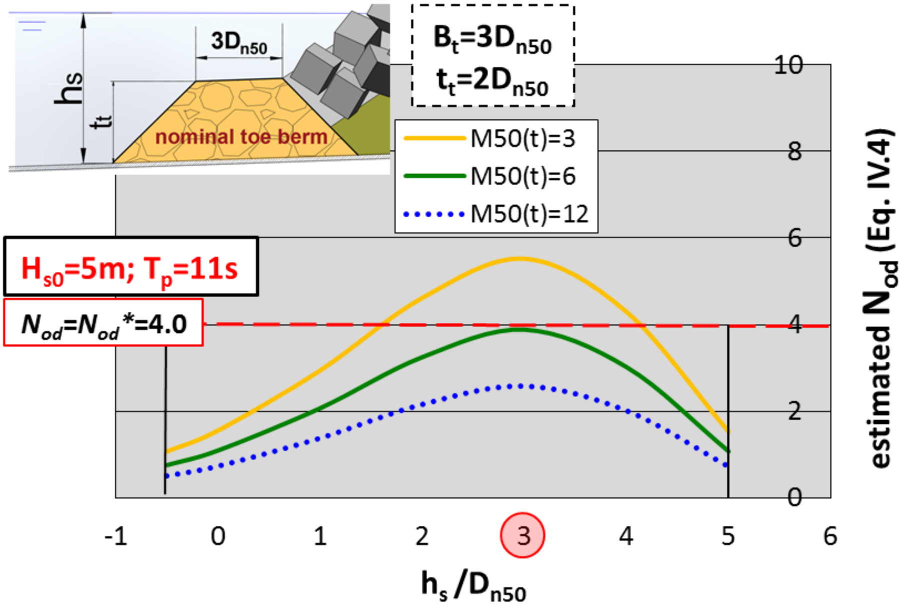

Figure IV.39. Toe berm damage (N_{od}=N_{od}*) given by Eq. IV.4 depending on h_s/D_{n50} for H_{s0}(m)=5 and T_p(s)=11.

IV.4.2. Wide toe berms (B_t>3D_{n50})

Eq. IV.4 considers that N_{od} is highest for h_s/D_{n50}=3.0 (h_t/D_{n50}=1.0). In these conditions, the required nominal diameter (D_{n50}) given by Eq. IV.4 may be so large for certain wave storms that it is not possible to obtain those rocks from the available quarries. In this case, the toe position should be moved to deeper or shallower water where the toe berm is more stable (see Fig. IV.39). However, this design change is not always possible due to environmental, economic or operational constraints. In this section, a new design method is proposed to construct wider toe berms (B_t>3D_{n50}) capable of resisting the wave conditions. As demonstrated in Section IV.3.2.2, the damage to the nominal toe berm, N_{od}*, must be considered when using wide toe berms.

IV.4.2.1. Hydraulic stability formula of wide toe berms

Eq. IV.4 was extended to design toe berms with $3D_{n50} \leq B_t \leq 12D_{n50}$ and $t_t=2D_{n50}$, placed on steep sea bottoms (m=1/10) when the SWL is close to the crest of the toe berm $1.5 \leq h_{ss}/D_{n50} \leq 2.6$, $0.02 \leq s_{0p} \leq 0.07$ and $0.4 \leq h_{ss}/H_{s0} \leq 1.0$.

Fig. IV.22 shows that under the same wave conditions (H_{s0}, T_p), the toe berm with D_{n50}(cm)=3.99 and n_t=5 provided almost the same N_{od}* as the toe berm with D_{n50}(cm)=5.17 and n_t=3. Analogously, the toe berm with D_{n50}(cm)=3.04 and n_t=5 gave values of N_{od}* similar to those of the toe berm with D_{n50}(cm)=3.99 and n_t=3. Fig. IV.40a illustrates the values of N_{od}* for all tests conducted with D_{n50}(cm)=3.99 with n_t=5 and D_{n50}(cm)=5.17 with n_t=3; Fig. IV.40b illustrates the values of N_{od}* for all tests conducted with D_{n50}(cm)=3.04 with n_t=5 and D_{n50}(cm)=3.99 with n_t=3.

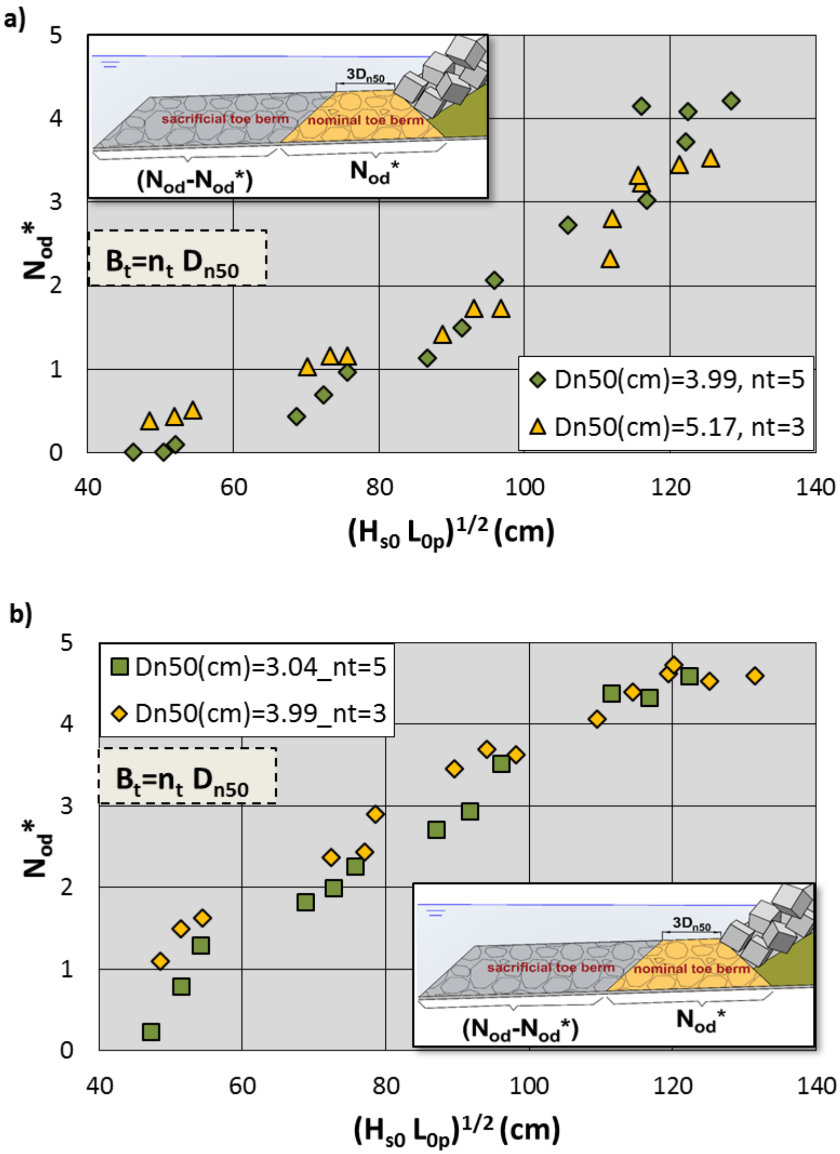

Figure IV.40. Measured nominal toe berm damage (N_{od}*) versus (H_{s0} L_{0p})$^{1/2}$ for tests conducted with (a) D_{n50}(cm)=3.99 with n_t=5 and D_{n50}(cm)=5.17 with n_t=3, and (b) D_{n50}(cm)=3.04 with n_t=5 and D_{n50}(cm)=3.99 with n_t=3.

These findings suggest that the rock size can be reduced by increasing the toe berm width. It is possible to keep N_{od}* constant by reducing D_{n50} and increasing n_t, or vice versa. Because Eq. IV.4 is valid to design nominal toe berms with $n_t=3$, the tested D_{n50} and n_t were related to the configuration of the nominal toe berm ($n_t=3$) with rock size $D_{n50}=D_{n50,3}$, following Eq. IV.8.

$$\frac{D_{n50,n_t}}{D_{n50,3}}=\left(\frac{3}{n_t}\right)^{\mu} \qquad [IV.8]$$

where $D_{n50,3}$ is the nominal diameter of rocks for the nominal toe berm ($n_t=3$), $D_{n50,nt}$ is the nominal diameter of rocks for wider toe berms ($3<n_t\leq 12$), and μ is a positive parameter to be calibrated using the test results described above (the best is μ=0.4). Eq. IV.8 indicates that, given a nominal toe berm with $n_t=3$ and $D_{n50}=D_{n50,3}$, an equivalent toe berm can be defined with higher n_t ($n_t>3$) and lower D_{n50} ($D_{n50,nt}<D_{n50,3}$) to provide similar N_{od}*.

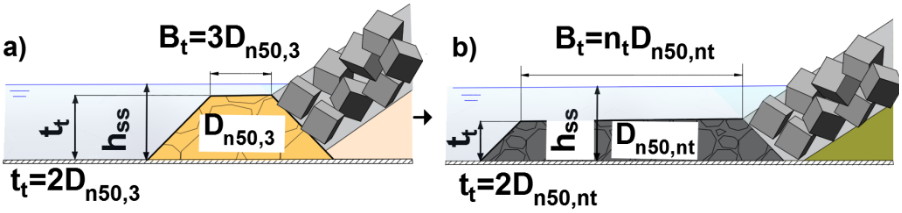

Figure IV.41. (a) Nominal toe berm ($n_t=3$) and (b) equivalent wider toe berm ($3<n_t\leq 12$).

Because Eq. IV.4 is valid to design rock toe berms with $n_t=3$, the estimated N_{od} given by Eq. IV.4 corresponds to the nominal toe berm damage (N_{od}*), the water depth at the toe (h_s) corresponds to the water depth at the toe of the nominal toe berm (h_{ss}) and the nominal diameter (D_{n50}) to $D_{n50,3}$. With these considerations, Eqs. IV.4 and IV.8 can be combined as follows (see Herrera et al., 2016):

$$N_{od}{*}=\left(\frac{(H_{s0}L_{0p})^{1/2}}{\Delta D_{n50,n_t}\left(\frac{n_t}{3}\right)^{\mu}}-5.5\right) \qquad [IV.9]$$

$$x\left[\left(-0.2\frac{h_{ss}}{D_{n50,n_t}\left(\frac{n_t}{3}\right)^{\mu}}+1.4\right)\exp\left(0.25\frac{h_{ss}}{D_{n50,n_t}\left(\frac{n_t}{3}\right)^{\mu}}-0.65\right)\right]^{1/0.15}$$

The best agreement between the measured N_{od}* and the estimated N_{od}* given by Eq. IV.9 was found for μ=0.4 (see Fig. IV.43).

Eq. IV.9 extends the application range of Eq. IV.4 to wider toe berms. Eq. IV.9 with μ=0.4 provides the rock size required for toe berms with $3D_{n50}\leq B_t\leq 12D_{n50}$ placed on a m=1/10 sea bottom and $1.5\leq h_{ss}/D_{n50}\leq 2.6$, $0.02\leq s_{0p}\leq 0.07$ and $0.4\leq h_{ss}/H_{s0}\leq 1.0$, using the damage parameter N_{od}*. When designing with N_{od}*, common values for acceptable damage may be used directly: initiation of damage (N_{od}*=1), moderate damage but toe berm still providing support to the armor (N_{od}*=2), and toe berm failure (N_{od}*=4).

For an acceptable level of damage (N_{od}*=0.5 or 1.0), Eq. IV.4 can be used first to calculate the rock size for a nominal toe berm, $D_{n50,3}$, and Eq. IV.8 can be used later to design a wider toe berm ($3<n_t\leq 12$) with smaller rocks ($D_{n50,nt}$). A practical application of this process is shown in Fig. IV.42. Fig. IV.42a shows the nominal diameter of rocks for the nominal toe berm ($D_{n50,3}$), estimated with Eq. IV.4 and μ=0.4, as a function of the deep water wave conditions, $(H_{s0}\,L_{0p})^{1/2}$, for the relative water depths at the toe of the nominal toe berm $h_{ss}/D_{n50,3}$=1.5, 2.0 and 2.5. Fig. IV.42b shows the relation between nominal diameters ($D_{n50,3}$ and $D_{n50,nt}$) as a function of the toe berm width ($3\leq n_t\leq 12$). $D_{n50,nt}$ can be selected by the designer considering the rock sizes available at the construction site. Red arrows in Fig. IV.42 indicate the relationship considered in Section IV.4.2.4.

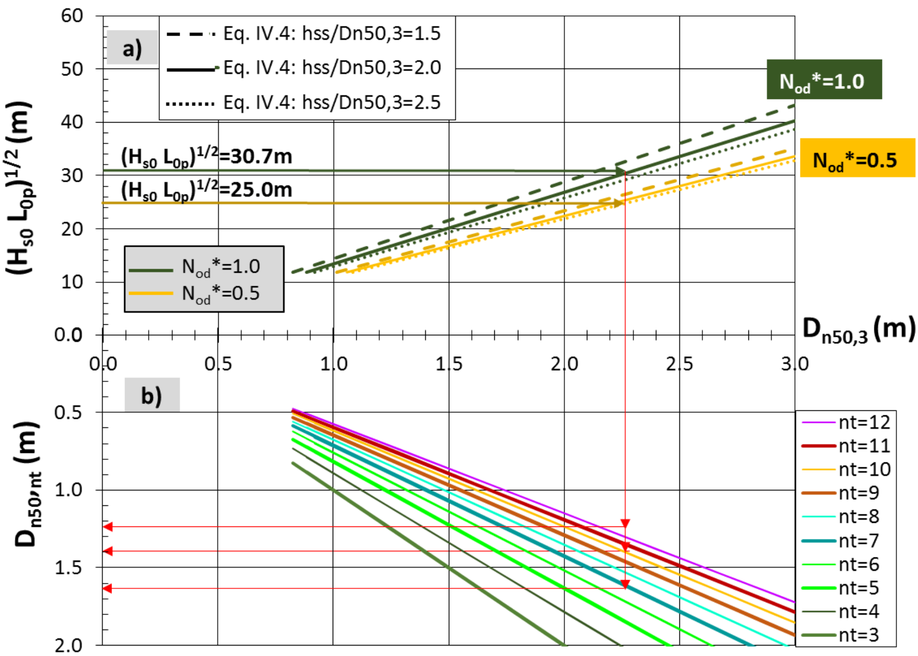

Figure IV.42. (a) $D_{n50,3}$ estimated with Eq. IV.4 and (b) $D_{n50,nt}$ as a function of $D_{n50,3}$ and the toe berm width (n_t).

IV.4.2.2. Confidence intervals

Assuming a Gaussian error distribution, the 90% confidence interval for the toe damage estimation given by Eq. IV.9 is provided by Eq. (IV.10).

$$N_{od}*\Big|_{5\ \%}^{95\ \%} = N_{od}* \pm 0.83 \qquad [IV.10]$$

Fig. IV.43 compares measured N_{od} and estimated N_{od} given by Eq. IV.9 as well as the 90% confidence interval given by Eq. IV.10. The rMSE and the r were used to determine the goodness of fit between the values of N_{od} measured in tests and those given by Eq. IV.9.

The rMSE=0.187 indicates the proportion of variance in N_{od}* not explained by Eq. IV.9 and r=0.91, the correlation between measured and estimated values of N_{od}*.

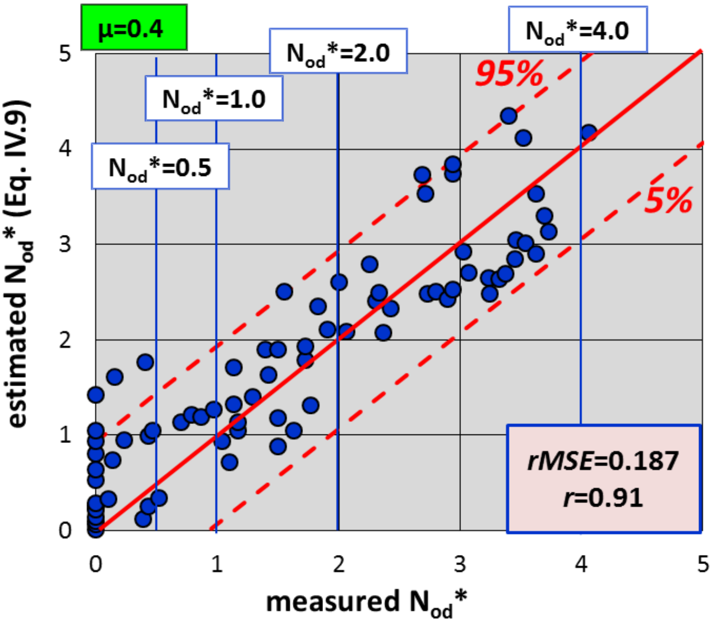

Figure IV.43. Comparison of the N_{od}* measured in tests and the N_{od} given by Eq. IV.9 with μ=0.4 and 90% confidence interval.

IV.4.2.3. Comparison with existing formulas

As mentioned in Section II.5.2, Van Gent and Van der Werf (2014) explicitly introduced the toe berm width (B_t) in the design equation for rock toe berms. For a given amount of acceptable damage, the required rock size, according to the study by Van Gent and Van der Werf (2014), is obtained with Eq. II.31, which was based on laboratory tests with a m=1/30 bottom slope, and no severe depth-limited wave breaking. Two toe berm widths were considered ($B_t=3D_{n50}$ and $9D_{n50}$), but only the total toe berm damage (N_{od}) was measured after each test. In order to consider that N_{od} increases with the toe berm width, these authors proposed multiplying the design N_{od} value by a factor f_B when $3D_{n50}<B_t \leq 9D_{n50}$.

$$f_B = \left(\frac{B_t}{3D_{n50}}\right)^{1/2} = \left(\frac{n_t}{3}\right)^{1/2} \qquad \text{[IV.11]}$$

Thus, when $B_t=3D_{n50}$, Eq. II.31 is directly applicable. If $3D_{n50}<B_t=n_t\,D_{n50}\leq 9D_{n50}$ and $t_t=2D_{n50}$, Eq. II.31 may be rewritten as follows:

$$D_{n50,n_t} = 0.32\left(\frac{H_s}{\Delta\left(N_{od}\,f_B\right)^{1/3}}\right)\left(\frac{2D_{n50,nt}}{H_s}\right)^{1/3}\left(\frac{n_t D_{n50,nt}}{H_s}\right)^{0.1}\left(\frac{\hat{u}_\delta}{\sqrt{gH_s}}\right)^{1/3} \qquad \text{[IV.12]}$$

Eq. IV.12 is equivalent to Eq. II.31 for n_t=3. Comparing Eqs. II.31 and IV.12, the relation between the required nominal diameters for the design of a nominal toe berm with n_t=3 and a toe berm with $3<n_t\leq 9$ also follows the potential relationship given by Eq. IV.8, but with the shape parameter μ=2/17 instead of μ=0.4 used in Eq. IV.9.

$$\frac{D_{n50,nt}}{D_{n50,3}}=\left(\frac{3}{n_t}\right)^{1/6}\left(\frac{D_{n50,nt}}{D_{n50,3}}\right)^{1/3}\left(\frac{nD_{n50,nt}}{3D_{n50,3}}\right)^{0.1}=\left(\frac{3}{n_t}\right)^{\frac{2}{17}} \qquad [IV.13]$$

Fig. IV.44 shows the N_{od}* measured in this study and that estimated by Eq. IV.9 when using μ=2/17 instead of μ=0.4; the agreement is poor, rMSE=1.07>>0.187 and r=0.77<<0.91.

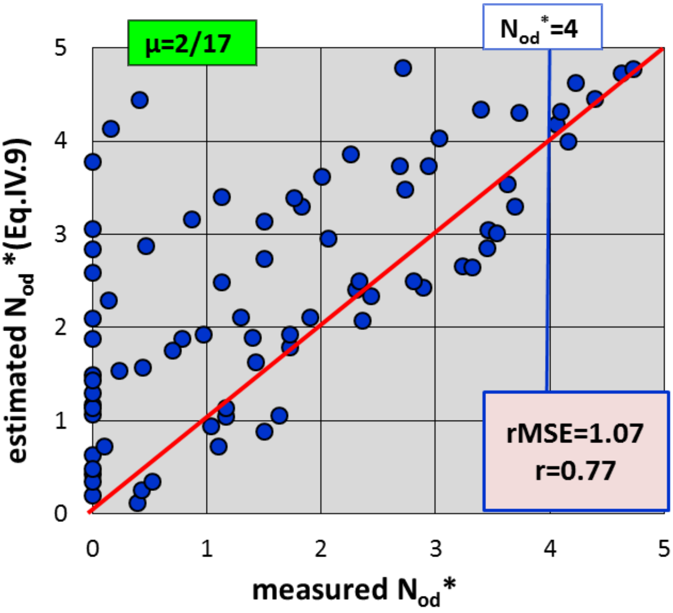

Figure IV.44. Comparison of the N_{od}* measured in tests and that estimated by Eq. IV.9 using μ=2/17 instead of μ=0.4.

Thus, although the relation $D_{n50,n}/D_{n50,s}=(3/n_t)^{\mu}$ could be valid for both studies (Van Gent and Van der Werf 2014, and the present study), the parameter μ depends on the test conditions. The divergence between μ=2/17 and 0.4 highlights the distinct performance of the toe berm when dealing with plunging waves breaking on a steep sea bottom (m=1/10) combined with very shallow waters (as seen in the case of this study), or when dealing with gentler sea bottoms (m=1/30) and no severe depth-limited wave breaking. Both cases indicate that rock size and toe berm width should be considered together when designing a rock toe berm.

IV.4.2.4. Example of application

A practical application is described here to design a rock toe berm placed on a m=1/10 sea bottom combined with the SWL close to the top of the berm ($h_{ss} \approx 2D_{n50}$). Eq. IV.4 was applied first to a standard rock toe berm ($B_t=3D_{n50}$ and $t_t=2D_{n50}$) as shown in Fig. IV.42a, using the recommended design value of $N_{od}*=1$. A design storm for the Alboran Sea area ($H_{s0}(m)=5$, $T_p(s)=11$) was assumed and the water depth at the toe was fixed at $h_{ss}(m)=4.5$. With these conditions ($(H_{s0}\ L_{0p})^{1/2}(m)=30.7$), the required rock size estimated by Eq. IV.4 was $D_{n50(3)}(m)=2.23$ ($M_{50}(t)=30$) for rocks with a mass density $\rho_r(g/cm^3)=2.70$. In order to reduce the required large rock size, Eq. IV.8 with $\mu=0.4$ was applied later (Fig. IV.42b). When considering a toe berm with six rock rows in the upper layer ($n_t=6$), the required rock size is reduced by 75%, leading to rocks with $D_{n50}(m)=1.7$ and $M_{50}(t)=13$. If the available rock size at the construction site is smaller, a wider toe berm is required with n_t in the range $3<n_t\leq 12$. Fig. IV.45 depicts the reduction in the rock mass (M_{50}) depending on n_t when using Eq. IV.8 and the initial rock mass $M_{50}(t)=30$ for $n_t=3$. Rocks with $M_{50}(t)=13.0$, 8.0 and 5.7 may be used when considering $n_t=6$, 9 and 12, respectively.

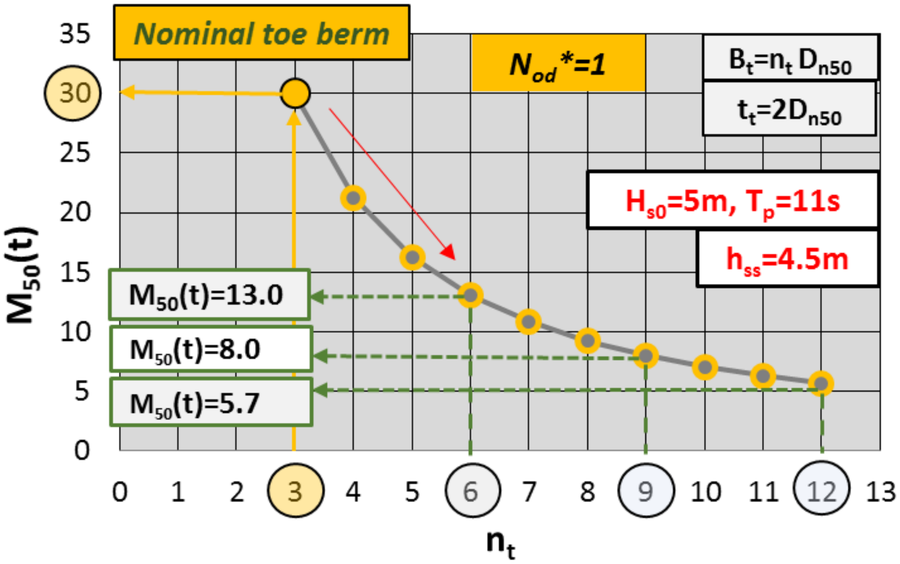

Figure IV.45. Rock mass (M_{50}) depending on the toe berm width ($B_t=n_t\ D_{n50}$).

IV.5. Influence of the placement technique on cube armor stability

IV.5.1. Introduction

Cubes and parallelepiped blocks are usually placed in two layers on the armor of conventional mound breakwaters without any predetermined orientation (random placement). However, randomness is not usually controlled in the prototypes or small scale models, which can lead to undesired arrangements during the construction and significant model effects. Cube units in a double-layer armor tend to change positions favoring face-to-face fitting although no cube is extracted from the armor during wave attack (HeP); this tendency can be influenced by the placement technique.

On the other hand, cube armors can also be placed with a uniform pattern like the cube revetment of the Maasvlakte 2, recently constructed in Rotterdam (Loman et al., 2012).

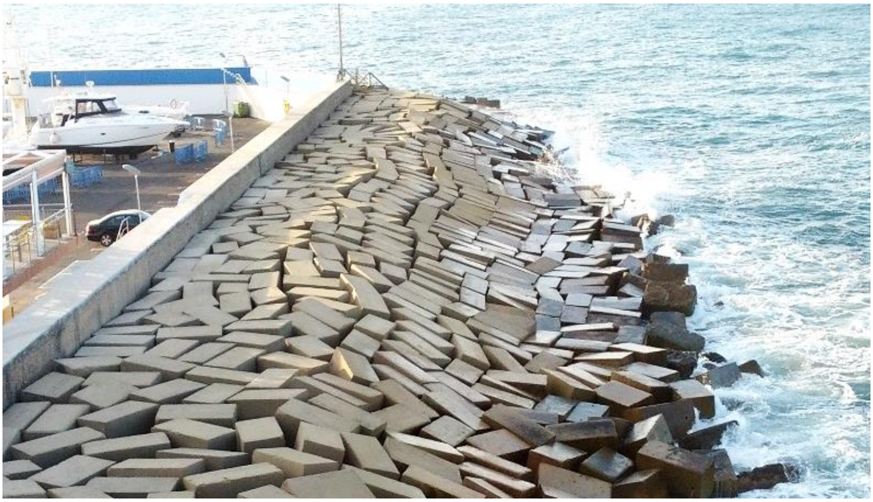

Figure IV.46. Double-layer armor with face-to-face fitting parallelepiped blocks. Mazarrón, Murcia (Spain).

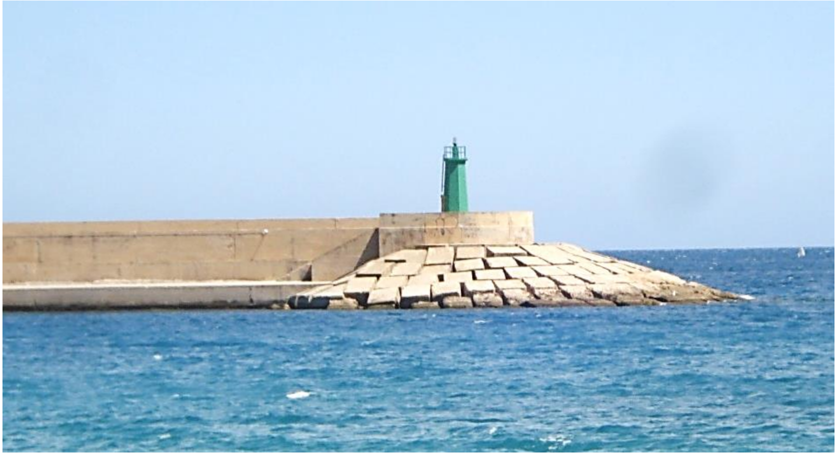

Figure IV.47. Uniformly-placed cube roundhead. Jávea, Alicante (Spain).

In this section, the influence of placement technique on cube armor stability is analyzed using Neural Networks (NNs). NN systems belong to a group of optimization techniques commonly-used in the artificial intelligence field (see Ansari and Hou, 1997). NNs can be used to extract patterns and detect trends when the interrelationships among parameters are complex. NNs are inspired in the human biological nervous system; they are organized in layers with units called neurons. Several types of NNs exist nowadays; the standard multi-layer feed-forward NN is frequently-used in maritime engineering. It has different layers of neurons connected without any feedback. NN models have been widely used to solve problems related to coastal structures (e.g. Mase et al., 1995; Van Gent and Van den Boogaard, 1998; Deo et al., 2002; Medina, 1999; Medina et al., 2002; Panizzo et al., 2003; Kim and Park, 2005; Panizzo and Briganti, 2007; Van Gent et al., 2007; Garrido and Medina, 2012).

In the present PhD, the armor damage (S_e) obtained in the laboratory tests conducted with uniformly- and randomly-placed cubes is analyzed using a multi-layer feed-forward NN with only one hidden layer and a backpropagation algorithm.

IV.5.2. Artificial neural network model for armor damage

The aim of the NN model was to examine the armor damage characterized in the experiments with the equivalent dimensionless armor damage (S_e) given by Eq. II.18. The basic experimental data were 114 tests carried out in the LPC-UPV wave flume with cubes of D_n(cm)=3.97, randomly-and uniformly-placed on the armor with similar armor porosity (ϕ=1.16), and a rock toe berm with D_{n50}(cm)=5.17, B_t=3D_{n50} and t_t=2D_{n50}; experiments were conducted in breaking wave conditions and without overtopping.

Experimental data were randomly separated for learning, testing and validation; 80% of the data were used to teach the NN model, 10% of the data were used for testing, 10% of the data were used for validation. Six input variables influenced the armor damage: incident spectral significant wave height at the wavemaker (H_{m0i}), deep water wave length ($L_{0p}=gT_p^2/2\pi$), cube nominal diameter (D_n), relative submerged mass density ($\Delta=[\rho_r-\rho_w]/\rho_w$), water depth at toe ($h_s$) and the placement technique (0=uniform; 1=random). However, only three dimensionless variables were used to feed the NN model: (1) $(H_{m0i}\, L_{0p})^{1/2}/\Delta D_n$, (2) $h_s/\Delta D_n$ and (3) placement technique (see Fig. IV.48).

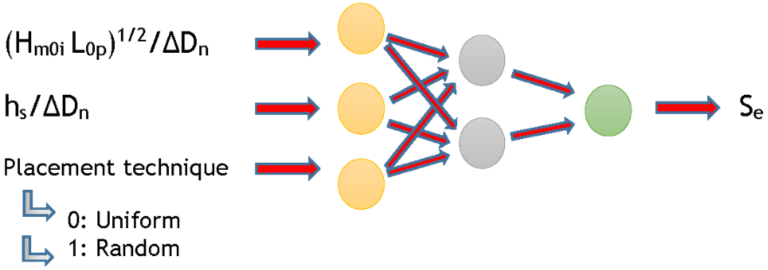

Figure IV.48. NN configuration.

The predicted squared error (PSE), suggested by Moody (1992), was used to calculate the number of neurons in the hidden layer (Eq. IV.14).

$$PSE = MSE\left[1+\frac{2N_p}{(N_o-N_p)}\right]=\frac{1}{N_o}\sum_{i=1}^{N_o}(t_i-e_i)^2\left[1+\frac{2N_p}{(N_o-N_p)}\right] \qquad [IV.14]$$

where N_p is the number of free parameters, N_o is the number of observations, t_i is the target value and e_i is the estimated value.

PSE decreases with the number of neurons in the hidden layer until the optimum; more hidden neurons lead to more degrees of freedom (more adjustable parameters) in the model. From the optimum number of neurons, PSE increases because the NN tends to model noisy fluctuations in the data set, which is unfavorable for the accuracy of the real predictions. When this occurs, the NN is said to be overlearning. To avoid overlearning of the NN, an early stopping criterion (Heskes, 1997) was used in the process. Fig. IV.49 shows the error obtained between the damage measured in tests and that estimated by the NN model when varying the number of neurons in the hidden layer from 1 to 5. Two neurons were required to explain armor damage.

Fig. IV.50 shows the armor damage measured in tests compared to that estimated by the NN model with two neurons in the hidden layer. The rMSE=0.114 obtained from the testing data set (blind data) was used to measure the goodness of fit.

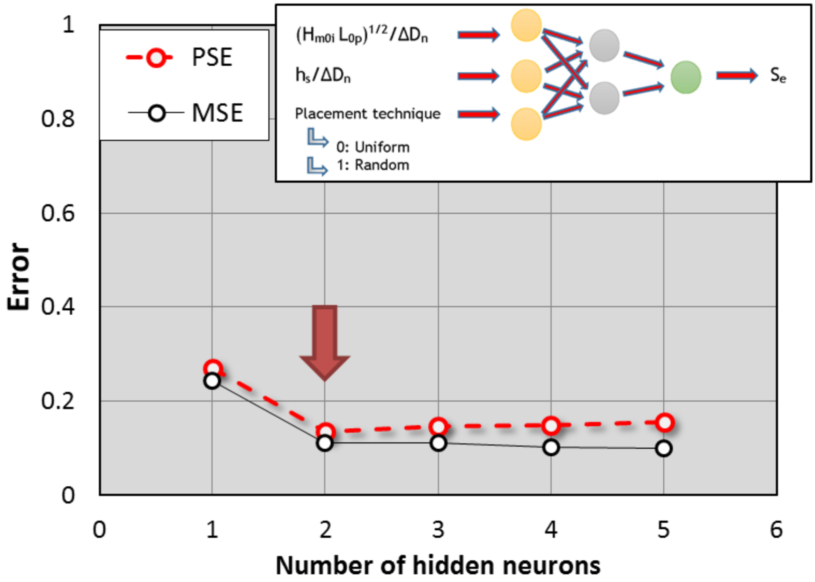

Figure IV.49. NN performance for configurations with different numbers of neurons in the hidden layer.

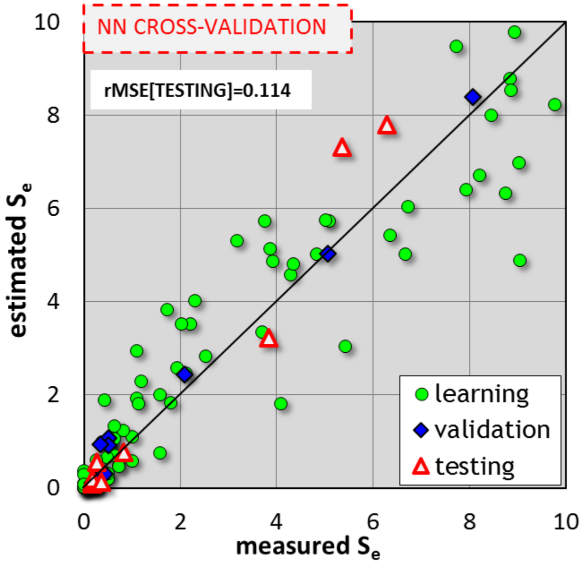

Figure IV.50. Comparison of NN estimations and experimental observations of S_e.

IV.5.3. Neural network simulations

The calibrated NN model was used as virtual wave flume (see Garrido and Medina, 2012) to simulate the behavior of cube armors with uniform and random placement.

Figs. IV.51 and IV.52 show the variations in armor damage estimations when different input variables are used. Fig. IV.51 shows the estimations of S_e given by the NN model when varying the input variable $(H_{m0i}\ L_{0p})^{1/2}/\Delta D_n$ and fixing the relative water depths at the toe at $h_s/\Delta D_n$=-0.4, 0.8 and 2.0. For all $h_s/\Delta D_n$, armor damage increased when increasing $(H_{m0i}\ L_{0p})^{1/2}/\Delta Dn$ for both random and uniform placement. More energetic waves (H_{m0i}, L_{0p}) and smaller armor unit sizes (ΔD_n) gave higher values of S_e. Armor damage was only slightly higher with uniform placement.

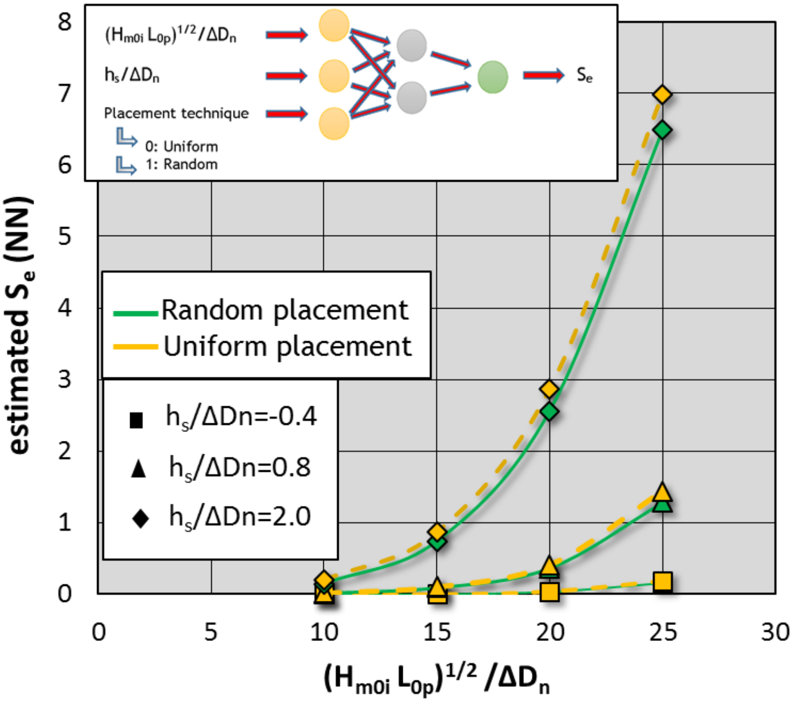

Figure IV.51. *S_e* estimated by NN depending on $(H_{m0i}\ L_{0p})^{1/2}/\Delta D_n$ for cubes randomly- and uniformly-placed on the armor layer.

Fig. IV.52 shows the estimations for S_e given by the NN model when varying the input variable $h_s/\Delta D_n$ and fixing $(H_{m0i}\ L_{0p})^{1/2}/\Delta D_n$ in the last step tested. Thus, the estimations of S_e shown in Fig. IV.52 correspond to the cumulative damage of all tests generated for a given water depth at the toe. Armor damage increases with the relative water depth up to $h_s/\Delta D_n$=2.8 and from this level, S_e decreases.

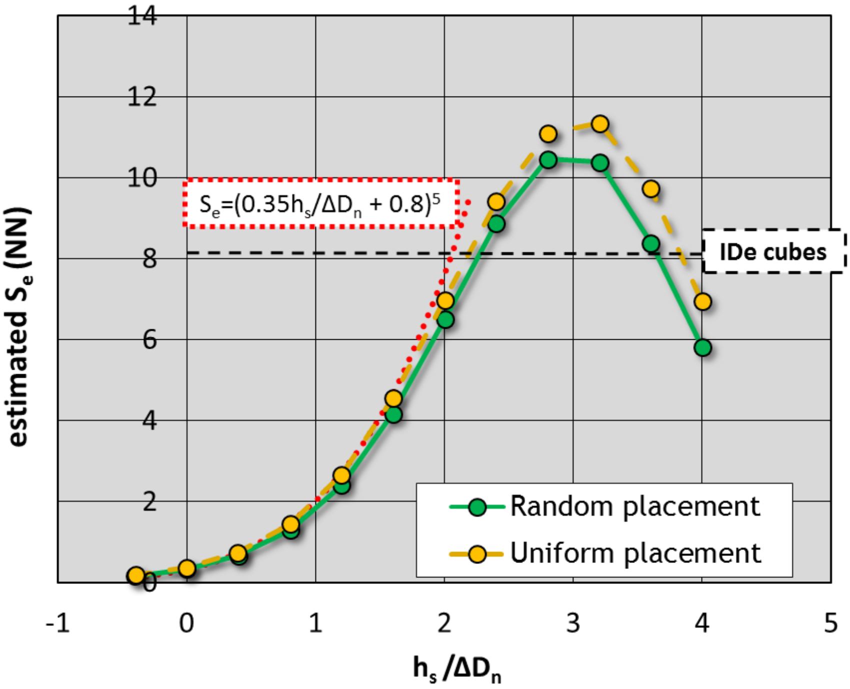

Figure IV.52. S_e estimated by NN depending on $h_s/\Delta D_n$ for cubes randomly- and uniformly-placed on the armor layer.

With low water depths, no severe cube extraction was observed during the tests; the most severe damage corresponded to HeP. In the range $-0.4<h_s/\Delta D_n<2$, no relevant differences were observed between random and uniform placement, and for both types of placement, low damage values were obtained ($S_e<8.3$, damage value for IDe according to Gómez-Martín and Medina, 2014). In the range $-0.4<h_s/\Delta D_n<2$, the cumulative armor damage, obtained after 35 to 40 wave runs of distinct wave characteristics within the range of the conducted experiments listed in Table IV.2 ($1.2<T_p(s)<2.4$ and $8<H_{m0}(cm)<22$), may be estimated by Eq. IV.15.

$$S_e = \left(0.35 \frac{h_s}{\Delta D_n} + 0.8 \right)^5 \qquad [IV.15]$$

Although cube armor hydraulic stability is significantly affected by armor porosity (see Medina et al., 2014), no clear differences were found when considering armor placement technique.

Chapter V

Conclusions and future research

Mutriku, País Vasco (Spain). July, 2012.

V.1. Summary and Conclusions

V.1.1. Introduction

Mound breakwaters are frequently designed with empirical formulas based on small-scale physical model tests in non-breaking wave conditions. A review of the literature concerning mound breakwater design indicates that most existing equations to estimate armor and toe berm stability are based on laboratory tests developed only in non-breaking wave conditions. Nevertheless, most rubble mound breakwaters are constructed in depth-limited wave conditions, where the bottom slope may have a significant influence.

The design of mound breakwaters usually focuses on the main armor. However, on rocky coastlines, with shallow waters and steep sea bottoms, mound breakwaters may even require emerged toe berms whose endurance is necessary to guarantee the armor stability. Thus, for the present study, the stability of rock armors and rock toe berms was analyzed through tests conducted in depth-limited breaking wave conditions with m=1/50 and 1/10 bottom slopes, respectively. The equations developed in this PhD thesis can be relevant to consider the sea level rise caused by the climate change, as this variation of the sea level specially affects to structures placed in shallow waters and studied in this thesis.

V.1.2. Hydraulic stability of rock armors placed in shallow waters and on gentle sea bottoms (m=1/50)

To analyze rock armor hydraulic stability in breaking wave conditions, physical tests with rock armors and slope $\cot\alpha=1.5$ were conducted with a bottom slope m=1/50 in the LPC-UPV wave flume.

Wave measurements obtained from laboratory tests were compared to numerical simulations given by the wave transformation model SwanOne. Wave height distributions and spectral moments were determined in both cases, and the values of the significant spectral wave height, (H_{m0}), the average wave height of the highest tenth waves ($H_{1/10}$) and the wave height exceeded by 2% of the waves ($H_{2\%}$) were analyzed. In all cases, laboratory measurements and numerical estimations were very similar.

Damage to double-layer randomly-placed rock armors, with slope $\cot\alpha=1.5$ and packing density $\phi=1.26$, was measured after each test run. The damage level, S_e, was found to be dependent on the stability number, $N_s=H/(\Delta D_{n50})$ when using $H=H_{m0}$, $H=H_{1/10}$ and $H=H_{2\%}$. Local wave steepness based on the mean wave length at the toe of the structure, $s_{m,toe}=H_{m0}/L_{m,toe}$, and water depth at the toe of the structure, h_s, were rejected as significant explanatory variables of S_e, with a 5% level of significance. Eqs. III.13 and III.16 were proposed to estimate armor damage considering the observed potential relationship between S_e and $N_s=H/(\Delta D_{n50})$. Eqs. III.13 and III.16were calibrated using $H=H_{m0}$, $H=H_{1/10}$ and $H=H_{2\%}$ obtained from laboratory tests and the SwanOne model; H_{m0} was a better descriptor of S_e than $H_{10\%}$ and $H_{2\%}$, after analyzing the variance in the errors using a bootstrapping technique.

When dealing with breaking waves, it is important to specify the exact point at which wave parameters should be determined, especially with steep sea bottoms. In order to know the optimum location to characterize the design spectral wave height attacking the structure, H_{m0} was estimated at different distances seaward from the structure toe. The estimations of H_{m0} given by SwanOne at $3h_s$ seaward from the structure toe were the most adequate to characterize waves in the depth-induced breaking zone. Thus, Eqs. III.13 and III.16 were finally selected to describe armor damage with $H= H_{m0}$ estimated by SwanOne at $3h_s$ seaward from the structure toe, with $K=0.066$ and $k_2=6.0$.

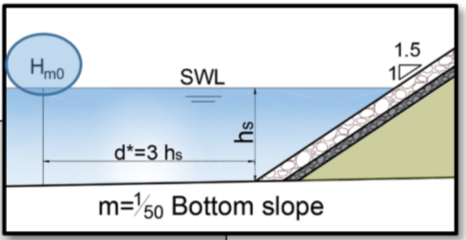

Eq. III.13: $$S_e = 0.066\left(\frac{H_{m0}}{\Delta D_{n50}}\right)^6$$

Eq. III.16: $$S_e\Big|_{5\%}^{95\%} = S_e \pm 0.52\cdot\sqrt{S_e}$$

Figure V.1. Final equations proposed to estimate rock armor damage.

A comparison was made between the armor damage measured in this study and the estimations given by the most commonly-used equations for rock armor design given in the literature (Eqs. II.20 to II.25), showing a high dispersion of results (see Fig. III.40). Most existing equations given in the literature were obtained from physical tests conducted in non-breaking wave conditions, and validated with waves measured from gauges located at a certain distance from the structure. However, they have been widely used for breaking wave conditions with H_s or $H_{2\%}$ estimated at the toe of the structure. Additionally, most equations require a method to consider the cumulative armor damage, while Eq. III.13 proposed in this study implicitly considers the cumulative damage of minor storms previously attacking the breakwater.

Eq. III.13 is valid to design double-layer rock armors with slope $\cot\alpha=1.5$, placed on a $m=1/50$ bottom slope within the ranges $0.98 \le H_{m0}/(\Delta D_{n50}) \le 2.5$ and

$3.75 \leq h_s/(\Delta D_{n50}) \leq 7.50$, using the mean values of S_e measured during tests for IDa, IIDa and IDe: S_e(IDa)=0.5, S_e(IIDa)=1.8 and S_e(IDe)=6.2.

V.1.3. Hydraulic stability of rock toe berms placed in very shallow waters and on steep sea bottoms (m=1/10)

To analyze the hydraulic stability of rock toe berms in breaking wave conditions, physical tests were conducted in the LPC-UPV wave flume with a bottom slope m=1/10, emerged and submerged toe berms, and cubes randomly- and uniformly-placed on the armor.

Firstly, the hydraulic stability of standard rock toe berms with $B_t=3D_{n50}$ and $t_t=2D_{n50}$ was analyzed. Within the ranges of $0.02<s_{0p}<0.07$, $-0.15<h_s/H_{s0}<1.5$ and $-0.5<h_s/D_{n50}<5.01$, Eq. IV.4 was proposed to estimate the toe berm damage ($N_{od} \leq 4$) with $N_{od}=1$ as a design criteria, using three parameters: (1) deep water wave height, H_{s0}, (2) deep water wave length, L_{0p}, and (3) water depth at the toe, h_s. For a given water depth (h_s), Eq. IV.4 considers the damage associated to the design storm (H_{s0}, T_p) as well as the cumulative damage of previous storms with lower or equal T_p and H_{s0}. Eq. IV.4 reveals a critical point when the SWL is near the top of the toe berm ($h_t=D_{n50}$). From $h_t=D_{n50}$, toe berm damage decreases with both increasing and decreasing water depths (Fig. IV.39).

The design of toe berms with rocks is almost always valid for emerged toe berms and very submerged toe berms. However, there is a range of water depths at the toe, h_s, in which the required rock size is so big that there is no available material. In these situations, it may be possible to either move the toe position in order to reduce the damaging effects of water depth or increase the width of the toe berm ($B_t=n_t D_{n50}$). Thus, the influence of toe berm width on toe berm stability was analyzed. When considering wide toe berms ($n_t>3$), common toe berm damage values ($0<N_{od} \leq 4$) cannot be directly applied as more rocks are displaced from wide toe berms even though these toe berms are more resistant. Therefore, two new concepts were introduced in this study: (1) the nominal toe berm, considered the most shoreward toe berm area which effectively supports the armor layer of $n_t=3$, and (2) the sacrificial toe berm, considered the most seaward toe berm area which serves to protect the nominal toe berm (see Fig. IV.1). Damage to the nominal toe berm (N_{od}^*) should be used to describe hydraulic stability of wider toe berms. Given a standard toe berm of three rocks wide (nominal toe berm), an equivalent toe berm with damage similar to the nominal toe berm may be defined by increasing the berm width and decreasing the rock size following Eq. IV.8; the reduction in rock size shows an inverse 0.4-power relation with the relative berm width. Eq. IV.8 can be used to design rock toe berms within the ranges m=1/10, $3D_{n50} \leq B_t \leq 12D_{n50}$, $t_t=2D_{n50}$, $1.5 \leq h_{ss}/D_{n50} \leq 2.6$, $0.02 \leq s_{0p} \leq 0.07$, $0.4 \leq h_{ss}/H_{s0} \leq 1.0$ and $0 \leq N_{od}^* \leq 4$.

Eq. IV.4: $$N_{od} = N_{od}{}^{*} = \left(\frac{(H_{s0}L_{0p})^{1/2}}{\Delta D_{n50,3}} - 5.5\right)\left[\left(-0.2\frac{h_s}{\Delta D_{n50,3}} + 1.4\right)\exp\left(0.25\frac{h_s}{\Delta D_{n50,3}} - 0.65\right)\right]^{1/0.15}$$

Eq. IV.8: $$D_{n50,n_t} = D_{n50,3}\left(\frac{3}{n_t}\right)^{0.4}$$

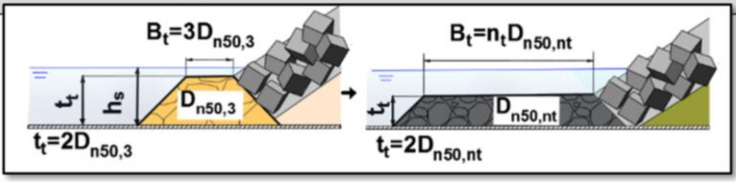

Figure V.2. Final equations proposed to estimate rock toe berm damage.

Finally, NN models were used to compare damage to randomly- and uniformly- placed cube armors. The NN methodology proved that there was no significant difference in armor damage when the packing density was similar (ϕ=1.16). Armor porosity and placement technique must be carefully considered in the design phase and during construction to prevent uncontrolled changes in hydraulic stability. In the case of double-layer cube armors, hydraulic stability is significantly affected by armor porosity but not by armor placement when the bottom slope is m=1/10.

V.2. Future research

Further research is required to examine how other bottom slopes (m≠1/50) affect double-layer rock armor stability. Studies should be designed for a wider range of water depths at the toe ($h_s/(\Delta D_{n50})<3.75$) and different armor slopes (cotα>1.5) with either rocks or other types of CAUs on the main armor.

The tests conducted for this research with m=1/50 and rock armors should be repeated with concrete armors, built with, for example, cubes in two layers, or Cubipods in single- and double-armor layers ($0.98 \le H_{m0}/(\Delta D_{n50}) \le 2.5$ and $3.75 \le h_s/(\Delta D_{n50}) \le 7.50$).

Regarding the toe berm design, future research is necessary to examine the transition area from the shallow waters with m=1/10 analyzed in this study, and the deeper waters and gentler bottom slopes tested by other authors (m<1/10 and $h_s/D_{n50}>5.01$). Research should also focus on different toe slope angles and thicknesses ($t_t>2D_{n50}$), as well as alternative designs for toe berms using CAUs rather than large rocks.

Finally, the influence of placement techniques on cube armor stability should be examined considering other slopes (cotα>1.5), gentler sea bottoms (m<1/10) and higher water depths ($h_s/\Delta D_n>4$).

References

α φ
β λ
χ μ
δ ξ
ε υ
η ρ

Aminti, P., Lamberti, A., 1996. Interaction between main armour and toe berm damage. Proc. 25th International Conference on Coastal Engineering, ASCE, 1542-1555.

Ansari, N., Hou, E., 1997. Computational Intelligence for Optimization. Kluwer Academic Publishers, Boston, USA.

Baart, S., Ebbens, R., Nammuni-Krohn, J., Verhagen, H.J., 2010. Toe rock stability for rubble mound breakwaters. Proc. 32nd International Conference on Coastal Engineering, World Scientific, 3005-3017.

Bakker, P., Van den Berge, A., Hakenberg, R., Klabbers, M., Muttray, M., Reedijk, B., Rovers, I., 2003. Development of concrete breakwater armour units. 1st Coastal, Estuary and Offshore Engineering Specialty Conference of the Canadian Society for Civil Engineering, Canada, CSC-395-1 - CSC-395-12.

Bakker, P., Klabbers, M., Muttray, M., Van den Berge, A., 2005. Hydraulic performance of Xbloc armour units. Proc. 1st International Conference on Coastal Zone Management and Engineering in the Middle East, 6 pages.

Baldock, T.E., Holmes, P., Bunker, S., Van Weert, P., 1998. Cross-shore hydrodynamics within an unsaturated surf zone. Coastal Engineering, 34, 173–196.

Baldock, T.E., Simmonds, D.J., 1999. Separation of incident and reflected waves over sloping bathymetry. Coastal Engineering, 38, 167–176.

Battjes, J.A., 1974. Surf similarity. Proc. 14th International Conference on Coastal Engineering, 466–479.

Battjes, J.A., Janssen, J.P.F.M., 1978. Energy loss and set-up due to breaking of random waves. Proc. 16th International Conference on Coastal Engineering, ASCE, 569-587.

Battjes, J.A., Groenendijk, H.W., 2000. Wave height distributions on shallow foreshores. Coastal Engineering, 40, 161–182.

Battjes, J.A., Bakkenes, H.J., Janssen, T.T., van Dongeren, A. R., 2004. Shoaling of subharmonic gravity waves. J. of Geophysical Research, 109, C02009, doi: 10.1029/2003JC001863.

Biésel, F., Suquet, F., 1951. Les Appareils generateurs de Houle en Laboratoire. La Houille Blanche, Vol. 6, nos. 2,4, 5.

Blenkinsopp, C. E., Chaplin, J. R., 2008. The effect of relative crest submergence on wave breaking over submerged slopes. Coastal Engineering, 55, 967–974.

Bonmarin, P., 1989. Geometric properties of deep-water breaking waves. J. of Fluid Mechanics, 209, 405-433.

Broderick, L.L., 1983. Riprap Stability A Progress Report. Proc. Specialty Conference on Design, Construction, Maintenance and Performance of Coastal Structures, Arlington, VA, March 9-11, 1983. Coastal Structures 1983, ASCE, 320-330.

Bruun, P., 1979. Common reasons for damage or breakdown of mound breakwaters. Coastal Engineering, 2, 261-273.

BSI Technical Committee CSB17, 1991. British Standard 6349: Maritime structures: part 7. Guide to the design and construction of breakwaters, BSI, London, UK.

Burchart, H.F., Liu, Z., 1992. Design of dolos armour units. In: B.L. Edge (Ed), Proc. 23rd International Conference on Coastal Engineering, 1053-1066.

Burchart, H.F., Liu, Z., 1995. Rubble mound breakwater failure modes. Proceedings Final Workshop: Rubble Mound Failure Modes. Sorrento, Italy, 14 pages.

Caires, S., Van Gent, M.R.A., 2012. Wave Height Distribution in Constant and Finite Depths. Proc. 33rd International Conference on Coastal Engineering, waves.15.

Camenen, B., Larson, M., 2007. Predictive formulas for breaking depth index and breaker type. J. Coastal Research, 23, 1028–1041.

Camfield, F., Street, R., 1968. The effects of bottom configuration on the deformation, breaking and run-up of solitary waves. Proc. 10th International Conference on Coastal Engineering, London, UK, 173–189.

CIRIA, CUR, 1991. Manual on the use of rock in coastal and shoreline engineering. CIRIA, London, UK.

CIRIA, CUR, CETMEF, 2007. The Rock Manual. The Use of Rock in Hydraulic Engineering (2nd edition). C683, CIRIA, London, UK.

Collins, J.I., Weir, W., 1969. Probabilities of wave characteristics in the surf zone. Tetra Technical Report, TC-149, 1–122.

Collins, J.I., 1970. Probabilities of breaking wave characteristics. Proc. 12th International Conference on Coastal Engineering, 399–414.

Cooker, M. J., Peregrine, D. H., Vidal, C., Dold, J. W., 1990. The interaction between a solitary wave and a submerged semicircular cylinder. J. of Fluid Mechanics, 215, 1–22.

Dally, W.R., Dean, R.G., Dalrymple, R.A., 1985. A model for breaker decay on beaches. Proc. 19th International Conference on Coastal Engineering, 82–98.

Dally, W.R., Dean, R.G., 1986. Transformation of random breaking waves on surf beat. Proc. 20th International Conference on Coastal Engineering, 109–123.

Dally, W.R., 1990. Random breaking waves: a closed-form solution for planar beaches. Coastal Engineering, 14, 233–263.

Dally, W.R., 1992. Random breaking waves: field verification of a wave-by-wave algorithm for engineering applications. Coastal Engineering, 16, 369–397.

Danel, P., 1952. On Limiting Clapotis, Gravity Waves. National Bureau of Standards, Circular, 521 (US Department of Commerce), 35–45.

Dean, R.G., Dalrymple, R.A., 1991. Water Wave Mechanics for Engineers and Scientists (2nd Edition). Advanced Series on Ocean Engineering, Vol.2. World Scientific Publishing, Singapore, 368 pages.

Deo, M.C., Gondane, D.S., Kumar, V.S., 2002. Analysis of wave directional spreading using neural networks. J. Waterway, Port, Coastal, Ocean Eng., 128, 30-37.

Docters van Leeuwen, L., 1996. Toe stability of rubble-mound breakwaters. M.Sc. thesis. Delft University of Technology, Delft, The Netherlands, 108 pages.

Donnars, P., Benoit, M., 1996. Interactions in the stability of toe-berm and main-armour for rubble-mound breakwaters: an experimental study. Proc. 25th International Conference on Coastal Engineering, ASCE, 1617-1630.

Dupray, S., Roberts, J., 2009. Review of the use of concrete in the manufacture of concrete armour units. Proc. International Conference of Coasts, Marine Structures and Breakwaters, ICE, 1, 245-259.

Ebbens, R.E., 2009. Toe Structures of Rubble Mound Breakwaters. Stability in Depth Limited Conditions. M.Sc. thesis. Delft University of Technology, Delft, The Netherlands, 114 pages.

Fenton, J., 1972. A ninth-order solution for the solitary wave. J. of Fluid Mechanics, 53, 257–271.

Feuillet, J., Coeffe, Y., Bernier, J., Chaloin, B., 1987. Le dimensionnement des digues à talus. Éditions Eyrolles, Collection de la direction des études et recherches d'électricité de France, Vol. 64, 172 pages.

Figueres, M., Medina, J.R., 2004. Estimation of incident and reflected waves using a fully non-linear wave model. Proc. 29th International Conference on Coastal Engineering, World Scientific, Singapore, 594–603.

Frens, A.B., 2007. The impact of placement method on Antifer-block stability. M.Sc. thesis. Delft University of Technology, Delft, The Netherlands, 146 pages.

Galvin, C. J., 1968. Breaker type classification on three laboratory beaches. J. of Geophysical Research, 73, 3651–3659.

Garrido, J.M., Medina, J.R., 2012. New neural network-derived empirical formulas for estimating wave reflection on Jarlan-type breakwaters. Coastal Engineering, 62, 9-18.

Gerding, E., 1993. Toe Structure Stability of Rubble Mound Breakwaters. M.Sc. thesis and Delft Hydraulics Report H1874. Delft University of Technology, Delft, The Netherlands, 113 pages.

Glukhovsky, B. K., 1966. Issledovanie morskogo vetrovogo volnenia (Study of sea wind waves). Leningrad, Gidrometeoizdat (in Russian), .

Goda, Y., 1970. A synthesis of breaker indices. Trans. Japan Soc. Civil Eng., 2, 227-230.

Goda, Y., 1975. Irregular wave deformation in the surf zone. Coastal Engineering in Japan 18, 13–26.

Goda, Y., Suzuki, Y., 1976. Estimation of incident and reflected waves in random wave experiments. Proc. 15th International Conference on Coastal Engineering, 828-845.

Goda, Y., 1985. Random seas and design of maritime structures. University of Tokyo Press, Tokyo, Japan.

Goda, Y., 2000. Random seas and design of maritime structures (2nd Edition).World Scientific Publishing, Singapore.

Goda, Y., 2010. Reanalysis of regular and random breaking wave statistics. Coastal Engineering Journal, 52 (1), 71–106.

Gómez-Martín, M.E., Medina, J.R., 2006. Damage progression on cube armored breakwaters. Proc. 30th International Conference on Coastal Engineering, World Scientific, 5229–5240.

Gómez-Martín, M.E., Medina, J.R., 2014. Heterogeneus Packing and Hydraulic Stability of Cube and Cubipod Armor Units. J. Waterway, Port, Coastal, Ocean Eng., ASCE, 140, 100-108.

Gómez-Martín, M.E., 2015. Análisis de la evolución de averías en el manto principal de diques en talud formado por escolleras, cubos y Cubípodos [Tesis doctoral no publicada]. Universitat Politècnica de València. doi:10.4995/Thesis/10251/59231, 332 pages.

Gourlay, M.R., 1992. Wave set-up, run-up and beach water table: Interaction between surf zone hydraulics and groundwater hydraulics. Coastal Engineering, 17, 93–144.

Grilli, S.T., Svendsen, I.A., Subramanya, R., 1997. Breaking criterion and characteristics for solitary waves on slopes. J. Waterway, Port, Coastal, Ocean Eng., 123, 102–112.

Haller, C.H., Catalan, C., 2005. Measurements of shallow water breaking wave rollers. Proc. of Coastal Dynamics 2005, 1–13.

Herrera, M.P., Medina, J.R., 2015. Toe berm design for very shallow waters on steep sea bottoms. Coastal Engineering, 103, 67-77.

Herrera, M.P., Molines, J., Medina, J.R., 2016. Hydraulic stability of nominal and sacrificial toe berms for mound breakwaters on steep sea bottoms. Coastal Engineering, 114, 361-368.

Heskes, T., 1997. Practical confidence and prediction intervals. In: Mozer, Jordan, Petsche (Eds.), Advances in neural information processing systems, vol. 9. MIT Press, Cambridge.

Hovestad, M., 2005. Breakwaters on steep foreshores: the influence of foreshore steepness on armour stability. M.Sc. thesis. Delft University of Technology, Delft, The Netherlands, 116 pages.

Hudson, R.Y., 1959. Laboratory investigation of rubble-mound breakwaters. J. Waterways and Harbors Div., ASCE, 85(WW3), 93–121.

Hughes, S.A., Borgman, L.E., 1987. Beta-Rayleigh distribution for shallow-water wave heights. In: R. Dalrymple (Ed.), Proc. International Conference on Coastal Hydrodynamics, 17–31.

Hunt, I.A., 1959. Design of Seawalls and Breakwaters. J. Waterways, Harbors and Coast. Eng. Div., ASCE, 85(WW3), 123-152.

IEC (International Electrotechnical Commission), 2009. IEC 61400-3, Wind Turbines —Part 3: Design Requirements for Offshore Turbines, Edition 1.0, 263 pages.

Iribarren, R., 1938. Una fórmula para el cálculo de los diques de escollera, M. Bermejillo-Pasajes, Madrid, Spain.

Iribarren, R., Nogales, C., 1950. Generalización de la Fórmula para el Cálculo de los Diques de Escollera y Comprobación de sus Coeficientes. Revista de Obras Públicas (Madrid), 239-277.

Iribarren, R., 1965. Formule pour le calcul des diques en enrochements naturels on elements artificieles. XXI Int. Navigation Congr., Sect. II-I, Stockholm, Sweden, 15-46.

Iverson, H.W., 1952. Laboratory study of breakers. Gravity Waves US Bureau of Standards, Circular, 52, 9–32.

Jensen, T., Andersen, H., Grlilnbeck, J., Mansard, E.P.D., Davies, M.H., 1996. Breakwater stability under regular and irregular wave attack. Proc. 25th International Conference on Coastal Engineering, World Scientific, 1679-1692.

Johnson, C.M., 2009. The effect of artificial reef configurations on wave breaking intensity relating to recreational surfing conditions. M.Sc. thesis. University of Stellenbosch, 137 pages.

Kamisky, G.M., Kraus, N.C., 1993. Evaluation of depth-limited wave breaking criterion. Proc. 2nd International Symposium on Ocean Wave Measurement and Analysis, New Orleans, LA, 437–448.

Kamphuis, J.W., 1991. Incipient wave breaking. Coastal Engineering, 15, 185–203.

Khayyer, A., Gotoh, H., Shao, S.D., 2008. Corrected incompressible SPH method for accurate water-surface tracking in breaking waves. Coastal Engineering, 55, 236–250.

Kim, D.H., Park, W.S., 2005. Neural network for design and reliability analysis of rubble mound breakwaters. Ocean Engineering, 32 (11–12), 1332–1349.

Kimura, A., 1980. Statistical properties of random wave groups. Proc. 17th International Conference on Coastal Engineering, ASCE, 2955-2973.

Klopman, G., 1996. Extreme wave heights in shallow water. Report H2486, WL/Delft Hydraulics, Delft, The Netherlands.

Kobayashi, N., Cox, D.T., Wurjanto, A., 1990a. Irregular wave reflection and runup on rough impermeable slopes. J. Waterway, Port, Coastal, Ocean Eng., 116(6), 708-726.

Kobayashi, N., Wurjanto, A., Cox, D.T., 1990b. Rock slopes under irregular wave attack. Proc. 22nd International Conference on Coastal Engineering, ASCE, 1307-1319.

Kraus, N.C., Larson, M., 1988. Beach profile change measured in the tank for large waves. Technical Report, CERC-88-6.

Kuriyama, Y., 1996. Models of wave height and fraction of breaking waves on a barred beach. Proc. 25th International Conference on Coastal Engineering, 247–260.

Lamberti, A., Aminti P., 1994. Program of tests on main armour - toe berm interaction and preliminary check of scale effects. MAST II RMBFM Project. Proc. of the 2nd workshop, Bressanone, Italy, 20-21.

Lamberti, A., Tomasicchio, G.R., Guiducci, F., 1994. Reshaping breakwaters in deep and shallow water conditions. Proc. 24th International Conference on Coastal Engineering, ASCE, 1343-1358.

Larson, M., Kraus, N.C., 1989. SBEACH: Numerical model for simulating storm-induced beach change, Report 1: Empirical foundation and model development. Technical Report CERC-89-9, US Army Engineer Waterways Experiment Station, Coastal Engineering Research Center, Vicksburg, MS.

Le Mehaute, B., Koh, R.C.Y., 1967. On the breaking of waves arriving at an angle to the shore. J. of Hydraulic Research, 5, 67–88.

Le Roux, J.P., 2007. A simple method to determine breaker height and depth for different deep water wave height/length ratios and seafloor slopes. Coastal Engineering, 54, 271–277.

Li, Y., 2000. Tsunamis: Non-breaking and breaking solitary wave run-up. Report KH-R-60, W. M. Keck Laboratory of Hydraulics and Water Resources, California Institute of Technology, Pasadena, CA.

Loman, G.J.A., Hofland, B., Van Der Biezen, S.C., Poot, J.G., 2012. Integral design of hard sea defense of Maasvlakte 2, Part II: Physical model testing of cube revetment and reef. 4th Conference on the Application of Physical Modelling to Port and Coastal Protection, 603-612.

Lomónaco, P., Vidal, C., Medina, J.R., Gómez-Martín, M.E., 2009. Evolution of damage on roundheads protected with Cube and Cubipod armour units. Proc., Coasts, Marine Structures and Breakwaters 2009, Institution of Civil Engineers (ICE), Vol. 1, Thomas Telford, London, 169–180.

Longuet-Higgins, M.S., 1952. On the statistical distributions of heights of sea waves. J. Marine Research, 11, 245–266.

Longuet-Higgins, M.S., 1982. Parametric solutions for breaking waves. J. of Fluid Mechanics, 121, 403–424.

Longuet-Higgins, M.S., 1983. On the joint distribution of wave periods and amplitudes in a random wave field. Proc. Roy. Soc. London, Ser. A, 347, 311−328.

Losada, M.A., Giménez-Curto, L.A., 1979. The joint effect of the wave height and period on the stability of rubble-mound breakwaters using Iribarren's number. Coastal Engineering, 3, 77-96.

Losada, M.A., Desiré, J.M., Alejo, L.M., 1986. Stability of blocks as breakwater armor units. J. of Structural Engineering, 112(11), 2392-2401.

Madsen, O.S., 1976. Wave climate of the continental margin: Elements of its mathematical description. In: D.J. Stanley and D.J.P. Swift (Eds.), Marine Sediment Transport in Environmental Management, John Wiley and Sons, New York, 65–87.

Mai, S., Wilhelmi, J., Barjenbruch, U., 2010. Wave height distributions in shallow waters. Proc. 32nd International Conference on Coastal Engineering, ASCE, 1–6.

Mansard, E.P.D., Funke, E.R., 1980. The measurement of incident and reflected spectra using a least squares method. Proc. 17th International Conference on Coastal Engineering, ASCE, 154–172.

Markle, D.G., 1989. Stability of toe berm armor stone and toe buttressing stone on rubble-mound breakwaters and jetties, physical model investigation.

Technical Report REMR-CO-12. U.S. Army Engineer Waterways Experiment Station, Vicksburg, MS, 82 pages.

Mase, H., Iwagaki, M., 1982. Wave height distributions and wave grouping in the surf zone. Proc. 18th International Conference on Coastal Engineering, 58–76.

Mase, H., Sakamoto, M., Sakai, T., 1995. Neural network for stability of rubble mound breakwaters. J. Waterway, Port, Coastal, and Ocean Eng., ASCE, 121 (6), 294–299.

Massel, S.R., Sobey, R.J., 2000. Distribution of the highest wave in a record. Coastal Engineering Journal, 42 (2), 153–173.

McCowan, J., 1894. On the Highest Waves of a Permanent Type. Philosophical Magazine, (Edinburgh) 38, 351–358.

Mead, S.T., Black, K., 2001. Predicting the breaking intensity of surfing waves. Special Issue of the Journal of Coastal Research on Surfing, 103–130.

Medina, J.R., Hudspeth, R.T., Fassardi, C., 1994. Breakwater Armor Damage due to Wave Groups. J. Waterway, Port, Coastal, Ocean Eng., ASCE, 120(2), 179-198.

Medina, J.R., 1996. Wave climate simulation and breakwater stability. Proc. 25th International Conference on Coastal Engineering, ASCE, 1789-1802.

Medina, J.R., 1999. Neural network modelling of runup and overtopping. In: A.A. Balkema (Ed.), Proc. of Coastal Structures, 1, 421–429.

Medina, J.R., 2001. Estimation of incident and reflected waves using simulated annealing. J. Waterway, Port, Coastal, and Ocean Eng., 127 (4), 213-221.

Medina, J.R., González-Escrivá, J.A., Garrido, J.M., De Rouck, J., 2002. Overtopping analysis using neural networks. Proc. 28th International Conference on Coastal Engineering, ASCE, 2165–2177.

Medina, J.R., Gómez-Martín, M.E., Corredor, A., 2010. Influence of armor unit placement on armor porosity and hydraulic stability. Proc. 32nd International Conference on Coastal Engineering, structures.41.

Medina, J.R., Molines, J., Gómez-Martín, M.E., 2014. Influence of armour porosity on the hydraulic stability of cube armour layers. Ocean Engineering, 88, 289-297.

Melby, J.A., Kobayashi, N., 1998. Progression and variability of damage on rubble mound breakwaters. J. Waterway, Port, Coastal, Ocean Eng., ASCE, 124(6), 286-294.

Melby, J. A., 1999. Damage progression on rubble mound breakwaters. Technical Report CHL-99-17, U.S. Army Engineer Research and Development Center, Vicksburg, MS. Ph.D. diss., University of Delaware, Newark, DE.

Méndez, F.J., Losada, I.J., Medina, R., 2004. Transformation model of wave height distribution on planar beaches. Coastal Engineering, 50 (3), 97–115.

Méndez, F.J., Castanedo, S., 2007. A probability distribution for depth-limited extreme wave heights in a sea state. Coastal Engineering, 54, 878-882.

Miche, R., 1944. Mouvements ondulatoires del le mer en prodeur constante ou decroissante. Annual des Ponts et Chaussees, 42–78.

Michell, J.H., 1893. On the highest wave in water. Philosophical Magazine, (Edinburgh) 36, 430–435.

Moody, J.E., 1992. The effective number of parameters: An analysis of generalization and regularization in non-linear learning systems. In: J.E. Moody, S.J. Hanson and R.P. Lipmann (Eds.), Advances in Neural Information Processing Systems 4, 847-854. San Mateo, CA, Morgan Kaufmann Publishers.

Munk, W.H., 1949. The solitary wave theory and its application to surf problems. Ann. New York Acad. Sci., 51, 376-424.

Muttray, M., Oumeraci, H., 2000. Wave transformation on the foreshore of coastal structures. Proc. 27th International Conference on Coastal Engineering, 2178–1191.

Muttray M., Reedijk, B., 2008. Reanalysis of breakwater stability with steep foreshore. Proc. 31st International Conference on Coastal Engineering, ASCE, 3346-3357.

Muttray, M., 2013. A pragmatic approach to rock toe stability. Coastal Engineering, 82, 56–63.

New, A.L., Mclever, P., Peregrine, D.H., 1985. Computations of overturning waves. J. of Fluid Mechanics, 150, 233-251.

Ostendorf, D.W., Madsen, O.S., 1979. An analysis of longshore current and associated sediment transport in the surf zone. Report No. 241, Department of Civil Engineering, MIT, 1165–1178.

Ogawa, Y., Shuto, N., 1984. Run-up of periodic waves on beaches of non-uniform slope. Proc. 19th International Conference on Coastal Engineering, 328–344.

Panizzo, A., Briganti, R., van der Meer, J.W., Franco, L., 2003. Analysis of wave transmission behind low-crested structures using neural networks. Proc. Coastal Structures 2003, ASCE, 555–566.

Panizzo, A., Briganti, R., 2007. Analysis of wave transmission behind low-crested breakwaters using neural networks. Coastal Engineering, 54 (9), 643–656.

Pardo, V., Herrera M.P., Molines J., Medina, J.R., 2012. Placement grids, porosity and randomness of armor layers. Proc. 33rd International Conference on Coastal Engineering, ASCE, 1131 – 1141.

Pardo, V., Herrera, M.P., Molines, J., Medina, J.R., 2014. Placement, porosity and randomness of cube and Cubipod armor layers. J. Waterway, Port, Coastal, Ocean Eng., ASCE, 140, 04014017.

Peregrine, D.H., 1983. Breaking waves on beaches, Annu. Rev. Fluid Mechanics, 15, 149–178.

Prevot, G., Boucher, O., Luck, M., Benoit, M., 2012. Stability of rubble mound breakwaters in shallow water and surf zone: an experimental study. Proc. 33rd International Conference on Coastal Engineering, ASCE, structures. 85.

Pullen, T., Allsop, N.W.H., Bruce, A., Kortenhaus, A., Schüttrumpf, H., van der Meer, J.W., 2007. EurOtop: Wave Overtopping of Sea Defenses and Related Structures — Assessment Manual, EA (UK), ENW (NL), and KFKI (DE), 1-181.

Qiao, H., Duncan, J., 2001. Gentle spilling breakers: crest flow-field evolution. J. of Fluid Mechanics, 439, 57–85.

Rattanapitikon, W., Shibayama, T., 2000. Verification and modification of breaker height formulas. Coastal Engineering Journal, 42 (4), 389-406.

Rattanapitikon, W., Vivattanasirak, T., Shibayama, T., 2003. A proposal of new breaker height formula. Coastal Engineering Journal, 45, 29–48.

Rattanapitikon, W., Shibayama, T., 2006. Breaking wave formulas for breaking depth and orbital to phase velocity ratio. Coastal Engineering Journal, 48, 395–416.

Robertson, B., Hall, K., Zytner, R., 2013. Breaking waves: Review of characteristic relationships. Coastal Engineering Journal, 55(1), 1350002 (40pages).

Sayao, O.J., 2007. Toe protection design for rubble mound breakwaters. Proc. 5th Coastal Structures International Conference, 104-115.

Scarfe, B.E., Elwany, H.S., Mead, S.T., Black, K.P., 2003. The science of surfing waves and surfing breaks — A review. Proc. 3rd International Surfing Reef Symposium, Raglan, NZ, 37-59.

Seyama, A., Kimura, A., 1988. The measured properties of irregular wave breaking and wave height change after breaking on a slope. Proc. 21st International Conference on Coastal Engineering, ACSE, 419–432.

Singamsetti, S.R., Wind, H.G., 1980. Characteristics of breaking and shoaling periodic waves normally incident on to plane beaches for constant slope. Report M1371, Delft Hydraulics Lab, Delft, The Netherlands.

Smith, E.R., Kraus, N.C., 1991. Laboratory study of wave breaking over bars and artificial reefs. J. Waterway, Port, Coastal, Ocean Eng., 117, 307–325.

Smith, G.M., Wallast, I., Van Gent, M.R.A., 2002. Rock slope stability with shallow foreshores. Proc. 28th International Conference on Coastal Engineering, ASCE, 1524 – 1536.

Smith, W.G., Kobayashi, N., Kaku, S., 1992. Profile changes of rock slopes by irregular waves. Proc. 23rd International Conference on Coastal Engineering, ASCE, 1559-1572.

Sunamura, T., Horikawa, K., 1974. Two-dimensional beach transformation due to waves. Proc. 14th International Conference on Coastal Engineering, ASCE, 920–938.

Sunamura, T., 1980. A laboratory study of offshore transport of sediment for eroding beaches. Proc. 17th International Conference on Coastal Engineering, 1051–1070.

Svendsen, I.A., Madsen, P.A., Buhr-Hansen, J., 1978. Wave characteristics in the surf zone. Proc. 16th International Conference on Coastal Engineering, ASCE, 520-539.

Tayfun, M.A., 1981. Breaking-limited wave heights. J. Waterway, Port, Coastal, Ocean Eng., ASCE, 107, 59-69.

Tayfun, M.A., 1999. Personal communication.

Teisson, C., 1990. Statistical approach of duration of extreme storms. Proc. 22nd International Conference on Coastal Engineering, ASCE, 1851-1860.

Thompson, D.M., Shuttler, R.M., 1975. Riprap design for wind wave attack. A laboratory study in random waves. Report EX 707, Hydraulic Research, Wallingford, UK, 144 pages.

Tsai, C., Chen, H., Hwung, H., Huang, M., 2005. Examination of empirical formulas for wave shoaling and breaking on steep slopes. Ocean Engineering, 32, 469–483.

TUDelft, 2016. SwanOne User Manual. Deft University of Technology, Delft, The Netherlands. http://www.kennisbank-waterbouw.nl/Software.

U.S. Army Corps of Engineers (USACE), 1975. Shore Protection Manual, U.S. Army Coastal Engineering Research Center, U.S. Army Engineer Waterways Experiment Station, Vicksburg, Mississippi.

U.S. Army Corps of Engineers (USACE), 1984. Shore Protection Manual, U.S. Army Coastal Engineering Research Center, U.S. Army Engineer Waterways Experiment Station, Vicksburg, Mississippi.

U.S. Army Corps of Engineers (USACE), 2002. Coastal Engineering Manual. Engineer Manual 1110-2-1100, U.S. Army Corps of Engineers, Washington, D.C.

U.S. Army Corps of Engineers (USACE), 2006. Coastal Engineering Manual. Engineer Manual 1110-2-1100, U.S. Army Corps of Engineers, Washington, D.C. (in 6 volumes).

Van der Meer, J.W., 1985. Stability of rubble mound revetments and breakwaters under random wave attack. ICE, Proc. Developments in Breakwaters, London, 141-154.

Van der Meer, J.W., 1988a. Rock slopes and gravel beaches under wave attack. PhD Thesis. Delft University of Technology, Delft, The Netherlands, 214 pages.

Van der Meer, J.W., 1988b. Deterministic and probabilistic design of breakwater armor layers. J. Waterway, Port, Coastal, Ocean Eng., ASCE, 114(1), 66-80.

Van der Meer, J.W., 1988c. Stability of cubes, tetrapods and Accropode. In: Design of breakwaters. Proc. Conference Breakwaters 1988, Eastbourne, 4-6 May. Thomas Telford, London, 71-80.

Van der Meer, J.W., 1990. Extreme shallow water wave conditions. Report H198, Delft Hydraulics, Delft, The Netherlands, 49 pages.

Van der Meer, J.W., D'Angremond, K., Gerding, E., 1995. Toe structure stability of rubble mound breakwaters. In: J.E. Clifford (Ed.), Advances in coastal structures and breakwaters, Thomas Telford, London, 379 pages.

Van der Meer, J.W., 1998a. Application and stability criteria for rock and artificial units (chapter 11). In: K.W. Pilarczyk (Ed.), Dikes and Revetments, Balkema, Rotterdam, 23 pages.

Van der Meer, J.W., 1998b. Geometrical Design of Coastal Structures (chapter 9). In: K.W. Pilarczyk (Ed.), Dikes and Revetments, Balkema, Rotterdam, 15 pages.

Van der Meer, J.W., 1999. Design of concrete armour layers. In: A.A. Balkema (Ed.), Proc. of Coastal Structures, 1, 213-221.

Van Gent, M.R.A., Van den Boogaard, H.F.P., 1998. Neural network modelling of forces on vertical structures. Proc. 26th International Conference on Coastal Engineering, ASCE, 2096–2109.

Van Gent, M.R.A., Smale, A.J., Kuiper, C., 2003. Stability of rock slopes with shallow foreshores. Proc. Coastal Structures 2003, Portland, Oregon, 100-112.

Van Gent, M.R.A., Van den Boogaard, H.F.P., Pozueta, B., Medina, J.R., 2007. Neural network modelling of wave overtopping at coastal structures. Coastal Engineering, 54 (8), 586–593.

Van Gent, M.R.A., Luis, L., 2013. Application of Cubes in a single layer. Proc. 6th SCACR Conference on Applied Coastal Research, Lisbon, Portugal, 1-10.

Van Gent, M.R.A., Van der Werf, I.M., 2014. Rock toe stability of rubble mound breakwaters. Coastal Engineering, 83, 166–176.

Verhagen, H.J., Reedijk, J., Muttray, M., 2006. The effect of foreshore slope on breakwater stability. Proc. 30th International Conference on Coastal Engineering, ASCE, 4828–4840.

Verhagen, H.J., Van Vledder, G., Eslami Arab, S., 2008. A practical method for design of coastal structures in shallow water. Proc. 31st International Conference on Coastal Engineering, World Scientific, 4, 2912-2922.

Vidal, C., Losada, M.A., Medina, R., 1991. Stability of mound breakwaters’ head and trunk. J. Waterway, Port, Coastal, Ocean Eng., ASCE, 117(6), 570-587.

Vidal, C., Losada, M. A., Mansard, E. P. D., 1995. Suitable wave height parameter for characterizing breakwater stability. J. Waterway, Port, Coastal, Ocean Eng., ASCE, 121(2), 88-97.

Vidal, C., Martin, F.L., Negro, V., Gironella, X., Madrigal, B., García-Palacios, J., 2003. Measurement of armor damage on rubble mound structures: comparison between different methodologies. Proc. International Conference on Coastal Structures 2003, World Scientific, 189-200.

Vidal, C., Medina, R., Lomónaco, P., 2006. Wave height parameter for damage description of rubble-mound breakwaters. Coastal Engineering, 53 (9), 711-722.

Vinje, T., Brevig, P., 1980. Numerical simulation of breaking waves. Finite Elements in Water Resources, 2, 196–210.

Weggel, J., 1972. Maximum breaker height for design. Proc. 13th International Conference on Coastal Engineering, 419-432.

Yagci, O., Kapdasli, S., 2003. Alternative placement technique for antifer blocks used on breakwaters. Ocean Engineering, 30, 1433-1451.

Yamada, O., Kimura, G., Okabe, J., 1968. Precise determination of the solitary waves of extreme height on water of uniform depth. Rep. Res. Inst. Applied Mech., Kyushu University, 15–32.

Yao, Y., Huang, Z., Monismith, S., Lo, E., 2012. Characteristics of monochromatic waves breaking over fringing reefs. J. of Coastal Research, 29, 94-104.

Appendix 1

Scientific papers

Varna (Bulgaria). October, 2014.

1. **Herrera, M.P., Molines, J., Medina, J.R., 2016. Hydraulic stability of nominal and sacrificial toe berms for mound breakwaters on steep sea bottoms. Coastal Engineering, 114, 361-368.**

Hydraulic stability of nominal and sacrificial toe berms for mound breakwaters on steep sea bottoms

Maria P. Herrera [a,*], Jorge Molines [b] and Josep R. Medina [c]

[a] Research Assistant, Dept. of Transportation, *Universitat Politècnica de València*, Camino de Vera s/n, 46022 Valencia, Spain. E-mail: maherram@upv.es (* corresponding author)

[b] Research Assistant, Dept. of Transportation, *Universitat Politècnica de València*, Camino de Vera s/n, 46022 Valencia, Spain. E-mail: jormollo@upv.es

[b] Professor, Dept. of Transportation, *Universitat Politècnica de València*, Camino de Vera s/n, 46022 Valencia, Spain. E-mail: jrmedina@upv.es

ABSTRACT

When mound breakwaters are placed on steep sea bottoms in combination with very shallow waters, the design of the toe berm becomes a relevant issue. Toe berms built close to the water surface on a steep sea bottom must withstand such high wave loads that their design may not be feasible with available quarrystones. In this study, a new design method was developed to reduce the rock size by increasing the toe berm width. The analysis involved specific 2D small-scale tests with toe berms of different rock sizes and widths, placed on a $m = 1/10$ bottom slope with the water surface close to the toe berm crest. Two new concepts were introduced to better characterize damage to wide toe berms: (1) the most shoreward toe berm area which effectively supports the armor layer, in this study referred to as the primary or "nominal" toe berm and (2) the most seaward toe berm area which serves to protect the nominal toe berm, in this study called the secondary or the "sacrificial" toe berm. Damage to the nominal toe berm was used to describe hydraulic stability of wider toe berms. Given a standard toe berm of three rocks wide (nominal toe berm), an equivalent toe berm with damage similar to the nominal toe berm was defined by increasing the berm width and decreasing the rock size. The reduction in rock size showed an inverse 0.4-power relation with the relative berm width.

Keywords: hydraulic stability; mound breakwater; nominal toe berm; sacrificial toe berm; shallow water; steep sea bottom; toe berm.

Highlights:

a) Toe berm is a relevant design element of mound breakwaters placed on steep sea bottoms combined with very shallow waters.
b) Toe berm damage is critical when the still water level is near the toe berm crest.
c) Toe berms may require rocks larger than the size available at the construction site.
d) Rock size for the toe berm can be reduced by increasing the toe berm width.

1. Introduction

The design of rubble mound breakwaters usually focuses on the main armor layer. When concrete armor units are used, it is common to construct a rock toe berm of three to four rocks wide to provide support for the armor layer (see CIRIA/CUR/CEFMEF, 2007). Toe berm stability depends mainly on design wave storm characteristics, water depth and the sea bottom slope existing at the construction site. Toe berms in very shallow waters behave in manner a completely different from those built in non-breaking conditions (see Hovestad, 2005). On gentle sea bottoms, it is common to design deep submerged rock toe berms. However, on rocky coastlines with steep sea bottoms, coastal structures may require emerged toe berms with heavy rocks; toe berm hydraulic stability may be even more critical than armor stability. Herrera and Medina (2015) conducted laboratory tests with a steep bottom slope (m = 1/10) and concluded that most damage occurs when the still water level (SWL) is near the crest of the toe berm. In these conditions, for certain wave storms, the required nominal diameter (D_{n50}) may be so large that it is not possible to design standard toe berms with rocks from available quarries. In these cases, Besley and Benechere (2009) and Herrera and Medina (2015) recommended moving the toe position to deeper or shallower waters where it is feasible to construct the toe berm with rock sizes available at the construction site. Nevertheless, if the toe position cannot be moved due to environmental, economic or operational requirements, this design change is not possible. Other design changes for toe berms are given in the literature; authors such as Burcharth and Liu (1995) or Van Gent and Van der Werf (2014) proposed using concrete units for the toe berm, while USACE (2006) suggested excavating trenches, drilling piles or anchoring bolts to the sea bottom to support the toe stones on rocky coastlines.

The most popular formulas to predict damage to rock toe berms were obtained from small-scale tests with different toe berm geometries. However, toe berm widths (B_t) and thicknesses (t_t) were not usually introduced as explicative parameters of the observed toe berm damage. Eq. (1) is equivalent to the formula given by Gerding (1993), which is based on laboratory tests with a bottom slope $m = 1/20$, two toe berm widths ($B_t = 3D_{n50}$ and $12D_{n50}$), two toe berm thicknesses ($t_t = 2.3D_{n50}$ and $8.8D_{n50}$), and different water depths at the toe ($7.5D_{n50} \leq h_s \leq 29.4D_{n50}$).

$$N_{od} = \frac{1}{\left(0.24\left(\frac{h_t}{D_{n50}}\right)+1.6\right)^{1/0.15}}\left(N_s\right)^{1/0.15} \qquad (1)$$

in which N_{od} is the damage number, $N_s = H_{st}/(\Delta D_{n50})$ is the stability number, $\Delta = (\rho_r - \rho_w)/\rho_w$ is the relative submerged mass density of rocks, ρ_r is the mass density of rocks, ρ_w is the mass density of sea water, H_{st} is the significant wave height at the toe of the structure, and h_t is the water depth above the toe berm.

Eq. (2) is equivalent to the formula proposed by Van der Meer (1998), based on the data given by Gerding (1993), but using the dimensionless parameter h_t/h_s.

$$N_{od} = \frac{1}{\left(6.2\left(\frac{h_t}{h_s}\right)^{2.7} + 2.0\right)^{1/0.15}} (N_s)^{1/0.15} \tag{2}$$

Ebbens (2009) and Baart et al. (2010) proposed Eq. (3) to estimate the toe berm damage from laboratory tests with three bottom slopes (m = 1/20, 1/50 and 1/10), two toe berm widths ($B_t = 3.7D_{n50}$ and $5.3D_{n50}$), two toe berm thicknesses ($t_t = 2.2D_{n50}$ and $3.2D_{n50}$), and different water depths at the toe ($2.7D_{n50} \leq h_s \leq 18D_{n50}$).

$$N_{\%} = 0.038\left(\xi_{0p}{}^{*}\right)^{3/2} (N_s)^3 \tag{3}$$

in which $N_{\%}$ is the percentage of damage, $\xi_{0p}{}^{*} = m/(H_{st}/L_{0p})^{1/2}$ is the surf similarity parameter where m is the bottom slope, and $L_{0p} = gT_p{}^2/2\pi$ is the deep water wave length corresponding to the peak period, T_p.
Eq. (4) is equivalent to the formula proposed by Muttray (2013), based on experiments conducted by different authors, including the data given by Gerding (1993) and Ebbens (2009).

$$N_{od} = \left(0.58 - 0.17\frac{h_t}{H_{st}}\right)^3 (N_s)^3 \tag{4}$$

Van Gent and Van der Werf (2014) obtained Eq. (5) from laboratory tests with a bottom slope m = 1/30, two toe berm widths ($B_t = 3D_{n50}$ and $9D_{n50}$), two toe berm thicknesses ($t_t = 2D_{n50}$ and $4D_{n50}$), and different water depths ($8.6D_{n50} < h_s < 27.4D_{n50}$ and $7D_{n50} \leq h_t \leq 25D_{n50}$). Eq. (5) explicitly considers the influence of B_t and t_t on toe berm stability.

$$N_{od} = 0.032\left(\frac{t_t}{H_{st}}\right)\left(\frac{B_t}{H_{st}}\right)^{0.3}\left(\frac{\hat{u}_\delta}{\sqrt{gH_{st}}}\right)(N_s)^3 \tag{5}$$

in which $\hat{u}_\delta = \frac{\pi H_{st}}{T_{m-1,0}} \frac{1}{\sinh(kh_t)}$, $k = \frac{2\pi}{L_{m-1,0}} = \frac{2\pi}{\frac{g}{2\pi} T_{m-1,0}{}^2}$, $T_{m-1,0} = \frac{m_{-1}}{m_0}$, m_i is the *i-th* spectral moment given by $m_i = \int_0^\infty S(f) f^i \, df$, being $S(f)$ the wave spectrum.

Van Gent and Van der Werf (2014) also proposed multiplying the design N_{od} value by a factor f_B (see Eq. 13) when $3D_{n50} < B_t \leq 9D_{n50}$, as described in Section 6.

Finally, Eq. (6) proposed by Herrera and Medina (2015) is based on laboratory tests with a steep bottom slope (m = 1/10), one toe berm width ($B_t = 3D_{n50}$), one toe berm thickness ($t_t = 2D_{n50}$), and water depths at the toe berm in the range of $-0.5D_{n50} \leq h_s \leq 5.01D_{n50}$.

$$N_{od} = \left[\left(\frac{(H_{s0}L_{0p})^{1/2}}{\Delta D_{n50}} - 5.5\right)\left[\left(-0.2\frac{h_s}{D_{n50}} + 1.4\right)\exp\left(0.25\frac{h_s}{D_{n50}} - 0.65\right)\right]\right]^{1/0.15} \tag{6}$$

in which H_{s0} is the significant deep water wave height. Herrera and Medina (2015) described the two toe berm damage definitions, N_{od} and $N_{\%}$, used in Eqs. (1) to (6).

$$N_{od} = \frac{N}{B/D_{n50}} \tag{7}$$

in which N is the number of displaced rocks and B is the total width of the wave flume. Herrera and Medina (2015) found that $N_{\%}$ is usually one order of magnitude lower than the damage number N_{od}. Both N_{od} and $N_{\%}$ take into account the total number of rocks displaced from the toe (N). However, N is not suitable to measure the damage to toe berms with different geometries, since a larger N is required to significantly damage larger toe berms. When increasing the toe berm width ($B_t > 3D_{n50}$), rocks situated in the most seaward area do not directly contribute to support the armor, but only to protect the most shoreward area of the toe berm. Since toe berm stability should be considered together with the stability of the main armor layer (see Lamberti, 1994), the most seaward area of the toe structure can be considered as a "sacrificial" toe berm, and the most shoreward area of three nominal diameters wide, as the "nominal" toe berm necessary to support the armor layer (see Fig. 1).

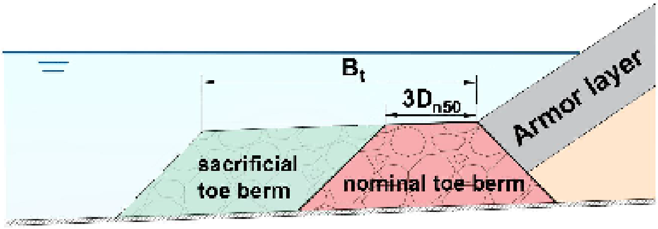

Fig. 1. Sketch of sacrificial and nominal toe berms.

This study analyzes the influence of the nominal diameter (D_{n50}) and the toe berm width ($B_t = nD_{n50}$) on the hydraulic stability of the nominal toe berm, where n is the number of rock rows placed on the upper layer of the toe berm. To this end, 2D physical tests were conducted using small-scale models of breakwaters with double-layer randomly-placed cube armors and rock toe berms, placed on a steep bottom slope (m = 1/10). Different pairs of (D_{n50}, B_t) were tested with the SWL close to the crest of the toe berms. The required rock size given by Eq. (6) for a nominal toe berm ($B_t = 3D_{n50}$) was modified to account for wider toe berms ($n > 3$) based on damage measurements of the nominal toe berm. In this paper, the experimental setup is described in Section 2. Tests with different toe berm sizes and widths are analyzed in Section 3. Section 4 describes a design method based on a new equation with its confidence intervals, providing an integrated graph to design rock toe berms. A practical application is given in Section 5. Formulas given in the literature are compared in Section 6. Finally, conclusions are drawn in Section 7.

2. Physical model tests

2D physical model tests were conducted in the wind and wave test facility (30m x 1.2m x 1.2m) of the Laboratory of Ports and Coasts at the *Universitat Politècnica de València*

(LPC-UPV) with a piston-type wavemaker and a steep sea bottom (*m* = 1/10). Fig. 2 shows a longitudinal cross section of the LPC-UPV wave flume with the location of the wave gauges used in this study.

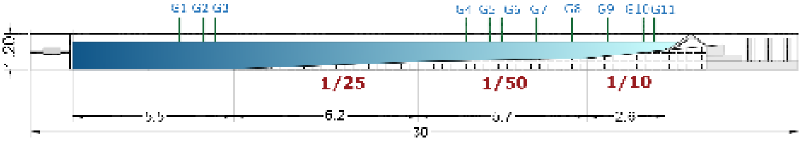

Fig. 2. Longitudinal cross section of the LPC-UPV wave flume (dimensions in meters).

The test model depicted in Fig. 3 corresponds to a conventional *cotα* = H/V = 3/2 non-overtopped mound breakwater, protected with a double-layer, randomly-placed cube armor with nominal diameter D_n(cm) = 3.97 and weight *W*(g) = 141.5. The cube armor was built on a filter layer with D_{n50}(cm) = 1.78 and D_{n85}/D_{n15} = 1.35. The granulometric characteristics of the core material were D_{n50}(cm) = 0.68 and D_{n85}/D_{n15} = 1.64.

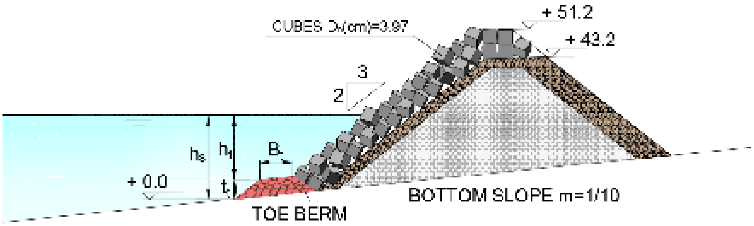

Fig. 3. Configuration of the cube armored model (dimensions in centimeters).

Toe berms were tested with three rock sizes, D_{n50}(cm) = 3.04, 3.99 and 5.12, with a mass density ρ_r(g/cm^3) = 2.70. Three toe berm widths (n = 3, 5 and 12) were applied with D_{n50}(cm) = 3.04 and 3.99; the nominal toe berm was considered as the most shoreward area of the berm with a width of three times the rock nominal diameter (B_t= 3D_{n50}). The nominal toe berm was placed first; later, the sacrificial toe berm was placed, using rocks painted in a different color to be easily distinguished. Only the nominal toe berm (n = 3) was tested with D_{n50} (cm) = 5.12. In all cases, the toe berm thickness was fixed at t_t = 2D_{n50}, and the water depth was h_{ss}(cm) = 8, measured at the toe of the nominal toe berm (*n = 3*) for all configurations (see Fig. 4). With h_{ss}(cm) = 8, the SWL was very close to the crest of the toe berms (1.5≤ h_{ss}/D_{n50} ≤2.6). Note that h_s = h_{ss} only when B_t= 3D_{n50}.

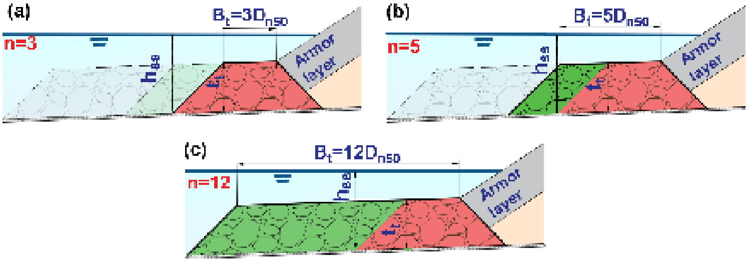

Fig. 4. Configuration of tested toe berms: (a) $B_t = 3D_{n50}$, (b) $B_t = 5D_{n50}$ and (c) $B_t = 12D_{n50}$.

Random wave runs of 500 waves were generated following JONSWAP ($\Upsilon = 3.3$) spectrum, and the AWACS Active Absorption System was activated to avoid multi-reflections. Test series were conducted following the methodology described by Herrera and Medina (2015). Five different peak periods were considered, $T_p(s) = 1.20, 1.50, 1.80, 2.20$ and 2.40; for each T_p, values of significant wave height at the wave generating zone (H_{sg}) were increased from no damage to wave breaking in front of the wavemaker. H_{sg} was increased in steps of 2cm in the range of $8 \leq H_{sg}$ (cm) ≤ 20. The toe berm was rebuilt after each test series defined by the water depth at the toe of the nominal toe berm (h_{ss}), the rock size (D_{n50}), and the toe berm width ($B_t = nD_{n50}$).

Two damage parameters were measured after each test: (1) N_{od}, corresponding to the total damage of the toe berm of width $B_t = nD_{n50}$ ($n \geq 3$); and (2) $N_{od}{}^*$ corresponding only to the damage of the nominal toe berm. Fig. 5 shows a model with D_{n50}(cm) = 3.99 and $B_t = 5D_{n50}$; blue rocks correspond to the nominal toe berm and brown rocks correspond to the sacrificial toe berm. Table 1 summarizes the test conditions and the range of parameters used in this study.

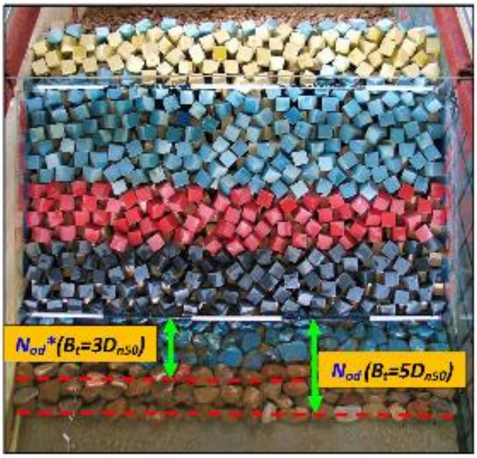

Fig. 5. Nominal (blue rocks) and sacrificial (brown rocks) toe berms with $B_t = 5D_{n50}$.

Table 1. Test conditions.

Parameter	Symbol	Value
Slope angle (-)	$cot\alpha$	3/2
Bottom slope (-)	m	1/10
Cube armor size (cm)	D_n	3.97
Rock filter size (cm)	D_{n50}	1.78
Rock core size (cm)	D_{n50}	0.68
Rock toe size (cm)	D_{n50}	3.04, 3.99 and 5.12
Rock toe density (g/cm³)	ρ_r	2.7
Relative toe width (-)	B_t/D_{n50}	3-12
Relative toe thickness (-)	t_t/D_{n50}	2
Relative water depth at toe berm (-)	h_s/D_{n50}	1.5-3.5
Relative water depth at the nominal toe berm (-)	h_{ss}/D_{n50}	1.5-2.6
Relative significant wave height at generating zone (-)	H_{sg}/h_{ss}	1.0-2.5

Wave steepness at generating zone ($s_{gp}=2\pi H_{sg}/gT_p^2$) (-)	s_{gp}	0.01-0.07
Stability number at generating zone ($N_s=H_{sg}/\Delta D_{n50}$) (-)	N_s	1.0-3.8
Damage level of the nominal toe berm (-)	N_{od}*	<4.8
Total damage level (-)	N_{od}	<11.1

Water surface elevation was measured using eleven capacitive wave gauges. One group of wave gauges (G1, G2 and G3) was placed near the wavemaker while ten wave gauges (G4 to G11) were placed along the wave flume (see Fig. 2). The LASA-V method described by Figueres and Medina (2004) was used to estimate incident and reflected waves at the generating zone (wave gauges G1, G2 and G3).

3. Data Analysis

3.1. Wave analysis

Using the water surface elevation, waves were characterized with a time and frequency domain analysis. When dealing with waves breaking on a m = 1/10 bottom slope combined with shallow waters, it is not easy to obtain reliable incident wave characteristics. The deep water wave conditions are the most reliable reference in these cases.

In this study, waves were characterized in deep water conditions following the methodology described in Herrera and Medina (2015). The average of the highest one-third incident waves ($H_{i,1/3}$) measured at G1, G2 and G3 was used to estimate the deep water significant wave height (H_{s0}) using the shoaling coefficients given by Goda (2000). Fig. 6 shows the measured $H_{1/3,i}$ versus the deep water significant wave height (H_{s0}) estimated using the methodology given in Goda (2000).

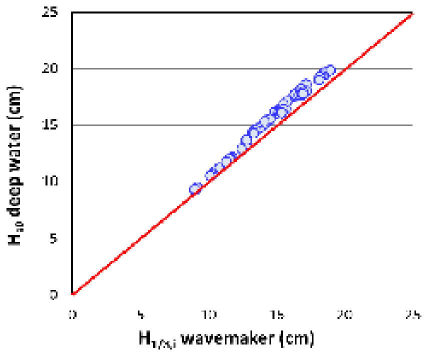

Fig. 6. Measured $H_{1/3,i}$ at the wave generating zone versus deep water significant wave height, H_{s0}.

The deep water significant wave height (H_{s0}) and the deep water wave length obtained from the peak period ($L_{0p}= gT_p^2/2\pi$) were used to characterize the toe berm damage. According to Herrera and Medina (2015), $(H_{s0}\,L_{0p})^{1/2}$ seems to be the best explicative variable to represent toe berm damage in very shallow waters combined with steep sea bottoms.

3.2. Damage analysis

Toe berm stability was analyzed using the total toe berm damage (N_{od}), along with the nominal toe berm damage (N_{od}*). After each test, the total number of rocks displaced from the toe berm (N) were counted and the damage parameter, N_{od}, was determined using Eq. (7). N_{od} corresponded to the damage to both the sacrificial and nominal toe berms. The damage parameter, N_{od}*, was also determined using Eq. (7) but considering only the number of rocks displaced from the nominal toe berm (Fig. 7). Both damage parameters considered the cumulative damage of each test series.

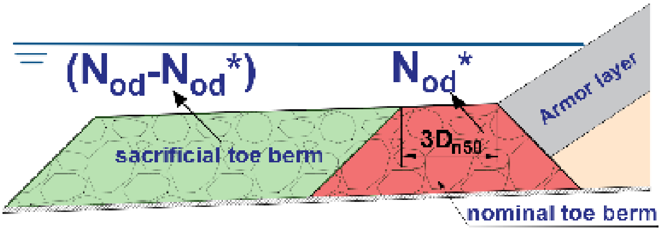

Fig. 7. Total toe berm damage (N_{od}) and nominal toe berm damage (N_{od}*).

Figs. 8 and 9 show total and nominal toe berm damage corresponding to D_{n50} (cm) = 3.04, 3.99 and 5.12 and different toe berm widths (n = 3, 5 and 12). Only the maximum cumulative damage obtained after test runs characterized by T_p is plotted here.

3.2.1. Total toe berm damage (N_{od})

Fig. 8 shows the measured N_{od} as a function of the variable $(H_{s0}\,L_{0p})^{1/2}$ for the seven tested models. N_{od} increased almost linearly with the variable $(H_{s0}\,L_{0p})^{1/2}$ in all cases. Given n, N_{od} was larger when reducing D_{n50}. Given D_{n50}, N_{od} increased when increasing n. Smaller rock sizes and wider toe berms led to larger values of total toe berm damage (N_{od}).

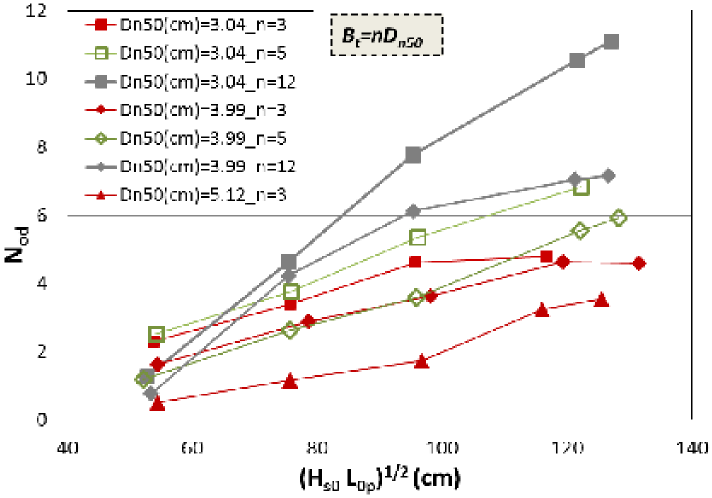

Fig. 8. Total toe berm damage (N_{od}) as a function of toe berm width ($B_t = nD_{n50}$) and rock size (D_{n50}).

3.2.2. Nominal toe berm damage (N_{od}*)

Fig. 9 shows the measured nominal toe berm damage (N_{od}*) as a function of the variable $(H_{s0}\ L_{0p})^{1/2}$. Given a toe berm width ($B_t = nD_{n50}$), N_{od}* was larger when reducing D_{n50}. Given a rock size (D_{n50}), N_{od}* increased when reducing the toe berm width (n). Thus, larger rock sizes as well as wider toe berms led to less nominal toe berm damage (N_{od}*).

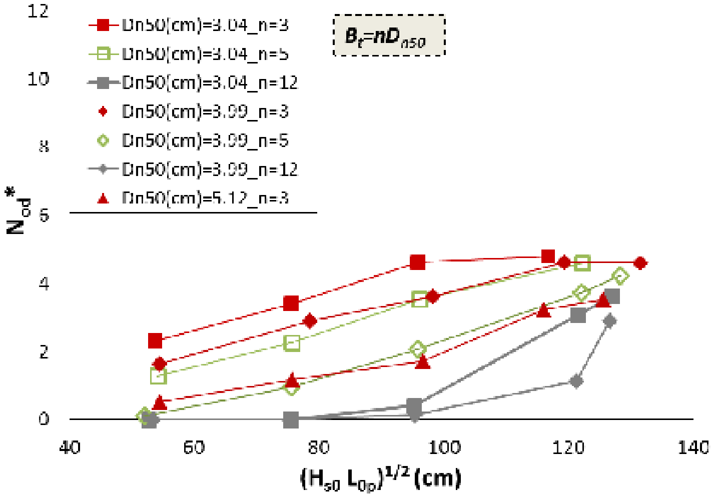

Fig. 9. Nominal toe berm damage (N_{od}*) as a function of toe berm width ($B_t = nD_{n50}$) and rock size (D_{n50}).

3.2.3. Comparison of total and nominal toe berm damage measurements

Fig. 10 compares measured total toe berm damage (N_{od}) and nominal toe berm damage (N_{od}*). The wider the toe berm, the lower the N_{od}* but the higher the N_{od}. Given a rock size (D_{n50}), a wider toe berm would reduce N_{od}*, although the N_{od} would increase. Thus, the total toe berm damage (N_{od}) is not a good estimator of the hydraulic stability of toe berms when comparing different berm widths ($B_t > 3D_{n50}$); the N_{od}* corresponding to the damage to the nominal toe berm, which is actually supporting the armor layer, is the toe berm damage which should be taken into account when analyzing breakwater hydraulic stability. Damage observed on the sacrificial toe berm is not relevant when analyzing the hydraulic performance of mound breakwaters.

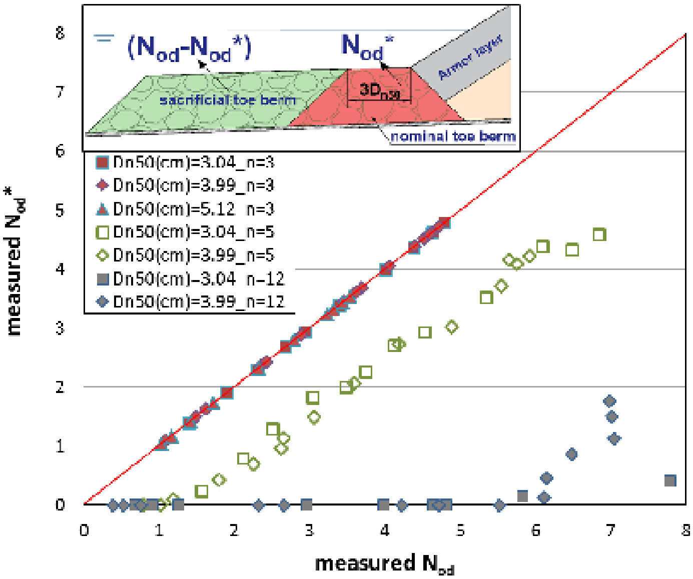

Fig. 10. Comparison of measured total toe berm damage (N_{od}) and measured nominal toe berm damage (N_{od}*).

Hereafter, only the damage to the nominal toe berm, N_{od}*, is considered. Eq. (6), proposed by Herrera and Medina (2015), is extended here to design toe berms with $3D_{n50} \leq B_t \leq 12D_{n50}$ and $t_t=2D_{n50}$, placed on steep sea bottoms (m = 1/10) when the SWL is close to the crest of the toe berm ($1.5 \leq h_s/D_{n50} \leq 2.6$), $0.02 \leq s_{0p} \leq 0.07$ and $0.4 \leq h_s/H_{s0} \leq 1.0$.

4. New design method for toe berms in shallow water and m =1/10

Fig. 9 shows that several tests with different D_{n50} and n provided similar values of N_{od}* for specific wave conditions, $(H_{s0} L_{0p})^{1/2}$. Under the same wave conditions (H_{s0}, T_p), the toe berm with D_{n50}(cm) = 3.99 and n = 5 provided almost the same N_{od}* as the toe berm with D_{n50}(cm) =5.12 and n=3. Analogously, the toe berm with D_{n50}(cm) = 3.04 and n = 5 gave values of N_{od}* similar to those of the toe berm with D_{n50}(cm) = 3.99 and n = 3. These findings suggest that the rock size can be reduced by increasing the toe berm width. It is possible to keep N_{od}* constant by reducing D_{n50} and increasing n, or *vice versa*. The relationship between D_{n50} and N_{od}* can be described by Eq. (8), using as a reference the nominal toe berm (n = 3) with rock size $D_{n50} = D_{n50,3}$.

$$\frac{D_{n50,n}}{D_{n50,3}}=\left(\frac{3}{n}\right)^{k} \qquad (8)$$

where $D_{n50,3}$ is the nominal diameter of rocks for the nominal toe berm ($n = 3$), $D_{n50,n}$ is the nominal diameter of rocks for wider toe berms ($3< n \leq 12$), and k is a positive parameter to be calibrated using the test results described above ($k = 0.4$). Eq. (8) indicates that given a nominal toe berm with $n = 3$ and $D_{n50} = D_{n50,3}$, an equivalent toe berm can be defined with higher n ($n > 3$) and lower D_{n50} ($D_{n50,n} < D_{n50,3}$) to provide similar N_{od}*.

Because Eq. (6) is valid to design toe berms using rocks with $n = 3$, the estimated N_{od} given by Eq. (6) corresponds to the nominal toe berm damage (N_{od}*), and Eqs. (6) and (8) can be combined as follows:

$$N_{od}{*} = \left(\frac{(H_{s0}L_{0p})^{1/2}}{\Delta D_{n50,n}\left(\frac{n}{3}\right)^{k}} - 5.5 \right) \qquad (9)$$
$$x \left[\left(-0.2\frac{h_{ss}}{D_{n50,n}\left(\frac{n}{3}\right)^{k}} + 1.4 \right) \exp\left(0.25\frac{h_{ss}}{D_{n50,n}\left(\frac{n}{3}\right)^{k}} - 0.65 \right) \right]^{1/0.15}$$

The best agreement between the measured N_{od}* and the estimated N_{od}* given by Eq. (9) was found for $k = 0.4$. The goodness of fit between measured and calculated values and the 90% confidence interval are described below.

Eq. (9) extends the application range of Eq. (6) to deal with wider toe berms. Eq. (9) with $k = 0.4$ provides the required rock size for toe berms with $3D_{n50} \leq B_t \leq 12D_{n50}$ and $t_t=2D_{n50}$, placed on a m = 1/10 sea bottom with $1.5 \leq h_{ss}/D_{n50} \leq 2.6$, $0.02 \leq s_{0p} \leq 0.07$, $0.4 \leq h_{ss}/H_{s0} \leq 1.0$, using the damage parameter N_{od}*.When designing with N_{od}*, common values for acceptable damage may be directly used. In this study, the criterion proposed by Herrera and Medina (2015) was considered: no significant movement of toe berm rocks ($N_{od}* < 0.5$), significant rock movements ($N_{od}* = 1.0$), moderate damage but toe berm still providing support to the armor ($N_{od}* = 2.0$), and toe berm failure ($N_{od}* = 4.0$).

4.1. Confidence intervals

Assuming a Gaussian error distribution, the 90% confidence interval for the toe berm damage estimation given by Eq. (9) is:

$$N_{od}{*}\Big|_{5\%}^{95\%} = N_{od}{*} \pm 0.83 \qquad (10)$$

Fig. 11 compares measured N_{od}* and that estimated given by Eq. (9) with the 90% confidence interval given by Eq. (10). The few outliers for small N_{od}* shown in Fig. 11 are on the safe side, estimated $N_{od}* >$ measured N_{od}*.

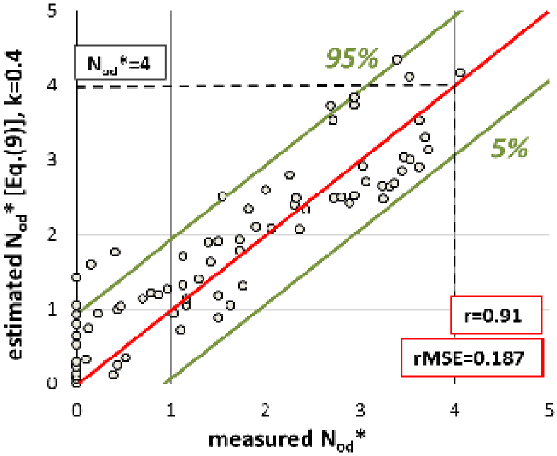

Fig. 11. 90% confidence interval of estimated N_{od}* given by Eq. (9) with $k = 0.4$.

In order to measure the goodness of fit between the N_{od}* measured in the tests and that estimated by Eq. (9), the relative mean squared error (*rMSE*) and the correlation coefficient (*r*) were calculated:

$$rMSE = \frac{MSE}{VAR} = \frac{\frac{1}{N_t}\sum_{i=1}^{N_t}(t_i - e_i)^2}{\frac{1}{N_t}\sum_{i=1}^{N_t}(t_i - \bar{t})^2} \qquad (11)$$

$$r = \frac{\sum_{i=1}^{N_t}(t_i - \bar{t})(e_i - \bar{e})}{\sqrt{\sum_{i=1}^{N_t}(t_i - \bar{t})^2 \sum_{i=1}^{N_t}(e_i - \bar{e})^2}} \qquad (12)$$

in which *MSE* is the mean squared error, N_t is the number of observations, t_i is the target value, e_i is the estimated value, *VAR* is the variance of target values, and $\bar{t}$ and $\bar{e}$ are the average of target and estimated values, respectively. $0 \leq rMSE \leq 1$ estimates the proportion of variance in the observed values not explained by Eq. (9); the lower the *rMSE*, the better the predictions. $0 \leq r \leq 1$ measures the degree of correlation between measured and estimated values of N_{od}*; the higher the *r*, the better the predictions. Eq. (9) with $k = 0.4$ provided $rMSE = 0.187$ and $r = 0.91$.

4.2. Design approach for equivalent toe berms

Given an acceptable level of damage (e.g. $N_{od}*$ = 0.5 or 1.0), Eq. (6) is used first to calculate the rock size for a nominal toe berm, $D_{n50,3}$, and Eq. (9) can be used later to define wider toe berms (3< n ≤12) with smaller rocks ($D_{n50,n}$).

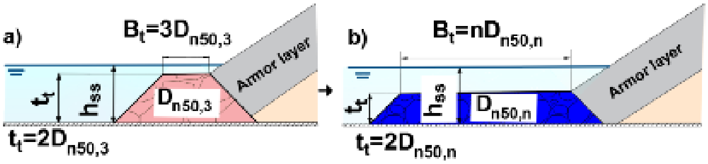

Fig. 12. (a) Nominal toe berm (n = 3) and (b) equivalent wider toe berm (3< n ≤12).

A practical application of this process is given by the design graph shown in Fig. 13, which is valid for $N_{od}*$ = 0.5 and 1.0. Fig. 13a shows the nominal diameter of rocks for a nominal toe berm ($D_{n50,3}$), estimated with Eq. (6), as a function of the deep water wave conditions, $(H_{s0}\ L_{0p})^{1/2}$, for $h_{ss}/D_{n50,3}$ = 1.5, 2.0 and 2.5. Fig. 13b shows the relation between nominal diameters ($D_{n50,3}$ and $D_{n50,n}$) as a function of the toe berm width (3≤ n ≤12). $D_{n50,n}$ can be selected by the designer considering the rock sizes available at the construction site. The ranges of application of Eq. (6) in Fig. 13 are 0.02< s_{0p} <0.07, -0.15< h_{ss}/H_{s0} <1.5, and -0.5≤ $h_{ss}/D_{n50,3}$ ≤5.01.

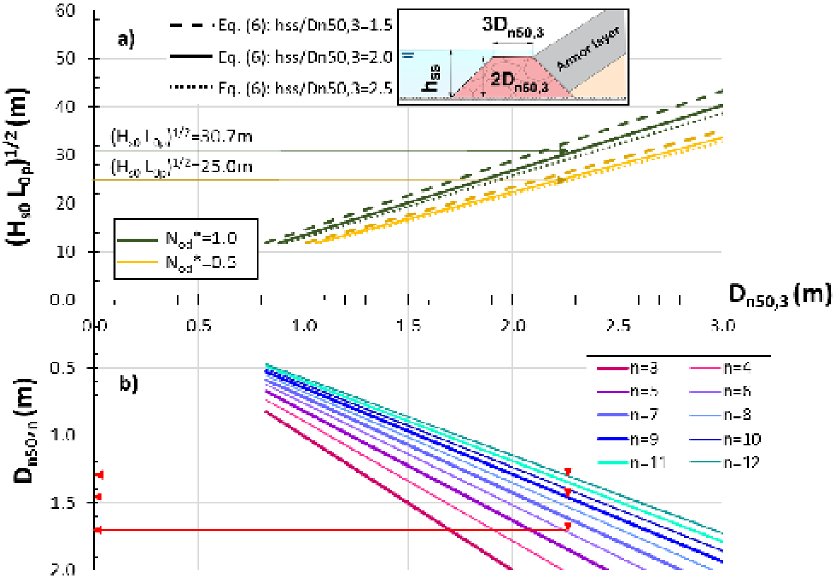

Fig. 13. (a) $D_{n50,3}$ estimated with Eq. (6) and (b) $D_{n50,n}$ as a function of $D_{n50,3}$ and the toe berm width (n).

Red arrows in Fig. 13 indicate the relationship considered in the example given below.

5. Application example

In this section, an example is given to design a rock toe berm placed on a m = 1/10 sea bottom combined with a SWL close to the crest of the toe berm ($h_{ss} \approx 2D_{n50}$); the recommended design value of $N_{od}{}^* = 1$, given by Herrera and Medina (2015) for Eq. (6), is considered first. According to Eq. (6) and given a typical design storm for the Alboran Sea (H_{s0}(m) = 5, T_p(s) = 11, $(H_{s0} L_{0p})^{1/2}$ = 30.7 m and water depth at the nominal toe berm h_{ss}(m) = 4.5), the required rock size for a nominal toe berm ($B_t = 3D_{n50}$ and $t_t = 2D_{n50}$) is $D_{n50,3}$(m) = 2.23, which corresponds to 30-tonne rocks if the mass density is ρ_r(g/cm³) = 2.70. In order to reduce the size of the required rocks (if not available at quarry), Eq. (9) with k = 0.4 is applied. When considering a double toe berm width (n = 6), the required rock size is reduced to $D_{n50,n}$(m) = 1.7 (13-tonne rocks). If only 6-tonne rocks are available at the construction site, a wider toe berm with n = 12 is required. Fig. 14 depicts the rock weight (W) in tonnes depending on the toe berm width (n). Rocks with W(t) = 30, 13, 8.0 and 5.7 (D_{n50} (m) = 2.23, 1.7, 1.44 and 1.28) could be used when considering toe berm widths having n = 3, 6, 9 and 12, respectively.

If $N_{od}{}^* = 0.5$ rather than $N_{od}{}^* = 1.0$ were considered as the design condition, the toe berms described above would withstand a design storm, $(H_{s0} L_{0p})^{1/2}$ = 25.0 m, which corresponds to a weaker design storm: H_{s0}(m) = 4 and T_p(s) = 10).

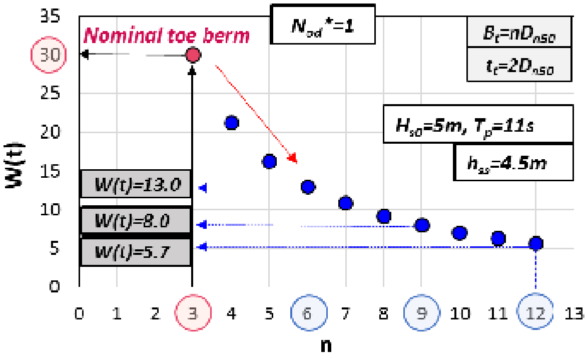

Fig. 14. Rock weight (W) depending on the toe berm width ($B_t = nD_{n50}$).

6. Comparison with existing formulas

As mentioned in Section 1, Van Gent and Van der Werf (2014) specifically introduced the toe berm width (B_t) as an explicative parameter of toe berm damage (N_{od}). For a certain amount of acceptable damage, the required rock size according to the study by these experts is given by Eq. (5), which was obtained from laboratory tests with a m = 1/30 bottom slope, and no severe depth-limited wave breaking. Two toe berm widths were considered ($B_t = 3D_{n50}$ and $9D_{n50}$), and only the total toe berm damage (N_{od}) was measured after each test. In order to consider that N_{od} increases with the toe berm width, these authors proposed multiplying the design N_{od} value by a factor f_B when $3D_{n50} < B_t \leq 9D_{n50}$.

$$f_B = \left(\frac{B_t}{3D_{n50}}\right)^{1/2} = \left(\frac{n}{3}\right)^{1/2} \tag{13}$$

Thus, when $B_t = 3D_{n50}$, Eq. (5) is directly applicable with $N_s = H_{st}/(\Delta D_{n50})$ and $D_{n50} = D_{n50,3}$. If $3D_{n50} < B_t = nD_{n50} \leq 9D_{n50}$ and $t_t = 2D_{n50}$, Eq. (5) may be rewritten as follows:

$$D_{n50,n} = 0.32\left(\frac{H_{st}}{\Delta(N_{od} f_B)^{1/3}}\right)\left(\frac{2D_{n50,n}}{H_{st}}\right)^{1/3}\left(\frac{nD_{n50,n}}{H_{st}}\right)^{0.1}\left(\frac{\hat{u}_\delta}{\sqrt{gH_{st}}}\right)^{1/3} \tag{14}$$

Eq. (14) is equivalent to Eq. (5) for $n = 3$. Manipulating Eqs. (5) and (14) and replacing f_B by the expression given by Eq. (13), the relation between the required nominal diameters for the design of a toe berm with $3 < n \leq 9$ and a nominal toe berm with $n = 3$, can be calculated using Eq. (15).

$$\frac{D_{n50,n}}{D_{n50,3}} = \left(\frac{3}{n}\right)^{1/6} \cdot \left(\frac{D_{n50,n}}{D_{n50,3}}\right)^{1/3} \cdot \left(\frac{nD_{n50,n}}{3D_{n50,3}}\right)^{0.1} = \left(\frac{3}{n}\right)^{\frac{2}{17}} \tag{15}$$

$D_{n50,n}/D_{n50,3}$ follows the potential relationship given by Eq. (8) but with the shape parameter $k = 2/17$ instead of $k=0.4$ used in Eq. (9). Fig. 15 shows the N_{od}* measured in this study and that estimated by Eq. (9) when using $k = 2/17$ rather than $k = 0.4$. Eqs. (5) and (14) given by Van Gent and Van der Werf (2014) are valid for toe structures placed on a m=1/30 bottom slope, with an armor slope cotα =2.0, $3D_{n50} \leq B_t \leq 9D_{n50}$, $2D_{n50} \leq t_t \leq 4D_{n50}$, $7D_{n50} < h_t \leq 25D_{n50}$, $1.2 \leq h_s/H_{st} \leq 4.5$ and $0.012 \leq s_{op} \leq 0.042$. Eqs. (5) and (14) are beyond the range of variables tested in this study; this explains the poor agreement between the N_{od}* measured in this study and that estimated by Eq. (9) when using $k = 2/17$ (instead of $k=0.4$). Further research is required to test the range of variables not included in Van Gent and Van der Werf (2014) or in the present study (e.g. $3.5D_{n50} < h_s < 8.6D_{n50}$ and $1/30 < m < 1/10$).

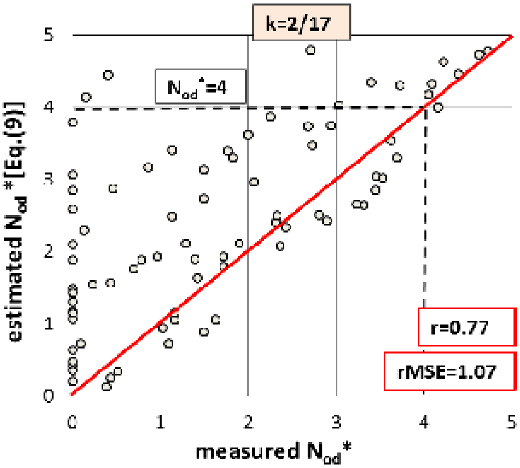

Fig. 15. Comparison of the N_{od}* measured in tests and that given by Eq. (9) using k = 2/17 rather then k = 0.4.

Thus, the parameter k depends on the test conditions. The divergence between k = 2/17 and 0.4 highlights the distinct performance of the toe berm when dealing with plunging waves breaking on a steep sea bottom (m = 1/10) combined with very shallow waters (as seen in the case of this study), or when dealing with gentler sea bottoms (m = 1/30) and no severe depth-limited wave breaking (as seen in Van Gent and Van der Werf, 2014). These two cases indicate that rock size and toe berm width should be considered together when designing a rock toe berm.

7. Summary and Conclusions

Although the hydraulic stability tests of toe berms reported in the literature consider different bottom slopes, ($1/50 \leq m \leq 1/10$), toe berm widths ($3D_{n50} \leq B_t \leq 9D_{n50}$) and toe berm thicknesses ($2D_{n50} \leq t_t \leq 8.8D_{n50}$), toe berm geometry is usually not taken as an explicative parameter of the toe berm damage. Only Van Gent and Van der Werf (2014) explicitly considered the influence of toe berm width ($B_t = nD_{n50}$) on toe berm stability. When considering wide toe berms ($n > 3$), common toe berm damage values ($0.5 \leq N_{od} \leq 4.0$) cannot be directly applied since more rock displacements are required to significantly damage wider toe berms.

This study proposes two new concepts to better characterize the hydraulic stability of wide toe berms ($3 < n \leq 12$): nominal and sacrificial toe berms. Two areas were distinguished for the toe berm: (1) the most shoreward area of the toe berm (nominal toe berm, n=3) which supports the armor layer and (2) the most seaward area (sacrificial toe berm) which protects the nominal toe berm. New physical tests were carried out at LPC-UPV with toe berms of different rock sizes (D_{n50}(cm) = 3.04, 3.99 and 5.12) and toe berm widths (n = 3, 5 and 12). Tests were conducted with a m = 1/10 bottom slope and a SWL close to the top of the berm ($1.5 \leq h_{ss}/D_{n50} \leq 2.6$). The toe berm damage was measured after each test considering: (1) the total toe berm damage (N_{od}), and (2) the damage to the nominal toe berm (N_{od}*). For wider toe berms ($n > 3$), N_{od}* turned out to be a better descriptor of toe berm damage; N_{od}* decreased when increasing the toe berm width (n). When using N_{od}*, recommended design values of conventional toe berm damage can be directly used ($0 \leq N_{od}^* \leq 4$).

Given an acceptable level of damage to the nominal toe berm (N_{od}*) as a design condition, it is possible to significantly reduce the rock size (D_{n50}) by increasing the toe berm width (n) according to Eq. (8). For steep sea bottoms (m = 1/10) and shallow waters, this reduction in rock size showed an inverse 0.4-power relationship with the relative toe berm width. Using the formula given by Van Gent and Van der Werf (2014) with a gentle bottom slope m = 1/30 and a toe berm thickness $t_t = 2D_{n50}$, the reduction in rock size also followed Eq. (8) but showed an inverse 2/17-power relationship with the toe berm width. Thus, the shape parameter k = 2/17 and 0.4 given in Eq. (8) depends on the water depth and the sea bottom slope existing at the construction site, and it determines the breaking type and the wave impact affecting the toe berm.

To design toe berms placed on m = 1/10 bottom slopes, the rock size reduction may be especially important when the wave conditions are so adverse that it is not possible to find the required rock sizes at the construction site. Thus, the proposed method can be used in these cases for the design of rock toe berms within the ranges m=1/10, $3D_{n50} \leq B_t \leq 12D_{n50}$, $t_t = 2D_{n50}$, $1.5 \leq h_{ss}/D_{n50} \leq 2.6$, $0.02 \leq s_{0p} \leq 0.07$, $0.4 \leq h_{ss}/H_{s0} \leq 1.0$ and $0 \leq N_{od}^* \leq 4$. The validity is limited to water depths close to the crest of the toe berm. Further research is required to examine the transition area from shallow waters with m=1/10 analyzed in this study, and the deeper waters and milder bottom slope tested by Van Gent and Van der Werf (2014). Also the effect of other slope angles and toe thicknesses should be investigated.

In shallow waters combined with steep sea bottoms (m=1/10), when using sacrificial toe berms, it is convenient to regularly monitor the toe berm. After severe storms, the sacrificial toe berm may be partially washed away and additional dumping of rocks at the toe may be necessary to continue providing full support to the armor layer.

References

Baart, S., Ebbens, R., Nammuni-Krohn, J., Verhagen, H.J., 2010. Toe rock stability for rubble mound breakwaters. Proceedings 32nd International Conference on Coastal Engineering, World Scientific, Shanghai, 3005-3017.

Besley, P., Denechere, M., 2009. Single Layer Armour Systems – Toe, Crest and Roundheads details. Proceedings of Coasts, Marine Structures and Breakwaters 2009 Conference.

Burchart, H.F., Liu, Z., 1995. Rubble Mound Breakwater Failure Modes. Proceedings Final Workshop: Rubble mound failure modes, Sorrento, Italy.

CIRIA, CUR, CETMEF, 2007. The Rock Manual. The Use of Rock in Hydraulic Engineering (2nd edition). C683, CIRIA, London.

Ebbens, R.E., 2009. Toe Structures of Rubble Mound Breakwaters. Stability in Depth Limited Conditions. M.Sc. thesis Delft. Delft University of Technology, Delft.

Figueres, M., Medina, J.R., 2004. Estimation of incident and reflected waves using a fully non-linear wave model. Proceedings 29th International Conference on Coastal Engineering, World Scientific, Singapore, 594–603.

Gerding, E., 1993. Toe Structure Stability of Rubble Mound Breakwaters. M.Sc. thesis Delft and Delft Hydraulics Report H1874. Delft University of Technology, Delft.

Goda, Y., 2000. Random seas and design of maritime structures (2nd Edition). World Scientific Publishing, Singapore, ISBN 981-02-3256-X.

Herrera, M.P., Medina, J.R., 2015. Toe berm design for very shallow waters on steep sea bottoms. Coastal Engineering, 103, 67-77.

Hovestad, M., 2005. Breakwaters on steep foreshores: the influence of foreshore steepness on armour stability. M.Sc. thesis Delft. Delft University of Technology, Delft.

Lamberti, A., 1994. Preliminary results on main-armour toe-berm interaction. RMBFM 3rd workshop-DH, De Voorst, The Netherlands.

Muttray, M., 2013. A pragmatic approach to rock toe stability. Coastal Engineering, 82, 56–63.

USACE, 2006. Coastal Engineering Manual. Engineer Manual 1110-2-1100, U.S. Army Corps of Engineers, Washington, D.C. (in 6 volumes).

Van der Meer, J.W., 1998. Geometrical Design of Coastal Structures. Pilarczyk, K.W. (Ed.), Seawalls, Dikes and Revetments. Balkema, Rotterdam.

Van Gent, M.R.A., Van der Werf, I.M., 2014. Rock toe stability of rubble mound breakwaters. Coastal Engineering, 83, 166–176.

2. Herrera, M.P., Medina, J.R., 2015. Toe berm design for very shallow waters on steep sea bottoms. Coastal Engineering, 103, 67-77.

Toe berm design for very shallow waters on steep sea bottoms

Maria P. Herrera [a,*] and Josep R. Medina [b]

[a] Research Assistant, Dept. of Transportation, *Universitat Politècnica de València*, Camino de Vera s/n, 46022 Valencia, Spain. E-mail: mahergam@upv.es (* corresponding author)

[b] Professor, Dept. of Transportation, *Universitat Politècnica de València*, Camino de Vera s/n, 46022 Valencia, Spain. E-mail: jrmedina@upv.es

ABSTRACT

The toe berm is a relevant design element when rubble mound breakwaters are built on steep sea bottoms in breaking conditions. Different design formulas can be found in the literature to predict the damage caused to submerged toe berms placed on gentle bottom slopes. However, these formulas are not valid for very shallow waters in combination with steep sea bottoms where toe berms receive the full force of breaking waves. To guarantee breakwater stability in these conditions, new design formulas are needed for toe berms. To this end, physical model tests were carried out and data were analyzed to characterize rock toe berm stability in very shallow water and with a bottom slope m = 1/10. Based on test results, a new formula was developed with three parameters to estimate the nominal diameter (D_{n50}) of the toe berm rocks: water depth at the toe (h_s), deep water significant wave height (H_{s0}) and deep water wave length (L_{0p}).

Keywords: Mound breakwater; Toe berm design; Shallow water; Steep sea bottom; Breaking conditions.

Highlights:

a) **In breaking conditions, toe berm stability is critically dependent on the bottom slope and water depth.**
b) **Existing formulas for toe berm design are mostly based on laboratory tests with submerged toe berms placed on gentle bottom slopes.**
c) **In shallow waters in combination with steep sea bottoms, wave attack may damage toe berms more than armor layers.**
d) **On rocky coastlines, mound breakwaters in very shallow water may require larger rocks for the toe berm than the armor.**

1. Introduction

Rubble mound breakwaters are usually protected by a toe berm when concrete armor units are used for the armor layer. This toe berm is placed on the seafloor or a bed layer, providing support to the concrete armor units which are placed later on the structure slope (USACE, 2006). Fig.1 shows a typical cross section for a conventional mound breakwater with a toe berm placed on a steep seafloor, where h_s is the sea bottom water depth at the toe, h_t is the water depth above the toe berm, B_t is the toe berm width and t_t is the toe berm thickness.

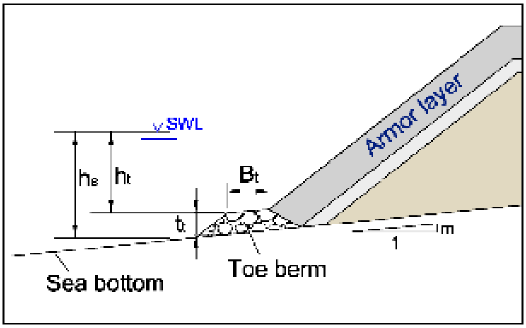

Fig. 1. Cross section of a conventional mound breakwater with a toe berm.

Many rubble mound breakwaters are constructed in breaking conditions and in shallow waters on steep sea bottoms. In these conditions, the highest waves start breaking on the sea bottom and impact the toe berm directly. This is particularly common for rocky sea bottoms with m = 1/10 or higher slopes; in this case, the toe berm must be designed to guarantee armor stability. In very shallow waters combined with steep seafloors, the stone size required for the toe berm may significantly exceed the armor unit size.

Several empirical formulas have been developed to predict damage to rock toe berms in depth-limited conditions. Most were obtained from laboratory tests with gentle bottom slopes and are only valid for submerged toe berms (h_t >>0); however, when constructed in very shallow waters on rocky coasts and steep seafloors, seawalls may require emerged toe berms (h_t<0) built with large rocks.

This research focuses on the design of toe berms placed in very shallow waters ($-0.15< h_s/H_{s0} <1.5$) in combination with steep seafloors (m = 1/10) since these conditions have not yet received sufficient attention in the literature. New physical model tests were carried out in the wave flume at the Universitat Politècnica de València (Spain) and data were analyzed to determine the influence of shallow waters and steep seafloors on toe berm stability. In this paper, existing formulas to design toe berms are first compared. The experimental setup is then described, test results are analyzed and a new design formula with confidence intervals is provided. Finally, conclusions are drawn.

2. Design formulas for toe berms

In this section, the most relevant formulas to design quarrystone toe berms are examined. The stability number, $N_s = H_{st} /(\Delta D_{n50})$, is used to characterize hydraulic stability, where D_{n50} is the nominal diameter of the rocks in the toe berm, $\Delta = (\rho_r - \rho_w)/\rho_w$

is the relative submerged mass density, ρ_r is the mass density of the rocks, ρ_w is the mass density of the sea water, and H_{st} is the significant wave height at the toe of the structure.

Markle (1989) performed physical tests in breaking conditions with a bottom slope m = 1/10. Regular waves were generated with increasing wave heights (9.1< H_{mt}(cm) <22.9) and wave periods (1.32< T_m(s) <2.82) for a given water depth at the toe (h_s(cm) = 12.2, 15.2, 18.3, 21.3, 24.4, 27.4), where H_{mt} is the average wave height at the toe of the structure and T_m is the mean wave period. Four rock nominal diameters were used (D_{n50}(cm) = 2.58, 2.95, 3.30, 4.06) for toe berms with $t_t = 2 \cdot D_{n50}$ and $B_t = 3 \cdot D_{n50}$. Eq. (1) is the lower bound formula obtained from Markle's data (see Muttray, 2013); the water depth ratio (h_t/h_s) was identified as the determining parameter for toe berm stability. Eq. (1) refers to moderate damage.

$$N_s{}^* = \frac{H_{mt}}{\Delta D_{n50}} = 1.6 + 5.5 \cdot \left(\frac{h_t}{h_s}\right)^3 \tag{1}$$

where $N_s^* = H_{mt}/(\Delta D_{n50})$ is the stability number for regular waves.

Gerding (1993) measured toe berm damage in physical tests using runs of 1,000 random waves and a bottom slope m = 1/20. Tests were characterized by a constant wave steepness at the wave generating zone ($s_{gp} = 2\pi H_{sg}/gT_p^2$ = 0.02 and 0.04), an increasing significant wave height at the wave generator (H_{sg}(cm) = 15, 20, 25) and a fixed water depth at the toe (h_s(cm) = 30, 40 and 50). Four stone sizes were tested (D_{n50}(cm) = 1.7, 2.5, 3.5 or 4.0), varying the toe berm height (t_t(cm) = 8, 15 and 22), and the toe berm width (B_t(cm) = 12 and 20). Gerding (1993) also proposed using the damage number N_{od} to quantify the damage observed on the toe berm. N_{od} is defined as the number of displaced rocks in a strip as wide as D_{n50} of the toe berm. N_{od} is independent of the shape and volume of the toe berm; therefore, damage geometry may differ significantly from quantitative N_{od}.

$$N_{od} = \frac{N}{B/D_{n50}} \tag{2}$$

where N is the number of displaced rocks and B is the total width of the wave flume. After each test, the damage number N_{od} was calculated and the model was rebuilt. The formula given by Gerding (1993) can be re-written to estimate toe berm damage as a function of the stability number.

$$N_{od} = \frac{1}{\left(0.24 \cdot \left(\frac{h_t}{D_{n50}}\right) + 1.6\right)^{1/0.15}} \cdot (N_s)^{1/0.15} \tag{3}$$

Docters van Leeuwen (1996) conducted tests on a bottom slope m = 1/50 to analyze the influence of the relative submerged mass density ($\Delta = (\rho_r - \rho_w)/\rho_w$) on Gerding's formula, concluding that Δ was well reproduced since different stone mass densities gave similar results for $H_{st}/(\Delta D_{n50})$ as a function of h_t/D_{n50}.

Van der Meer (1998) re-analyzed the data given by Gerding (1993) for rock toe berms, using the water depth ratio (h_t/h_s) as the explanatory variable; the new Van der Meer formula can be re-written as follows:

$$N_{od} = \frac{1}{\left(6.2 \cdot \left(\frac{h_t}{h_s}\right)^{2.7} + 2.0\right)^{1/0.15}} \cdot (N_s)^{1/0.15} \qquad (4)$$

CIRIA/ CUR/ CETMEF (2007) made reference to the formulas given by Gerding (1993) and Van der Meer (1998) to calculate the rock size for toe berms of rubble mound breakwaters. Gerding (1993) recommended using $N_{od} = 2.0$ for safe designs while Van der Meer (1998) recommended $N_{od} = 0.5$ for conservative designs. For a standard toe berm size of 3 to 5 rocks wide and a thickness of 2 to 3 rocks, CIRIA/ CUR/ CETMEF (2007) criteria indicated $N_{od} = 0.5$ for start of damage, $N_{od} = 2.0$ for moderate damage and $N_{od} = 4.0$ for failure.

Ebbens (2009) conducted physical tests to analyze the influence of three bottom slopes (m = 1/50, 1/20 and 1/10). Random waves were generated with seven water levels varying in the range of $7.3 < h_s(\text{cm}) < 25.3$. The four lowest water levels (h_s(cm) = 7.3, 9.3, 11.3 and 13.3) were tested with two values for wave steepness at the wave generating zone ($s_{gp} = 2\pi H_{sg}/gT_p^2 = 0.04$ and 0.02). Tests with the three highest water levels (h_s(cm) = 15.3, 20.3, or 25.3) were only performed with $s_{gp} = 2\pi H_{sg}/gT_p^2 = 0.03$ for calibration. For each water level, wave runs were generated with four significant wave heights at the wave generator (H_{sg}(cm) = 6, 8, 10 or 12). Three rock sizes were tested (D_{n50}(cm) = 1.88, 2.15 and 2.68) with toe berm thickness t_t(cm) = 6 and toe berm width B_t(cm) = 10 (above a 2cm-thick bed layer). Three rock porosities were used for each D_{n50} (n = 0.36, 0.33, 0.32). For the bottom slope m = 1/10, only D_{n50}(cm) = 2.15 and 2.68 were tested. To characterize toe berm damage, the damage parameter given by Eq. (5) was used.

$$N_{\%} = N \cdot \frac{D_{n50}{}^3}{(1-n) \cdot V_{total}} \qquad (5)$$

where n is the void porosity and V_{total} is the apparent volume of the toe berm.

A difference in damage was observed when varying the wave steepness from $s_{gp} = 0.04$ to $s_{gp} = 0.02$. Steeper waves ($s_{0p} = 0.04$) led mainly to a downward movement of rocks, while longer waves ($s_{0p} = 0.02$) pushed rocks in an upward direction. Thus, for tests with $s_{0p} = 0.04$, only downward rock movements were considered to characterize toe berm damage. For tests with $s_{0p} = 0.02$, the number of displaced rocks was counted considering the number of stones moving downwards (away from the toe berm) and upwards.

Using $N_{\%}$, Ebbens (2009) proposed the following design equation for toe berm stability:

$$N_{\%} = 0.038 \cdot \left(\xi_{0p}*\right)^{3/2} \cdot \left(N_s\right)^3 \tag{6}$$

where $\xi_{0p}^{*} = m/(H_{st}/L_{0p})^{1/2}$ is the surf similarity parameter in which $1/m$ is the bottom slope, and $L_{0p} = gT_p^2/2\pi$ is the deep water wave length. Although higher toe berm damage was measured during the tests, Eq. (6) only provides reliable values if $N_{\%} < 0.3$.

The toe berm was not rebuilt after each test but rather before each change in the water level. The cumulative toe berm damage did not always increase for a certain water depth, but it sometimes decreased when wave steepness increased (s_{0p}=0.04 after s_{0p}=0.02).

Fig. 2 represents the experimental results given by Ebbens (2009) who recommended using $N_{\%}$ = 5% ($N_{od} \approx 0.5$) as a safe toe berm design level for swell waves and $N_{\%}$ = 10% ($N_{od} \approx 1.0$) for wind waves. Fig. 2 also indicates the values of N_{od} and $N_{\%}$ obtained for toe berm sizes (D_{n50}(cm) = 1.88, 2.15 and 2.68), in which $N_{\%}$ is approximately one order of magnitude lower than the damage number N_{od}.

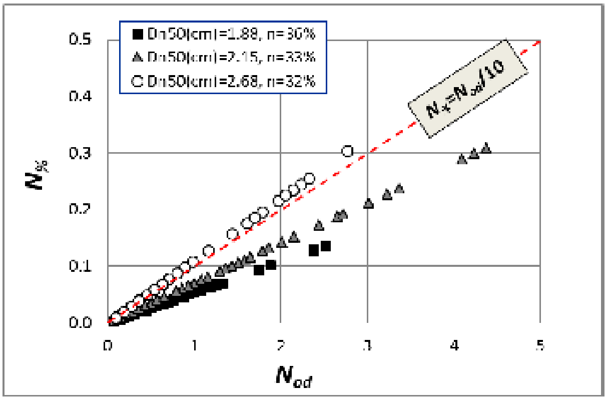

Fig. 2. Values of N_{od} corresponding to $N_{\%}$ measured by Ebbens (2009).

The experimental results obtained by Markle (1989), Gerding (1993) and Ebbens (2009) were re-analyzed by Muttray (2013), who proposed the following formula:

$$N_{od} = \left(0.58 - 0.17 \cdot \frac{h_t}{H_{st}}\right)^3 \cdot \left(N_s\right)^3 \tag{7}$$

Van Gent and Van der Werf (2014) performed tests with runs of 1,000 random waves with m = 1/30 bottom slope. Three water levels in front of the toe (h_s(cm) = 20, 30, and 40) were tested, mostly without severe wave breaking on the foreshore. Two wave steepness values at the wave generating zone were tested ($s_{gp} = 2\pi H_{sg}/gT_p^2$ = 0.015 and 0.04) increasing the significant wave height until reaching a high damage level or H_{sg}(cm)

5

= 28. Two stone sizes were used (D_{n50}(cm) = 1.46 and 2.33) with a toe berm thickness t_t = $2 \cdot D_{n50}$ and $4 \cdot D_{n50}$, and a toe berm width $B_t = 3 \cdot D_{n50}$ and $9 \cdot D_{n50}$. The model was rebuilt after each test series of four or seven wave runs of increasing H_{sg}. These authors proposed the following formula to estimate damage to the toe berm:

$$N_{od} = 0.032 \cdot \left(\frac{t_t}{H_{st}}\right) \cdot \left(\frac{B_t}{H_{st}}\right)^{0.3} \cdot \left(\frac{\hat{u}_\delta}{\sqrt{g \cdot H_{st}}}\right) \cdot (N_s)^3 \tag{8}$$

where $\hat{u}_\delta = \frac{\pi \cdot H_{st}}{T_{m-1,0}} \frac{1}{\sinh(kh_t)}$, $k = \frac{2\pi}{L_{m-1,0}} = \frac{2\pi}{\frac{g}{2\pi} \cdot T_{m-1,0}{}^2}$, $T_{m-1,0} = \frac{m_{-1}}{m_0}$ and m_i is the *i-th* spectral moment, $m_i = \int_0^\infty S(f) \cdot f^i \cdot df$, being $S(f)$ the wave spectra.

Given a design wave storm (H_{st}, $T_{m-1,0}$), the larger the toe berm (B_t or t_t), the larger the N_{od}.

Eqs. (1) to (4) can be used to estimate the toe berm damage caused by a single wave storm, characterized by H_{mt} or H_{st} measured at the toe of the structure. For Eqs. (6) and (7), the model was rebuilt after test series as defined by a given water. For Eq. (8), the model was rebuilt after test series as defined by a given wave steepness. Eqs. (6) to (8) also include the wave period T_p or $T_{m-1,0}$ to characterize the design wave storm. Test characteristics are summarized in Table 1.

Table 1. Range of parameters (min, max) used in the toe berm stability tests described in the literature and considered in this study.

Parameter	Symbol	Markle (1989)	Gerding (1993)	Ebbens (2009)	Van Gent and Van der Werf (2014)	This study
Waves	-	Regular	Random	Random	Random	Random
Bottom slope (-)	m	1/10	1/20	(1/50,1/10)	1/30	1/10
Rock toe berm size (cm)	D_{n50}	(2.6, 4.1)	(1.7, 4)	(1.9, 2.7)	(1.5, 2.3)	(3.99, 5.17)
Water depth at toe (cm)	h_s	(12.2, 27.4)	(30, 50)	(7.3, 34.0)	(20, 40)	(-2, 20)
Relative water depth at toe (-)	h_s/D_{n50}	(3.0, 10.6)	(7.5, 29.4)	(2.7, 18.0)	(8.6, 27.4)	(-0.5, 5.01)
Relative significant wave height at toe (-)	H_{st}/h_s	(0.6, 1.1)^a	(0.3, 0.6)^b	(0.2, 1.4)	(0.2, 0.8)	(-9.9, 10.1)^c
Wave steepness at toe ($s_{tp}=2\pi H_{st}/gT_p{}^2$)(-)	s_{tp}	(0.009,0.068)^a	(0.01,0.04)^b	(0.008,0.04)	(0.012,0.042)	(0.008,0.08)^c
Relative toe width (-)	B_t/D_{n50}	3	(3, 12)	(3.7, 5.3)	3 and 9	3

Relative toe thickness (-)	t_t/D_{n50}	2	(2.3, 8.8)	(2.2, 3.2)	2 and 4	2
Stability number at toe ($N_s=H_{st}/\Delta D_{n50}$) (note $H_{st}=H_{m0}$ at toe)(-)	N_s	(1.96,4.39)[a]	(2.1,8.37)[b]	(1.07,4.16)	(1.2,10.5)	(0.81,3.36)[c]
Damage level (-)	N_{od}	moderate	<9.2	≤4.4	<7.3	<4.7
Cumulative damage	-	no	no	yes	yes	yes
Number of waves per run	N	-	1000	1000	1000	500
Number of test runs	N_t	1	1	4	4 to 7	35 to 40

[a] Refers to average wave height, H_{mt}, and wave period, T_m, at the toe of the structure.

[b] Refers to the average wave height of the one-third highest waves at the toe of the structure, $H_{st}=H_{1/3}$.

[c] Refers to significant wave height measured at the wave generating zone, $H_{sg}=(4\cdot m_0)^{1/2}$.

Fig. 3 shows an example of a typical case ($B_t=3\cdot D_{n50}$ and $t_t=2\cdot D_{n50}$) of toe berm damage estimated by Eqs. (3) to (8) as a function of N_s. The wave steepness at the toe is fixed at $s_{tp}=2\pi H_{st}/gT_p^2=0.02$, the water depth ratio is $h_t/h_s=0.78$, and the relative water depth at the toe is $h_s/D_{n50}=9.4$. The damage parameter obtained from Eq. (6) was considered $N_\% = N_{od}/10$ (see Fig. 2).

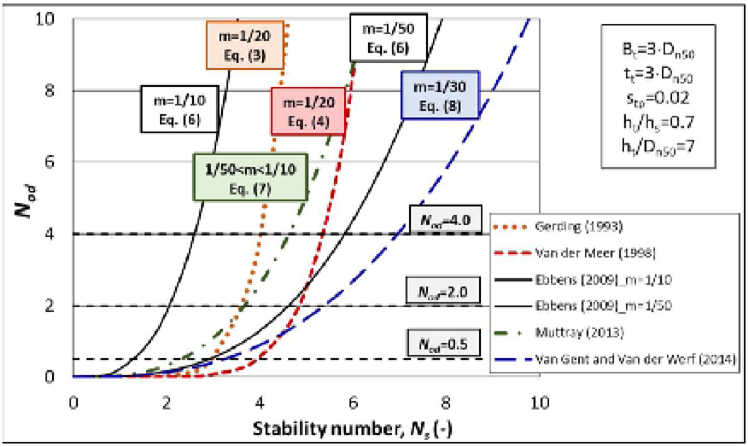

Fig. 3. Example of toe berm damage estimated by different formulas.

Fig. 3 illustrates the relevant dispersion of toe berm damage estimations calculated using Eqs. (3), (4) and (6) to (8).

The available literature for submerged toe structures in depth-limited conditions and gentle seafloors suggests that the primary parameters for toe stability are the relative water depth at the toe and the wave height, while other parameters such as berm width/berm height appear to be less relevant (see e.g. Van Gent and Van der Werf, 2014). However, for emergent toe structures and steeper seafloors no information is available. Only Ebbens (2009) performed physical tests with random waves and a steep bottom (m = 1/10). Nevertheless, the effect of water depth on toe berm stability was not considered nor was the stability of emerged toe berms.

In this paper, the influence of the water depth in submerged (h_t>0) and emerged (h_t<0) toe berms is investigated, considering the cumulative toe berm damage corresponding to a variety of wave storm conditions with the same still water level (SWL).

3. Methodology

2D physical model tests were conducted in the wind and wave test facility (30 x 1.2 x1.2 m) of the Laboratory of Ports and Coasts at the Universitat Politècnica de València (LPC-UPV) with a steep sea bottom (m = 1/10). Fig. 4 shows a longitudinal cross section of the LPC-UPV wave flume while Fig. 5 shows the cross section of the model tested.

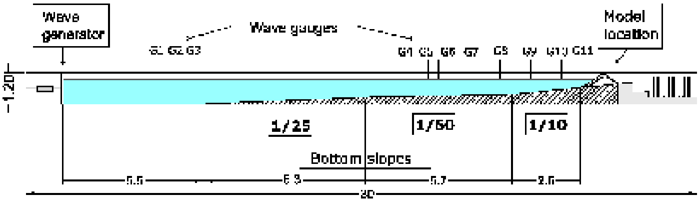

Fig. 4. Longitudinal cross section of the LPC-UPV wave flume (dimensions in meters).

The model depicted in Fig. 5 is a conventional tanα = H/V = 1.5 non-overtopping mound breakwater, protected with a conventional double-layer randomly-placed cube armor with nominal diameter D_n(cm) = 3.97 and W(g) = 141.5. The mean value of the measured packing density of the tested armor layer was ϕ = 1.16, very close to the recommended value ϕ = 1.17 given by CIRIA/ CUR/ CETMEF (2007). Rocks with D_{n50}(cm) = 3.99 and 5.17 and mass density ρ_r(g/cm^3) = 2.70 were used for the toe berms. Toe berm thickness and width were fixed at $t_t = 2 \cdot D_{n50}$ and $B_t = 3 \cdot D_{n50}$, similar to those tested by Markle (1989), Gerding (1993), Ebbens (2009) and Van Gent and Van der Werf (2014).

The double-layer randomly-placed cube armor was built on a filter layer with D_{n50}(cm) = 1.78 and D_{n85}/D_{n15} = 1.35. The characteristics of the core material were D_{n50}(cm) = 0.68 and D_{n85}/D_{n15} = 1.64.

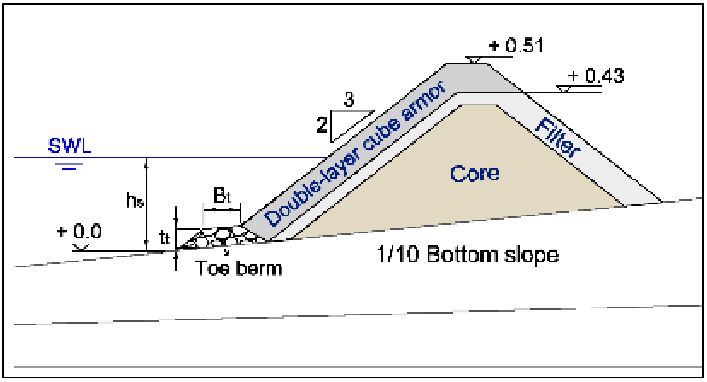

Fig. 5. Cross section of the cube armored model (dimensions in meters).

Random wave runs of 500 waves were generated following JONSWAP (γ = 3.3) spectra, and incident and reflected waves were estimated at the wave generating zone (wave gauges G1, G2 and G3). The AWACS Active Absorption System was activated to avoid multi-reflections.

Test series were associated to the water depth at the toe (h_s). For a specific h_s, five different peak periods were used, T_p(s) = 1.20, 1.50, 1.80, 2.20 and 2.40; for each peak period (T_p), increasing values of significant wave height at the wave generating zone (H_{sg}) were produced from no damage to wave breaking. H_{sg} was varied in steps of 2cm in the range of 8< H_{sg} (cm) <22. The tested water depths at the toe of the structure were h_s(cm) = -2, 0, 2, 4, 6, 8, 10, 12, 14, 16, 18 and 20.

The methodology used in these experiments considered the fact that on steep seafloors and in very shallow waters seawalls must withstand not just a design storm, but also numerous wave storms slightly less intense than the design storm. For each water depth (h_s), five peak periods with approximately seven significant wave heights were generated. The toe berm was repaired after a test series of a specific h_s (35 to 40 tests for each rock size tested: D_{n50}(cm) = 3.99 and 5.17). A total of 775 tests were performed.

Surface elevation was measured using eleven capacitive wave gauges, three acoustic gauges and four pressure sensors placed along the flume. One group of wave gauges (G1, G2 and G3) was placed near the wave generator while the other wave gauges were placed along the wave flume near the model (see Fig. 4). The distances (in meters) from wave gauges G9, G10 and G11 to the toe berm were 1.90, 1.40 and 0.70, respectively.

The damage to the toe berm was measured after each test. The damage parameter, N_{od}, was obtained considering the cumulative number of rocks displaced from the toe berm during each test series (h_s constant). Comparing the photographs taken perpendicularly to the armor slope after each test, armor damage was also measured using the Virtual Net method described by Gómez-Martín and Medina (2014).

4. Data analysis

4.1. Wave analysis

Using the measured surface elevations, wave height distributions and spectral moments were obtained. In several tests performed for this study, the water depth at the toe was null or negative ($h_s < h_t < 0$). Only in tests conducted with h_s(cm) ≥8, was it possible to obtain reliable values for wave heights near the structure. Fig. 6 shows a comparison between H_{m0} measured in the wave gauge G1 (wave generation zone) and G11 (model zone) for tests conducted in the range 8≤ h_s(cm) ≤20.

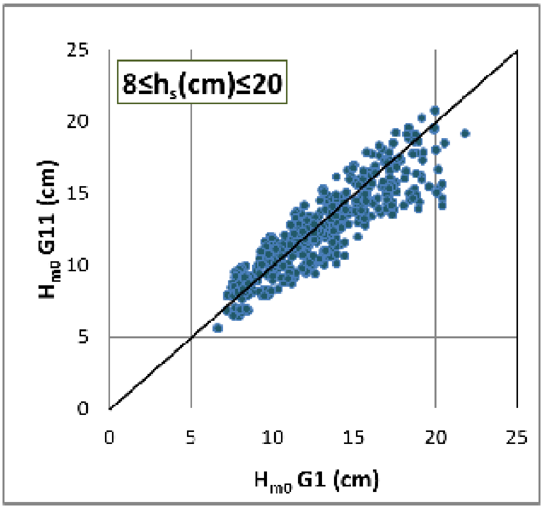

Fig. 6. Comparison between H_{m0} measured in the wave gauge G1 and G11 for tests conducted in the range 8≤ h_s(cm) ≤20.

Thus, it was necessary to refer all measurements to a location independent from the toe berm. The deep water wave conditions were selected as a clear reference for wave characteristics in these experiments. Using the three wave gauges placed near the wave generator, incident and reflected waves were separated into non-linear and non-stationary waves using the LASA-V method developed by Figueres and Medina (2004). The incident significant wave heights measured at the wave generating zone were propagated to deep water using the shoaling coefficients proposed by Goda (2000).

In these conditions, it is not clear *'a priori'* if wave transformation corresponding to the steep sea bottom m = 1/10 in the wave breaking zone is different depending on the foreshore. In order to check the sensitivity of H_s to the foreshore, a simple numerical experiment was conducted. To this end, the numerical model SwanOne (see Verhagen et al., 2008) was used to compare the significant wave height estimated at several points near the structure (A, B, C, D, E, F, G, H and T) in three virtual wave flumes with different configurations for the sea bottom (see Fig. 7). Flume #1 (Fig. 7a) corresponds to the configuration used in the experiments; flume #2 (Fig. 7b) and flume #3 (Fig. 7c) consider different lengths of the bottom slope m = 1/10 and different water depths at the wave generator.

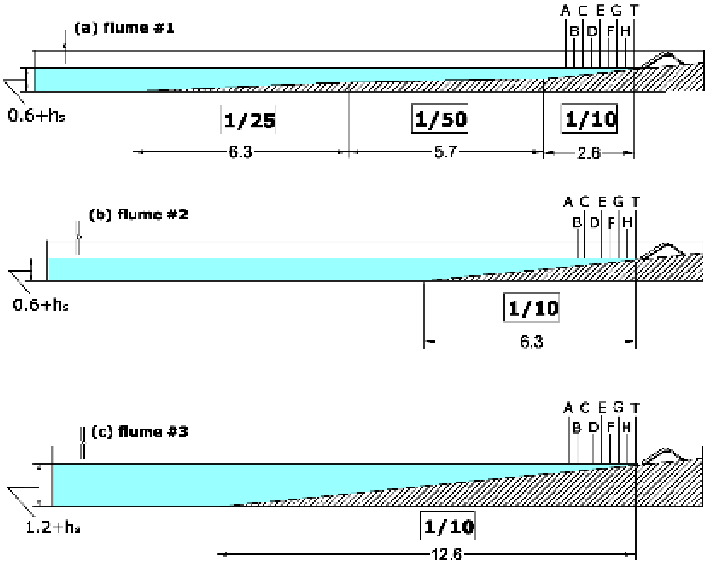

Fig. 7. Virtual wave flumes: (a) flume #1, (b) flume #2 and (c) flume #3 (dimensions in meters).

The analysis considered different water depths at the toe (h_s), peak periods (T_p) and deep water significant wave heights (H_{s0}). Table 2 shows the input data used for the SwanOne model. H_{st} values, given by SwanOne at the toe of the structure, were taken as reference to characterize the bottom profile's influence on waves attacking the structure. The input energy in the model was exactly the same; the same deep water significant wave height (H_{s0}) and peak period (T_p) were applied for the three virtual flumes.

Table 2. Significant wave height at the toe (H_{st}) as provided by the SwanOne numerical model for the virtual wave flumes #1, #2 and #3, shown in Fig. 7.

Deep water			Toe				Toe	
Input data			Depth	H_{st}			Relative H_{st}	
Case	T_p (s)	H_{s0} (cm)	h_s (cm)	H_{st}#1 (cm)	H_{st}#2 (cm)	H_{st}#3 (cm)	H_{st}#2/ H_{st}#1 (-)	H_{st}#3/ H_{st}#1 (-)
1	1.2	11.4	4	4.78	4.69	4.77	0.981	0.998
2	1.5	15.8	4	5.85	5.84	5.85	0.999	0.999
3	2.2	16.8	4	5.92	5.92	5.91	1.000	0.999
4	1.2	11.4	6	6.27	6.25	6.25	0.997	0.997
5	1.5	15.6	6	7.43	7.43	7.46	0.999	1.004
6	2.2	17.2	6	8.82	8.82	8.82	1.000	1.000
7	1.2	10.9	14	9.68	9.68	9.44	1.000	0.975
8	1.5	14.6	14	11.91	11.98	11.76	1.005	0.987
9	1.8	15.3	14	12.67	13.01	12.90	1.027	1.019
10	1.2	11.4	18	10.33	10.41	10.12	1.008	0.980
11	1.5	15.8	18	13.46	13.53	13.21	1.006	0.982
12	2.2	17.7	18	16.27	16.37	16.51	1.006	1.015

The relative mean squared error (*rMSE*) was used to measure the error between two significant wave heights estimated by the SwanOne numerical model for two virtual flumes. Flume #1 was taken as reference (target) because it corresponds to the wave flume used for the physical experiments described in this study.

$$rMSE = \frac{MSE}{\sigma^2(t)} = \frac{\frac{1}{N}\sum_{i=1}^{N}(t_i - e_i)^2}{\sigma^2(t)} \tag{9}$$

where *MSE* is the mean squared error, *N* is the number of observations, t_i is the target value, e_i is the estimated value and σ^2 is the variance of target values. The *rMSE* estimates the proportion of variance in the target values t_i (i=1 to N) not explained by the estimated values, e_i.

Table 3 shows the rMSE corresponding to points "A" to "T" when $H_s = (4{\cdot}m_0)^{1/2}$ measured at the same point in flume #1 is compared to H_s measured in flumes #2 and #3. Input data for the SwanOne model are given in Table 2.

Table 3. *rMSE* corresponding to H_s given by the SwanOne model at different points along wave flume #1 (target) as compared to values given for flumes #2 and #3.

rMSE			
Point	Toe distance (m)	H_s#2	H_s#3
A (G9)	1.90	0.040	0.036
B	1.40	0.028	0.027
C (G10)	1.30	0.023	0.025
D	1.00	0.016	0.019
E (G11)	0.70	0.009	0.014
F	0.60	0.007	0.014
G	0.40	0.002	0.010
H	0.20	0.003	0.005
T	0.00	0.001	0.002

At the toe of the structure, the *rMSE* of H_{st} was 0.1% (flume #2) and 0.2% (flume #3). The H_s errors were very low, especially at the points near the structure.

The results of this numerical experiment clearly indicate that changes in the bottom profile do not significantly affect the H_s near the structure, if the toe is placed on a bottom slope m = 1/10 (regardless of how far away the bottom profile is from the structure). Thus, when the breakwater is placed on a bottom slope m = 1/10 in very shallow waters, the slope will determine the waves that can actually reach the toe berm. In this study, it was assumed that the wave storm attacking the structure depends only on the bottom slope (m = 1/10), water level and deep water wave storm characteristics.

One should take into account that deep water wave conditions are the obvious reference when dealing with incident and reflected waves breaking on the seafloor. Existing methods to separate incident and reflected waves on steep sea bottoms combined with shallow waters are not reliable when applied near the structure (Baldock and Simmonds, 1999; Battjes et al., 2004).

4.2. Damage analysis

The rocks displaced from the toe berm were counted after each test to calculate the damage number N_{od}. Because this study deals with shallow water wave breaking conditions, the influence of the water depth on toe berm stability was analyzed first.

Fig. 8 shows the evolution of the observed toe berm damage depending on the water depth at the toe (h_s) for tests with D_{n50}(cm) = 3.99 and 5.17. Roughly speaking, toe berm damage (N_{od}) increased with water depths up to h_s(cm) = 12, and decreased from there up to h_s(cm) = 20.

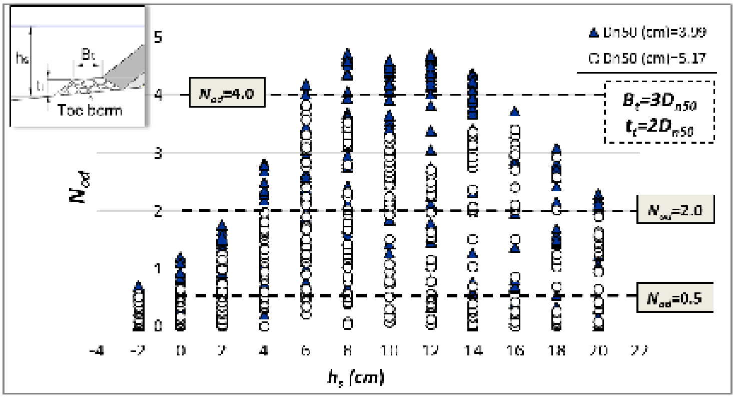

Fig. 8. Measured toe berm damage (N_{od}) depending on water depth at the toe (h_s).

Most toe berm damage occurred during the run-down events. Run-up and run-down mainly depend on the wave height and period of incident waves. According to Hunt (1959), the run-up (R_{up}) on a structure due to monochromatic waves can be estimated by Eq. (10).

$$R_{up} = (H \cdot L_0)^{1/2} \cdot \tan\alpha \qquad (10)$$

where tan α is the slope of the breakwater. Different formulas have been obtained to characterize wave run-up and run-down based on Eq. (10). Test results by Thompson and Shuttler (1975) indicated that the run–down level (R_d) on porous slopes is also proportional to $(H{\cdot}L_0)^{1/2}$.

In the experiments conducted for this study, N_{od} seemed to increase almost linearly with the variable $(H_{s0}{\cdot}L_{0p})^{1/2}$ for a given water depth (h_s) up to failure ($N_{od} \approx 4.0$). Fig. 9 shows N_{od} as a function of $(H_{s0}{\cdot}L_{0p})^{1/2}$ and h_s, for tests carried out with D_{n50}(cm) = 3.99 and 5.17. Straight lines correspond to h_s(cm) = -2, 0, 2, 4 and 6.

14

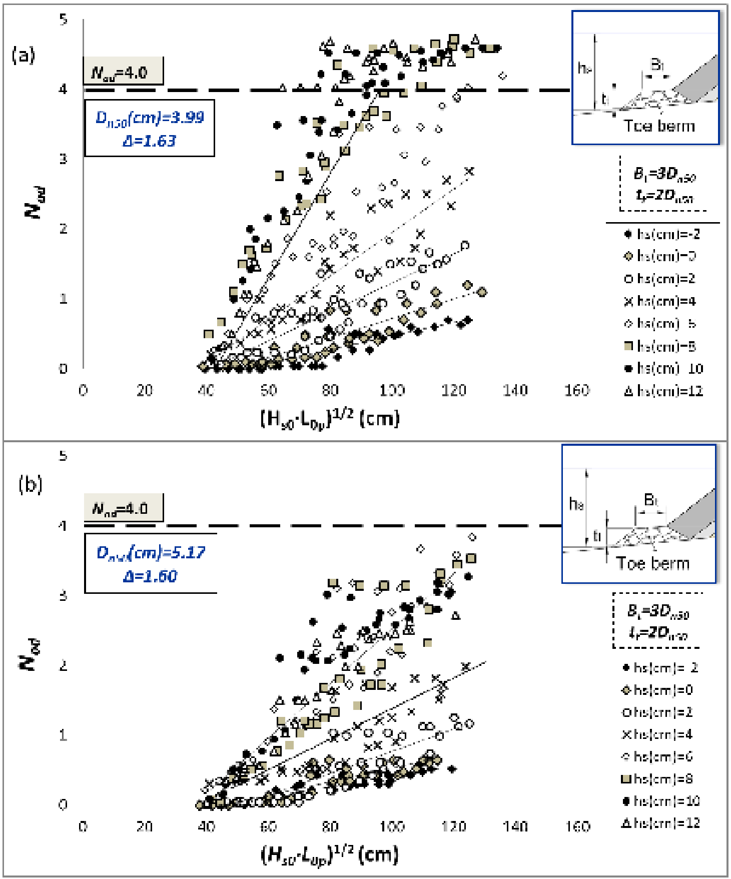

Fig. 9. Measured toe berm damage (N_{od}) compared with $(H_{s0}\cdot L_{0p})^{1/2}$.
For toe berm damage N_{od}>4, an increase in $(H_{s0}\cdot L_{0p})^{1/2}$ did not significantly increase the damage (failure according to CIRIA/ CUR/ CETMEF, 2007). Only tests with $N_{od} \leq 4$ were selected for further analysis.

5. A new toe berm stability formula

A new design formula was developed in this study to include the most relevant parameters affecting the stability of toe berms placed on steep (m = 1/10) sea bottoms in combination with very shallow waters. The analysis in the previous section showed that toe berm damage was greater with increasing wave conditions, $(H_{s0}\cdot L_{0p})^{1/2}$, and decreasing rock size, D_{n50}. Thus, the ratio $(H_{s0}\cdot L_{0p})^{1/2}/\Delta D_{n50}$ was used as an explanatory dimensionless parameter for the design equation. The influence of the water depth was introduced using the relative water depth (h_s/D_{n50}), which is a structural dimensionless variable independent from the climate conditions. As N_{od} increased with $(H_{s0}{\cdot}L_{0p})^{1/2}/\Delta D_{n50}$ as a function of h_s/D_{n50} (see Fig. 10), the corresponding general formula is given by Eq.(11).

$$N_{od}=\left(\frac{(H_{s0}\cdot L_{0p})^{1/2}}{\Delta D_{n50}}-c\right)\cdot f\left(\frac{h_s}{D_{n50}}\right) \qquad (11)$$

in which c is a constant, and $f\,(h_s/D_{n50})$ is a function of the relative water depth h_s/D_{n50}.

To calibrate the general expression of the design formula, only tests corresponding to the maximum significant wave height generated for each peak period and water depth were taken into account. In each test series defined by a water depth at the toe (h_s), cumulative toe berm damage (N_{od}) generally increased with increasing deep water significant wave height (H_{s0}) and peak period (T_p). However, for a specific T_p, only the higher H_{s0} significantly increased the toe berm damage N_{od}. Therefore, only the toe berm damage value obtained at the highest H_{s0} of each T_p was considered for calibration purposes.

One should take into account that the toe berm damage associated to a specific water level (h_s) and wave condition (H_{s0}, T_p), refers to the cumulative damage of the previous tests with lower H_{s0} and T_p, and the same h_s.

The new formula for toe berm design is obtained by calibrating c and $f\,(h_s/D_{n50})$ in Eq. (11) with the test results from this study. $f\,(h_s/D_{n50})$ considers that given D_{n50}, H_{s0} and T_p, N_{od} is highest when h_s/D_{n50} = 3.0 (h_t/D_{n50} = 1). From h_s/D_{n50} = 3.0, N_{od} decreases with increasing h_s/D_{n50}.

$$N_{od}=\left(\frac{(H_{s0}\cdot L_{0p})^{1/2}}{\Delta D_{n50}}-5.5\right)\cdot\left[\left(-0.2\frac{h_s}{D_{n50}}+1.4\right)\cdot\exp\left(0.25\frac{h_s}{D_{n50}}-0.65\right)\right]^{1/0.15} \qquad (12)$$

Eq. (12) is valid for a standard toe berm ($B_t = 3{\cdot}D_{n50}$ and $t_t = 2{\cdot}D_{n50}$) placed on a steep seafloor (m = 1/10) in the range $N_{od} \leq 4.0$, $0.02 < s_{0p} = 2\pi H_{s0}/gT_p^2 < 0.07$, $-0.15 < h_s/H_{s0} < 1.5$ and $-0.5 < h_s/D_{n50} < 5.01$.

Fig. 10 compares the test results and the proposed formula (Eq. (12)) corresponding to four relative water depths, in which the toe berm was completely emerged (h_s/D_{n50} = -0.4), partially emerged (h_s/D_{n50} = 0.8 and 1.5) and submerged (h_s/D_{n50} = 3.0).

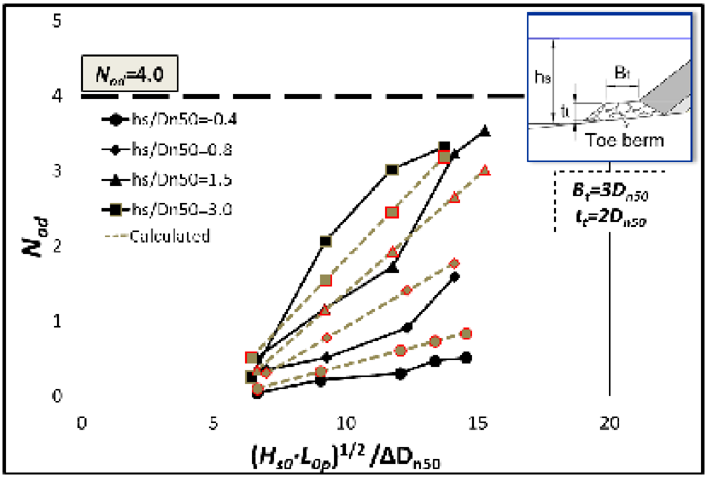

Fig. 10. Comparison of measured and estimated damage for emerged and submerged toe berms.

The agreement between measured and estimated N_{od} was reasonable as N_{od} errors were lower than 0.5. The goodness of fit considering all measured and calculated values is described in the next section.

5.1 Confidence intervals for the new stability formula

Assuming a Gaussian error distribution, the 90% confidence interval for the toe damage estimation given by Eq. (12) is:

$$N_{od}\Big|_{5\%}^{95\%} = N_{od} \pm 1.64 \cdot \sqrt{\sigma^2(\varepsilon)} \qquad (13)$$

where N_{od} is given by Eq. (12) and $\sigma^2(\varepsilon)$ is the variance of the estimation errors. $\sigma^2(\varepsilon)$ was not considered as constant but rather as a linear function of N_{od} given by Eq. (14). N_{od} data were ordered and grouped in ten data sets as shown in Fig. 11. The *MSE* was calculated for each data set (black rhombus in Fig. 11). As the *MSE* increases with increasing N_{od}, the variance of the errors can be estimated by:

$$\sigma^2(\varepsilon) = 0.14 \cdot N_{od} + 0.05 \qquad (14)$$

where N_{od} is given by Eq. (12). The 90% confidence interval is given by:

$$N_{od}\Big|_{5\%}^{95\%} = N_{od} \pm 1.64 \cdot \sqrt{(0.14 \cdot N_{od} + 0.05)} \qquad (15)$$

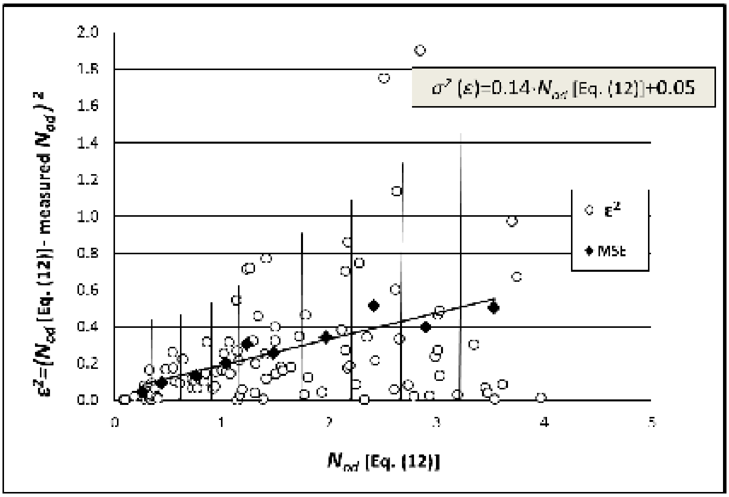

Fig. 11. Squared toe berm damage errors as a function of the N_{od} given by Eq. (12).

Fig. 12 compares measured N_{od} and estimated N_{od} given by Eq. (12) as well as the 90% confidence interval given by Eq. (15). The *rMSE* and the correlation coefficient (*R*) were used to determine the goodness of fit between the values of N_{od} measured in tests and the N_{od} given by Eq. (12).

$$R=\frac{\sum_{i=1}^{N}(t_i-\mu_t)(e_i-\mu_e)}{\sqrt{\sum_{i=1}^{N}(t_i-\mu_t)^2\sum_{i=1}^{N}(e_i-\mu_e)^2}} \tag{16}$$

where N is the number of observations, t_i is the target value, e_i is the estimated value and μ_t and μ_e are the sample means of target and estimated values, respectively.
The *rMSE*=1-R² =0.208 indicates the proportion of variance of N_{od} not explained by Eq. (12) and *R*=0.89, the degree of correlation between measured and estimated values of N_{od}.

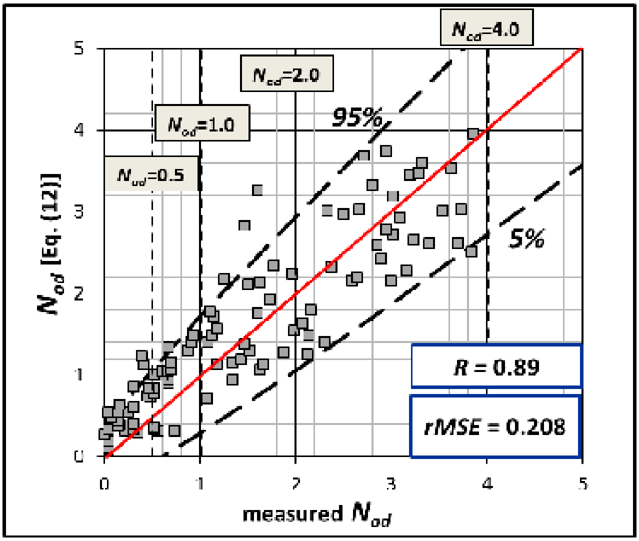

Fig. 12. Comparison of the N_{od} measured in tests and the N_{od} given by Eq. (12) and 90% confidence interval.

5.2 Validation with additional tests

In order to validate the new toe berm design formula given by Eq. (12), those tests carried out with lower wave heights, and not considered to calibrate Eq. (12), were used. Only tests with parameters defined within the range of application of Eq. (12) were taken into account in this analysis.

Fig. 13 compares the measured toe berm damage N_{od} and the estimated N_{od} using Eq. (12). Most validation test results fall within the 90% confidence interval, and the *rMSE* was 0.124. Thus, Eq. (12) is valid for all data within the specified range of application.

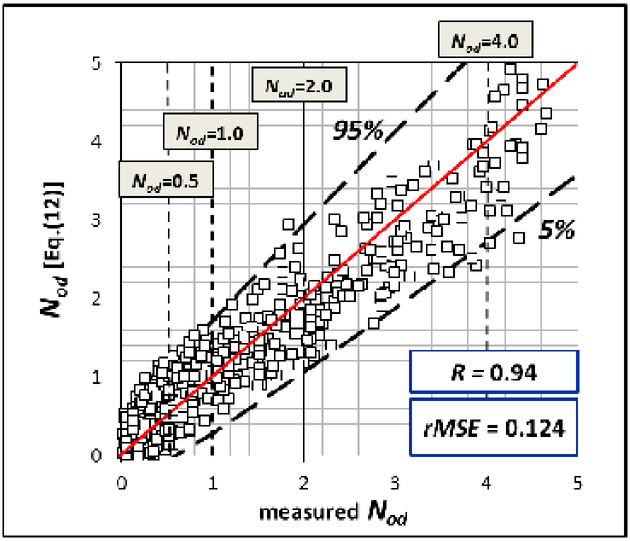

Fig. 13. Comparison of the N_{od} measured in tests and the N_{od} given by Eq. (12) and 90% confidence intervals given by Eq. (15) for all tests within the range of application specified for Eq. (12).

From the qualitative point of view, four levels of toe berm damage were distinguished in this study: (1) no significant movement of toe berm rocks (N_{od} <0.5), (2) significant rock movements (N_{od} = 1.0), (3) moderate damage but toe berm still providing support to the armor (N_{od} = 2.0), and (4) toe berm failure (N_{od} = 4.0).

Using this damage scale, a value of N_{od} = 1.0 is considered a reasonable design criteria when using Eq. (12). If the toe berm is much larger than the standard size tested in this study ($B_t = 3 \cdot D_{n50}$ and $t_t = 2 \cdot D_{n50}$), the design criteria N_{od} = 1.0 and the new formula are no longer valid (see Van Gent and Van der Werf, 2014).

5.3 Comparison of measurements with existing formulas

As mentioned in Section 2, different formulas can be used to predict toe berm damage (Eqs. (3), (4) and (6) to (8)). Although they were obtained from laboratory tests with different conditions and foreshore slopes, a comparison was made between the toe berm damage measured in this study and the predictions given by these five formulas. Only tests conducted with submerged toe berms (h_t >0) were compared because emerged toe berms are out of the range of applicability of the formulas given in the literature. The significant wave height obtained in this study in the gauge G11 was used to estimate the wave height at the toe in the prediction formulas.

Fig. 14 shows the N_{od} measured in this study and the toe berm damage prediction given by Eqs. (3), (4) and (6) to (8) for those tests conducted in the range 10≤ h_s(cm) ≤20 (h_t >0). The 90% confidence intervals of the proposed equation (Eq. (12)) are also depicted in Fig. 14.

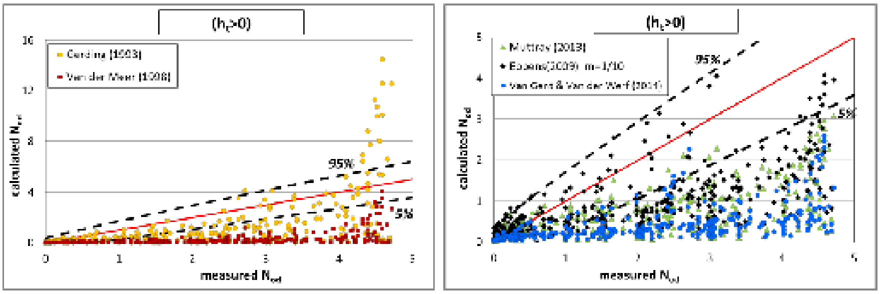

Fig. 14. Measured damage (N_{od}) compared with prediction formulas and 90% confidence intervals of Eq.(12) for submerged toe berms (h_t>0).

Only tests performed with water depths in the range 10≤ h_s(cm) ≤20 were compared; however, the validity of most of the equations is limited to relatively deep submerged toe berms placed in gentler seafloors. Eq. (12) usually provides conservative predictions of toe berm damage N_{od} compared to the other formulas given in the literature, for toe berms in shallow water depths.

5.4 Applications

In this section, Eq. (12) is applied to a standard rock toe berm ($B_t = 3 \cdot D_{n50}$ and $t_t = 2 \cdot D_{n50}$) within the aforementioned validity ranges. Small, medium and large rocks were considered (W(t) = 3, 6 and 12) with a mass density of ρ_r(t/m^3) = 2.70. A typical design storm for the Alboran Sea area was assumed (H_{s0}(m) = 6 and T_p(s) = 12).

Fig. 15 depicts the toe berm damage (N_{od}) given by Eq. (12) depending on h_s/D_{n50} when considering H_{s0}(m) = 6 and T_p(s) = 12 as the design wave storm. Toe berm damage is greatest when h_s/D_{n50} = 3 ($h_t = D_{n50}$). In this case, failure (N_{od} ≥4) or near failure is predicted for small, medium and large rocks. From h_s/D_{n50} = 3 ($h_t = D_{n50}$), toe berm damage decreases with both increasing and decreasing water depths at the toe ($h_t > D_{n50}$ and $h_t < D_{n50}$). For the cases h_s/D_{n50} = 0 (h_t<<0) and h_s/D_{n50} = 5 (h_t>>0), low to moderate toe berm damage (N_{od}<2) is predicted when using toe berm rocks larger than W(t) = 3 (D_{n50} = 1.04).

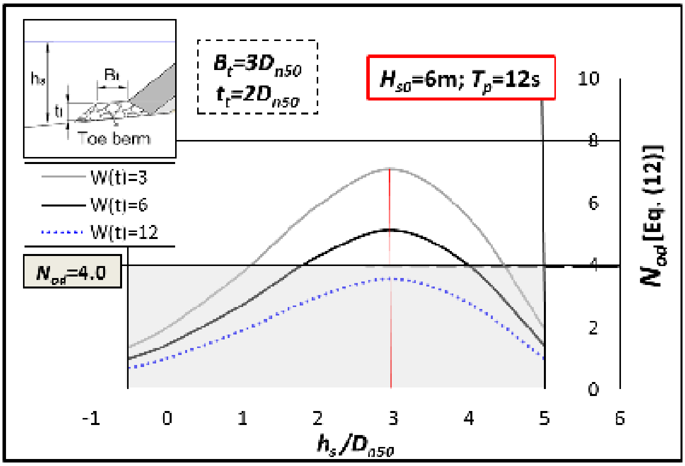

Fig. 15. Toe berm damage (N_{od}) given by Eq. (12) depending on h_s/D_{n50}.

Eq. (12) can be used to determine a more stable toe berm position, changing the strictly submerged toe berm to an emerged or completely submerged toe berm within the range $-0.5< h_s/D_{n50} <5.0$ ($-2.5< h_t/D_{n50} <3.0$). If large rocks are not available at the construction site, the structure design should be modified, for instance, moving the toe berm to a deeper position, where the same toe berm is more stable, or using concrete units for the toe berm.

Toe berm damage also varies with the design wave storm. Fig. 16 shows the influence of the design wave storm on toe berm damage if $h_s/D_{n50} = 0$. When considering H_{s0}(m) = 6 and T_p(s) = 12, low damage is estimated with medium-sized rocks ($N_{od} \approx 1$). If waves are stronger, for instance H_{s0}(m) = 8 and T_p(s) = 14, moderate damage ($N_{od} \approx 2$) is estimated for this rock size (W(t) = 6, D_{n50} = 1.30).

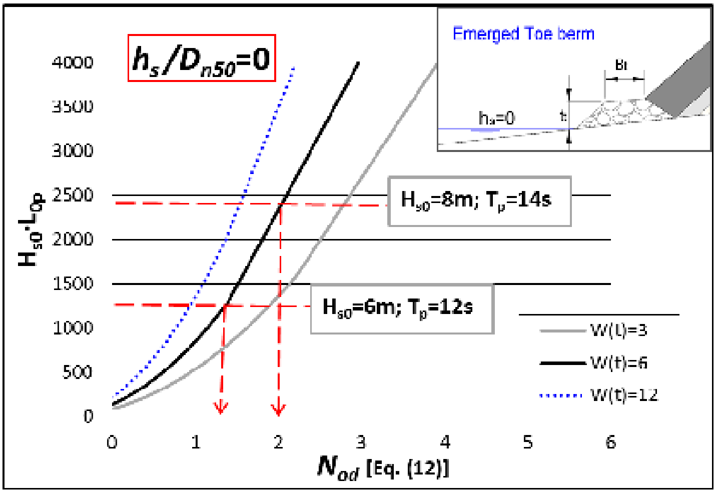

Fig. 16. Toe berm damage (N_{od}) given by Eq. (12) for h_t<<0 and h_s/D_{n50} = 0.

Formulas given in the literature are only valid for submerged toe berms (h_t >>0). Thus, the case h_s/D_{n50} = 5 (h_s/D_{n50} = 3) is compared with equations given in Section 2, although Eqs. (3), (4) and (8) are out of the range of application.

Table 4 shows the toe berm damage (N_{od}) estimated by Eqs. (3), (4), (6), (7), (8) and (12) for the specified rock sizes tested (W(t) = 3, 6 and 12) with B_t=3·D_{n50}, t_t=2·D_{n50} and the design wave storm H_{s0}(m) = 6 and T_p(s) = 12. For Eqs. (3), (4), (6), (7) and (8), the specified design wave storm was propagated from deep water to the water depth h_s = 5·D_{n50} using the SwanOne numerical model to calculate the significant wave height at the toe, H_{st}.

Table 4. Toe berm damage (N_{od}) estimated with (3), (4), (6), (7) and (8) for three rock sizes (W(t) = 3, 6 and 12) and h_s/D_{n50} = 5.

			N_{od}			
	Gerding (1993)	Van der Meer (1998)	Ebbens (2009)	Muttray (2013)	Van Gent and Van der Werf (2014)	This study
W(t)	Eq. (3) [b]	Eq. (4) [b]	Eq. (6)[a]	Eq. (7)	Eq. (8) [b]	Eq. (12)
3	5.5	0.3	5.5[b]	2.9	0.6	2.0
6	1.9	0.1	3.2 [b]	1.6	0.4	1.4
12	0.5	0.03	1.7	0.7	0.2	1.0

[a] N_{od} = 10·$N_{\%}$.

[b] Out of the range of application.

To estimate toe berm damage with a steep sea bottom m = 1/10, only Eqs. (6) and (7) can be taken for comparison because the other formulas are based on tests carried out with gentler bottom slopes (m = 1/20, m = 1/30 or m = 1/50). Eqs. (4) and (8) provide similar values for N_{od} but lower than those obtained with Eq. (12) because toe berms on steep seafloors undergo direct wave attack due to plunging breakers, resulting in higher values for N_{od}. Although Eqs. (3) and (4) were obtained from the same test database, Eq. (3) estimates higher values for N_{od}.

Eqs. (6), (7) and (12) provide similar values of N_{od} for the largest rock size (W(t) = 12, D_{n50} = 1.66). Eq. (6) differs from Eqs. (7) and (12) especially when using small- and medium-sized rocks, but the estimated toe berm damage values are beyond its range of application.

6. Conclusions

The design of the toe berm which supports the armor layer is usually considered as a secondary element in mound breakwater designs. However, when the toe berm is built close to the water surface on a steep sea bottom, it must withstand high wave loads due to wave breaking directly on the toe berm. In this case, the toe berm stability is a critical element of the breakwaters and, thus, the toe berm may require stones larger than those used in the armor layer. A review of the existing literature regarding toe berm stability indicates that there is no reasonable method to design toe berms on steep sea bottoms in combination with very shallow waters.

Using quarrystones, most existing formulas for toe berm design (Eqs. (1) to (8)) are based on laboratory tests with gentle bottom slopes and toe berms below the *SWL* ($h_s > h_t >> 0$). In these conditions, toe berm damage usually decreases with increasing water depths at the toe, h_s. However, on rocky coastlines with steep sea bottoms, sea defenses may require emerged toe berms ($h_t << 0$). Toe berms in very shallow waters behaves completely different from those built in non-breaking conditions, and toe berm damage shows a critical point when the *SWL* is near the top of the berm ($h_t = D_{n50}$). From $h_t = D_{n50}$, toe berm damage decreases with increasing as well as decreasing water depth at the toe ($h_t > D_{n50}$ and $h_t < D_{n50}$).

Within the ranges $0.02 < s_{0p} < 0.07$, $-0.15 < h_s/H_{s0} < 1.5$ and $-0.5 < h_s/D_{n50} < 5.01$, Eqs. (12) and (15) estimate the toe berm damage ($N_{od} \leq 4$) and 90% confidence interval for standard toe berms ($B_t = 3 \cdot D_{n50}$ and $t_t = 2 \cdot D_{n50}$) placed on steep ($m = 1/10$) sea bottoms in very shallow waters. Using $N_{od} = 1.0$ as a design criteria is recommended since the toe berm still provides good support to the armor layer.

The rock material required for toe berms built in these conditions depends on three parameters: water depth at the toe (h_s), deep water significant wave height (H_{s0}) and deep water wave length corresponding to the peak period (L_{0p}). The toe berm damage given by Eq. (12) takes into account the cumulative toe berm damage which corresponds to numerous lower intensity wave storms. For a given water depth (h_s), Eq. (12) considers the damage associated to the design storm (H_{s0}, T_p) and the cumulative damage of storms with lower or equal T_p and H_{s0}.

The design of toe berms using quarrystone is usually feasible for emerged toe berms ($h_t << 0$) and deeply submerged toe berms ($h_t >> 0$). However, there is a range of water depths at the toe (h_s) which requires rocks larger than the size that may be available at some construction sites. In these situations, the toe position may be moved to deeper or shallower waters to avoid the critical water depth ($h_t \approx D_{n50}$); toe berms with concrete units may also be another design alternative.

Acknowledgments

The first author was financially supported through the FPU program (*Formación del Profesorado Universitario*) funded by the Spanish Ministry of Education (*Ministerio de Educación, Cultura y Deporte*) FPU13/01872. The authors also acknowledge financial support from the Spanish Ministry of Economy and Competitiveness (grant BIA2012-33967). The authors thank Debra Westall for revising the manuscript.

References

Baldock, T.E. and Simmonds, D.J., 1999. Separation of incident and reflected waves over sloping bathymetry. Coastal Engineering, 38, 167–176.

Battjes, J.A., Bakkenes, H.J., Janssen, T.T. and van Dongeren, A. R., 2004. Shoaling of subharmonic gravity waves. Journal of Geophysical Research, 109, C02009, doi:10.1029/2003JC001863.

CIRIA, CUR, CETMEF, 2007. The Rock Manual. The Use of Rock in Hydraulic Engineering (2nd edition). C683, CIRIA, London.

Docters van Leeuwen, L., 1996. Toe stability of rubble-mound breakwaters. M.Sc. thesis Delft. Delft University of Technology, Delft.

Ebbens, R.E., 2009. Toe Structures of Rubble Mound Breakwaters. Stability in Depth Limited Conditions. M.Sc. thesis Delft. Delft University of Technology, Delft.

Figueres, M. and Medina, J.R., 2004. Estimation of incident and reflected waves using a fully non-linear wave model. Proc. 29th International Conference on Coastal Engineering, World Scientific, Singapore, 594–603.

Gerding, E., 1993. Toe Structure Stability of Rubble Mound Breakwaters. M.Sc. thesis Delft and Delft Hydraulics Report H1874. Delft University of Technology, Delft.

Goda, Y., 2000. Random seas and design of maritime structures (2nd Edition).World Scientific Publishing, Singapore, ISBN 981-02-3256-X.

Gómez-Martín, M.E. and Medina, J.R., 2014. Heterogeneus Packing and Hydraulic Stability of Cube and Cubipod Armor Units. J. Waterway, Port, Coastal, Ocean Eng., 140, 100-108.

Hudson, R.Y., 1959. Laboratory investigation of rubble-mound breakwaters. Journal of the Waterways and Harbors Division, ASCE, 85(WW3), 93–121.

Hunt, I.A., 1959. Design of Seawalls and Breakwaters, ASCE, 85(WW3), 123-152.

Markle, D.G., 1989. Stability of toe berm armor stone and toe buttressing stone on rubble-mound breakwaters and jetties, physical model investigation. Technical Report REMR-CO-12. U.S. Army Engineer Waterways Experiment Station, Vicksburg, Mississippi.

Muttray, M., 2013. A pragmatic approach to rock toe stability. Coastal Engineering, 82, 56–63.

Thompson, D.M. and Shuttler, R.M., 1975. Riprap design for wind wave attack. A laboratory study in random waves. Report EX 707, Hydraulic Research, Wallingford.

USACE, 2006. Coastal Engineering Manual. Engineer Manual 1110-2-1100, U.S. Army Corps of Engineers, Washington, D.C. (in 6 volumes).

Van der Meer, J.W., 1998. Geometrical Design of Coastal Structures. Pilarczyk, K.W. (Ed.), Seawalls, Dikes and Revetments. Balkema, Rotterdam.

Van Gent, M.R.A. and Van der Werf, I.M., 2014. Rock toe stability of rubble mound breakwaters. Coastal Engineering, 83, 166–176.

Verhagen, H.J., Van Vledder, G., Eslami Arab, S., 2008. A practical method for design of coastal structures in shallow water. Proceedings 31st International Conference on Coastal Engineering. World Scientific vol 4, pp. 2912-2922.

3. **Herrera, M.P., Hoyos, A., Molines, J., Medina, J.R., 2015. Influence of placement technique on double-layer cube armor stability of breakwaters constructed on steep foreshores. Proc. 36th IAHR World Congress, 28 June-3 July, 2015 (The Hague, the Netherlands), in press.**

INFLUENCE OF THE PLACEMENT TECHNIQUE ON DOUBLE-LAYER CUBE ARMOR STABILITY OF BREAKWATERS CONSTRUCTED ON STEEP FORESHORES

MARIA P. HERRERA (1), AINOHA HOYOS(2), JORGE MOLINES (3) & JOSEP R. MEDINA (4)

(1) *Research Assistant, Universitat Politècnica de València, València, SPAIN, mahergam@upv.es*

(2) *Research Assistant, Universitat Politècnica de València, València, SPAIN, aihoal@upv.es*

(3) *Research Assistant, Universitat Politècnica de València, València, SPAIN, jormollo@upv.es*

(4) *Professor, Universitat Politècnica de València, València, SPAIN, jrmedina@upv.es*

ABSTRACT

The stability of cube-armored breakwaters, with random and uniform placement, was analyzed using artificial neural networks (NN). Small-scale 2D physical tests were conducted in the wind and wave test facility of the Laboratory of Ports and Coasts at the Universitat Politècnica de València (UPV). The tested models corresponded to double-layer cube-armored breakwaters, with null or low overtopping rates in wave breaking conditions, placed on a m=1/10 steep sea bottom. Armor damage was calculated after each test using the Virtual Net method. Results of armor damage were compared for randomly- and uniformly-placed cube armors using NN models. The NN methodology proved that there is no significant difference in armor damage for randomly- and uniformly-placed cube armors with the same packing density ϕ = 1.16.

Keywords: Mound breakwater, Cube armor, Placement technique, Heterogeneous Packing, Neural Network.

1. INTRODUCTION

For centuries, mound breakwaters have been constructed with natural stone to protect harbor areas from wave attack. In the 19th century, conventional cubes and parallelepiped blocks were introduced as artificial armor units to protect the underlayers and the breakwater core. Since 1950, different types of concrete armor units (CAUs) have been developed in order to optimize breakwater design, increasing safety while reducing economic and environmental costs. Figure 1 shows different types of CAUs used to construct mound breakwaters according to Dupray and Roberts (2009).

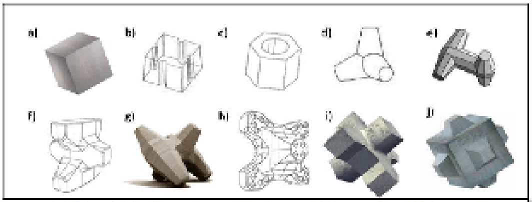

a) Cube; b) Antifer cube; c) Seabee; d) Tetrapod; e) Dolosse; f) Accropode; g) Core-Loc; h) Accropode II; i) Xbloc; j) Cubipod

Figure 1. Concrete armor units (CAUs) described by Dupray and Roberts (2009).

Armor units may be placed uniformly, patterned, oriented or randomly. The specific placement technique is directly related to armor porosity and interlocking (see Medina et al., 2010) which significantly affects armor stability. Small-scale models are usually constructed by hand, without water and with excellent visibility; however, it is not easy to follow specific placement rules at prototype scale with poor visibility and continuous wave action. Real breakwater armors tend to increase armor porosity above the recommended values (see Medina et al., 2014), and the armor unit placement technique is a critical issue to be taken into account in the design phase.

Structural strength (massive, bulky and slender), placement technique (uniform, patterned, oriented and random) and number of layers (one or two layers) are the armor characteristics which highly condition the CAU to be used in the armor layer. In this paper, the double-layer cube armor is analyzed considering random and uniform placement. Conventional cube armors are double-layer armors with random placement; however, cube armors can be also placed with a uniform pattern like the cube revetment of the Maasvlakte 2, recently constructed in Rotterdam (Loman et al., 2012).

Cube units in a conventional, randomly-placed double-layer armor tend to change positions favoring face-to-face fitting although no cube is extracted from the armor during wave attack (see Figure 2). The tendency to face-to-face fitting of cube units reduces the porosity in the lower area of the armor, increasing the porosity in the upper zone. This cube armor behavior is referred to the failure mode *Heterogeneous Packing* (Gómez-Martín and Medina, 2014), and can be influenced by the placement technique.

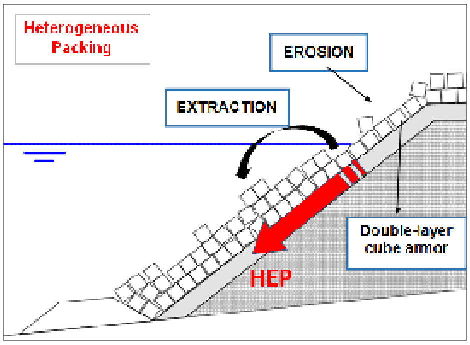

Figure 2. Heterogeneous packing failure mode (HEP) described by Gómez-Martín and Medina (2014).

Different methods to characterize armor damage have been proposed in the literature (see Gómez-Martín and Medina, 2014). In this study, the Virtual Net Method developed by Gómez-Martín and Medina (2014) was used to calculate the observed damage of cube armors placed randomly and uniformly. The Virtual Net Method considers the armor divided into individual strips of a constant width (*a*) and length (*b*); it allows us to measure the dimensionless damage in each strip (S_i) considering porosity evolution in time and space. Integrating this dimensionless armor damage over the slope, the Virtual Net Method also provides the equivalent dimensionless armor damage parameter (S_e).

$$S_i = k \cdot \left(1 - \frac{1-n_{vi}}{1-n_{v0i}}\right) \qquad [1]$$

$$S_e = \sum_{i=1}^{I} S_i \qquad \forall S_i \geq 0 \qquad [2]$$

where k is the number of rows in each strip, $n_{vi}=1-(N_i \cdot D_n^2/a \cdot b)$ is the porosity of the strip, N_i is the number of armor units whose center of gravity is within each strip, D_n is the nominal diameter, n_{v0i} is the initial porosity of each strip and I is the number of strips.

In this paper, the armor damage is compared for cubes randomly- and uniformly-placed. Due to the number of variables involved in the process, artificial neural networks (NN) were used to analyze the problem. Firstly, the model tests performed at the UPV wave flume are described. Secondly, the methodology used to obtain a NN model based on armor damage observations is explained. Thirdly, the influence of placement technique on double-layer cube armor stability is analyzed. Finally, conclusions are given.

2. EXPERIMENTAL METHODOLOGY

Small-scale 2D physical tests were conducted in the wave flume (30 x 1.2 x1.2 m) of the Laboratory of Ports and Coasts at the Universitat Politècnica de València (UPV) with a bottom slope *m*=1/10. The models were tested in wave breaking conditions with null or low overtopping rates.

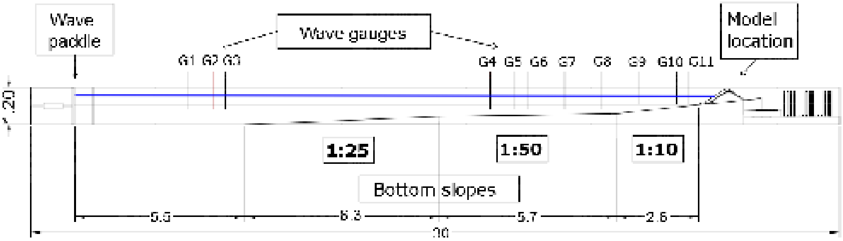

Figure 3. Longitudinal section of the UPV wave flume. Dimensions in meters.

Two small-scale models with cube units placed randomly and uniformly were constructed. These models corresponded to conventional non-overtopping mound breakwaters, protected with a double-layer cube armor with equivalent cube size or D_n[cm]=3.97, ρ_c [g/cm^3]=2.27 and W[g]= 142. The mean value of the measured packing density was ϕ = 1.16, very close to the recommended value ϕ = 1.17 given by CIRIA/ CUR/ CETMEF (2007). In the toe berm, stones with a nominal diameter D_{n50}[cm]=5.17, ρ_r [g/cm^3]=2.70 and W[g]= 373 were used with two times the nominal diameter high and three times the nominal diameter wide ($t_t = 2{\cdot}D_{n50}$ and $B_t = 3{\cdot}D_{n50}$).

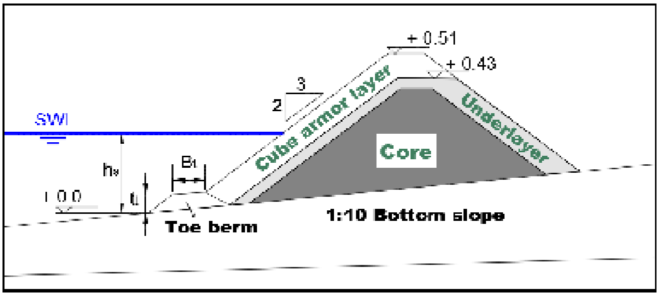

Figure 4. Cross section of the double layer cube armored model. Dimensions in meters.

Irregular wave trains were generated with a m=1/10 steep bottom slope, following JONSWAP (γ=3.3) spectra. Reflected waves were absorbed by the wave paddle (Active Absorption System AWACS) to avoid multi-reflections.

Each test series was characterized by the water level at the toe h_s[cm]= -2,0, 2, 4, 6, 8, 10, 12, 14, 16, 18 and 20, and the peak period T_p[s]=1.2, 1.5, 1.8, 2.2 and 2.4. For each water level and wave period, wave heights were generated from values which did not cause much damage to values at which waves broke in the generating zone due to the high wave steepness. The significant wave height at wave paddle was varied in the range 8<H_s[cm]<22. The storm duration was set to 500 waves.

Cumulative armor damage was considered and the model was not rebuilt after each test run, but rather after each test series defined by h_s (35 to 40 tests). Tests characteristics are summarized in Table 1.

Table 1. Small-scale parameters tested (min, max).

Parameter	Symbol	Value
Foreshore angle	$\tan(\alpha_{shore})$	1/10
Slope angle	$\tan(\alpha)$	2/3
Cube size [cm]	D_n	3.97
Stone size [cm]	D_{n50}	5.17
Water depth at toe[cm]	h_s	(-2, 20)
Peak period [s]	T_p	(1.2, 2.4)

Wave height at paddle[cm]	H_s	(8, 22)
Number of waves	N	500

Eleven capacitive wave gauges, three acoustic gauges and four pressure sensors were placed along the flume to measure surface elevation. One group of wave gauges was placed near the paddle and the other wave gauges were placed along the wave flume near the model. Using the three wave gauges placed near the wave paddle, incident and reflected waves were separated using the LASA-V method proposed by Figueres and Medina (2004), which is able to separate non-linear and non-stationary waves.

Armor damage was measured after each test run. Comparing the photographs taken perpendicularly to the armor slope after each test, armor damage was quantified using the Virtual Net method described by Gómez-Martín and Medina (2014). A virtual net was projected over each photograph (see Figure 5), dividing the armor into four strips of $3\cdot D_n$ wide (strips A, B, C and D) and another strip of $2\cdot D_n$ wide (strip E). Dimensionless armor damage was calculated for each strip (S_i); integrating this dimensionless armor damage over the slope, the equivalent dimensionless armor damage parameter was obtained (S_e). Figure 5 shows two photographs of the two armors with cubes randomly- and uniformly-placed, and the virtual net used during the experiments.

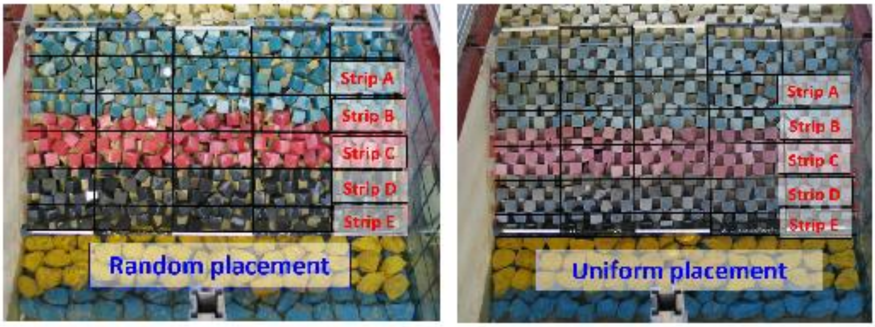

Figure 5. Application of the Virtual Net method proposed by Gómez-Martín and Medina (2014) to measure armor damage in the experiments.

Different damage levels were also identified following the criteria given by Vidal et al. (1991): (1) Initiation of Damage, (2) Initiation of Iribarren's Damage, (3) Initiation of Destruction and (4) Destruction.

3. NEURAL NETWORK MODELING OF ARMOR DAMAGE

3.1 Neural Network Models in Coastal Engineering

Neural network (NN) systems belong to a group of optimization techniques commonly-used in the artificial intelligence field. NN can be used to extract patterns and detect trends in which the interrelationships among parameters are unclear or complex. NN are inspired in the way biological nervous systems process information; they are organized in layers with one or more processing units called neurons. Different types of NN models exists; the standard multi-layer feed-forward NN is the most commonly used scheme in maritime engineering. It is composed of different layers of neurons connected without any feedback. Different NN models have been used to solve problems related to coastal structures (e.g. Mase et al., 1995 or Van Gent et al., 2007).

In this paper, a multi-layer feed-forward NN with only one hidden layer and a backpropagation algorithm was used to analyze the armor damage (S_e) obtained in the experiments carried out with uniformly- and randomly-placed cubes.

3.2 NN model for armor damage

The experimental data were comprised of observations from 114 experiments carried out in the UPV wave flume. The NN model was prepared in two phases, the learning or training phase and the testing phase. Observations were randomly separated in the learning data set (80%), testing data set (10%) and validation data set (10%). Armor damage was analyzed considering the equivalent dimensionless armor damage (S_e) given by Eq. (2). Six variables were considered relevant to describe armor damage in this problem: incident significant wave height at wave paddle ($H_{m0,i}$), deep water wave length ($L_{0p}=gT_p^2/2\pi$), cube nominal diameter (D_n), relative submerged mass density ($\Delta=[\rho_r-\rho_w]/\rho_w$), water depth at toe ($h_s$) and the placement technique (0=uniform, 1=random). However, only three dimensionless variables were considered to feed the NN model: (1) $(H_{m0,i}\cdot L_{0p})^{1/2}/\Delta D_n$, (2) $h_s/\Delta D_n$ and (3) placement technique (see Figure 6).

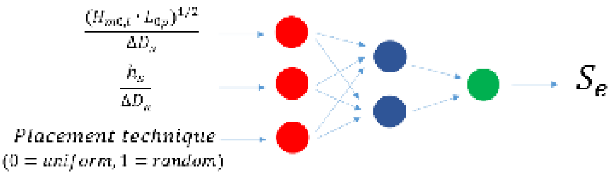
$\frac{(H_{m0,i}\cdot L_{0p})^{1/2}}{\Delta D_n}$
$\frac{h_s}{\Delta D_n}$
$Placement\ technique$
$(0 = uniform, 1 = random)$
S_e

Figure 6. NN configuration to analyze armor damage.

In order to find the appropriate size of the hidden layer, the predicted squared error (*PSE*) proposed by Moody (1992) was used:

$$PSE = MSE\left[1+\frac{2P}{(N-P)}\right]=\frac{1}{N}\cdot\sum_{i=1}^{N}(o_i-e_i)^2\left[1+\frac{2P}{(N-P)}\right] \qquad [3]$$

where *MSE* is the mean squared error, *P* is the number of free parameters, *N* is the number of training samples, o_i is the observed value and e_i is the estimated value. *MSE* decreases when the number of neurons in the hidden layer increases; however, a lower *MSE* does not imply a better prediction because the number of free parameters (*P*) increases. *PSE* predicts the performance of the NN better because it takes into consideration both *MSE* and *P*. If *P* is too high compared to *N*, the NN model fits the learning data very well but the prediction performance is poor (overlearning). To avoid overlearning, an early stopping criterion (Heskes, 1997) was used in the process. Figure 7 shows the performance of the NN for different numbers of neurons in the hidden layer. At least, two neurons were necessary to properly characterize armor damage.

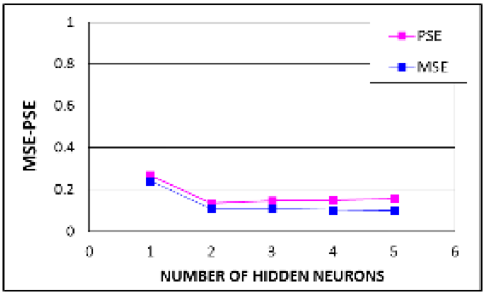

Figure 7. NN performance for configurations with different numbers of neurons in the hidden layer.

Figure 8 compares the estimated and measured armor damage. The relative Mean Squared Error (*rMSE*) was used to measure the goodness of fit for the testing data set (not used for learning).

$$rMSE = \frac{MSE}{Var} = \frac{1}{N} \cdot \sum_{i=1}^{N} \frac{(o_i - e_i)^2}{Var(o_i)} \qquad [4]$$

where *MSE* is the Mean Squared Error, *Var* is the variance of the observed armor damage data, *N* is the number of data, o_i is the observed value and e_i is the estimated value. Using the testing data, *rMSE*=11.4% is a measurement of the proportion of variance not explained by the NN model.

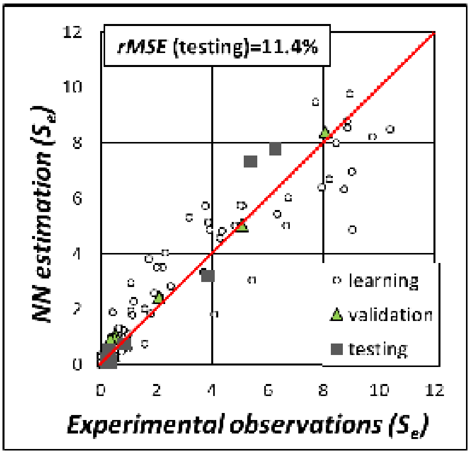

Figure 8. Comparison of NN estimations and experimental observations of armor damage S_e.

4. APPLICATIONS OF THE NEURAL NETWORK

In this section, the NN model described above was used as a simulator (virtual wave flume) as done by Garrido and Medina (2012) to characterize the behavior of randomly- and uniformly-placed cube

7

armors. Firstly, the equivalent dimensionless armor damage (S_e) was considered and the main variables were analyzed. Figure 9 shows the NN estimation of S_e depending on the variable $(H_{m0,i}\cdot L_{0p})^{1/2}/\Delta D_n$ for three relative water depths at the toe: $h_s/\Delta D_n$ = -0.4, 0.8 and 2.0. S_e increases with the dimensionless variable $(H_{m0,i}\cdot L_{0p})^{1/2}/\Delta D_n$ regardless of the water depth. More intense wave storms ($H_{m0,i}$, L_{0p}) and smaller armor unit size (ΔD_n), resulted in more armor damage (S_e). No clear differences were observed in the placement technique.

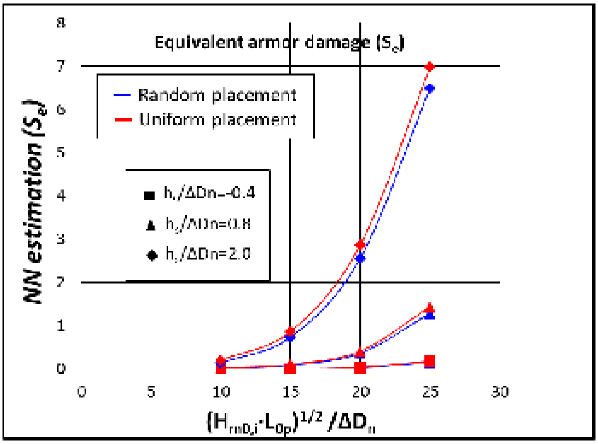

Figure 9. NN armor damage (S_e) estimation depending on $(H_{m0,i}\cdot L_{0p})^{1/2}/\Delta D_n$ and the placement technique.

The influence of the relative water depth at the toe was also analyzed. Figure 10 shows the armor damage (S_e) estimated by the NN model when considering the cumulative damage of all tests generated for a given water depth at the toe. Armor damage increases with the relative water depth up to $h_s/\Delta D_n$ =2.8; from this level, S_e decreases.

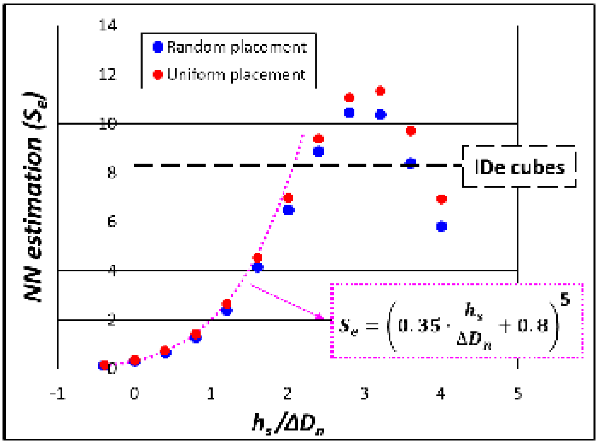

Figure 10. NN equivalent armor damage (S_e) estimation depending on $h_s/\Delta D_n$ and the placement technique (uniform or random) for a conventional double-layer cube armor.

No severe damage was observed with low water levels. In the range $-0.4 < h_s/\Delta D_n < 2$, the equivalent armor damage was lower than $S_e \approx 8.3$ for Initiation of Destruction (see Gómez-Martín and Medina, 2014). In this range, the cumulative armor damage considered may be estimated by Eq. [5]. Note that armor damage is cumulative damage corresponding to 35 to 40 wave runs of differing wave characteristics within the range of the conducted experiments listed in Table 1 ($1.2<T_p[s]<2.4$ and $8<H_s[cm]<22$).

$$S_e = \left(0.35 \cdot \frac{h_s}{\Delta D_n} + 0.8\right)^5 \qquad [5]$$

where h_s is the water depth at the toe, D_n is the cube nominal diameter and $\Delta = ([\rho_c - \rho_w]/\rho_w)$ is the relative submerged mass density.

Double layer randomly- and uniformly-placed cube armors have a similar hydraulic stability. With low water depths, no severe cube extraction was observed during the tests; the most severe damage corresponded to Heterogeneous Packing. Although cube armor hydraulic stability is significantly affected by armor porosity (see Medina et al., 2014), no clear differences were found when considering armor placement technique.

5. SUMMARY AND CONCLUSIONS

As a general rule, placement technique is a critical issue when analyzing armor stability. Placement technique may affect armor porosity, interlocking and armor damage. Armor units may be placed uniformly, patterned, oriented, or randomly. Cube units are massive CAUs usually placed randomly. However, measurements for armor randomness are not usually given for small-scale models or prototypes, and as a result randomness could affect structural response.

In order to study the influence of the placement technique on double-layer cube armor stability, 2D physical tests were conducted in the LPC-UPV. Small-scale models were constructed to correspond to mound breakwaters armored with cubes placed randomly and uniformly. Amor damage was characterized using the Virtual Net method proposed by Gómez-Martín and Medina (2014) which allows us to analyze the common Heterogeneous Packing undergone by cube armors. NN models were used in this study to analyze the data.

Using the NN model as a simulator, several virtual results were obtained and analyzed to compare armor damage with randomly- and uniformly-placed cubes. Armor stability and the tendency to face-to-face fitting of cube units were found to be similar for conventional double-layer randomly- or uniformly-placed units if the packing density was φ=1.16.

Armor porosity and placement technique must be carefully considered in the design phase and during construction to avoid uncontrolled changes in hydraulic stability. In the case of double-layer cube armors, hydraulic stability is significantly affected by armor porosity but not by armor placement.

ACKNOWLEDGMENTS

The authors received financial support from the Spanish Ministry of Economy and Competitiveness (grant BIA2012-33967). The first and third author were financially supported through the FPU program (Formación del Profesorado Universitario) funded by the Spanish Ministry of Education (Ministerio de Educación, Cultura y Deporte). The authors also thank Debra Westall for revising the manuscript.

REFERENCES

CIRIA, CUR, CETMEF (2007). The Rock Manual. The Use of Rock in Hydraulic Engineering (2nd edition). C683, CIRIA, London.

Dupray, S. and Roberts, J. (2009). Review of the use of concrete in the manufacture of concrete armour units. Proc., Int. Conf. of Coasts, Marine Structures and Breakwaters, ICE, Edinburgh, UK, 1, 245-259.

Figueres, M., and Medina, J. R. (2004). Estimation of incident and reflected waves using a fully non-linear wave model. Proc. 29th Int. Conf. on Coastal Engineering, World Scientific, Singapore, 594–603.

Garrido, J.M. and Medina, J.R. (2012). New neural network-derived empirical formulas for estimating wave reflection on Jarlan-type breakwaters. Coastal Engineering, 62, 9-18.

Gómez-Martín, M.E. and Medina, J.R. (2014). Heterogeneous Packing and Hydraulic Stability of Cube and Cubipod Armor Units. J. Waterway, Port, Coastal, and Ocean Eng., 140, 100-108.

Heskes, T. (1997). Practical confidence and prediction intervals. In: Mozer, Jordan, Petsche (Eds.), Advances in neural information processing systems, vol. 9. MIT Press, Cambridge.

Loman, G.J.A., Hofland, B., Van Der Biezen, S.C. and Poot, J.G. (2012). Integral design of hard sea defense of Maasvlakte 2 Part II: Physical model testing of cube revetment and reef. 4th Conference on the Application of Physical Modelling to Port and Coastal Protection.

Mase, H., Sakamoto, M. and Sakai, T. (1995). Neural network for stability of rubble mound breakwaters. J. Waterway, Port, Coastal, and Ocean Eng., 121 (6), 294–299.

Medina, J.R., Gómez-Martín, M.E. and Corredor, A. (2010). Influence of armor unit placement on armor porosity and hydraulic stability. Coastal Proceedings, 32(1), structures,41.

Medina, J.R., Molines, J. and Gómez-Martín, M.E. (2014). Influence of armour porosity on the hydraulic stability of cube armour layers. Ocean Engineering, 88, 289-297.

Moody, J.E. (1992). The effective number of parameters: An analysis of generalization and regularization in nonlinear learning systems. In J.E. Moody, S.J. Hanson & R.P. Lipmann (eds.), Advances in Neural Information Processing Systems 4, 847-854. San Mateo California: Morgan Kaufmann Publishers.

Van Gent, M.R.A., Van den Boogaard, H.F.P., Pozueta, B. and Medina, J.R. (2007). Neural network modelling of wave overtopping at coastal structures. Coastal Engineering, 54 (8), 586–593.

Vidal, C., Losada, M.A. and Mansard, E.P.D. (1991). Stability of mound breakwater's head and trunk. J. Waterway, Port, Coastal, and Ocean Eng., 117(6), 570–587.

4. **Herrera, M.P., Molines, J., Medina, J.R., 2014. Toe protection stability for rubble mound breakwaters in very shallow waters. Proc. 5th International Conference on the Application of Physical Modelling to Port and Coastal Protection, 231-239.**

TOE PROTECTION STABILITY FOR RUBBLE MOUND BREAKWATERS IN VERY SHALLOW WATER

M.P. HERRERA(1), J. MOLINES(2) & J.R. MEDINA(3)
(1) *Universitat Politècnica de València, València, Spain, mahergam@cam.upv.es*
(2) *Universitat Politècnica de València, València, Spain, jormollo@cam.upv.es*
(3) *Universitat Politècnica de València, València, Spain, jrmedina@tra.upv.es*

Abstract

Most mound breakwaters are constructed in the surf zone, where they are attacked by waves breaking on the sea bottom. When they are built on steep foreshore slopes, most are placed in very shallow water; in these conditions the toe berm stability is a critical issue. Several empirical formulas have been published to predict damage to toe protections. However, most of them are not valid for very shallow water conditions; so 2D tests were carried out in the wave flume at the Universitat Politècnica de València (Spain) to analyze the influence of the toe berm on the breakwater stability in these conditions.

Keywords: toe protection, breaking conditions, mound breakwater, steep foreshore slope

1. Introduction

A depth-limited condition is common for most rubble-mound breakwaters.

Eq. [1] proposed by Hudson (1959) and popularized later by SPM (1975 and 1984) is one of the most widely used hydraulic stability formulas for armors. It includes the stability coefficient (K_D) to consider the geometry of the armor unit, number of layers, breakwater zone (trunk or head) and breaking or non-breaking conditions.

$$W = \frac{\rho_r * g * H^3}{K_D * \Delta^3 * cot\alpha} \qquad [1]$$

where W is the median mass of the armor units, K_D is the stability coefficient; ρ_r is the material density; Δ is the relative submerged mass density; α is the slope angle; and H is the design wave height. In non-breaking conditions, SPM (1975) and SPM (1984) proposed using $H=H_s$ and $H_{1/10}$, respectively. In breaking conditions, SPM (1975) and SPM (1984) proposed using the design breaking wave height $H=H_b$ considering the concepts of breaking depth and breaker travel distance for regular waves. Design height in breaking conditions estimated by SPM (1984) depends on the deep-water wave height and period, as well as the bottom slope.

In non-breaking conditions, the mass of toe rocks is one order of magnitude lower than the armor unit mass (see SPM, 1984). However, a more complex situation arises for shallow water where combined with steep foreshore slopes as the waves may break on the foreshore but impact directly on the toe protection. For these situations, the required stone size for the toe berm must be increased.

Different empirical formulas have been obtained to predict the toe berm damage, including those given by Gerding (1993), Van der Meer (1998), Muttray (2013) and Van Gent (2014). These authors used the damage number N_{od}, which describes the relationship between the amount of damage observed in a scale model and the test conditions. The value represents the number of displaced rocks in a strip as wide as the nominal stone size of toe rock.

$$\mathrm{N_{od}} = \frac{\mathrm{N}}{\mathrm{B/D_{n50}}} \qquad [2]$$

where N is the number of displaced stones and B the total width of the wave flume.

Gerding (1993) carried out specific tests on a structure with a 1:1.5 slope and a seabed slope of 1:20. His formula can be written as follows depending on the damage parameter N_{OD}:

$$N_{od} = \Big(\frac{\frac{Hs}{\Delta D_{n50}}}{(0.24\frac{h_t}{D_{n50}}+1.6)}\Big)^{6.67} \qquad [3]$$

where h_t is the water depth above the toe; H_s is the significant wave height; D_{n50} is the nominal diameter; and Δ is the relative submerged mass density of the rock material.

Based on the data given by Gerding (1993), Van der Meer (1998) published the following formula:

$$N_{od} = \Big(\frac{\frac{Hs}{\Delta D_{n50}}}{(6.2(\frac{h_t}{h})^{2.7}+2)}\Big)^{6.67} \qquad [4]$$

where h is the water depth in front of the toe.

Ebbens (2009) performed model tests in the laboratory of Delta Marine Consultants (DMC) in Utrech, The Netherlands. The test set up was similar to the tests of Gerding (1993) involving a rubble mound breakwater with a slope of

1:1.5. In this case, foreshore slopes of 1:10, 1:20 and 1:50 were examined and the influence of the foreshore slope on toe protections was studied. Ebbens (2009) reported that toe berm damage increased on steeper seabeds.

Based on a re-analysis of existing data, Muttray (2013) proposed another formula for rock toe structures. This formula can be written as follows:

$$N_{od} = (\frac{Hs}{\Delta D_{n50}}(0.58 - 0.17\frac{ht}{Hs}))^3 \qquad [5]$$

The Rock Manual (2007) refers to Eqs. [3] and [4] for the design of toe berms of rubble-mound breakwaters. Both equations were obtained from laboratory tests with gentle foreshore slopes and in the range of:

$$0.4<h_t/h_m<0.9$$

$$3<h_t/D_{n50}<25$$

The design of toe berms placed on steep foreshore slopes in very shallow water has not received much attention in the literature although they are common shore protection structures for rocky coastlines. The aim of this paper is therefore to study the influence of the toe protection on the breakwater stability for steep foreshore slopes and very shallow water conditions.

2. Experimental methodology

Small-scale model tests were conducted in the wave flume (30 x 1.2 x1.2 m) of the Laboratory of Ports and Coasts at the Universitat Politècnica de València (LPC-UPV). Regular and irregular wave trains were generated with a 10% steep foreshore (reference scale of 1/60). Irregular waves following JONSWAP (γ=3.3) spectra were generated using AWACS active absorption system.

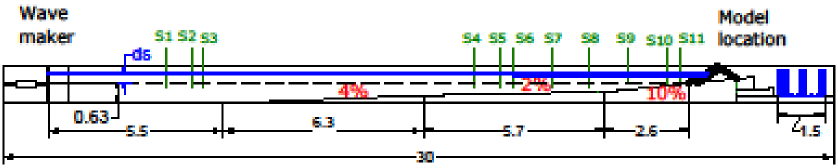

Figure 1. Longitudinal section of the wind and wave flume at the UPV. Levels in meters.

The series of tests were characterized by the water level and the peak period (prototype Tp[s]=9.3, 11.6, 13.9, 17 and 18.6). For each water level and wave period, wave heights were generated from values which did not cause much damage to values which provoked wave breaking in the generation zone due to the steepness (s=H/L). Then, the prototype significant wave height was varied in the range 4<Hs[m]<12. The storm duration was set to 500 waves.

The tested model corresponded to a conventional mound breakwater with zero or minor overtopping, protected with a double-layer cube armor with equivalent cube size D_n[cm]=4.00 and W[g]= 141.5g (W[t]=17 at prototype scale). The configuration of the toe structure was varied. Different rock diameters were placed (D_{n50}[cm]=4.00 and D_{n50}[cm]=5.00), maintaining the configuration at a thickness (t_t) of two times the nominal diameter and a width (B_t) of three times the nominal diameter (see Figure 2). Cumulative damage was observed as the model was not rebuilt for a given depth.

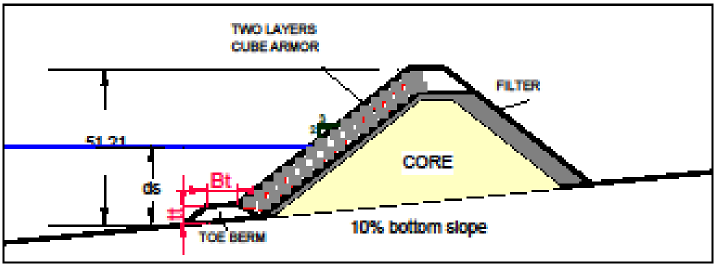

Figure 2. Cube cross section for s=10% bottom slope. Levels in centimeters.

The water depth was measured at the toe of the structure being d_s[cm]= -2,0, 2, 4, 6, 8, 10, 12, 14, 16, 18 and 20 (d[m]=-1.2, 0, 1.2, 2.4, 3.6, 4.8, 6, 7.2, 8.4, 9.6, 10.8 and 12 at prototype scale). Tests characteristics are summarized in Table 1 below.

Table 1. Overview of tested parameters at model scale.

Parameter	Value
d_s [cm]	-2, 0, 2, 4, 6, 8, 10, 12, 14, 16, 18, 20
H_s [cm]	8, 10, 12, 14, 16, 18, 20
T_p [s]	1.2, 1.5, 1.8, 2.2, 2.4
tan (α_{shore})	1:10
Rock size, D_{n50} [cm]	4.00, 5.00

With these conditions, most waves broke before reaching the structure. In order to measure the surface elevation at different positions and to characterize the breaking process, eleven capacitive wave gauges, three acoustic gauges and four pressure sensors were placed along the flume.

3. Data analysis and results

3.1 Wave analysis

Using the measured surface elevation, wave height distributions and spectral moments were determined. Incident and reflected waves were separated using the LASA-V method, allowing wave separation of non-linear and non-stationary waves.

Test data were compared with existing methods to obtain the wave distribution in the breaking zone. In the first analysis, the wave gauge measurements were related with the estimation given by the SwanOne model. It is a popular free wave propagation model developed by Delft University of Technology which is appropriate to estimate wave propagation in 1D bathymetry (wave flume). The model simulates the wave propagation in time and space, shoaling, refraction due to current and depth, as well as frequency shifting due to currents and non-stationary depth. It also takes into account depth-induced breaking.

In order to measure the goodness of fit, the relative mean square error rMSE was used,

$$MSE = \frac{1}{N}\sum_{i=1}^{N}(t_i - a_i)^2 \qquad rMSE = \frac{MSE}{\sigma^2(t)}$$

[6]

where MSE=mean squared error, N=number of observations, t_i= target value, a_i=measured value and σ^2= variance of measured values. The relative mean square error rMSE gives an estimation of the proportion of variance not explained by the model. In this study, the rMSE value was 6.8% (see Figure 3).

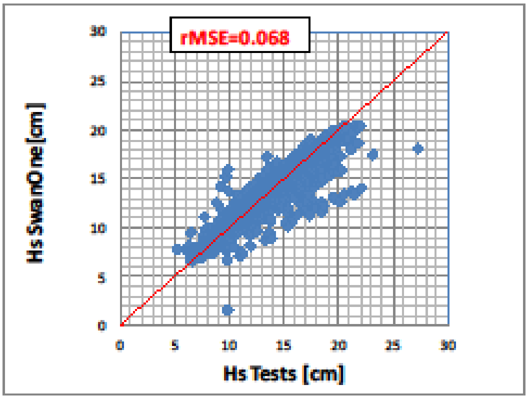

Figure 3. Comparison of the significant wave height values obtained in the tests and those provided by the numerical model SwanOne.

3.2 Damage analysis

Having characterized the trains of waves, the influence of the test parameters (see Table 1) on toe protection stability was studied. The damage of the toe protection was measured before and after each test. To this end, the damage values were obtained depending on the damage parameter N_{od}, which considers the number of stones displaced from the toe. The water depth at the toe seemed to be a very relevant factor. Figure 4 shows the toe protection damage observed at the end of each group of tests (defined by a water depth), compared to the water depth measured at the toe of the structure, for those tests conducted with rock diameters of 4 and 5 cm.

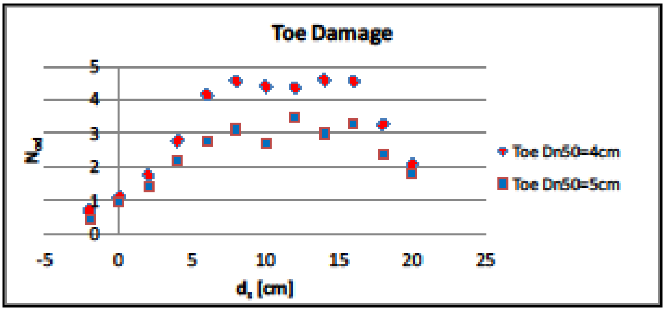

Figure 4. Toe damage and water depth measured at the toe of the structure.

The damage increased until a certain water depth (d_s=6cm). At this water level, the amount of damage remained constant until the water depth reached 16 cm where the greater depth in front of the toe meant less damage.

The influence of the period and the wave height on the damage was studied. The analysis showed that the amount of damage increases with increasing wave height and with increasing wave period while the toe damage reduces with increasing rock size. Figures 5 illustrates the values of the toe damage compared to the wave height, depending on the peak period and the toe rock nominal diameter, for the specific case of the tests conducted with a water level in front of the toe (d_s) of 2cm.

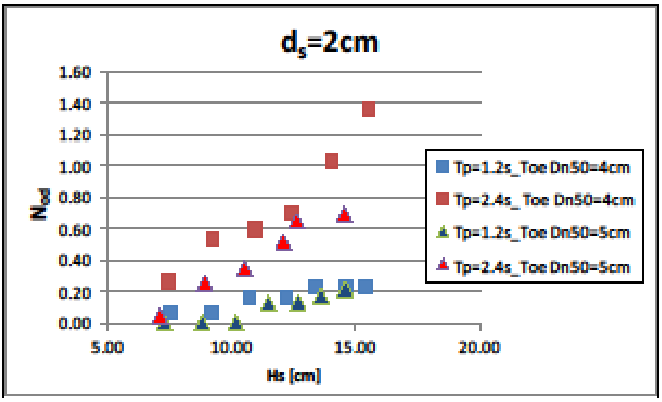

Figure 5. Toe damage compared to wave height as a function of peak period and toe size.

Comparing the photographs taken perpendicularly to the slope before and after each test, armor damage (S_e) was calculated using the Virtual Vet method developed by Gómez-Martín and Medina (2006). This method considers the effect of heterogeneous packing commonly suffered by regular-shaped armor units. To determine if the breakwater was at the initiation of damage, initiation of Iribarren's Damage or initiation of destruction, the criterion given by Losada et al. (1986) and Vidal et al. (1991) was used. Figure 6 shows the relation between the armor damage obtained with the Virtual Net method proposed by Gómez-Martín and Medina (2006), and the water depth. At a certain water depth (d_s=16cm), the armor damage decreased because the role of the toe protection becomes less relevant. In any case, the armor damage was lower in those tests conducted with the toe protection of D_{n50}=5cm. In addition, some tests were carried out without toe protection in order to analyze the effect on armor damage.

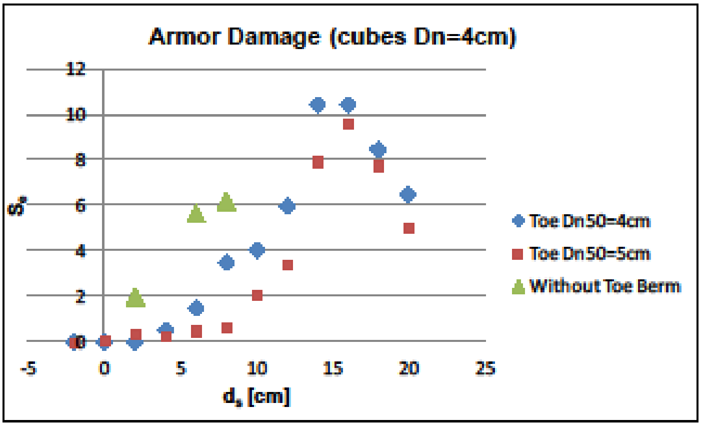

Figure 6. Final armor damage calculated using the Virtual Net method and water depth measured at the toe of the structure.

Armor damage was also measured using the definition of the damage parameter N_{od}. With this definition of damage, heterogeneous packing was not taken into account; only the armor unit extractions were considered.

Figure 7 shows the relation between the armor and toe stability for each test. With low water depths, toe stability was essential for the whole armor stability and most of the damage was absorbed by toe protection. However, greater water depths led to more severe armor damage.

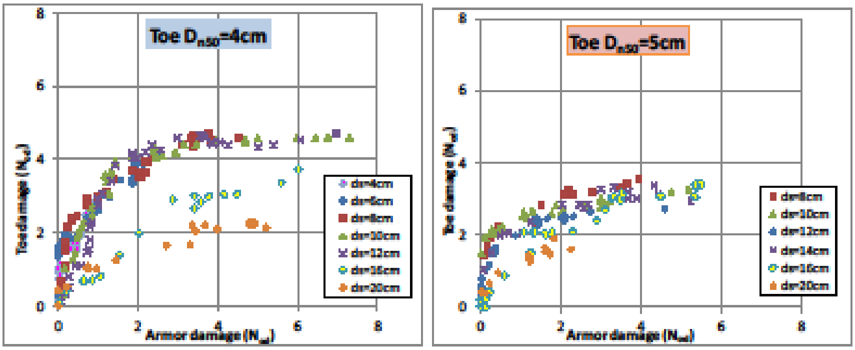

Figure 7. Armor damage compared to toe damage measured with the parameter N_{od}.

8

4. Summary and conclusions

Several empirical formulas have been published to predict the toe protection damage, such as those given by Gerding (1993), Van der Meer (1998), Muttray (2013) and Van Gent (2014). Nevertheless, these are not suitable for the design of toe structures placed on steep foreshore slopes in very shallow water.

In order to study the stability of toe protection structures in these conditions, mound breakwater models were placed in very shallow water with 10% foreshore slope. Specific tests were carried out in the LPC-UPV.

In deep water conditions it is common to use the relation of 1/10 between the weight of the armor units and the weight of the toe rocks (see SPM, 1984). In very shallow water and on steep foreshores, the stability of the toe berm is critical to ensure the entire armor stability. As a rule of thumb, the units in the toe berm must be larger in size than those in the armor.

For low water depths, toe stability affects armor stability and most of the damage is absorbed by toe protection. On the other hand, greater water depths lead to more armor damage.

One of the parameters determining toe stability is the water depth measured at the toe of the structure (d_h). For very shallow waters and steep foreshore slopes, the waves may break directly on the breakwater toe. To improve the breakwater stability in these situations, it may be possible to move the toe position in order to reduce the damaging effects of water depth. (see Figure 4).

Acknowledgments

The authors received financial support from the Spanish Ministry of Economy and Competitiveness (grant BIA2012-33967). The second author was financially supported through the FPU program (Formación del Profesorado Universitario) funded by the Spanish Ministry of Education (Ministerio de Educación, Cultura y Deporte). The authors thank Debra Westall for revising the manuscript.

References

CIRIA, CUR, CETMEF, 2007. 'The Rock Manual: The Use of Rock in Hydraulic Engineering'. 2nd edition. CIRIA C683, London.

Ebbens, R.E., 2009. 'Toe Structures of Rubble Mound Breakwaters. Stability in Depth Limited Conditions'. (Master's Thesis) Delft University of Technology 84.

Gerding, E., 1993. 'Toe Structure Stability of Rubble Mound Breakwaters'. M.Sc. thesis Delft and Delft Hydraulics Report H1874. Delft University of Technology, Delft.

Gómez-Martín, M.E. and Medina, J.R., 2006. 'Damage progression on cube armored breakwaters'. *Proc. 30th ICCE*, ASCE, 5229-5240.

Hudson, R.Y., 1959. 'Laboratory investigation of rubble-mound breakwaters'. *Journal of the Waterways and Harbors Division*, ASCE, 85(WW3), 93–121.

Losada, M. A., Desire, J. M., and Alejo, L. M., 1986. 'Stability of blocks as breakwater armor units'. *J. Struct. Eng.*, 112(11), 2392–2401.

Muttray, M., 2013. 'A pragmatic approach to rock toe stability'. *Coastal Engineering*, 82, 56–63.

Shore Protection Manual (1975 and 1984). 'Shore Protection Manual'. U.S. Army Coastal Engineering Research Center, U.S. Army Engineer Waterways Experiment Station, Vicksburg, Mississippi.

Van der Meer, J.W., 1998. 'Geometrical Design of Coastal Structures'. Pilarczyk, K.W. (Ed.), Seawalls, Dikes and Revetments. Balkema, Rotterdam.

Van Gent, M.R.A. and Van der Werf, I.M., 2014. 'Rock toe stability of rubble mound breakwaters'. *Coastal Engineering* 83, 166–176.

Vidal, C., Losada, M. A., and Mansard, E. P. D., 1991. 'Stability of mound breakwater's head and trunk'. *J. Waterway, Port, Coastal, and Ocean Eng.*, 117(6), 570–587.

Appendix 2

Transformation of Eq. II.20 in terms of armor damage following the methodology used by Medina et al. (1994)

Puerto Blanco. Calpe, Alicante (Spain). July, 2016.

Eq. II.20 has been related to different levels of armor damage, S, following the methodology described by Medina et al. (1994). The values of armor damage, D, given by USACE (1975) and USACE (1984) for rough quarrystones, were used for this purpose as a function of $H/H_{D=0}$, where H is the wave height corresponding to damage D, and $H_{D=0}$ is the design wave height corresponding to D=0-5% (note that $H=H_s$ for USACE (1975) and $H=H_{1/10}$ for USACE (1984)).

The damage, D, was based on the volume of rocks displaced from the active zone of the armor. USACE (1975) and USACE (1984) defined the active zone as the area which extends from the middle of the breakwater crest down the seaward face to a depth equivalent to $H_{D=0}$ below the SWL. Considering this definition, the corresponding active zone for the tests conducted in the present study was approximately $28D_{n50}^2$ for $H=H_s$ and $27.2D_{n50}^2$ for $H=H_{1/10}$. In both cases, the damage D provided by USACE (1975 and 1984) was related to the dimensionless armor damage, S, as listed in Table A2.1.

		Relative wave height, $H/H_{D=0}$						
		1.00	1.08	1.19	1.27	1.37	1.47	1.56
		Damage (D) in Percent						
		0-5	5-10	10-15	15-20	20-30	30-40	40-50
Damage (S=0.28D)	$H=H_s$(USACE,1975)	0.7	2.1	3.5	4.9	7.0	9.8	12.6
	$H=H_{1/10}$(USACE,1984)	0.7	2.0	3.4	4.8	6.8	9.5	12.2

Table A2.1. Dimensionless armor damage (S) for H=Hs and H=H1/10, as a function of H/HD=0 and the damage in percent (D).

The damage data shown in Table A2.1 were fitted by Eq. A2.1 for both $H=H_s$ and $H=H_{1/10}$, as observed in Fig. A2.1.

$$\frac{H}{H_d}=\left(\frac{S}{1.4}\right)^{0.2} \tag{A2.1}$$

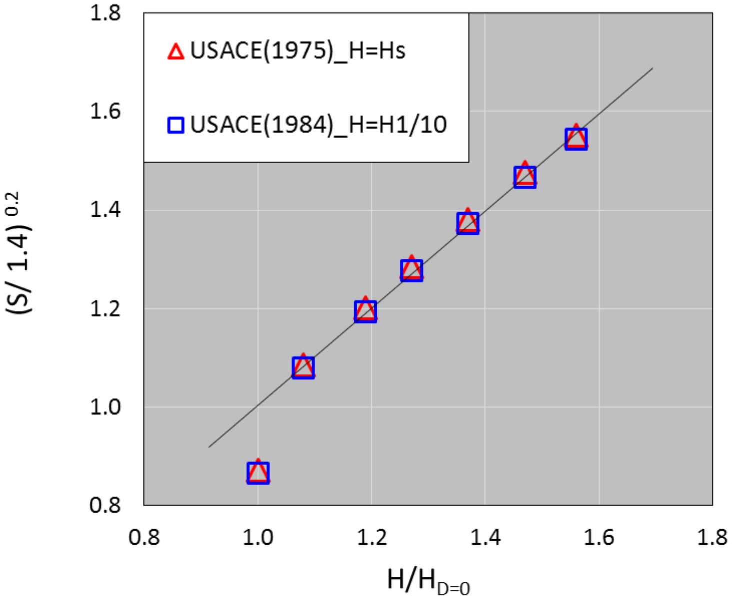

Figure A2.1. Linear damage function obtained from the data provided by USACE (1975 and 1984).

Relating Eqs. II.20 and A2.1, Eq. A2.2 was obtained to estimate the stability number for higher levels of armor damage, using the dimensionless damage parameter, S.

$$\frac{H}{\Delta D_{n50}} = \left(\frac{S}{1.4}\right)^{0.2} (K_D \cot\alpha)^{1/3} \qquad [A2.2]$$